frontiers | Research Topics

74th annual meeting of the Italian society of physiology: breakthroughs and key discoveries

Edited by
Myriam Catalano and Roberto Piacentini

Published in
Frontiers in Physiology

ISSN 1664-8714
ISBN 978-2-8325-7285-6
DOI 10.3389/978-2-8325-7285-6

Generative AI statement
Any alternative text (Alt text) provided alongside figures in the articles in this ebook has been generated by Frontiers with the support of artificial intelligence and reasonable efforts have been made to ensure accuracy, including review by the authors wherever possible. If you identify any issues, please contact us.

About Frontiers

Frontiers is more than just an open access publisher of scholarly articles: it is a pioneering approach to the world of academia, radically improving the way scholarly research is managed. The grand vision of Frontiers is a world where all people have an equal opportunity to seek, share and generate knowledge. Frontiers provides immediate and permanent online open access to all its publications, but this alone is not enough to realize our grand goals.

Frontiers journal series

The Frontiers journal series is a multi-tier and interdisciplinary set of open-access, online journals, promising a paradigm shift from the current review, selection and dissemination processes in academic publishing. All Frontiers journals are driven by researchers for researchers; therefore, they constitute a service to the scholarly community. At the same time, the *Frontiers journal series* operates on a revolutionary invention, the tiered publishing system, initially addressing specific communities of scholars, and gradually climbing up to broader public understanding, thus serving the interests of the lay society, too.

Dedication to quality

Each Frontiers article is a landmark of the highest quality, thanks to genuinely collaborative interactions between authors and review editors, who include some of the world's best academicians. Research must be certified by peers before entering a stream of knowledge that may eventually reach the public - and shape society; therefore, Frontiers only applies the most rigorous and unbiased reviews. Frontiers revolutionizes research publishing by freely delivering the most outstanding research, evaluated with no bias from both the academic and social point of view. By applying the most advanced information technologies, Frontiers is catapulting scholarly publishing into a new generation.

What are Frontiers Research Topics?

Frontiers Research Topics are very popular trademarks of the *Frontiers journals series*: they are collections of at least ten articles, all centered on a particular subject. With their unique mix of varied contributions from Original Research to Review Articles, Frontiers Research Topics unify the most influential researchers, the latest key findings and historical advances in a hot research area.

Find out more on how to host your own Frontiers Research Topic or contribute to one as an author by contacting the Frontiers editorial office: frontiersin.org/about/contact

74th annual meeting of the Italian society of physiology: breakthroughs and key discoveries

Topic editors

Myriam Catalano — Sapienza University of Rome, Italy

Roberto Piacentini — Catholic University of the Sacred Heart, Italy

Citation

Catalano, M., Piacentini, R., eds. (2025). *74th annual meeting of the Italian society of physiology: breakthroughs and key discoveries*. Lausanne: Frontiers Media SA. doi: 10.3389/978-2-8325-7285-6

Table of contents

frontiers | Frontiers in Physiology

TYPE Editorial
PUBLISHED 05 December 2025
DOI 10.3389/fphys.2025.1756505

OPEN ACCESS

EDITED AND REVIEWED BY
Geoffrey A. Head,
Baker Heart and Diabetes Institute, Australia

*CORRESPONDENCE
Myriam Catalano,
myriam.catalano@uniroma1.it

RECEIVED 28 November 2025
ACCEPTED 30 November 2025
PUBLISHED 05 December 2025

CITATION
Catalano M and Piacentini R (2025) Editorial: 74th annual meeting of the Italian society of physiology: breakthroughs and key discoveries.
Front. Physiol. 16:1756505.
doi: 10.3389/fphys.2025.1756505

Editorial: 74th annual meeting of the Italian society of physiology: breakthroughs and key discoveries

Myriam Catalano[1]* and Roberto Piacentini[2,3]

[1]Department of Physiology and Pharmacology, Faculty of Pharmacy and Medicine, Sapienza University of Rome, Rome, Italy, [2]Department of Neuroscience, Università Cattolica del Sacro Cuore, Rome, Italy, [3]IRCCS Fondazione Policlinico Universitario A. Gemelli, Rome, Italy

KEYWORDS

cellular physiology, environmental factors, human physiology, neuro-glial communication, synaptic plasticity

Editorial on the Research Topic
74th annual meeting of the italian society of physiology: breakthroughs and key discoveries

The 74th Annual Congress of the Italian Society of Physiology, which took place in Rome in September 2024, provided a valuable platform for interdisciplinary dialogue, fostering communication among researchers and presenting novel perspectives in physiological research. This Research Topic compiles contributions reflecting the richness of discussions and presentations during the congress, offering an overview of topics of great current interest and scientific relevance.

The articles range from cellular and molecular aspects to neurobiological and systemic processes. They focus on the mechanisms that regulate synaptic plasticity, neuro-glial communication, and the impact of environmental factors on human physiology.

In particular:

Synapse regulation depends on post-translational modifications, including SUMOylation, which modulates the conformation, stability, and localization of synaptic proteins. Bertozzi et al. have demonstrated that sumoylation, a physiological process occurring on proteins, ensures spatiotemporal control of synaptic transmission and plasticity. Conversely, its alteration is associated with the appearance of neurodegenerative illnesses, such as Alzheimer's diseases, which opens up therapeutic prospects based on SUMO modulation.

Cannata et al. investigated the role of α7 nicotinic acetylcholine receptors (α7-nAChRs) in glutamatergic transmission using a mouse model. Deletion of the gene that encodes these receptors in both neurons and astrocytes, induces a phenotype similar to Alzheimer's disease (AD), characterized by abnormal β-amyloid accumulation, tau phosphorylation, and neuroinflammation in aged mice (>12 months). However, in young α7-KO mice (4–6 months-old) functional and molecular alterations in glutamatergic transmission, including reduced NMDA currents and altered expression of synaptic proteins, such as Synapsin-1, GluN2A, GluN2B, and the post-synaptic

scaffold protein Homer-1 were found. Selective neuronal re-expression of the α7-nAChR gene in α7-KO mice via AAV infection restored post-synaptic functional alterations, but not presynaptic ones. The authors hypothesize that early synaptic dysfunction in Alzheimer's disease results from an altered cholinergic-glutamatergic dialogue that precedes overt neurodegeneration. They also suggest that clarifying the specific contribution of the α7-nAChR receptor in different cell types could lead to new therapies aimed at preserving circuit functionality in the early stages of Alzheimer's disease.

Growing global plastic production has made plastic pollution a critical environmental and public health issue, prompting particular attention to nanoplastics (NPs) due to their prevalence and potential biological risks. Giordano et al.'s study investigated the effects of exposure to polyethylene terephthalate (PET) nanoplastics on NIH-3T3 murine fibroblasts, a relevant cell model for processes such as cell migration, which is important for tissue regeneration. The PET NPs realistically represent environmental microplastics because they were obtained using a top-down approach that simulates the mechanical abrasion occurring in the atmosphere. Furthermore, the PET NPs exhibit autofluorescence, which is useful for interaction studies without the use of additional dyes. The results show that PET NPs are internalized by fibroblasts in a dose-dependent manner and localize in the cytoplasm. After 24 h, cell viability decreased by only ≤20% at concentrations of 10–100 μg/mL, but migration was significantly impaired, as evidenced by the scratch assay. This suggests a potential impact on tissue repair. Additionally, exposure induced a dose-dependent increase in reactive oxygen species (ROS), suggesting that intracellular oxidative stress may be a mechanism underlying the migratory deficit. These data underscore the risks that PET NPs pose to cellular functions and highlight the need for further research on the underlying mechanisms.

Loi et al. examined cortical plasticity in older adults using paired associative stimulation (PAS) and new indices were introduced to evaluate the response to stimulation. Curve concavity (CC) was found to be the most effective discriminator between responders and non-responders, significantly correlating with cognitive status as measured by the Montreal Cognitive Assessment (MoCA). The study suggests that CC could be a useful biomarker for monitoring PAS-induced cortical plasticity and its relationship with cognitive status, potentially aiding in the treatment of cognitive disorders.

Among environmental factors modulating endogenous neurogenesis, enriched environment (EE) plays a key role. Marrocco et al. showed that transplanting microbiota from mice raised in an EE to those in a standard environment (SE) decreases anxiety and increases neurogenesis and neurotrophins release in the hippocampus. These findings confirm the role of gut microbiota in mediating the beneficial effects of lifestyle on the brain and suggest prospects for therapeutic interventions based on fecal transplantation for mood disorders.

Masoli et al.'s work is a systematic review of the scientific literature on Purkinje cells, the most complex neurons in the nervous system. These neurons have a vast dendritic tree rich in spines that receive excitatory inputs from parallel and climbing fibers. The study highlighted that, although the total number of spines is lower than initial estimates, they are more efficient given the identification of more complex structures, such as double-headed spines, and functional mechanisms modulated by post-learning morpho-functional changes in glial cells. These recent structural and functional findings on Purkinje cells contribute to synaptic recognition and cerebellar plasticity.

The study by Morrone et al. investigates cross-education, which is the increase in strength of the untrained limb after training the contralateral limb. This process is mediated by interhemispheric dynamics through the corpus callosum. To clarify these mechanisms, the authors employed a lesion model in which nine patients with relapsing-remitting multiple sclerosis and focal lesions of the corpus callosum participated in a six-week, high-intensity, isokinetic training program targeting the dorsiflexors of the stronger ankle. After training, both limbs showed significant increases in strength and reduced asymmetry. However, patients with lesions in the rostral corpus callosum reported less cross-education and reduced improvement in asymmetry between the two limbs. No correlations were found for the other subregions of the corpus callosum. This study underscores the pivotal role of the rostral corpus callosum in mediating cross-education mechanisms and suggests that routinely assessing callosal lesions could inform targeted rehabilitation interventions.

In the review by Porcari et al., glial cell-derived neurotrophic factor (GDNF) emerges as an essential trophic factor for neuronal survival and synaptic plasticity. In addition to protecting dopaminergic neurons, GDNF influences GABAergic hippocampal circuits. It interacts with glial cells and contributes to the regulation of neuroinflammation and the blood-brain barrier. GDNF also plays a role in the peripheral nervous system, controlling the development of sympathetic and parasympathetic fibers, maintaining somatic sensory neurons, and innervating motor neurons at the neuromuscular junction. The importance of GDNF in the biology of many tumors (e.g., neuroendocrine, prostate, and colorectal) has also been emphasized, particularly the fact that the GDNF-RET axis is a double-edged sword that requires precise regulation to achieve therapeutic benefits. GDNF was then explored in depth as a promising therapeutic target for neurodegenerative diseases and other neurological conditions.

Ranieri et al. used the hindlimb unloading (HU) mouse model to evaluate the effects of microgravity on body fluid distribution and kidney function. The kidney is the primary regulator of water and salt balance. Specifically, they analyzed vasopressin levels and renal aquaporin (AQP2) expression. The study showed that 1 week of suspension leads to early activation of the system. After 4 weeks, however, there is inhibition of the process associated with protein degradation mechanisms and reduced translation of AQP2 mRNA. These adaptations reflect physiological strategies that balance central venous pressure and water homeostasis in microgravity conditions. They also provide insight into managing nephropathies associated with prolonged immobility.

Storniolo et al. explore how muscle fatigue affects anticipatory postural adjustments (APAs) when initiating walking. Walking is a task that requires feedforward control of posture coordinated with the focal movement. Sixteen trained men performed walking onset tests before and after a one-minute sequence of counter-movement jumps. Muscle activity was recorded via electromyography, and centre of pressure (CoP) shifts and kinematics were recorded. Fatigue delayed both excitatory and inhibitory APAs, as well as reducing the speed and amplitude of posterior CoP shifts. While most participants maintained a “diving” strategy (bilateral dorsal

inhibition and ventral excitation), three subjects adopted a "turning" strategy characterized by reciprocal activations compatible with trunk rotation. These results suggest that the central nervous system possesses a variety of postural strategies that can be selected based on factors such as fatigue, training level, and task constraints.

As Physiology research continues to evolve, it is important to recognize the contributions of scientists and clinicians who drive its progress. The 74th Annual Congress of the Italian Society of Physiology exemplified collaboration and the exchange of ideas that promote the advancement of the biomedical sciences.

We thank all the authors, reviewers, and contributors who made this Research Topic possible.

This Research Topic reflects the curiosity and commitment of the scientific community. We hope the presented results will stimulate new research and bring us closer to understanding the complex mechanisms that regulate human physiology.

Author contributions

MC: Writing – original draft, Writing – review and editing. RP: Writing – original draft, Writing – review and editing.

Funding

The author(s) declared that financial support was not received for this work and/or its publication.

Conflict of interest

The author(s) declared that this work was conducted in the absence of any commercial or financial relationships that could be construed as a potential conflict of interest

Generative AI statement

The author(s) declared that generative AI was not used in the creation of this manuscript.

Any alternative text (alt text) provided alongside figures in this article has been generated by Frontiers with the support of artificial intelligence and reasonable efforts have been made to ensure accuracy, including review by the authors wherever possible. If you identify any issues, please contact us.

Publisher's note

frontiers | Frontiers in Physiology

TYPE Original Research
PUBLISHED 13 January 2025
DOI 10.3389/fphys.2024.1520578

OPEN ACCESS

EDITED BY
Roberto Piacentini,
Catholic University of the Sacred Heart, Italy

REVIEWED BY
Rinaldo André Mezzarane,
University of Brasilia, Brazil
Oscar Crisafulli,
University of Pavia, Italy

*CORRESPONDENCE
Paolo Cavallari,
paolo.cavallari@unimi.it

RECEIVED 31 October 2024
ACCEPTED 09 December 2024
PUBLISHED 13 January 2025

CITATION
Storniolo JL, Farinelli V, Esposti R and Cavallari P (2025) Impact of muscle fatigue on anticipatory postural adjustments during gait initiation. *Front. Physiol.* 15:1520578.
doi: 10.3389/fphys.2024.1520578

Impact of muscle fatigue on anticipatory postural adjustments during gait initiation

Jorge L. Storniolo[1,2], Veronica Farinelli[1], Roberto Esposti[1] and Paolo Cavallari[1,2]*

[1]Human Physiology Section of the Department of Pathophysiology and Transplantation, Università Degli Studi, Milano, Italy, [2]Laboratorio Sperimentale di Fisiopatologia Neuromotoria, IRCCS Istituto Auxologico Italiano, Meda, Italy

Introduction: Prolonged or strenuous exercise leads to a temporary decrease in muscle function and performance, which interferes with activity of both prime movers and postural muscles. This effect of fatigue has been reported both for single segment movements and for locomotion. However, little is known regarding the effects of fatigue on anticipatory postural adjustments (APAs) during gait initiation, a task in which the control of focal movement should be strictly coupled to a feedforward control of posture.

Methods: We studied APAs during gait initiation in 16 healthy well-trained adult males, searching for muscle activities that precede the backward shift of the Center of Pressure (CoP). Participants stood on a force plate for about 10 s and then started walking at their natural speed. APAs were evaluated before and after a 1 min exhausting sequence of countermovement jumps. An optoelectronic system captured the heel-off events while a force plate measured the CoP position and vertical ground reaction force. Wireless probes recorded the electromyogram of trunk and leg muscles from both sides.

Results: It was observed that muscle fatigue delayed excitatory and inhibitory APAs, of about 40 and 80 ms, respectively, and a parallel delay was induced on prime movers; moreover, velocity and amplitude of backward CoP shift were reduced. Regarding APAs sign and occurrence, most of the participants showed bilateral inhibition in dorsal muscles and excitation in the ventral ones, displaying a forward "diving" strategy that was almost unaffected by fatigue. However, after fatigue, three of the "diving" participants switched to a "turning" strategy, i.e., they displayed a reciprocal activation/inhibition pattern in the dorsal muscles, compatible with a trunk rotation.

Discussion: The "turning" strategy has been previously described in untrained individuals and in a toes-amputee mountain climber, who showed a "diving" approach to gait initiation when wearing his prosthetic shoes and switched to the "turning" approach when barefoot. Altogether, these results support the idea that one and the same person may develop a repertoire of postural strategies among which the central nervous system will choose, according to the personal fitness and the constraints in which the action is performed.

KEYWORDS

postural strategies, APAs, trunk muscles, exhausting exercise, human

1 Introduction

Physiological fatigue is a complex process involving various factors leading to a decline in muscle performance (Bigland-Ritchie and Woods, 1984). Fatigue, characterized by reduced maximal muscle force or power due to prolonged or strenuous exercise, may result from peripheral mechanisms including metabolic by-products, depletion of energy substrates, accumulation of extracellular potassium ions, and alterations in neuromuscular function (Davies et al., 1991). Additionally, also central fatigue, stemming from changes in the central nervous system (spinal motor neurons, motor cortex, or structures upstream of the motor cortex), has been shown to contribute to tiredness and reduced muscle output, leading to twitching, cramps, aches, and pains (Gandevia, 2001). These processes may interact and influence each other, leading to a temporary decrease in muscle function and performance (for a recent review, see Behrens et al., 2023).

Actually, it has been demonstrated that the increase in blood lactate levels after fatigue not only impairs cognitive and executive functions, but also exert direct cortical influences by increasing primary motor cortex excitability and depressing supplementary motor area (Coco et al., 2016; 2020). In turn, Bolzoni et al. (2015) showed that changes in supplementary motor area excitability modulates Anticipatory Postural Adjustments (APAs) without affecting the primary movement. Taken together, the above cited results support the idea that the fatigue effects may also involve the postural control, in particular the APAs that stabilize posture prior to the execution of the focal movement.

A few studies reported that fatigue impairs postural control and locomotion in young adults and older participants; actually, increased occurrence of falls is not only caused by biological aging, but also by fatigue in lower leg muscles (Helbostad et al., 2007; Parijat and Lockhart, 2008). Specifically, in healthy young adults it was observed that localized muscle fatigue of the quadriceps affected various kinematic and kinetic parameters linked with a high risk of slip-induced falls (Parijat and Lockhart, 2008). In parallel, a repeated sit-to-stand task impaired locomotion control in older persons with regard to increased step width and length variability (Helbostad et al., 2007).

The intrinsic complexity of walking becomes apparent at its very beginning, i.e., at gait initiation, when the control of focal movement should be strictly coupled to a feedforward control of posture. Indeed, starting gait implies not only to propel the Center of Gravity (CoG), but also to build-up the postural scheme needed to grant body stability in the transition from quiet standing to locomotion (Farinelli et al., 2021). In this framework, fatigue should likely affect not only the movement itself but also the postural actions preceding it. Actually, a conclusion in this direction is reported by Yiou et al. (2011), who showed an increased duration of the APAs after acute fatigue of Tibialis Anterior (TA) muscles. This prolonged activity was however expressed as the time difference between the onset of forward acceleration of the CoG and the take-off of the leading foot. In parallel, TA activation was depressed, while its onset remained locked to that of CoG acceleration. From a functional point of view, decreased electrical activity during gait initiation in both TAs may reflect a protective strategy, aiming to attenuate the intensity of the contraction and thus optimally preserve the integrity of the fatigued muscle. In turn, such result is in agreement with the "pain-adaptation model" (Lund et al., 1991), which predicts a decrease in EMG activity of agonist muscles, an increase in EMG activity of antagonist muscles, and slower and less powerful movements during muscle pain to protect the painful muscle.

However, such results are not exhaustive for the following reasons: i) the TA and its antagonist Soleus (Sol) should be considered prime movers, not postural muscles, since they shift the Center of Pressure (CoP) backward and consequently propel the CoG forward; ii) the forward CoG acceleration and the ensuing take-off of the leading foot are intrinsic part of the focal movement, thus the APAs should be searched for before those events. In this perspective, the APAs associated with gait initiation has been detailed by Farinelli et al. (2021); in this paper we address the question on whether APAs associated with gait initiation may be affected by whole-body fatigue.

2 Methods

2.1 Participants

Seeking homogeneity in the effectiveness of the fatigue procedure (see below), the study was conducted on healthy male adults, free from any musculoskeletal or neurological dysfunction and systematically practicing physical activity, so as to control for effects of age, gender and training status. Specifically, there were enrolled sixteen men with an age of 26 ± 6 years (mean ± SD), a height of 1.76 ± 0.1 m, a weight of 75 ± 10.1 kg and practicing physical activity at least three times per week. All participants were right-footed, as ascertained by asking them which leg they used to kick a ball, as well as by observing the limb used to initiate walking spontaneuosly. The experimental procedure was carried out in accordance with the standards laid down in the Declaration of Helsinki and approved by the "Comitato Etico di Ateneo dell'Università degli Studi di Milano" (counsel 23/23).

2.2 Experimental setup

The experimental session consisted of a gait initiation task. Specifically, participants wearing sports shoes were asked to stand on the force plate for 10 s and then start walking at their own will after a vocal prompt. Ten trials were collected before and after muscle fatigue. The fatiguing procedure consisted of a 1-min of uninterrupted countermovement jumps (CMJ), i.e., a sequence of vertical jumps performed by quickly squatting with the hands on the hips, then jumping as high as possible and repeating the squat-jump sequence immediately after each landing (Bosco et al., 1983; Figure 1). Simultaneously, the participant was verbally encouraged to reinforce the maximal effort required for the test.

2.3 Recordings

A dynamometric force plate (9286AA, KISTLER, Winterthur, Switzerland, sampling frequency: 400 Hz) was used to compute the CoP position and measure the vertical Ground Reaction Force

FIGURE 1
Starting the countermovement jump sequence: 1: standing position; 2: knees flexion to squat; 3: jump and take off from the force plate; 4: landing on the force platform; 5: pushing to jump again.

(vGRF) while jumping. Wireless probes (FREEEMG 1000, BTS, Milan, Italy, sampling frequency: 1,000 Hz) were employed bilaterally to record the surface electromyographic (EMG) activity of TA, Sol, Obliquus Abdominis (OA), Erector Spinae at L2 vertebra (ES), Vastus Medialis (VM) and Biceps Femoris (BF). Electrodes were placed according to the Surface Electromyography for the Non-Invasive Assessment of Muscles (SENIAM) guidelines (Hermens et al., 2000). Markers on the heels were recorded through an eight-camera optoelectronic system (SMART-DX, BTS, Milan, Italy, sampling frequency 100 Hz), allowing the estimation of the heel-off events.

2.4 Data processing

EMG data were processed as described elsewhere (Farinelli et al., 2021). In brief, after high-pass filtering (50 Hz for all muscles except OA, in which 150 Hz was used to reject cardiac artifacts), EMG traces were full-wave rectified, then time-aligned to the heel-off of the leading foot and averaged across trials. The same averaging was applied to CoP and heel traces. The mean level and SD of the CoP trace from 3 to 1 s before the heel-off was measured, then the onset of the backward CoP shift was identified by a custom-made algorithm, which searched for the time point where the trace fell below −2 SD with respect to the mean level and remained below that value for at least 50 ms. CoP onset was then assigned to Time 0. The averaged EMGs were integrated with a 25 ms moving window (the window outcome was assigned to the central sample to avoid phase-lags) and the mean level and SD of the traces were measured from 3 to 1 s before the CoP onset. The onset of the EMG changes was identified by applying the same algorithm used for CoP setting the threshold to mean ±2 SD and restraining the search from −300 to +100 ms with respect to CoP onset. Amplitude and latency of the first backward peak of CoP were also measured.

To assess the effectiveness of the fatigue procedure, the number of jumps and the average of the vGRF peaks in the propulsive phase, i.e., the last peak before flight, were considered. Both variables were calculated in two time windows: in the first and in the last 15 s of the 1-min fatigue procedure.

2.5 Statistical analysis

First, the occurrence of the EMG changes was scored by assigning +1 to excitation, −1 to inhibition, and 0 in case of absence; then, considering the categorical nature of such variable, the effect of fatigue was assessed by Wilcoxon matched pairs test. The latency of EMG changes was considered only for those participants who showed changes of the same sign in both conditions. In view of the continuous nature of the variable, the normality was preliminarily checked in each muscle by Shapiro-Wilk test; then the effect of fatigue on APA latency was evaluated either by paired t-tests, for those muscles in which normality was not violated, or by Wilcoxon matched pairs test where the normality assumption did not hold true. The same procedure was used to compare amplitude and latency of backward CoP shift before and after fatigue as well as for evaluating the outcome of the fatiguing procedure, in which the number of jumps and the average peak of the vGRF were compared in the first and last 15 s of exercise. The normality assumption did not hold true only for the latency of BF on the trailing side and of TA on the leading side. Significance threshold was set at $p = 0.05$.

3 Results

3.1 Efficacy of the fatiguing protocol

The CMJ procedure did not decrease the jump frequency, indeed the number of jumps performed by the participants was, in average, comparable during the first and last 15 s of the exercise (13.8 ± 0.4 vs. 14.1 ± 0.6; t-test $p = 0.48$). On the contrary, the explosive force dropped by about 18%: the peak force of each jump being 1,471 ± 41 N (mean ± SE) in the first 15 s and 1,203 ± 40 N in the last 15 s (t-test $p < 0.0001$).

3.2 Impact of muscle fatigue on APAs during gait initiation

Our protocol of muscle fatigue induced visible changes in sign and occurrence of APAs, as well as in their latency.

For what regards sign and occurrence (inhibition, excitation or absence) fatigue induced effects of increased severity from distal to proximal postural muscles. This could be appreciated by examining both the occurrence of excitation/inhibition (left side of Table 1) and the number of those participants who showed EMG changes of the same sign in both conditions (i.e., the matched pairs, right side of Table 1). For example, the inhibition of BF muscle in the trailing side

TABLE 1 Effect of fatigue on Signs, Occurrence and Latency of APAs in postural muscles Erector Spinae (ES), Obliquus Abdominis (OA), Biceps Femoris (BF) and Vastus Medialis (VM), as well as on EMG activity of prime movers Soleus (Sol) and Tibialis Anterior (TA). On the left side, number of participants showing inhibition (blue), excitation (red) or absence (black) of APA/EMG activity, compared by Wilcoxon matched pairs test. On the right, the Mean Latency was calculated only for matched pairs (i.e., those participants who showed EMG changes of the same sign in both conditions) and compared either by t-test (^{t}), where data distribution did not deviate from normality, or by Wilcoxon matched pairs test (^{W}) where the normality assumption was violated. Significant p-values in bold.

		Sign and occurrence (n/16 participants)			Mean latency ± SE (ms) for matched pairs		
		Control	Fatigue	p	Control	Fatigue	p (n pairs)
Leading side	ES	12 1 3	11 - 5	>0.5	−158 ± 15 - -	−91 ± 18 - -	**0.011** (11) t - -
	OA	- 7 9	2 3 11	**0.028**	- −77 ± 26 -	- −43 ± 10 -	- n.c. (3) -
	BF	9 - 7	12 - 4	0.225	−173 ± 16 - -	−97 ± 33 - -	**0.020** (8) t - -
	VM	- 12 4	- 11 5	>0.5	- −105 ± 11 -	- −51 ± 18 -	- **0.009** (11) t -
	Sol	13 - 3	12 - 4	>0.5	−123 ± 29 - -	−61 ± 20 - -	**0.007** (12) t - -
	TA	- 13 3	- 14 2	>0.5	- −79 ± 21 -	- −36 ± 19 -	- **0.046** (13) W -
Trailing side	ES	11 1 4	9 4 3	0.176	−139 ± 19 −24 -	−76 ± 32 39 -	**0.037** (7) t n.c. (1) -
	OA	- 12 4	- 12 4	>0.5	- −45 ± 12 -	- −5 ± 16 -	- **0.017** (12) t -
	BF	12 - 4	13 - 3	>0.5	−167 ± 24 - -	−80 ± 16 - -	**0.005** (10) W - -
	VM	- 14 2	- 14 2	>0.5	- −69 ± 12 -	- −23 ± 17 -	- **0.011** (13) t -
	Sol	16 - -	15 - 1	>0.5	−147 ± 16 - -	−78 ± 19 - -	**0.003** (15) t - -
	TA	- 16 -	- 15 1	>0.5	- −78 ± 15 -	- −41 ± 12 -	- **0.04** (15) t -

was observed in 12 participants in control condition and in 13 after fatigue. However, only 10 individuals showed inhibition in both conditions. This means that two individuals missed the original inhibition after fatigue while 3 displayed inhibitions only after fatigue. It is then clear that fatigue had no systematic effect, as witnessed by the Wilcoxon test. The most severe effects were observed in the ES of the trailing side and in the OA of the leading side, in which the Wilcoxon test reached significance. Indeed, out of the 7 participants showing excitation in control, 4 dropped it after fatigue; instead, two further individuals displayed inhibition instead of excitation, but only in fatigue.

The disturbing effect of fatigue was not limited to the EMG pattern (sign and occurrence), but also became apparent in the latency of both excitation and inhibition (right side of Table 1). In fact, all trunk and

10.3389/fphys.2024.1520578

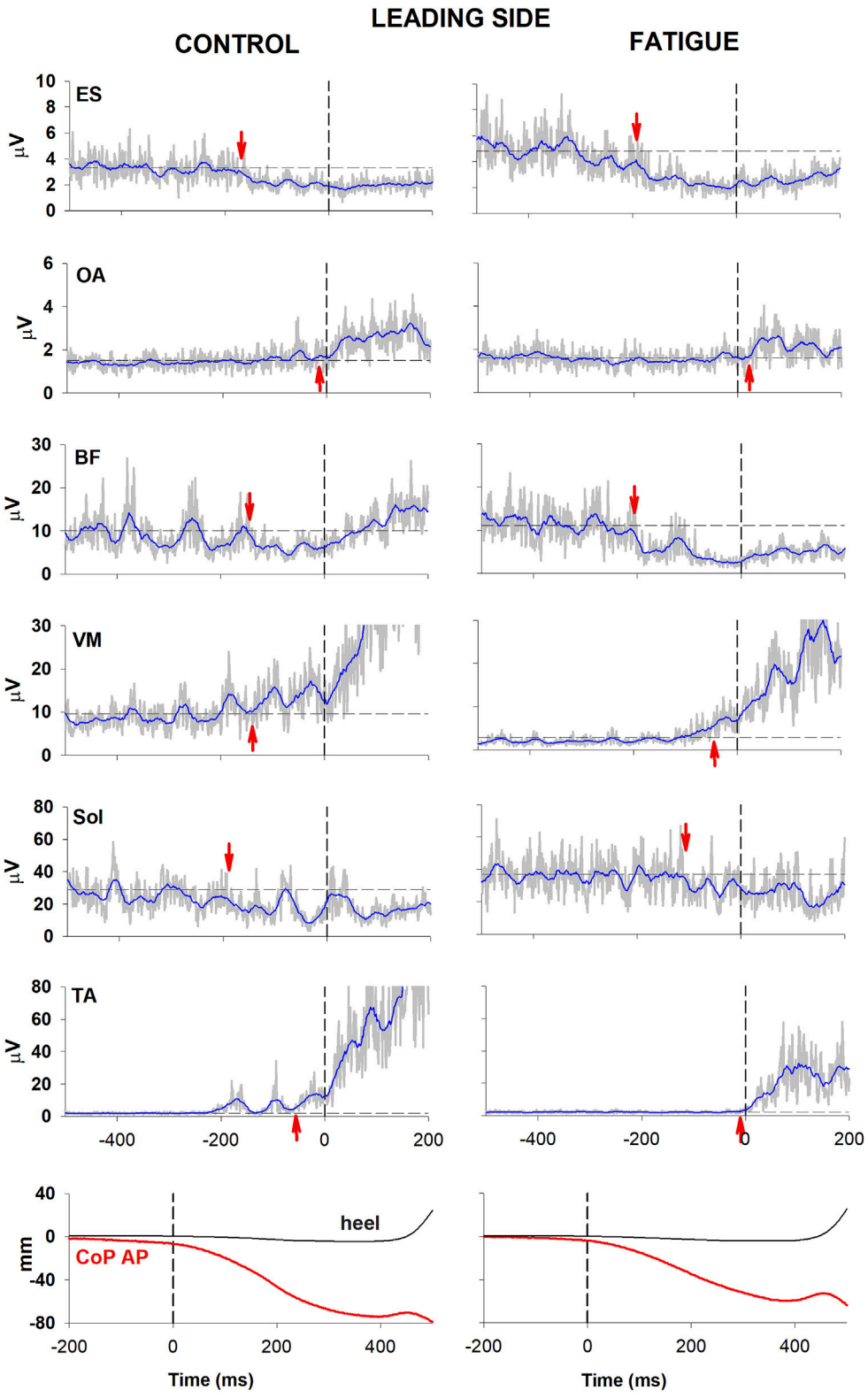

FIGURE 2
Comparison of raw (grey) and integrated (blue) EMG activity in control (left) and fatigue (right) condition on the leading side. One participant in which all muscular activities kept the same sign before and after fatigue. From the top: Erector Spinae (ES), Obliquus Abdominis (OA), Biceps Femoris (BF), Vastus Medialis (VM) and prime movers Soleus (Sol) and Tibialis Anterior (TA). Arrows mark the onset of excitation (upward arrow) or inhibition (downward arrow). Black dashed lines at time 0 mark the onset of the backward whole-body CoP shift while the horizontal lines represent the average muscle activity at baseline. The lowermost plot shows the anteroposterior CoP displacement (red) as well as the heel vertical displacement (black).

10.3389/fphys.2024.1520578

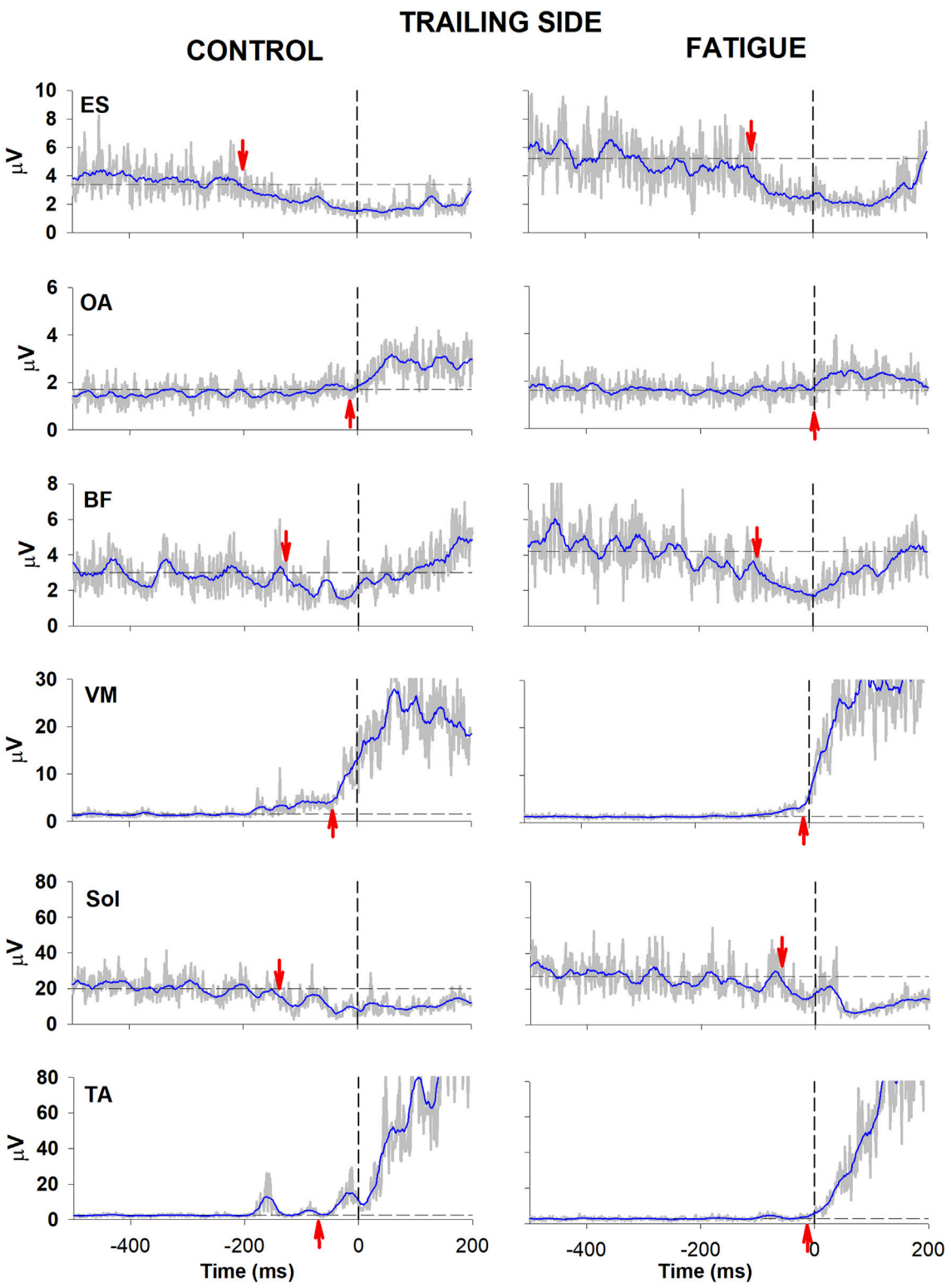

FIGURE 3
Comparison of raw (grey) and integrated (blue) EMG activity in control (left) and fatigue (right) condition on the trailing side. Same participant and graphic conventions as in Figure 2.

thigh muscles demonstrated a significant delay in APA activity after fatigue, which was confirmed by statistics. This was also paralleled by the activity of the prime movers (TA recruitment and Sol inhibition). Moreover, it is worth to note that the amount of delay was comparable among muscles showing excitation (~40 ms) as well as among those showing inhibition (~80 ms).

Figures 2, 3 illustrate the behaviour of one participant in which all muscular activities kept the same sign before and after fatigue. In the control condition, EMG changes preceding CoP shift could be identified in the trunk and lower limb muscles of both the trailing and the leading sides (left panel, Figures 2, 3). Specifically, as in most participants, a reciprocal activity was observed in dorsal and ventral postural muscles. Indeed, ES and BF showed an inhibition of tonic EMG activity while OA and VM showed an excitation. These APAs accompanied the well-known reciprocal activity observed in the prime movers (inhibition in Sol and excitation in TA). After the fatiguing procedure (right panel, Figures 2, 3), a clear increase in latency occurred in all muscular activities.

Fatigue also affected the CoP trajectories. Indeed, in the illustrated participant the fatigue procedure reduced the amplitude of the peak backward shift, without changing its latency (bottom traces in Figure 2). This was measured in the whole population, resulting into a significant reduction of peak amplitude (46.55 mm ± 4.91 SE in control condition vs. 40.71 mm ± 4.07 SE in fatigue; t-test $p = 0.047$) while latency was almost unchanged (449 ms ± 26 vs. 439 ms ± 20; t-test $p > 0.5$).

4 Discussion

4.1 Neuromuscular and biomechanical factors affecting APA timing and pattern

With the aim of assessing whether the effect of fatigue alters the APAs and the prime movers activity in physically active participants, our results highlighted that the CMJ procedure mainly delayed APAs and reduced the speed of the backward CoP shift, with minor effects on sign and occurrence of APAs.

There is an apparent problem in comparing our findings with those reported by literature. Indeed, 1) most studies on the effect of fatigue on APAs consider upper limb movements, not gait initiation; 2) only few studies employed a fatigue task affecting both prime movers and postural muscles, like our CMJ task; 3) the definition of the reference time for measuring APA latency is different among papers. Specific references are provided in the following paragraphs.

In regard to APA timing, it should be noted that we employed a novel approach (Farinelli et al., 2021) which reinterpreted the posturo-kinetic chain related to gait initiation. In fact, classical literature searched for APAs in the time window from the first CoP displacement to the onset of heel-off or foot-off (Crenna and Frigo, 1991; Assaiante et al., 2000; Yiou et al., 2011; Yiou et al., 2017), including activities in TA and Sol. This approach neglected the fact that initiating gait requires to push forward the CoG, an action that is attained by shifting the CoP backward. In our view, the CoP displacement is the effect of prime movers, meaning that Sol and TA activity should no longer be considered APAs but rather the expression of the primary motor command. Consequently, APAs should be ideally searched for in a time window preceding the backward CoP displacement, i.e., well before the heel-off. Thus, the timing of our EMG activities is not directly comparable with that measured in previous studies on gait initiation, like in Yiou et al. (2011), who reported an earlier onset of APAs after fatigue. However, we observed a reduction in backward CoP velocity, as described by Yiou.

Our approach is instead much more congruent with that used in classical papers on APAs accompanying movements of single segments (for a review see Bouisset and Do, 2008). In this regard, literature on arm raising movements reports contrasting results. Kanekar et al. (2008) described a minimal APAs anticipation (less than 10 ms with respect to prime mover activation) in ES, BF and Semitendinosus after fatiguing postural muscles. This result is also supported by Monjo and Forestier (2014), who induced muscle fatigue by electrical stimulation, as well as by Schouppe et al. (2019) who studied APAs after physical and cognitive exertion. No changes in APAs after fatigue were also reported by Yiou et al. (2009) during bilateral forward reach task. Conversely, Strang and Berg (2007) described up to 25 ms advance in Paraspinals muscles. Slightly larger advances (about 30–40 ms) were reported by Vuillerme et al. (2002) in the Semitendinosus. Similarly, Allison and Henry (2002) found about 30–40 ms advance in Rectus Abdominis and OA, but only in 4 participants. Our results are in contrast with those of Strang and Berg (2007) and Vuillerme et al. (2002) but in agreement with Kanekar et al. (2008), Monjo and Forestier (2014) and Schouppe et al. (2019). Indeed, we observed that prime movers and postural muscles underwent a comparable time shift both for excitatory and inhibitory actions, witnessing that the time difference between APAs and prime movers onset did not change more than 10 ms. The high variability of outcomes has been also addressed in a review by Yiou et al. (2012) concerning the APA adaptability to biomechanical, physiological, temporal and psychological constraints. In regard to fatigue, a neurophysiological constraint, these authors concluded that its effect on APAs depends on the fatiguing procedure and the mechanical requirements of the motor task.

4.2 APA pattern associated with different strategies of gait initiation

Another aspect to discuss is the pattern of APAs in back muscles. When we introduced the new perspective on APAs in gait initiation (Farinelli et al., 2021) we observed that healthy participants systematically adopted a “turning” strategy around the trailing body side, which acted as a pivot. Indeed, the ES and abdominal muscles were excited on the trailing side while, on the leading side, ES was inhibited and abdominals excited.

On the contrary, in the current work, ES APAs were usually inhibitory on the leading and trailing sides, thus promoting a “diving” strategy, both in control and fatigue conditions. There are however a few exceptions: one participant showed reciprocal APAs in ES (i.e., the “turning” strategy) in both conditions and, interestingly, 3 participants developed reciprocal activation of the ES specifically after fatigue. The question then arises as to why there is a different pattern of ES activity not only between participants but also even in one and the same individual. This suggests that different strategies may be available to the Central Nervous System (CNS), which then chooses the most suitable one according to the individual’s needs.

This perspective is sustained by a recent observation (Storniolo et al., 2024) that a change in gait initiation strategy occurred in a very trained individual (professional climber) who undergone bilateral amputation of all five toes. When barefoot, a condition of greater

instability due to the amputation, such participant adopted the slower and seemingly safer "turning" strategy, while when wearing prosthetic shoes, which restored the total length of the feet and likely increased the self-confidence, he adopted the "diving" strategy. It should also be noted that participants in Farinelli et al. (2021) were untrained and barefoot people, while in the present paper the participants were well-trained and shod. For what concerns the level of physical activity, here we enrolled trained participants, seeking for homogeneity in the effectiveness of the fatigue procedure. On the other hand, with regard to the barefoot vs. shod condition, we know that donning or doffing shoes may influence the gait initiation strategy (Storniolo et al., 2024). However, shoes were required in the present study to protect lower limb joints from the strong impacts with the ground during the CMJ. It could then be argued that to compare actual data with those of Farinelli et al. (2021) shoes might have been donned only during CMJ. Unfortunately, we have no idea of how long it would take, after doffing shoes, to restore the "barefoot" gait strategy, while we had to speed-up the gait initiation recording before fatigue fading. Thus, we chose to keep the *disturbing* effect of shoes throughout the experimental session, in the aim of evaluating the pure effect of fatigue.

Both of the above differences clearly preclude a direct comparison of present data on gait initiation with those of Farinelli et al. (2021). At the same time, however, the fact that present participants were well-trained and shod likely increased their self-confidence, as it occurred in the amputated climber when shod. It can then be argued that the "diving" strategy may be changed into the "turning" one when self-confidence decreases, a condition that may occur after fatigue. Indeed, it has been observed in rugby players that neuromuscular fatigue induced by the CMJ procedure can manifest itself not only in the reduction of physical production, such as jump height, but mainly as an altered motor strategy (Kennedy and Drake, 2017). This perspective is also in agreement with the conclusion by Yiou et al. (2012) that "depending on the constraints, the priority of the CNS was focused on postural stability maintenance, on body protection and/or on maintenance of focal movement performance". Therefore, the CNS can adapt strategies according to different conditions. As an example, different strategies for body progression are adopted by toddlers after a few months of independent walking (Bisi and Stagni, 2015): some of them use the "stepper" strategy, with a trunk rotation (similar to our "turning" strategy) while others display a "controlled forward fall" (similar to our "diving" approach). This seems also to occur in elderly people who adopt the "turning" strategy as long as they lose their self-confidence (Onuma et al., 2020). Interestingly enough, Rowland et al. (2021) reported delayed APAs in ES muscles of elderly people performing bilateral arm rising, a situation that can be reconducted to the APA delay observed in our fatigued participants.

In conclusion, present results, combined with those of Farinelli et al. (2021) and Storniolo et al. (2024), support the existence of a repertoire of postural strategies among which the CNS chooses, according to the specific constraints in which the action is to be performed; a view in agreement with that proposed by Yiou et al. (2012). This concept can be also reconducted to Bernstein's idea that any voluntary movement may be associated with an arborized pattern of postural commands, each tailored to a specific context. Accordingly, an APA pattern may be shaped to fit the mechanical needs and be maintained subliminal until necessary; by amplifying transmission to certain targets and attenuating transmission to others, the APA chain is brought to action wherever needed (Baldissera et al., 2002; Baldissera and Esposti, 2005).

4.3 Limitations and future directions

We purposely limited the experimental sample to healthy male adults, well fitted and shod. While this selected sample allowed to rule-out possible confounding factors (see Methods), it would be of interest to enrol a more variate sample and stratify the outcomes according with the different anthropometric characteristics, ages, gender and level of physical activity. In this regard, it would also be of interest to compare athletes practicing disciplines that require different postural approaches.

Another limitation regards the analysis of body kinematics, which we restrained to antero-posterior CoP displacement as such variable has been recently introduced to set the APA time window for the analysis of postural muscles (Farinelli et al., 2021). Future studies could investigate the CoP/CoM displacements in both antero-posterior and medio-lateral directions, with or without fatigue. Such topic has been already addressed (Honeine et al., 2016), but using the classical approach of searching for APAs in the time window from the first CoP displacement to the onset of heel-off, and without applying fatigue.

Data availability statement

The raw data supporting the conclusions of this article will be made available by the authors, without undue reservation.

Ethics statement

The studies involving humans were approved by Comitato Etico di Ateneo dell'Università degli Studi di Milano. The studies were conducted in accordance with the local legislation and institutional requirements. The participants provided their written informed consent to participate in this study.

Author contributions

JS: Conceptualization, Formal Analysis, Investigation, Resources, Writing–original draft, Writing–review and editing. VF: Formal Analysis, Investigation, Resources, Software, Writing–original draft, Writing–review and editing. RE: Formal Analysis, Investigation, Supervision, Writing–original draft, Writing–review and editing. PC: Conceptualization, Funding acquisition, Supervision, Writing–original draft, Writing–review and editing.

Funding

The author(s) declare that financial support was received for the research, authorship, and/or publication of this article. This study

has been supported by internal funds from Università degli Studi di Milano and by funds from Fondazione Pierfranco e Luisa Mariani.

Acknowledgments

The authors would like to express their gratitude for the availability and effort of all participants who adhered to this research. The Department of Pathophysiology and Transplantation, University of Milan, is funded by the Italian Ministry of Education and Research (MUR): Dipartimenti di Eccellenza Program 2023 to 2027.

Conflict of interest

The authors declare that the research was conducted in the absence of any commercial or financial relationships that could be construed as a potential conflict of interest.

The author(s) declared that they were an editorial board member of Frontiers, at the time of submission. This had no impact on the peer review process and the final decision.

Generative AI statement

The author(s) declare that no Generative AI was used in the creation of this manuscript.

Publisher's note

References

Allison, G. T., and Henry, S. M. (2002). The influence of fatigue on trunk muscle responses to sudden arm movements, a pilot study. *Clin. Biomech. (Bristol, Avon)* 17 (5), 414–417. doi:10.1016/s0268-0033(02)00029-3

Assaiante, C., Woollacott, M., and Amblard, B. (2000). Development of postural adjustment during gait initiation: kinematic and EMG analysis. *J. Mot. Behav.* 32 (3), 211–226. doi:10.1080/00222890009601373

Baldissera, F., Borroni, P., Cavallari, P., and Cerri, G. (2002). Excitability changes in human corticospinal projections to forearm muscles during voluntary movement of ipsilateral foot. *J. Physiol.* 539 (Pt 3), 903–911. doi:10.1113/jphysiol.2001.013282

Baldissera, F., and Esposti, R. (2005). Postural constraints to coupling of ipsilateral hand-foot movements. *Neuroreport* 16 (15), 1615–1619. doi:10.1097/01.wnr.0000181586.49130.48

Behrens, M., Gube, M., Chaabene, H., Prieske, O., Zenon, A., Broscheid, K. C., et al. (2023). Fatigue and human performance: an updated framework. *Sports Med.* 53 (1), 7–31. doi:10.1007/s40279-022-01748-2

Bigland-Ritchie, B., and Woods, J. J. (1984). Changes in muscle contractile properties and neural control during human muscular fatigue. *Muscle Nerve* 7 (9), 691–699. doi:10.1002/mus.880070902

Bisi, M. C., and Stagni, R. (2015). Evaluation of toddler different strategies during the first six-months of independent walking: a longitudinal study. *Gait Posture* 41 (2), 574–579. doi:10.1016/j.gaitpost.2014.11.017

Bolzoni, F., Bruttini, C., Esposti, R., Castellani, C., and Cavallari, P. (2015). Transcranial direct current stimulation of SMA modulates anticipatory postural adjustments without affecting the primary movement. *Behav. Brain Res.* 291, 407–413. doi:10.1016/j.bbr.2015.05.044

Bosco, C., Komi, P. V., Tihanyi, J., Fekete, G., and Apor, P. (1983). Mechanical power test and fiber composition of human leg extensor muscles. *Eur. J. Appl. Physiol. Occup. Physiol.* 51 (1), 129–135. doi:10.1007/BF00952545

Bouisset, S., and Do, M. C. (2008). Posture, dynamic stability, and voluntary movement. *Neurophysiol. Clin.* 38 (6), 345–362. doi:10.1016/j.neucli.2008.10.001

Coco, M., Buscemi, A., Guerrera, C. S., Di Corrado, D., Cavallari, P., Zappalà, A., et al. (2020). Effects of a bout of intense exercise on some executive functions. *Int. J. Environ. Res. Public Health* 17 (3), 898. doi:10.3390/ijerph17030898

Coco, M., Perciavalle, V., Cavallari, P., and Perciavalle, V. (2016). Effects of an exhaustive exercise on motor skill learning and on the excitability of primary motor cortex and supplementary motor area. *Med. Baltim.* 95 (11), e2978. doi:10.1097/MD.0000000000002978

Crenna, P., and Frigo, C. (1991). A motor programme for the initiation of forward-oriented movements in humans. *J. Physiol.* 437, 635–653. doi:10.1113/jphysiol.1991.sp018616

Davies, N. W., Standen, N. B., and Stanfield, P. R. (1991). ATP-dependent potassium channels of muscle cells: their properties, regulation, and possible functions. *J. Bioenerg. Biomembr.* 23, 509–535. doi:10.1007/BF00785809

Farinelli, V., Bolzoni, F., Marchese, S. M., Esposti, R., and Cavallari, P. (2021). A novel viewpoint on the anticipatory postural adjustments during gait initiation. *Front. Hum. Neurosci.* 15, 709780. doi:10.3389/fnhum.2021.709780

Gandevia, S. C. (2001). Spinal and supraspinal factors in human muscle fatigue. *Physiol. Rev.* 81 (4), 1725–1789. doi:10.1152/physrev.2001.81.4.1725

Helbostad, J. L., Leirfall, S., Moe-Nilssen, R., and Sletvold, O. (2007). Physical fatigue affects gait characteristics in older persons. *J. Gerontol. A Biol. Sci. Med. Sci.* 62, 1010–1015. doi:10.1093/gerona/62.9.1010

Hermens, H. J., Freriks, B., Disselhorst-Klug, C., and Rau, G. (2000). Development of recommendations for SEMG sensors and sensor placement procedures. *J. Electromyogr. Kinesiol.* 10 (5), 361–374. doi:10.1016/s1050-6411(00)00027-4

Honeine, J. L., Schieppati, M., Crisafulli, O., and Do, M. C. (2016). The neuro-mechanical processes that underlie goal-directed medio-lateral APA during gait initiation. *Front. Hum. Neurosci.* 10, 445. doi:10.3389/fnhum.2016.00445

Kanekar, N., Santos, M. J., and Aruin, A. S. (2008). Anticipatory postural control following fatigue of postural and focal muscles. *Clin. Neurophysiol.* 119 (10), 2304–2313. doi:10.1016/j.clinph.2008.06.015

Kennedy, R. A., and Drake, D. (2017). The effect of acute fatigue on countermovement jump performance in rugby union players during preseason. *J. Sports Med. Phys. Fit.* 57 (10), 1261–1266. doi:10.23736/S0022-4707.17.06848-7

Lund, J. P., Donga, R., Widmer, C. G., and Stohler, C. S. (1991). The pain-adaptation model: a discussion of the relationship between chronic musculoskeletal pain and motor activity. *Can. J. Physiol. Pharmacol.* 69 (5), 683–694. doi:10.1139/y91-102

Monjo, F., and Forestier, N. (2014). Unexperienced mechanical effects of muscular fatigue can be predicted by the Central Nervous System as revealed by anticipatory postural adjustments. *Exp. Brain Res.* 232 (9), 2931–2943. doi:10.1007/s00221-014-3975-0

Onuma, R., Hoshi, F., Matsuda, T., and Jinno, T. (2020). Trunk movement characteristics of the elderly at gait initiation. *Rigakuryoho Kagaku* 35, 329–333. doi:10.1589/rika.35.329

Parijat, P., and Lockhart, T. E. (2008). Effects of lower extremity muscle fatigue on the outcomes of slip-induced falls. *Ergonomics* 51, 1873–1884. doi:10.1080/00140130802567087

Rowland, R. S., Jenkinson, N., and Chiou, S. Y. (2021). Age-related differences in corticospinal excitability and anticipatory postural adjustments of the trunk. *Front. Aging Neurosci.* 13, 718784. doi:10.3389/fnagi.2021.718784

Schouppe, S., Danneels, L., Van Damme, S., Van Oosterwijck, S., Palmans, T., and Van Oosterwijck, J. (2019). Physical and cognitive exertion do not influence feedforward activation of the trunk muscles: a randomized crossover trial. *Exp. Brain Res.* 237 (11), 3011–3021. doi:10.1007/s00221-019-05585-0

Storniolo, J. L., Farinelli, V., Onesti, M., Correale, L., Peyré-Tartaruga, L. A., Esposti, R., et al. (2024). Case report: new perspectives on gait initiation strategies from a case of

full toes amputation in a professional mountain climber. *Front. Hum. Neurosci.* 18, 1463249. doi:10.3389/fnhum.2024.1463249

Strang, A. J., and Berg, W. P. (2007). Fatigue-induced adaptive changes of anticipatory postural adjustments. *Exp. Brain Res.* 178 (1), 49–61. doi:10.1007/s00221-006-0710-5

Vuillerme, N., Nougier, V., and Teasdale, N. (2002). Effects of lower limbs muscular fatigue on anticipatory postural adjustments during arm motions in humans. *J Sport Med. Phys. Fit.* 42 (3), 289–294.

Yiou, E., Caderby, T., Delafontaine, A., Fourcade, P., and Honeine, J. L. (2017). Balance control during gait initiation: state-of-the-art and research perspectives. *World J. Orthop.* 8 (11), 815–828. doi:10.5312/wjo.v8.i11.815

Yiou, E., Caderby, T., and Hussein, T. (2012). Adaptability of anticipatory postural adjustments associated with voluntary movement. *World J. Orthop.* 3 (6), 75–86. doi:10.5312/wjo.v3.i6.75

Yiou, E., Ditcharles, S., and Le Bozec, S. (2011). Biomechanical reorganisation of stepping initiation during acute dorsiflexor fatigue. *J. Electromyogr. Kinesiol.* 21 (5), 727–733. doi:10.1016/j.jelekin.2011.04.008

Yiou, E., Mezaour, M., and Le Bozec, S. (2009). Anticipatory postural adjustments and focal performance during bilateral forward-reach task under different stance conditions. *Mot. Control* 13 (2), 142–160. doi:10.1123/mcj.13.2.142

frontiers | Frontiers in Physiology

TYPE Original Research
PUBLISHED 24 February 2025
DOI 10.3389/fphys.2025.1554742

OPEN ACCESS

EDITED BY
Roberto Piacentini,
Catholic University of the Sacred Heart, Italy

REVIEWED BY
Giuseppe Coratella,
University of Milan, Italy
Okobi Eko Ekpo,
Khalifa University, United Arab Emirates

*CORRESPONDENCE
Franca Deriu,
deriuf@uniss.it

RECEIVED 02 January 2025
ACCEPTED 06 February 2025
PUBLISHED 24 February 2025

CITATION
Morrone M, Martinez G, Achene A, Scaglione M, Masala S, Manca A and Deriu F (2025) Size and site matter: the influence of corpus callosum subregional lesions on the magnitude of cross-education of strength. *Front. Physiol.* 16:1554742. doi: 10.3389/fphys.2025.1554742

Size and site matter: the influence of corpus callosum subregional lesions on the magnitude of cross-education of strength

Marco Morrone[1], Gianluca Martinez[1], Antonio Achene[2], Mariano Scaglione[2], Salvatore Masala[2], Andrea Manca[1] and Franca Deriu [1,3]*

[1]Department of Biomedical Sciences, University of Sassari, Sassari, Italy, [2]Department of Medicine, Surgery and Pharmacy, University of Sassari, Sassari, Italy, [3]Unit of Endocrinology, Nutritional and Metabolic Disorders, AOU Sassari, Sassari, Italy

Introduction: Cross-education is an established yet not fully understood phenomenon involving interhemispheric processes within the corpus callosum (CC) that result in strength gains in the untraining limb following training of the contralateral homologous muscles. There is a substantial lack of cross-education studies employing lesional models. This study employed the model of multiple sclerosis, a condition typically featuring demyelinating callosal lesions, to pinpoint CC subregions that mediate cross-education, potentially fostering the mechanistic understanding of the interlimb transfer.

Methods: Nine individuals with relapsing-remitting multiple sclerosis (median Expanded Disability Status Scale: 3.5) and focal CC lesions underwent a 6-week, high-intensity isokinetic training program (≥80% maximal effort at 10°/s) targeting their stronger ankle dorsiflexors. Sagittal FLAIR MRI scans were segmented into five CC subregions (CC1–CC5), with lesion volumes quantified for each subregion. Strength (peak concentric torque at 10°/s) was measured bilaterally before (PRE) and after (POST) training to determine cross-education, defined as the percentage increase in torque of the untrained, weaker limb. Correlations between lesion volumes in CC subregions and cross-education were analyzed.

Results: Both the trained (+21.5 ± 15.8%, p = 0.002) and untrained (+35.2 ± 24.9%, p = 0.003) limbs demonstrated post-training strength gains, reducing but not eliminating inter-limb asymmetry. Lesions specifically in the rostral body (CC2) correlated with reduced cross-education magnitude

Abbreviations: CC, corpus callosum; M1, primary motor cortex; MRI, Magnetic resonance imaging; PM, premotor area; SMA, supplementary motor area; TMS, Transcranial magnetic stimulation.

(rs = −0.670, p = 0.048) and smaller improvements in strength asymmetry (rs = 0.809, p = 0.008). No associations were detected in other CC subregions.

Conclusion: These findings highlight the pivotal role of specific CC subregions, particularly the rostral body, in mediating cross-education of strength. These findings advance our understanding of CC role in the interhemispheric dynamics underpinning cross-education. Routine MRI can identify patients without CC2 lesions who may benefit from cross-education, providing a practical approach to improving muscle strength when weaker muscles cannot be directly trained.

Clinical Trial Registration: ClinicaTrials.Gov, identifier NCT02010398

KEYWORDS

interlimb transfer, contralateral strength training, multiple sclerosis, MRI, rehabilitation, callosal damage

Introduction

Cross-education is a long-known phenomenon first introduced in 1894 (Scripture et al., 1894). It refers to increased motor output (i.e., force generation, skill) of the opposite, untrained limb following a period of unilateral exercise training (Manca et al., 2021). This interlimb transfer of strength has been consistently observed in healthy individuals (Lee and Carroll, 2007; Coratella et al., 2022; Altheyab et al., 2024), orthopedic (Farthing et al., 2009) and neurological populations displaying predominantly unilateral motor impairment and muscle weakness, such as stroke survivors (Dragert and Zehr, 2013; Urbin et al., 2015) and persons with multiple sclerosis (Manca et al., 2017a; Manca et al., 2020) with reported strength gains in the untrained homologous muscles from aggregated data ranging from 9% to 18% in healthy subjects (Manca et al., 2017b) and up to 29% in mixed patient populations (Green and Gabriel, 2018a). The underlying neurophysiological mechanisms are thought to involve cortical and subcortical adaptations, including increased excitability and plasticity within motor networks of the untrained hemisphere. Interhemispheric interactions facilitated by transcallosal pathways are considered crucial for these adaptations (Green and Gabriel, 2018b; Lee and Carroll, 2007; Manca et al., 2018; Ruddy et al., 2017b).

The corpus callosum (CC) is the largest fiber bundle in the human brain, comprising approximately 300-million fibers that connect cortical regions across the two hemispheres (Hofer and Frahm, 2006). It plays a fundamental role in integrating sensory, motor, and cognitive information, enabling coordinated bilateral activities (Jokinen et al., 2007; Ruddy et al., 2017a; Wahl and Ziemann, 2008). Topographically, the CC is organized into subregions responsible for connecting specific cortical areas, each associated with distinct functional networks. While different segmentation schemes exist (Hofer and Frahm, 2006; Jokinen et al., 2007; Witelson, 1989), anatomically the anterior midbody (i.e., the section immediately behind the rostrum and the genu) connects premotor and supplementary motor areas (PMs, SMAs), whereas the posterior midbody (i.e., the midbody part ahead of the isthmus) links primary motor cortices (M1s) (Hofer and Frahm, 2006). These subregions facilitate the interhemispheric communication essential for motor ideation/planning, and execution (Fling et al., 2011). Despite compelling evidence indicating that transcallosal motor pathways play a key role in cross-education of skills following acute, single-session trainings (Ruddy et al., 2017b), to the best of our knowledge no studies have directly investigated the contribution of specific CC subregions to the magnitude of interlimb transfer of strength following chronic training. Understanding this structure-function relationship could be important for elucidating the precise neural mechanisms underlying cross-education and designing targeted rehabilitation protocols that harness interhemispheric signaling.

In this context, multiple sclerosis offers a unique opportunity to study how CC lesions influence cross-education of strength due to the impact of the disease on white matter integrity. Callosal pathology in multiple sclerosis is common and can disrupt interhemispheric communication, affecting motor coordination and cognitive functions (Degraeve et al., 2023; Hoppner et al., 1999; Kern et al., 2011; Peterson et al., 2017).

Clinically, individuals with multiple sclerosis frequently present unilateral weakness, spasticity, and impaired motor control (Larson et al., 2013), especially in the ankle dorsiflexion muscles (Lantis et al., 2024). Cross-education could serve as a valuable approach for these patients, allowing strength gains in the weaker muscles through training of the contralateral homologous stronger ones (Manca et al., 2017a). Since lesions vary in size and location within the CC, this population provides a "natural experiment" for exploring how specific patterns of callosal damage may facilitate or limit cross-education outcomes. In healthy cohorts, the integrity of interhemispheric pathways is generally preserved, thereby masking the specific contribution of distinct CC subregions to cross-education. By contrast, individuals with multiple sclerosis often exhibit isolated lesions in different segments of the CC, providing researchers with an opportunity to parse and differentiate how focal damage in regions linking homologous areas modulates the neurophysiological adaptation to unilateral training. New knowledge on this topic could have direct clinical relevance, as a better understanding of how CC integrity influences contralateral strength gains would help tailor rehabilitation programs to individual patients based on their neuroradiological profiles.

Based on the recognized role of transcallosal pathways in interlimb transfer and the signature callosal damages due to multiple sclerosis that could impair it, the present study aimed at identifying key callosal subregions involved in cross-education. We examined

the effects of a 6-week, high-intensity unilateral training of the less-affected ankle dorsiflexors, starting from the hypothesis that the extent and site of lesions in key CC subregions would associate with the magnitude of strength gains in the contralateral, more-affected untrained limb.

Methods

Participants

Persons with multiple sclerosis were enrolled in the study from those referring to the Neurological Unit of the University Hospital of Sassari. Inclusion criteria were as follows: (1) definite diagnosis of MS; (2) clinical, radiological, and pharmacological stability for at least 6 months; (3) unilateral muscle weakness of the ankle dorsiflexors of at least 1 point on the Medical Research Council scale; (4) absence of white matter demyelinating lesions in the spinal cord, and underneath premotor, cingulate, and motor areas. Following the medical assessment, performed by a neurologist with a 15-year experience in MS evaluation and management, nine patients (7 females, 2 males) met all inclusion criteria and were included in the study.

MRI segmentation and analysis of the corpus callosum subregions and their lesions

All MRI scans were acquired using a standardized protocol on a 1.5 T Philips Achieva® scanner (Best, Netherlands). Sagittal FLAIR sequences were utilized with the following parameters: repetition time (TR) = 4,800 ms, echo time (TE) = 297 ms, slice thickness = 1.5 mm with continuous axial slices, a matrix size of 200 × 200, and a field of view (FOV) of 240 × 240 mm^2. Three neuroradiologists with over 20 years of experience in MRI analysis in persons with multiple sclerosis performed the MRI analysis and segmentation. Experts were blinded to clinical information. In cases where their initial segmentations or lesion detections differed, they reached a consensus through discussion.

Segmentation of the CC followed the approach described by Jokinen et al. (2007), dividing the corpus callosum into five subregions: the genu (CC1), rostral body (CC2), midbody (CC3), isthmus (CC4), and splenium (CC5). Lesions within the CC were defined as hyperintensities present across at least three consecutive slices. Manual segmentation of the CC was performed slice by slice on the sagittal planes, followed by verification in the axial and coronal views to correct any potential contouring inaccuracies or artifacts. After completing the manual segmentation, the open-source 3D Slicer software was employed to generate 3D reconstructions and conduct volumetric analysis.

The total volume of the CC was calculated and expressed in cubic centimeters (cc). Lesion volume within the CC was also measured in cc, and the lesion load was calculated as the percentage of the total CC volume occupied by lesions for each subregion. This approach provided a detailed analysis of both the structural integrity and the lesion burden within the CC in the study participants.

Strength assessments

The maximal isokinetic peak torque of the ankle dorsiflexors on both the trained (less affected) and untrained (more affected) side was measured before (PRE) and after the intervention (POST) using isokinetic dynamometry (Biodex System-3, Biodex, Shirley, NY, United States). Participants were seated on the system's chair with the trunk inclined at 85°, knee flexed at 30°, and ankle in full plantar flexion, stabilized with custom belts and straps. Participants underwent a light warm-up and familiarization with the system by completing two sets of 2–4 submaximal repetitions with a three-min rest in between at 10°/s isokinetic angular velocity. A short warm-up was chosen to avoid early onset of muscle fatigue, which can be pronounced in individuals with multiple sclerosis (Lambert et al., 2001) yet giving them enough practice to get acquainted with the isokinetic movement over the predefined range of motion. Following the warm-up, participants were instructed to dorsiflex as hard and fast as possible against the ankle attachment. Participants were asked to perform three maximal concentric contractions from full plantarflexion to their maximal dorsiflexion at an angular velocity of 10°/s for both sides. Peak torque of the dorsiflexors was recorded. The choice of testing and training concentrically was justified by the fact that patients had difficulties in actively dorsiflexing their ankle, particularly at the transition from push-off to swing where a concentric, open-kinetic chain contraction of the dorsiflexors is needed to ensure the clearance of the foot. A very low angular velocity (10°/s) was chosen to provide participants adequate time to achieve maximal torque, and to align with clinical isokinetic testing in persons with multiple sclerosis (Dvir, 2025). This facilitates higher torque outputs compared to faster velocities and takes into account the reduced neural drive and neuromuscular recruitment, which are signature features of multiple sclerosis (Kent-Braun et al., 1998). Dynamic isokinetic rather than isometric testing was chosen as it is more closely related to ankle function during gait, and to study participants' capability to generate torque over the entire range of motion (Dvir, 2025).

Strength asymmetry was calculated both PRE and POST intervention as the difference between the trained and untrained sides using the following formula:

$$\text{Torque asymmetry} = \frac{\text{peak torque (trained)-peak torque (untrained)}}{\text{peak torque (untrained)}} \times 100$$

Additionally, the gain in strength on the trained side and the cross-education effect on the untrained side were quantified in both Newton-meters (Nm) and percentage (%). During testing, visual feedback and strong verbal encouragement were provided to ensure maximal effort.

Intervention

The intervention was administered using the same isokinetic device employed for the strength assessments. As per recent recommendations on transparent reporting of exercise variables in resistance training protocols (Coratella, 2022), the protocol consisted of high-intensity isokinetic concentric training of the ankle dorsiflexors of the stronger side. Participants completed three

sets of four maximal efforts at 10°/s, with a three-min passive rest between sets. The ROM used was individualized for each participant according to baseline testing measurements. We chose to exercise the ankle dorsiflexors over a full ROM Before starting, participants underwent the same warm-up procedures described for the muscle strength measurements. The training was performed 3 days per week on alternate days over a 6-week period, with each session lasting approximately 30 min. All training sessions were supervised by a physiotherapist with a 10-year expertise in the rehabilitative management of persons with multiple sclerosis. As with the strength testing procedures, visual feedback and strong verbal encouragement were provided to maximize effort throughout the intervention.

Statistical analysis

Volumetric data from the CC segmentations were obtained using 3D Slicer version 5.6.2. All statistical analyses were performed using SPSS version 29 (IBM Corp., Armonk, NY, United States). Descriptive statistics were used to report demographic and clinical characteristics of the participants, with continuous variables expressed as mean ± standard deviation (SD) or median and interquartile range (IQR) depending on the distribution of the data.

Normality and sphericity of the data were assessed using the Shapiro-Wilk and Mauchly's tests, respectively. To evaluate the presence of strength asymmetry and cross-education effects, a repeated-measures analysis of variance (RM-ANOVA) was to test for changes in isokinetic peak torque of both the trained and untrained following the intervention. Main effects of TIME (PRE vs. POST), SIDE (trained vs. untrained) as well as TIME*SIDE interaction were tested. In case of significant differences, pairwise comparisons were carried out to locate the source of the difference. Effect sizes (Cohen's d and partial eta-squared, η_p^2) were calculated alongside p-values to determine the magnitude of the observed differences. Effect sizes were interpreted taking (1) a Cohen's d of 0.2 as small, 0.5 medium and 0.8 large; (2) a η_p^2 of 0.01 as small, 0.06 medium and 0.14 large (Cohen, 1988; Richardson, 2011). A p-value <0.05 was considered statistically significant for all analyses.

Correlation analyses were conducted using Spearman's rank-order correlation to assess the relationship between lesion volume in the CC subregions and both the magnitude of cross-education and changes in strength asymmetry (Δstrength asymmetry). Correlation coefficients (r_s) and p-values were reported to indicate the strength and significance of these associations.

Results

Participants' characteristics

Nine persons with multiple sclerosis (7F, 2 M), aged 38 ± 13 years, withrelapsing-remitting course of disease satisfied the inclusion criteria and were included in the study. Demographic and clinical characteristics are detailed in Table 1 both at the individual and group level. Median EDSS was 3.5 (IQR: 2) indicating mild to moderate disability, with a mean disease duration of 11 ± 6 years. Four patients were on IFN-B1a, 4 on fingolimod and 1 on glatiramer acetate.

Corpus callosum lesions and segmentations volumetrics

Volumetrics analysis showed a mean total CC volume of 0.523 ± 0.791 cc. Lesion volumes in the five CC subregions are detailed in Table 2, while Figure 1 displays the distribution of lesions load and volumes across CC subregions.

Cross-education

RM-ANOVA on peak isokinetic torque showed a main effect of TIME ($p = 0.001$, $\eta_p^2 = 0.744$, $d = 0.987$) and SIDE ($p = 0.005$, $\eta_p^2 = 0.656$, $d = 0.926$), but no TIME*SIDE interaction ($p = 0.076$, $\eta_p^2 = 0.659$, $d = 0.111$). Pairwise comparisons showed a substantial asymmetry in isokinetic peak torque at baseline (29.3% ± 77.8%, $p = 0.005$, $\eta_p^2 = 0.649$, $d = 0.919$), with the trained ankle dorsiflexors generating 26.9 ± 9.2 Nm, and the untrained ones 20.8 ± 10.3 Nm. Post-training, strength asymmetry was still detected ($p = 0.01$, $\eta_p^2 = 0.587$, $d = 0.838$) yet reduced to 19.3% ± 59.9%. Subjects N5 and N9 were the only ones with a higher asymmetry POST (12.6% vs. 1.3%, and 9.2% vs. 1.6%, respectively).

Following the 6-week training there was an increase in strength of the trained side (+21.5 ± 15.8%, $p = 0.002$, $\eta_p^2 = 0.718$, $d = 0.976$) except for subjects N7 and N8, and in the untrained side (cross-education) (35.2% ± 24.9%, $p = 0.003$, $\eta_p^2 = 0.689$, $d = 0.956$), with no relevant differences by side. Individual and group-level data for the strength tests are reported in Table 3.

Correlation analysis

Spearman's rank-order correlation analysis revealed an association between lesion volume in CC2 and both cross-education magnitude ($r_s = -0.670$; $p = 0.048$), and Δstrength asymmetry ($r_s = 0.809$; $p = 0.008$). Conversely, no associations were observed between either variable and lesion volumes in the other CC subregions or with total lesion volume. Figure 2 illustrates the spaghetti plot depicting the individual cross-education magnitude and its correlation with lesion volume in CC2.

Discussion

The present study was planned and executed to elucidate the relationship between callosal lesions due to MS and the magnitude of contralateral strength gains in the untrained limb (*i.e.*, cross-education). In doing so, we attempted to identify CC subregion/s mostly involved in the interhemispheric connectivity, a condition long known to lead to diffuse callosal damage and atrophy (Degraeve et al., 2023; Hoppner et al., 1999). CC, the major commissure interconnecting the two hemispheres, was chosen in view of its functional role that makes it the key anatomical node for

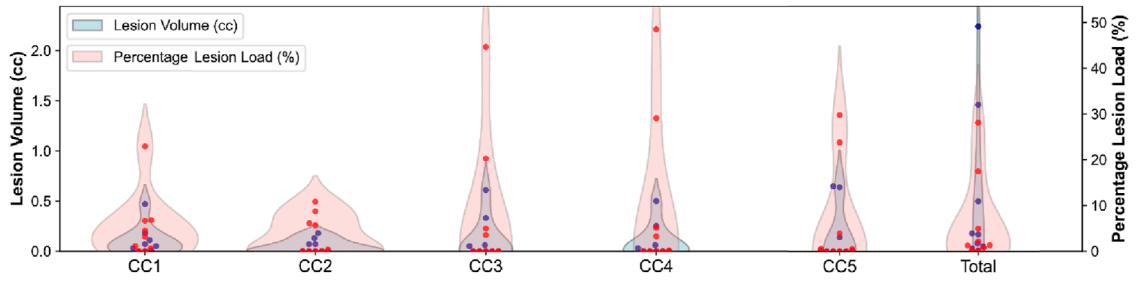

FIGURE 1
Distribution of lesion load and volume across subregions. Red dots indicate individual subjects' lesion load, while blue dots represent individual subjects' lesion volume.

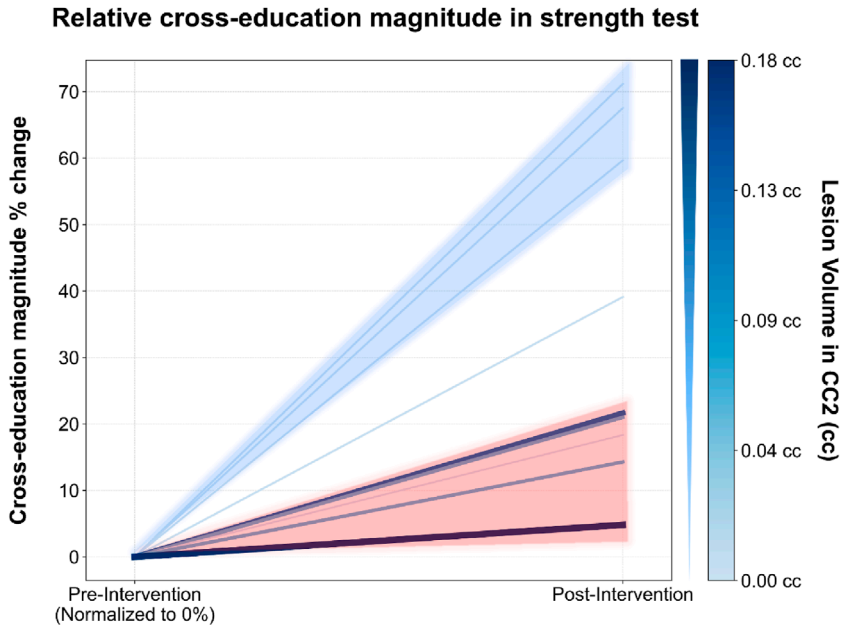

FIGURE 2
Relative cross-education magnitude (%) change in strength test before and after training. Each line represents an individual subject. The color and thickness of the lines indicate lesion volume in CC2 (rostral body) of the corpus callosum: thicker and darker lines correspond to larger lesion volumes. Cross-education magnitude is shown on the y-axis, with pre- and post-intervention time points on the x-axis.

the interhemispheric bidirectional interactions thought to mediate cross-education (Ruddy et al., 2017b).

The first finding of this interventional study was confirmation of cross-education occurrence in persons with multiple sclerosis (Manca et al., 2017a). The novelty resides in the fact that, despite evidence of diffuse callosal damage, the average magnitude of effect here observed overlapped with those observed in neurologically intact individuals (+15–30% strength in the contralateral homologous, untrained muscles) (Manca et al., 2017b). Following the 6-week strength training, the magnitude of cross-education in the untrained muscles was found to scale only with the lesional volume of CC2 subregion, which represents the portion of CC immediately posterior to rostrum and genu and anterior to midbody on the midsagittal plane (Jokinen et al., 2007). Importantly, if normalized by total CC volume, unlike the other subregions, even very low lesions in CC2 were associated with substantial reductions in the extent of cross-education, suggesting a major role of cortical areas interconnected at this level to ensure the interhemispheric inhibitory and facilitatory dynamics underpinning cross-education. Previous findings from seminal studies using diffusion tensor imaging (DTI) tractography (Huang et al., 2005) and functional magnetic resonance imaging (fMRI) activation in white matter (Fabri et al., 2011) support that CC subregions are associated with distinct functions of the human brain. According to this functional partition, anterior activation foci are associated with taste stimuli, central-anterior foci with motor tasks, central-posterior foci with tactile stimuli, and splenium foci with visual stimuli (Fabri et al., 2011). While the transcallosal connections of the cortical motor network have yet to be fully revealed, due to its complex architecture and the number and density of crossing fibers (Jeurissen et al., 2013), evidence from studies using resting-state functional connectivity of white-matter indicate that the

TABLE 1 Demographic and clinical characteristics of the participants.

	Subj. N1	Subj. N2	Subj. N3	Subj. N4	Subj. N5	Subj. N6	Subj. N7	Subj. N8	Subj. N9	Subjs 1–9[a]
Age (yrs)	48	43	32	27	33	52	24	59	20	38 ± 13
Sex	F	F	F	M	F	F	F	F	M	7F; 2M
Disease course	RR	RR	RR	RR	RR	RR	RR	RR	RR	9RR
Disease duration (yrs)	10	10	11	12	8	13	6	23	3	11 ± 6
EDSS	3.0	4.0	4.5	2.0	5.5	5.0	2.0	3.5	2.5	3.5 (2)[b]
DMT	IFN-β1a	IFN-β1a	Fingolimod	fingolimod	fingolimod	GA	fingolimod	IFN-β1a	IFN-β1a	

Abbreviations: yrs, years; RR, relapsing-remitting; EDSS, expanded disability status scale; DMT, disease modifying therapy; F, female; M, male; IFN, interferon; GA, glatiramer acetate.
[a]All data reported as mean ± standard deviation.
[b]EDSS reported as median (interquartile range).

TABLE 2 Corpus callosum lesion volumes by subregion and total.

Site of lesions	Subj. N1	Subj. N2	Subj. N3	Subj. N4	Subj. N5	Subj. N6	Subj. N7	Subj. N8	Subj. N9	Subjs 1–9[a]
CC1 (*cc*)	0.068	0	0.046	0.471	0.109	0.011	0.026	0.184	0	0.102 ± 0.151
CC2 (*cc*)	0	0	0	0.005	0.134	0.066	0	0.065	0.179	0.050 ± 0.067
CC3 (*cc*)	0	0	0	0.612	0.328	0.061	0	0.046	0	0.116 ± 0.214
CC4 (*cc*)	0	0	0	0.499	0.249	0.027	0	0.060	0.003	0.093 ± 0.172
CC5 (*cc*)	0.013	0.014	0	0.654	0.639	0	0	0.140	0	0.162 ± 0.278
Total (*cc*)	0.081	0.014	0.046	2.241	1.459	0.165	0.026	0.495	0.182	0.523 ± 0.791

Abbreviations: cc, cubic centimeters; CC1, rostrum and genu, CC2, rostral body, CC3, midbody; CC4, isthmus; CC5 splenium.
[a]All data reported as mean ± standard deviation.

10.3389/fphys.2025.1554742

10.3389/fphys.2025.1554742

TABLE 3 Isokinetic strength test results.

		Subj. N1	Subj. N2	Subj. N3	Subj. N4	Subj. N5	Subj. N6	Subj. N7	Subj. N8	Subj. N9	Subjs 1–9[a]
PRE training	PT at 10°/s untrained side (Nm)	17	19.1	6.2	27.1	15.7	20	22.9	15.4	43.6	20.8 ± 10.3
	PT at 10°/s trained side (Nm)	22.4	26.0	20.5	39.5	15.9	26.0	26.2	21.0	44.3	26.9 ± 9.2
	Strength asymmetry (%)	31.8	36.1	230.6	45.8	1.3	30	14.4	36.4	1.6	29.3 ± 77.8
POST training	PT at 10°/s untrained side (Nm)	29.1	32	9.9	37.7	19.1	24.2	27.1	17.6	45.7	26.9 ± 10.9
	PT at 10°/s trained side (Nm)	31.7	37.2	26.1	42.1	21.5	30.9	27.1	22.1	49.9	32.1 ± 9.5
	Strength asymmetry (%)	8.9	16.2	107.1	11.7	12.6	27.7	0	22.6	9.2	19.3 ± 59.9
	Strength gain in trained side (%)	41.5	43.1	27.3	6.6	35.2	18.8	3.4	5.2	12.6	21.5 ± 15.8
	Cross-education effect in the untrained side (%)	71.1	67.5	59.7	39.1	21.7	21	18.3	14.3	4.8	35.3 ± 24.9

Abbreviations: PT, peak torque; Nm, Newton-metres.
[a]All data reported as mean ± st. dev.

anterior midbody is the most important interhemispheric hub for the cortical grey-matter sensorimotor system (Wang et al., 2020). Interhemispheric connections at this level bridge the two hemispheres (mainly PM and SMA) to be executed by the M1 to allow sharing of resources and information for the successful ideation and planning of voluntary movements.

Our finding on the influence of lesions specifically located in CC2 on the extent of interlimb transfer are founded on topographic studies that employed DTI-based tractography to evidence the massive crossing of fibers from PM and SMA to their contralateral homologous areas occurring in this specific subregion (Hofer and Frahm, 2006). More specifically, within the human CC, SMA-SMA crossing fibers are more in number and strength than those connecting M1 and dorsal premotor (PMd) cortices and pre-SMA (Fling et al., 2011).

Ruddy et al. (2017b) used a combination of neuroimaging methods (fMRI and diffusion weighted imaging-based tractography) to investigate the pathways in the human brain that mediate cross-education. They found elevated functional connectivity of the white matter pathways connecting bilateral SMAs in the resting motor network following a single session of ballistic unilateral, dominant-hand wrist flexion training that resulted in increased performance by >35% in the untrained wrist of healthy participants. However, the individual transfer did not correlate with the observed increases in activation. Conversely, in our cohort of persons with multiple sclerosis with callosal damage, we found robust association between the lesion load harming the integrity of interhemispheric fibers of the premotor system and the amount of individual transfer. The different duration, nature and site of the behavioral training administered in the two studies (6-week, ankle dorsiflexors' high intensity resistance training in our case, single session wrist flexors' ballistic training in Ruddy et al.'s study) may be accounted for the discrepant neuroradiological-functional relationships observed. In a secondary analysis by the same group (Ruddy et al., 2017b), data on corticospinal excitability (MEP recruitment curves by single-pulse transcranial magnetic stimulation, TMS) were also appraised, revealing no neurophysiological correlates of the improved performance in the untrained limb. This was in line with a previous TMS study, which also assessed M1 intracortical facilitation, M1-M1 interhemispheric inhibition and sensory-motor integration and revealed no evidence of neural adaptations following 4 weeks of unilateral training of the intrinsic muscles of the hand (Manca et al., 2016). Overall, these reports seem to confirm that the acute adaptations that underpin the contralateral performance gains following unilateral training would be mediated by neural elements other than those occurring between M1 cortices or within M1, though the latter has been the typical target of TMS-based investigations attempting to elucidate the neurophysiological mechanisms of cross-education, with mixed results due to the paucity of studies that shared common hypotheses, outcomes and procedures (Hortobagyi et al., 2011; Manca et al., 2018).

Our findings align with an increasing corpus of studies that locate in the premotor rather than primary motor areas the anatomo-functional site of motor control of unilateral and bilateral movements and interhemispheric transfer, as well. However, while most investigations have dealt with acute exercise generally targeting hand muscles, we demonstrated a negligible contribution of M1 following a chronic (18 sessions) intervention targeting the lower limb, as demonstrated by the lack of association between CC3

(where most M1-M1 connecting fibers cross) and cross-education. Indeed, while CC3 was the subregion with the largest cumulative lesional load (along with CC5), lack of anatomical integrity did not translate in reduced magnitude of the transfer.

In a translational perspective, the present data bridging specific anatomical lesions to function may hold potentially relevant clinical implications. Beyond the observed increase in strength in the weaker, untrained side, the training here administered reduced the group-level asymmetry recorded at baseline, thus mitigating the common warning of clinical practitioners and neurorehabilitation specialists that contralateral training may enhance interhemispheric imbalance and strength/skill asymmetry. This consideration is in line with data showing no worsening of asymmetry with contralateral training of the stronger muscles (Manca et al., 2020), and with a recent consensus statement on cross-education where topic experts agreed that asymmetry is less important if there are benefits for the more affected limb (Manca et al., 2021).

Study limitations

The first limitation to the findings of this study relates to the stringent criteria applied to identify candidate persons with multiple sclerosis who displayed callosal lesions but intact spinal cord. Additionally, to be enrolled they had to be free from evidence of lesions in motor and premotor areas. Consequently, the sample size was reduced to a cohort of highly selected persons with multiple sclerosis, narrowing the external validity and generalizability of our results to populations with similarly isolated neuroradiological features.

Another limitation is the lack of neurophysiological testing, which would have allowed to directly test, among others, hypotheses on PM-PM, SMA-SMA and M1-M1 connections and intracortical circuits, and their integrated influence on cross-education. Future studies paralleling neuroradiological methods with TMS-based protocols probing inhibitory and facilitatory intracortical (both ipsi- and contra-laterally to the training) and interhemispheric dynamics in the context of cross-education are warranted.

Conclusion

Data showed that both site and size of the lesions influence cross-education. In particular, it was shown that the presence of lesions in the rostral body directly affected cross-education and that the lesion size was associated with the transfer magnitude. This new knowledge can be immediately translated into practice considering that it is based on a routine examination (conventional MRI), as patients who are not able to fully exercise their weaker side and do not display lesions in this subregion might be considered good candidates to cross-education protocols. Such information would allow the development of targeted rehabilitation strategies for persons with multiple sclerosis and other populations with callosal pathology, optimizing the use of cross-education to improve muscle strength.

Patient consent statement

A written consent was obtained by all participants.

Author's note

This article has received the Best Oral Presentation Award (presenter: Marco Morrone) at the 74th Congress of the Italian Society of Physiology (SIF).

Data availability statement

The raw data supporting the conclusions of this article will be made available by the authors, without undue reservation.

Ethics statement

The studies involving humans were approved by ASL n.1-Sassari, Italy; Prot. number 1160L2013. The studies were conducted in accordance with the local legislation and institutional requirements. The participants provided their written informed consent to participate in this study.

Author contributions

MM: Conceptualization, Data curation, Formal Analysis, Investigation, Writing–original draft, Writing–review and editing. GM: Conceptualization, Data curation, Formal Analysis, Investigation, Methodology, Visualization, Writing–original draft, Writing–review and editing. AA: Resources, Supervision, Validation, Visualization, Writing–original draft, Writing–review and editing. MS: Supervision, Writing–original draft, Writing–review and editing. SM: Supervision, Writing–original draft, Writing–review and editing. AM: Conceptualization, Data curation, Formal Analysis, Investigation, Methodology, Writing–original draft, Writing–review and editing. FD: Conceptualization, Funding acquisition, Project administration, Supervision, Writing–original draft, Writing–review and editing.

Funding

The author(s) declare that financial support was received for the research, authorship, and/or publication of this article. 1) Fondazione Italiana Sclerosi Multipla (FISM grant 2016R11, recipient Franca Deriu). 2) European Union - NextGenerationEU, DM 737/ 2021 risorse 2021–2022 - CUP J55F21004240001 (recipient Andrea Manca).

Conflict of interest

The authors declare that the research was conducted in the absence of any commercial or financial relationships that could be construed as a potential conflict of interest.

Generative AI statement

The author(s) declare that no Generative AI was used in the creation of this manuscript.

Publisher's note

References

Altheyab, A., Alqurashi, H., England, T. J., Phillips, B. E., and Piasecki, M. (2024). Cross-education of lower limb muscle strength following resistance exercise training in males and females: a systematic review and meta-analysis. *Exp. Physiol.* doi:10.1113/EP091881

Cohen, J. (1988). *Statistical power analysis for the behavioral Sciences*.

Coratella, G. (2022). Appropriate reporting of exercise variables in resistance training protocols: much more than load and number of repetitions. *Sports Med. - Open* 8, 99. doi:10.1186/s40798-022-00492-1

Coratella, G., Galas, A., Campa, F., Pedrinolla, A., Schena, F., and Venturelli, M. (2022). The eccentric phase in unilateral resistance training enhances and preserves the contralateral knee extensors strength gains after detraining in women: a randomized controlled trial. *Front. Physiol.* 13, 788473. doi:10.3389/fphys.2022.788473

Degraeve, B., Sequeira, H., Mecheri, H., and Lenne, B. (2023). Corpus callosum damage to account for cognitive, affective, and social-cognitive dysfunctions in multiple sclerosis: a model of callosal disconnection syndrome? *Mult. Scler.* 29 (2), 160–168. doi:10.1177/13524585221091067

Dragert, K., and Zehr, E. P. (2013). High-intensity unilateral dorsiflexor resistance training results in bilateral neuromuscular plasticity after stroke. *Exp. Brain Res.* 225 (1), 93–104. doi:10.1007/s00221-012-3351-x

Dvir, Z. (2025). *Isokinetics: muscle testing, interpretation and clinical applications*. Routledge: Chapman and Hall, Incorporated.

Fabri, M., Polonara, G., Mascioli, G., Salvolini, U., and Manzoni, T. (2011). Topographical organization of human corpus callosum: an fMRI mapping study. *Brain Res.* 1370, 99–111. doi:10.1016/j.brainres.2010.11.039

Farthing, J. P., Krentz, J. R., and Magnus, C. R. (2009). Strength training the free limb attenuates strength loss during unilateral immobilization. *J. Appl. Physio.* 106 (3), 830–836. doi:10.1152/japplphysiol.91331.2008

Fling, B. W., Walsh, C. M., Bangert, A. S., Reuter-Lorenz, P. A., Welsh, R. C., and Seidler, R. D. (2011). Differential callosal contributions to bimanual control in young and older adults. *J. Cogn. Neurosci.* 23 (9), 2171–2185. doi:10.1162/jocn.2010.21600

Green, L. A., and Gabriel, D. A. (2018a). The cross education of strength and skill following unilateral strength training in the upper and lower limbs. *J. Neurophysiol.* 120 (2), 468–479. doi:10.1152/jn.00116.2018

Green, L. A., and Gabriel, D. A. (2018b). The effect of unilateral training on contralateral limb strength in young, older, and patient populations: a meta-analysis of cross education. *Phys. Ther. Rev.* 23 (4-5), 238–249. doi:10.1080/10833196.2018.1499272

Hofer, S., and Frahm, J. (2006). Topography of the human corpus callosum revisited–comprehensive fiber tractography using diffusion tensor magnetic resonance imaging. *Neuroimage* 32 (3), 989–994. doi:10.1016/j.neuroimage.2006.05.044

Hoppner, J., Kunesch, E., Buchmann, J., Hess, A., Grossmann, A., and Benecke, R. (1999). Demyelination and axonal degeneration in corpus callosum assessed by analysis of transcallosally mediated inhibition in multiple sclerosis. *Clin. Neurophysiol.* 110 (4), 748–756. doi:10.1016/s1388-2457(98)00075-3

Hortobagyi, T., Richardson, S. P., Lomarev, M., Shamim, E., Meunier, S., Russman, H., et al. (2011). Interhemispheric plasticity in humans. *Med. Sci. Sports Exerc.* 43 (7), 1188–1199. doi:10.1249/MSS.0b013e31820a94b8

Huang, H., Zhang, J., Jiang, H., Wakana, S., Poetscher, L., Miller, M. I., et al. (2005). DTI tractography based parcellation of white matter: application to the mid-sagittal morphology of corpus callosum. *Neuroimage* 26 (1), 195–205. doi:10.1016/j.neuroimage.2005.01.019

Jeurissen, B., Leemans, A., Tournier, J. D., Jones, D. K., and Sijbers, J. (2013). Investigating the prevalence of complex fiber configurations in white matter tissue with diffusion magnetic resonance imaging. *Hum. Brain Mapp.* 34 (11), 2747–2766. doi:10.1002/hbm.22099

Jokinen, H., Ryberg, C., Kalska, H., Ylikoski, R., Rostrup, E., Stegmann, M. B., et al. (2007). Corpus callosum atrophy is associated with mental slowing and executive deficits in subjects with age-related white matter hyperintensities: the LADIS Study. *J. Neurol. Neurosurg. Psychiatry* 78 (5), 491–496. doi:10.1136/jnnp.2006.096792

Kent-Braun, J. A., Ng, A. V., Castro, M., Weiner, M. W., Gelinas, D., Dudley, G. A., et al. (1998). Strength, skeletal muscle composition, and enzyme activity in multiple sclerosis. *J. Appl. Physiol.* 83, 1998–2004. doi:10.1152/jappl.1997.83.6.1998

Kern, K. C., Sarcona, J., Montag, M., Giesser, B. S., and Sicotte, N. L. (2011). Corpus callosal diffusivity predicts motor impairment in relapsing-remitting multiple sclerosis: a TBSS and tractography study. *Neuroimage* 55 (3), 1169–1177. doi:10.1016/j.neuroimage.2010.10.077

Lambert, C. P., Archer, R. L., and Evans, W. J. (2001). Muscle strength and fatigue during isokinetic exercise in individuals with multiple sclerosis. *Med. Sci. Sports Exerc.* 33 (10), 1613–1619. doi:10.1097/00005768-200110000-00001

Lantis, D. J., Cantrell, G. S., Bemben, D. A., Black, C. D., Larson, D. J., Pardo, G., et al. (2024). Ankle dorsiflexion asymmetry and the relationship with walking performance in people with multiple sclerosis. *Gait Posture* 107, 194–198. doi:10.1016/j.gaitpost.2023.10.002

Larson, R. D., McCully, K. K., Larson, D. J., Pryor, W. M., and White, L. J. (2013). Bilateral differences in lower-limb performance in individuals with multiple sclerosis. *J. Rehabil. Res. Dev.* 50 (2), 215–222. doi:10.1682/jrrd.2011.10.0189

Lee, M., and Carroll, T. J. (2007). Cross education: possible mechanisms for the contralateral effects of unilateral resistance training. *Sports Med.* 37 (1), 1–14. doi:10.2165/00007256-200737010-00001

Manca, A., Cabboi, M. P., Dragone, D., Ginatempo, F., Ortu, E., De Natale, E. R., et al. (2017a). Resistance training for muscle weakness in multiple sclerosis: direct versus contralateral approach in individuals with ankle dorsiflexors' disparity in strength. *Arch. Phys. Med. Rehabil.* 98 (7), 1348–1356. doi:10.1016/j.apmr.2017.02.019

Manca, A., Dragone, D., Dvir, Z., and Deriu, F. (2017b). Cross-education of muscular strength following unilateral resistance training: a meta-analysis. *Eur. J. Appl. Physiol.* 117 (11), 2335–2354. doi:10.1007/s00421-017-3720-z

Manca, A., Ginatempo, F., Cabboi, M. P., Mercante, B., Ortu, E., Dragone, D., et al. (2016). No evidence of neural adaptations following chronic unilateral isometric training of the intrinsic muscles of the hand: a randomized controlled study. *Eur. J. Appl. Physiol.* 116 (10), 1993–2005. doi:10.1007/s00421-016-3451-6

Manca, A., Hortobagyi, T., Carroll, T. J., Enoka, R. M., Farthing, J. P., Gandevia, S. C., et al. (2021). Contralateral effects of unilateral strength and skill training: modified Delphi consensus to establish key aspects of cross-education. *Sports Med.* 51 (1), 11–20. doi:10.1007/s40279-020-01377-7

Manca, A., Hortobagyi, T., Rothwell, J., and Deriu, F. (2018). Neurophysiological adaptations in the untrained side in conjunction with cross-education of muscle strength: a systematic review and meta-analysis. *J. Appl. Physiol.* 124 (6), 1502–1518. doi:10.1152/japplphysiol.01016.2017

Manca, A., Peruzzi, A., Aiello, E., Cereatti, A., Martinez, G., Deriu, F., et al. (2020). Gait changes following direct versus contralateral strength training: a randomized controlled pilot study in individuals with multiple sclerosis. *Gait Posture* 78, 13–18. doi:10.1016/j.gaitpost.2020.02.017

Peterson, D. S., Gera, G., Horak, F. B., and Fling, B. W. (2017). Corpus callosum structural integrity is associated with postural control improvement in persons with multiple sclerosis who have minimal disability. *Neurorehabil. Neural Repair* 31 (4), 343–353. doi:10.1177/1545968316680487

Richardson, J. T. E. (2011). Eta squared and partial eta squared as measures of effect size in educational research. *Educ. Res. Rev.* 6, 135–147. doi:10.1016/j.edurev.2010.12.001

Ruddy, K. L., Leemans, A., and Carson, R. G. (2017a). Transcallosal connectivity of the human cortical motor network. *Brain Struct. Funct.* 222 (3), 1243–1252. doi:10.1007/s00429-016-1274-1

Ruddy, K. L., Leemans, A., Woolley, D. G., Wenderoth, N., and Carson, R. G. (2017b). Structural and functional cortical connectivity mediating cross-education of motor function. *J. Neurosci.* 37 (10), 2555–2564. doi:10.1523/JNEUROSCI.2536-16.2017

Scripture, E. W., Smith, T. L., and Brown, E. M. (1894). *On the education of muscular control and power*. Studies from the Yale Psychological Laboratory 2.

Urbin, M. A., Harris-Love, M. L., Carter, A. R., and Lang, C. E. (2015). High-intensity, unilateral resistance training of a non-paretic muscle group increases active range of motion in a severely paretic upper extremity muscle group after stroke. *Front. Neurol.* 6, 119. doi:10.3389/fneur.2015.00119

Wahl, M., and Ziemann, U. (2008). The human motor corpus callosum. *Rev. Neurosci.* 19 (6), 451–466. doi:10.1515/revneuro.2008.19.6.451

Wang, P., Meng, C., Yuan, R., Wang, J., Yang, H., Zhang, T., et al. (2020). The organization of the human corpus callosum estimated by intrinsic functional connectivity with white-matter functional networks. *Cereb. Cortex* 30 (5), 3313–3324. doi:10.1093/cercor/bhz311

Witelson, S. F. (1989). Hand and sex differences in the isthmus and genu of the human corpus callosum: a postmortem morphological study. *Brain* 112 (3), 799–835. doi:10.1093/brain/112.3.799

frontiers | Frontiers in Physiology

TYPE Original Research
PUBLISHED 15 April 2025
DOI 10.3389/fphys.2025.1535053

OPEN ACCESS

EDITED BY
Myriam Catalano,
Sapienza University of Rome, Italy

REVIEWED BY
Roberto Piacentini,
Catholic University of the Sacred Heart, Italy
Xiaoming Zhou,
Uniformed Services University of the Health Sciences, United States

*CORRESPONDENCE
Marianna Ranieri,
marianna.ranieri@uniba.it
Giovanna Valenti,
giovanna.valenti@uniba.it

RECEIVED 26 November 2024
ACCEPTED 31 March 2025
PUBLISHED 15 April 2025

CITATION
Ranieri M, Venneri M, Storlino G, Ferrulli A, D'Agostino M, Centrone M, Di Mise A, Zerlotin R, Tamma G, Grano M and Valenti G (2025) Alteration of vasopressin-aquaporin system in hindlimb unloading mice. *Front. Physiol.* 16:1535053. doi: 10.3389/fphys.2025.1535053

Alteration of vasopressin-aquaporin system in hindlimb unloading mice

Marianna Ranieri[1]*, Maria Venneri[2], Giuseppina Storlino[3], Angela Ferrulli[1], Mariagrazia D'Agostino[1], Mariangela Centrone[1], Annarita Di Mise[1,4], Roberta Zerlotin[5], Grazia Tamma[1], Maria Grano[5] and Giovanna Valenti[1]*

[1]Department of Biosciences, Biotechnologies and Environment, University of Bari, Bari, Italy, [2]Istituti Clinici Scientifici Maugeri SPA SB IRCCS, Bari, Italy, [3]Department of Clinical and Experimental Medicine, University of Foggia, Foggia, Italy, [4]Department of Biotechnology and Biosciences, University of Milano-Bicocca, Milan, Italy, [5]Department of Precision and Regenerative Medicine and Ionian Area, University of Bari, Bari, Italy

Murine hindlimb unloading (HU) is considered a model of choice for simulating the physiological effects of microgravity on several functions, including fluid and electrolyte homeostasis. Microgravity causes changes in blood redistribution, modulating vasopressin secretion, a major hormone controlling water reabsorption through the vasopressin-sensitive water channel AQP2. In this study, mice were hindlimb suspended over 4 weeks or rested in the ground as controls, and vasopressin levels, along with renal aquaporins expression were investigated. Copeptin, a stable precursor of the hormone vasopressin, significantly increased as early as 1 week of unloading which correlated with a significant increase in AQP2 total protein expression and decrease in serum osmolality, suggesting early activation of the vasopressin/AQP2 axis in this model. Conversely, in 4 weeks HU suspended mice, copeptin decreased significantly and both AQP2 mRNA and AQP2 total protein expression were significantly reduced. Consistent with a downregulation of the vasopressin/AQP2 axis an increase in serum osmolality was observed at 4 weeks HU. The basolateral water channels AQP3 and AQP4 were, on the other hand, unaffected. Immunolocalization studies confirmed reduced expression of AQP2 in renal collecting ducts of HU mice at 4 weeks. A significantly increased amount of the expressed AQP2 was found phosphorylated at Ser261, a site regulating AQP2 protein stability and degradation. In line, p38-MAPK, committed to phosphorylate Ser261 and to increase miR137 expression, an AQP2 mRNA-targeted microRNA, was significantly increased in HU, suggesting that reduced AQP2 expression was mainly due to increased protein degradation and downregulation of AQP2-mRNA translation. Our results suggest that vasopressin/AQP2 axis is upregulated as early as 1 week and may be involved in the antidiuretic response also observed in early spaceflight period in astronauts. Contrariwise, the vasopressin-AQP2 system is downregulated after 4 weeks HU, likely to counteract the persistent central venous pressure due to cephalic shift of fluids.

KEYWORDS

AQP2, vasopressin (ADH), vasopressin type 2 receptor, hindlimb suspension (unloading), microgravity, microRNA, calcium-sensing receptor (CaSR)

Introduction

Body fluid regulation is affected by microgravity causing reno-vascular changes (Olde Engberink et al., 2023). In particular, microgravity causes fluid redistribution from the legs to the upper part of the body, which impacts kidney function and volume homeostasis (Moore and Thornton, 1987; Thornton et al., 1992; Olde Engberink et al., 2023; Beysens and Loon, 2015). The major hormone regulating body fluid distribution is the antidiuretic hormone vasopressin. Vasopressin is secreted in response to an increase in plasma osmolality or decreased extracellular volume. In the kidney, it binds its receptor (vasopressin V2 receptor) in the collecting duct principal cells, initiating a signal transduction cascade leading to redistribution of aquaporin-2 (AQP2) water channels to the luminal plasma membrane, thereby increasing water permeability. Thus, water can be reabsorbed in the renal collecting duct to fine-tune water balance and plasma osmolality (Centrone et al., 2022; Ranieri et al., 2019; Kharin and Klussmann, 2024). In the light of the above considerations, is of interest to study the modulation of the vasopressin-aquaporin system occurring during exposure to microgravity.

Several models for simulating the effects of microgravity exist for various species. In humans, a well-established terrestrial model is head-down bed rest which induces a cephalic fluid shift and results in the loss of impact loading on the musculoskeletal system (Convertino et al., 1990; Barkaszi et al., 2022; Le Roux et al., 2022; Qaisar et al., 2020). Similarly, water immersion of humans causes a rapid cephalad fluid shift, unloading of the immersed systems (Watenpaugh, 2016; Valenti et al., 2006).

Hindlimb unloading (HU) of rodents in a head-down position, is an animal model to simulate the physiological effects of microgravity on ground (Globus and Morey-Holton, 2016; Morey-Holton and Globus, 2002). The HU model was developed in the 1980s to study mechanisms, responses, and treatments for the adverse consequences of space flight. In this model, the hindlimbs of rodents are elevated to produce a 30° head-down tilt, which results in a cephalad fluid shift (Morey-Holton and Globus, 2002). Although the rat hindlimb unloading (HU) model was initially developed in particular to study alterations of the musculoskeletal and cardiovascular systems caused by weightlessness (Morey, 1979), several studies have demonstrated that this model can be used to study alterations of many physiological properties including fluid and electrolyte homeostasis (Globus and Morey-Holton, 2016; Morey-Holton and Globus, 2002; Chung et al., 2012). However, data obtained from hindlimb unloading experiments must be interpreted with caution since in humans the entire body is unloaded during spaceflight, whereas the forelimbs, head, and upper back remain weightbearing in hindlimb-unloaded animals. Moreover, in HU fluid shifts may be greater in hindlimb-unloaded rodents because the animal is quadruped. Despite these cautions, studies in hindlimb-unloaded rats have been instrumental in defining the time course and mechanisms of physiological changes that occur due to unloading. A previous study using HU rat model examined time dependent alterations of vasopressin for 1 (HU1), 7 (HU7), 14 days (HU14) showing a peak value of both plasma vasopressin levels and AQP2 at HU7. Alterations were however restored at HU14 (Chung et al., 2012) suggesting that in this model, vasopressin system may require 2 weeks for adaptation to microgravity. These results differ however from another study showing higher vasopressin levels at HU14 (Chung et al., 2012). In the present contribution, mice were hindlimb suspended over 4 weeks or rested in the ground as controls, and vasopressin levels along with renal aquaporins expression was investigated. For the first time in rodent HU models, plasma copeptin levels were measured as validated surrogate for plasma vasopressin levels. Measurement of copeptin is increasingly preferred over measurement of vasopressin because of the technical constraints of the conventional assays for vasopressin (Heida et al., 2017).

Obtained results indicate that in mice, while vasopressin-AQP2 axis is upregulated as early as 1 week, 4 weeks hindlimb unloading results in downregulation of the vasopressin - AQP2 system, likely as a consequence of the persistent cephalic shift of fluids.

Results

Evaluation of serum copeptin, aquaporins expression and serum osmolality in HU mice

Serum copeptin levels were measured (ELISA kit) as validated surrogate for serum vasopressin levels.

At 1 week HU suspension, copeptin levels were significantly increased in HU mice compared to the Rest mice (HU: 2,029 ± 59.98 pg/mL vs. REST: 1,483 ± 170.1 pg/mL; $p = 0.016$) (Figure 1A).

In line with this data, total AQP2 expression in kidney homogenate from 1 week HU suspended mice significantly increased with respect to Rest mice (HU: 1.227 ± 0.081 O.D. vs. REST: 1.000 ± 0.062 O.D.; $p = 0.047$) (Figure 2A), along with a significant reduction in pS261-AQP2 (HU: 0.659 ± 0.065 O.D. vs. REST: 1.000 ± 0.086 O.D.; $p = 0.008$) (Figure 2B), a phosphorylation site crucial for the degradation processes via proteasome (Nedvetsky et al., 2010; Isobe et al., 2017). This indicates that AQP2 is less degraded at early timepoint of HU.

In agreement with the increase in copeptin levels, serum osmolality was significantly reduced in HU mice, reflecting higher water reabsorption resulting in reduction in serum osmolality (HU: 319.3 ± 9.26 mmol/kg vs. REST: 549.7 ± 60.09 mmol/kg; $p = 0.019$) (Figure 1B).

Conversely, at 4 weeks HU, copeptin levels were significantly decreased in HU mice compared to Rest mice (HU: 815.9 ± 82.49 pg/mL vs. REST: 1,319.0 ± 77.29 pg/mL; $p = 0.002$) (Figure 3A), along with a significant increase in serum osmolality (HU: 242.7 ± 8.22 mmol/kg vs. REST: 215.8 ± 6.54 mmol/kg; $p = 0.043$) suggesting that mice are in negative fluid balance at 4 weeks of suspension (Figure 3B).

AQP2 expression was therefore evaluated both at mRNA and protein levels, in kidneys from 4 weeks HU mice and compared to Rest mice. Both mRNA (HU: 0.522 ± 0.091 vs. REST: 1.000 ± 0.122; $p = 0.007$) (Figure 4A) and protein levels (HU: 0.625 ± 0.037 O.D. vs. REST: 1.000 ± 0.093 O.D.; $p = 0.002$) (Figure 4B) revealed a significant decrease in AQP2 expression.

In contrast, AQP3 and AQP4 expressions evaluated by Western blotting technique demonstrated no significant alteration after 4 weeks of suspension in HU mice compared

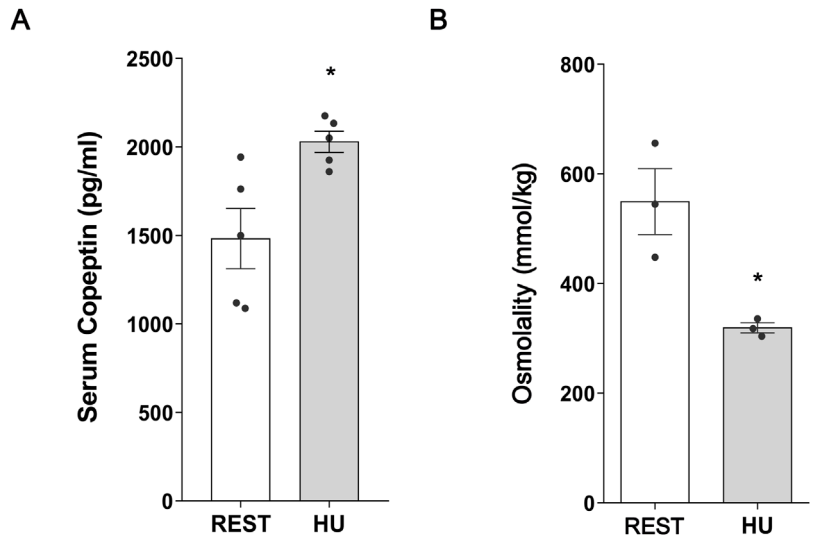

FIGURE 1
(A) Serum Copeptin in 1 week hindlimb unloading rodent model (HU) compared to control (REST). ELISA assay was performed on serum obtained from HU and REST mice. Data are expressed as mean ± S.E.M. (pg/mL). Statistical analysis was done using Unpaired t-test (*$p < 0.05$). **(B)** Serum Osmolality in hindlimb unloading rodent model (HU) compared to control (REST). Data are expressed as mean ± S.E.M. (mmol/kg). Statistical analysis was done using Unpaired t-test (*$p < 0.05$).

to Rest mice (Supplementary Figure S1) indicating a selective downregulation of AQP2.

HU mice displayed higher levels in AQP2 phosphorylated at Ser261 and AQP2-mRNA targeted miRNA137

Next, the intracellular pathways responsible for AQP2 downregulation were investigated. The regulation of both AQP2 gene and protein expression levels occurs by different regulatory factors: kinases, such as p38MAPK, known as upstream AQP2 degradation, or microRNA, such as miR137, known as a mRNA-AQP2 targeting microRNA. To evaluate the involvement of p38MAPK in regulating the degradation of AQP2, via phosphorylation in Ser261, and of miRNA137 in downregulating the mRNA-AQP2 translation, we performed Western blotting experiments to measure phosphorylated levels of AQP2 (AQP2-pS261) and Phospho-p38MAPK, the active form of this kinase, and RT-PCR assays to compare miR137 levels in HU mice with that in Rest mice.

In line to reduced AQP2 expression, 4 weeks HU mice displayed a significant increase in AQP2 phosphorylated at Ser261 (HU: 1.529 ± 0.194 O.D. vs. REST: 1.000 ± 0.133 O.D.; $p = 0.039$) (Figure 5A) suggesting activation of the degradation pathways.

Confocal microscopy and visualization confirmed the decreased expression of AQP2 and the increased phosphorylation levels in Ser261 of AQP2 observed in HU mice kidneys with respect to Rest mice kidneys (Figure 5B).

p38MAPK is a candidate kinase to phosphorylate AQP2 at Serine 261 (Hoffert et al., 2006; Nedvetsky et al., 2010), and its phosphorylation represents a hallmark for ubiquitination and protein degradation via proteasome (Nedvetsky et al., 2010; Isobe et al., 2017).

Using specific phosphoantibodies recognizing p38MAPK (Pp38MAPK, the active form of the kinase) significantly higher levels of Pp38MAPK were found in HU mice compared to Rest mice (HU: 2.144 ± 0.323 O.D. vs. REST: 1.000 ± 0.118 O.D.; $p = 0.004$) (Figure 6A).

RT-PCR experiments demonstrated higher levels of miRNA137 in HU mice, an AQP2-mRNA targeted miRNA137 (Kim et al., 2015) (HU: $2.290^{*}10^{-5}$±$2.736^{*}10^{-6}$ ng vs. REST: $1.533^{*}10^{-5}$±$1.522^{*}10^{-6}$ ng; $p = 0.029$) (Figure 6B).

AQP2 levels in kidney from HU mice treated with p38MAPK inhibitor SB203580

To understand the actual involvement of p38MAPK in phosphorylating AQP2 and inducing reduced AQP2 expression, we performed experiments exposing kidney slices obtained from HU mice to SB203580 (10 μM for 30 min) a specific inhibitor of p38MAPK.

Of interest, both AQP2 mRNA (HU SB203580: 1.589 ± 0.402 vs. HU ctrl: 1.000 ± 0.337; $p = 0.013$) (Figure 7A) and protein levels (HU SB203580: 1.686 ± 0.211 O.D. vs. HU ctrl: 1.000 ± 0.224 O.D.; $p = 0.042$) (Figure 7B) were upregulated in kidney slices from HU treated with SB203580 (HU SB203580) compared to kidney slices left under basal condition (HU ctrl), indicating that this kinase is a downstream effector.

Moreover, a significative reduction in AQP2-pS261 levels was observed in the presence of SB203580 (HU SB203580: 0.510 ± 0.244 O.D. vs. HU ctrl: 1.000 ± 0.259 O.D.; $p = 0.028$) (Figure 8A), suggesting that p38MAPK inhibition prevents AQP2 degradation via phosphorylation at Ser261 in HU mice.

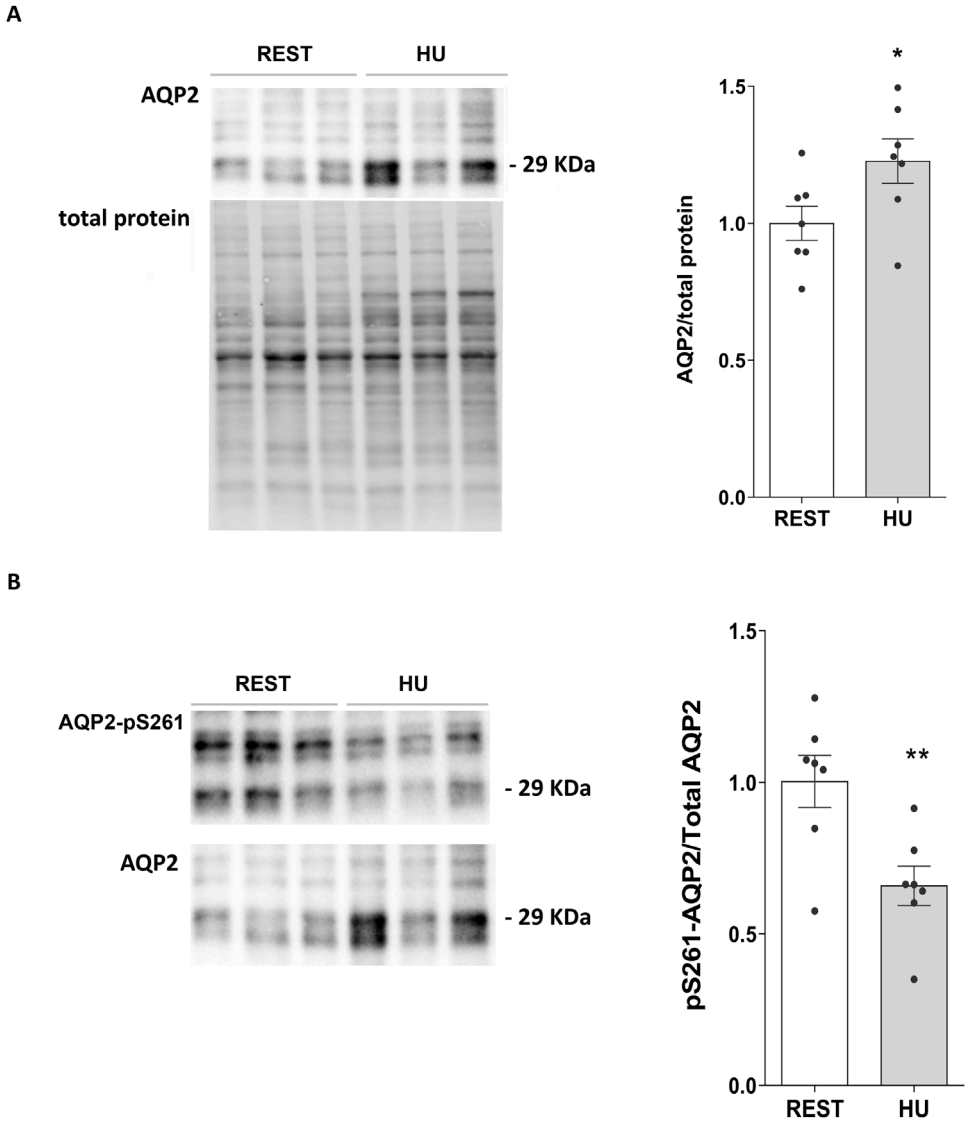

FIGURE 2
(A) Expression of AQP2 in 1 week HU and REST mice. Kidneys from HU and REST mice were lysed, and immunoblotting experiments were performed using specific antibodies against total AQP2. Densitometric analysis of total AQP2 bands normalized to the total protein content is reported in the histogram. Data are expressed as mean ± S.E.M. (O.D.). Statistical analysis was done using Unpaired t-test (*$p < 0.05$). **(B)** Expression of AQP2 in 1 week HU and REST mice. Kidneys from HU and REST mice were lysed, and immunoblotting experiments were performed using specific antibodies against total AQP2. Densitometric analysis of total AQP2 bands normalized to the total protein content is reported in the histogram. Data are expressed as mean ± S.E.M. (O.D.). Statistical analysis was done using Unpaired t-test (**$p < 0.01$).

Of note, under these experimental conditions, a significative reduction of the AQP2-mRNA targeted miR137 was observed in HU mice (HU SB203580: $8.815^{*}10^{-9} \pm 8.686^{*}10^{-10}$ ng vs. HU ctrl: $1.141^{*}10^{-8} \pm 5.008^{*}10^{-10}$ ng; $p = 0.015$) (Figure 8B).

In line with this, SB203580 reduced phosphorylated p38MAPK levels in HU mice (HU SB203580: 0.482 ± 0.207 O.D. vs. HU ctrl: 1.000 ± 0.113 O.D.; $p = 0.042$) (Figure 8C).

All the described experiments were conducted in mice matched by sex (4 males and 4 females in 4 weeks suspension and 4 males and 3 females in 1 week suspension). No significant difference emerged between the two groups, indicating that the obtained results were apparently not influenced by sex.

Discussion

The hindlimb unloading (HU) mouse has been confirmed to be a useful model for studying the impact of microgravity or the effects of prolonged immobilization in humans (Globus and Morey-Holton, 2016; Milstead et al., 2004). Exposure to microgravity leads to a redistribution of body fluid to the upper part of the body and an extravasation very early in-flight. These physiological alterations significantly affect renal function, an organ playing a pivotal role in regulating fluid balance, electrolytes, and waste removal in the body. In the absence of gravity, some key changes lead to alterations in how the kidneys function: fluid redistribution, decreased blood volume, altered filtration, electrolyte imbalance and

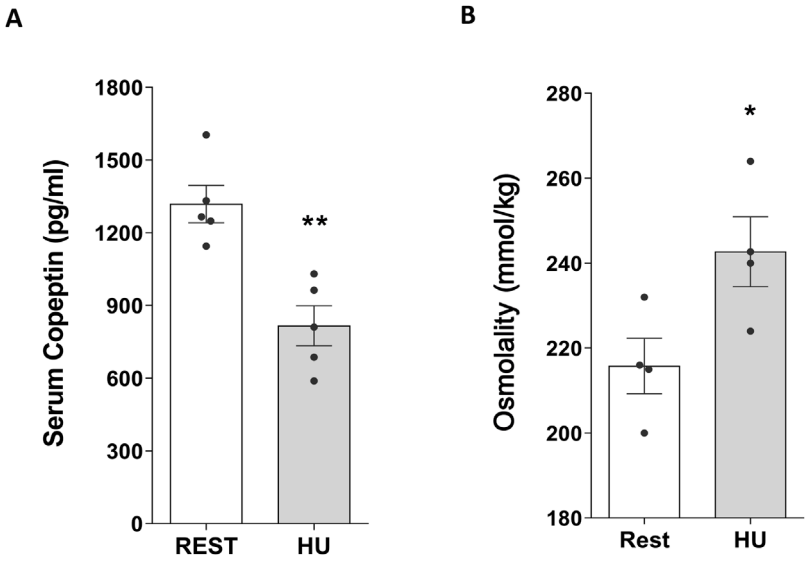

FIGURE 3
(A) Serum Copeptin in 4 weeks hindlimb unloading rodent model (HU) compared to control (REST). ELISA assay was performed on serum obtained from HU and REST mice. Data are expressed as mean ± S.E.M. (pg/mL). Statistical analysis was done using Unpaired t-test (**$p < 0.01$). **(B)** Serum Osmolality in hindlimb unloading rodent model (HU) compared to control (REST). Data are expressed as mean ± S.E.M. (mmol/kg). Statistical analysis was done using Unpaired t-test (*$p < 0.05$).

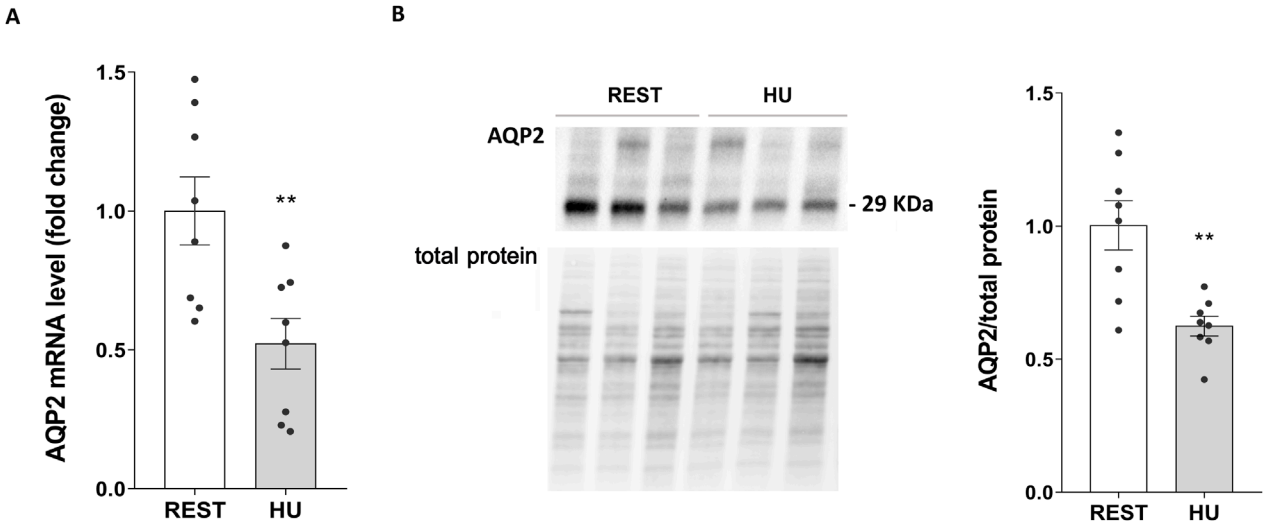

FIGURE 4
(A) AQP2 mRNA levels in 4 weeks HU and REST mice. RNA was extracted from HU and REST mice kidneys as described in Methods Section. Data are expressed as mean ± S.E.M. Statistical analysis was done using Unpaired t-test (**$p < 0.01$). **(B)** Expression of AQP2 in HU and REST mice. Kidneys from HU and REST mice were lysed, and immunoblotting experiments were performed using specific antibodies against total AQP2. Densitometric analysis of total AQP2 bands normalized to the total protein content is reported in the histogram. Data are expressed as mean ± S.E.M. (O.D.). Statistical analysis was done using Unpaired t-test (**$p < 0.01$).

bone loss and calcium metabolism (Olde Engberink et al., 2023). Studying kidney function in microgravity provides valuable insights into how the human body adapts to extreme environments and may offer clues for managing conditions such as kidney disease on Earth or kidney consequences during aging bed rest. In the present contribution vasopressin levels, evaluated for the first time monitoring copeptin, a validated surrogate for plasma vasopressin levels, along with renal aquaporins expression were investigated in HU mice over 4 weeks. Obtained results can be summarized as follows: *a.* vasopressin (copeptin) increased as early as 1 week of unloading which correlated with a significant increase in AQP2 total protein expression and decrease in serum osmolality, suggesting early activation of the vasopressin/AQP2 axis; *b.* at 4 weeks of HU, vasopressin decreased significantly along with reduction of both

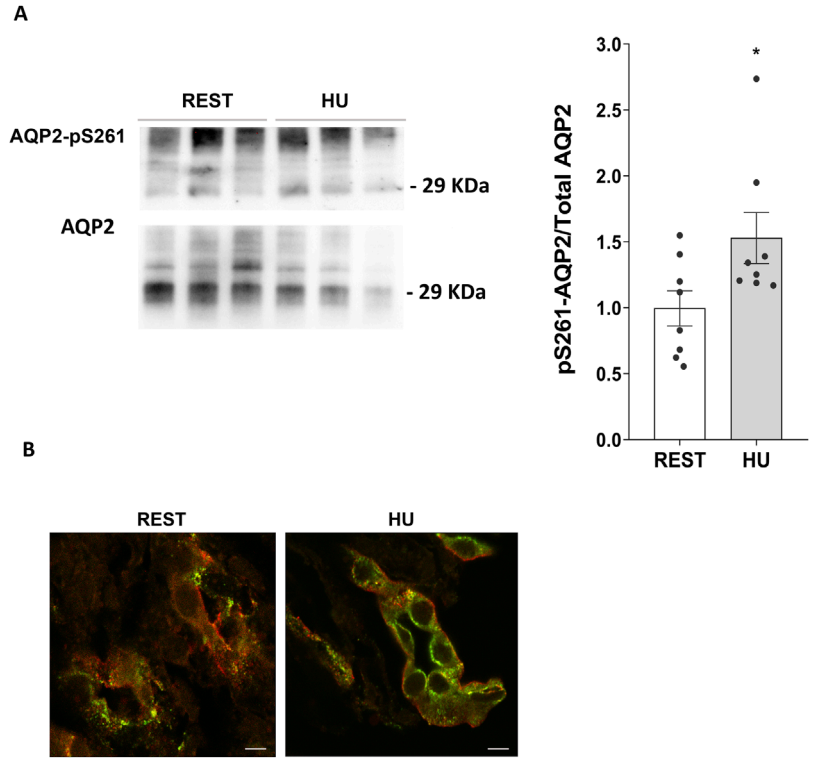

FIGURE 5
(A) Expression of AQP2-pS261 in 4 weeks HU compared to REST mice. Kidneys from HU and REST mice were lysed, and immunoblotting experiments were performed using specific antibodies against phosphorylated AQP2 in Ser261 and total AQP2. Densitometric analysis of AQP2-pS261 bands normalized to total AQP2 is reported in the histogram. Data are expressed as mean ± S.E.M. (O.D.). Statistical analysis was done using Unpaired t-test (*$p < 0.05$). **(B)** Localization of AQP2-pS261 and total AQP2. Immunofluorescence staining of AQP2-pS261, in green (AlexaFluor 488), and total AQP2, in red (AlexaFluor 555), in renal sections of HU and REST mice (scale bar: 5 μm).

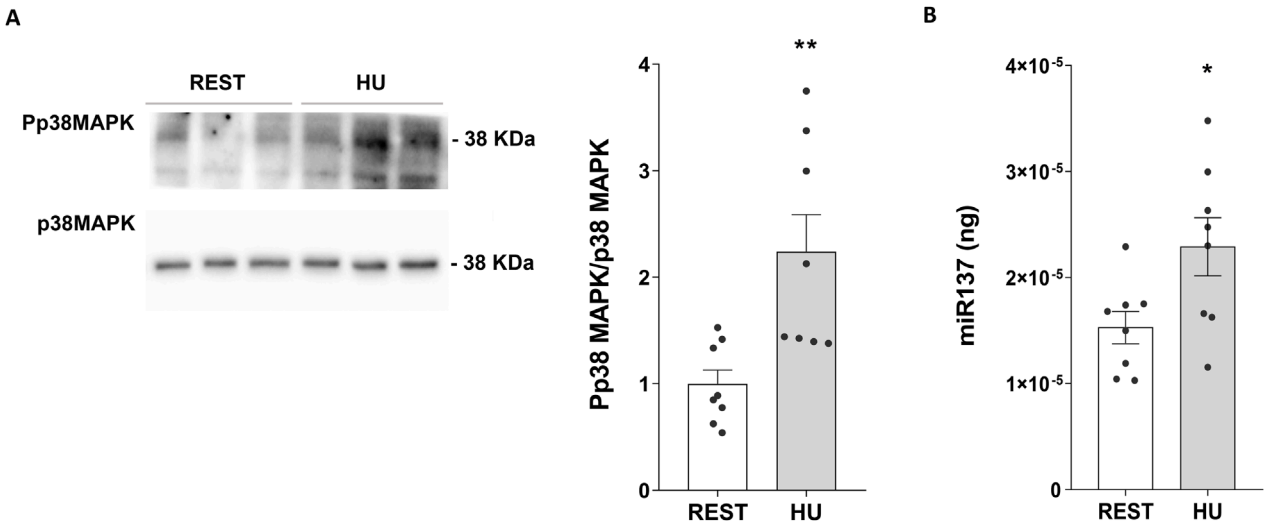

FIGURE 6
(A) Expression of Phosphorylated p38-MAPK (Pp38MAPK) in 4 weeks HU and REST mice. Kidneys from HU and REST mice were lysed, and immunoblotting experiments were performed using specific antibodies against phospho-p38MAPK (Pp38MAPK) and total p38MAPK. Densitometric analysis of Pp38MAPK bands, normalized to total p38MAPK, is reported in the histogram. Data are expressed as mean ± S.E.M. (O.D.). Statistical analysis was done using Unpaired t-test (**$p < 0.01$). **(B)** Evaluation of miR-137 in HU and REST mice. Total RNA was extracted from HU and REST mice kidneys, and the cDNA was obtained as described in Materials and Methods. Synthetic RNA with 59-phospho, miR-137 (UUAUUGCUUAAGAAUACGCGUAG), was synthesized and used to perform a calibration curve and interpolate miRNA sample values from HU and REST mice. Data from RT-PCR experiments were interpolated in the calibration curve obtained with synthetic miRNA. Data are expressed as mean ± S.E.M. (ng). Statistical analysis was done using Unpaired t-test (*$p < 0.05$).

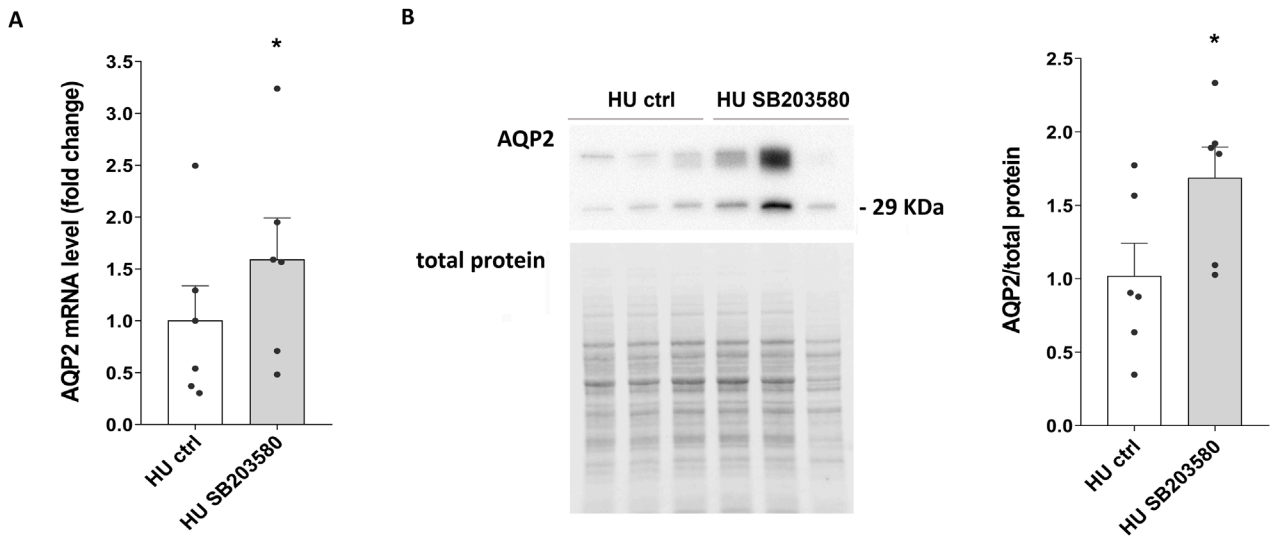

FIGURE 7
(A) AQP2 mRNA levels in 4 weeks HU mice treated with p38MAPK inhibitor SB203580. RNA was extracted from HU mice kidneys left in basal condition or treated with SB203580, as described in Methods Section. Data are expressed as mean ± S.E.M. Statistical analysis was done using paired t-test (*$p < 0.05$). **(B)** Expression of AQP2 in HU mice treated with the inhibitor SB203580. Kidneys from HU mice were left in basal condition or treated with SB203580 and subsequently lysed. Immunoblotting experiments were performed using specific antibodies against total AQP2. Densitometric analysis of total AQP2 bands normalized to the total protein content is reported in the histogram. Data are expressed as mean ± S.E.M. (O.D.). Statistical analysis was done using paired t-test (*$p < 0.05$).

AQP2 mRNA and AQP2 total protein expression; *c.* the basolateral water channels AQP3 and AQP4 were unaffected.

As mentioned, the observation that vasopressin and AQP2 levels rise at 1 week HU is in agreement with a previous study using HU rat model showing a peak value of both plasma vasopressin levels and AQP2 at HU7 (Chung et al., 2012). Since it is well described that about 10%-15% fluid transfer from the intravascular to interstitial compartment occurs very early in astronauts within the first 24 h (Leach et al., 1996) and in HU rats (Sullivan et al., 2004), this increase in vasopressin might reflect the need to restore vascular fluid loss. In line with that, serum osmolality decreased at 1 week HU. Another study however reported that fluid loss may not occur in spaceflight in quadrupeds such as the rat (Wade and Morey-Holton, 1998). We cannot exclude that stress can also contribute to the observed increase in vasopressin since it is known that stress is often associated with water retention and its resolution with diuresis (Bhattacharya et al., 1998). Nevertheless, the timepoint showing increase in vasopressin is not an early time and it has been reported that HU model is not a stress model (Drummer et al., 2001). We show here that mice suspended for 4 weeks had instead a significant decrease in serum copeptin, associated with reduced expression of AQP2 both in terms of mRNA and protein levels. Functional alterations of vasopressin observed in the HU model are compatible with an adaptation to the fluid redistribution towards the cephalic part of the body, causing central hypervolemia and consequently a reduction of vasopressin. We observed that the reduction in vasopressin levels was paralleled by the downregulation of AQP2 expression. These effects are expected to limit fluids reabsorption, counteracting central hypervolemia. To our knowledge this is the first study evaluating vasopressin levels in HU mice suspended for 4 weeks. As discussed, a previous study using HU rat model showed a peak value of plasma vasopressin (measured with RIA method) after 1 week associated with reduction in AQP2 expression. These alterations were however restored after 2 weeks (Chung et al., 2012), and the authors suggest that, in this model, vasopressin system may require 2 weeks for adaptation to microgravity. In contrast, in HU mice evaluated in our study, vasopressin levels remained significantly lower with respect to the starting timepoint. If 4 weeks suspension can be considered a period of chronic adaptation microgravity, then our results differ from data in astronauts during long-term spaceflights displaying instead increased levels of vasopressin (Drummer et al., 2000; Grigoriev et al., 1994) despite no change in plasma osmolality that can be the consequence of decreased plasma volume. We cannot explain this discrepancy that can be related to a different behavior of mice with respect to humans. In addition, it is possible that body fluid regulation in microgravity in space differs from that on earth as suggested by other studies (Drummer et al., 2000). In fact, in humans, renal responses during exposure to simulated microgravity are consistently weaker than those during simulation experiments before spaceflight (Norsk et al., 2000).

HU causes a cephalad fluid shift and removal of ground reaction forces from the hindlimbs as occurs in astronauts. However, gravity is still present in the HU model with a headward shift of internal organs and fluid. The internal organs still exert pressure against each other with HU, unlike in spaceflight, during which organs free float.

In our study we provide evidence that the downregulation of the vasopressin-sensitive water channel AQP2 is mainly the consequence of activation of its degradation. AQP2 trafficking and expression are fine controlled by various post-translational events, like phosphorylation, ubiquitination, and degradation (Moeller et al., 2011; Ranieri et al., 2018), and glutathionylation

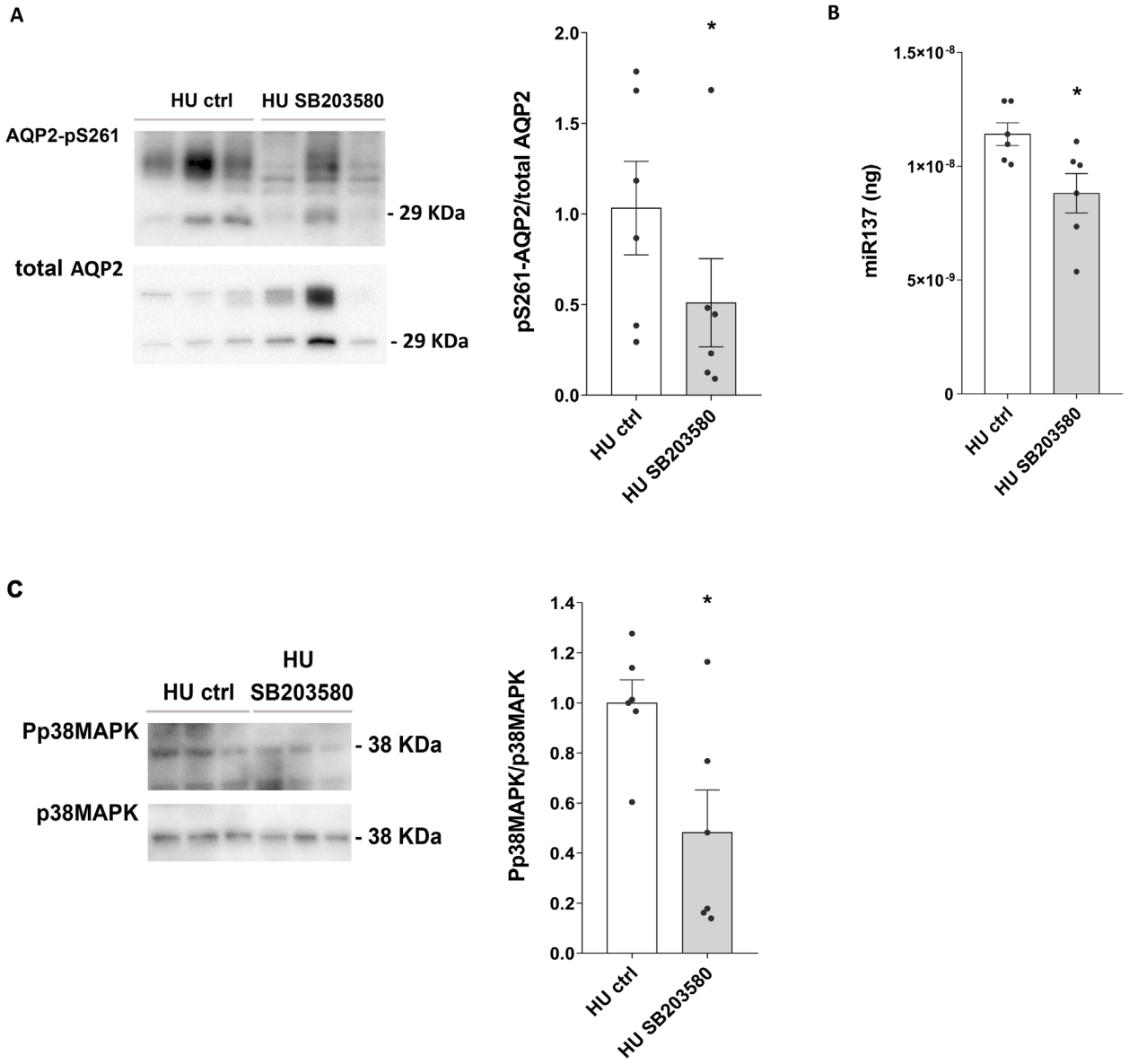

FIGURE 8
(A) Expression of AQP2-pS261 and of Phosphorylated p38-MAPK (Pp38MAPK) in 4 weeks HU mice treated with p38MAPK inhibitor SB203580. HU mice kidneys were left in basal condition or treated with SB203580. Subsequently, kidneys were lysed, and immunoblotting experiments were performed using specific antibodies against AQP2-pS261 and total AQP2. Densitometric analysis of AQP2-pS261 bands normalized to total AQP2 is reported in the histogram. Data are expressed as mean ± S.E.M. (O.D.). Statistical analysis was done using paired t-test (*$p < 0.05$). **(B)** Evaluation of the effect of SB203580 treatment in HU mice on miR-137 levels. Total RNA was extracted from HU mice kidneys left in basal condition or treated with SB203580, and the cDNA was obtained as described in Materials and Methods. Synthetic RNA with 59-phospho, miR-137 (UUAUUGCUUAAGAAUACGCGUAG), was synthesized and used to perform a calibration curve and interpolate miRNA sample values from HU and REST mice. Data from RT-PCR experiments were interpolated in the calibration curve obtained with synthetic miRNA. Data are expressed as mean ± S.E.M. (ng). Statistical analysis was done using paired t-test (*$p < 0.05$). **(C)** Expression of Phosphorylated p38-MAPK (Pp38MAPK) in HU mice treated with p38MAPK inhibitor SB203580. Kidneys from HU mice were left in basal condition or treated with SB203580 prior to lysis. Immunoblotting experiments were performed using specific antibodies against phospho-p38MAPK (Pp38MAPK) and total p38MAPK. Densitometric analysis of Pp38MAPK bands, normalized to total p38MAPK, is reported in the histogram. Data are expressed as mean ± S.E.M. (O.D.). Statistical analysis was done using paired t-test (*$p < 0.05$).

(Tamma et al., 2014). The binding of vasopressin to its receptor causes AQP2 phosphorylation at Serine 256, 264 and 269 at short term; while, at long term, AQP2 mRNA expression increases and, consequently, rises AQP2 protein level (Matsumura et al., 1997; Fenton et al., 2008; Hoffert et al., 2008). On the other hand, under vasopressin stimulation, phosphorylation at Serine 261 of AQP2 decreases (Hoffert et al., 2006; Matsumura et al., 1997; Hoffert et al., 2007; Nedvetsky et al., 2010). Both events, AQP2 phosphorylation at Serine 261 and polyubiquitination induce AQP2 internalization, recycling or degradation via p38MAPK (Nedvetsky et al., 2010; Trepiccione et al., 2014). p38MAPK is a candidate kinase to phosphorylate AQP2 at Serine 261 (Hoffert et al.,

2006; Nedvetsky et al., 2010), and its phosphorylation represents a hallmark for ubiquitination and protein degradation via proteasome (Nedvetsky et al., 2010; Isobe et al., 2017).

HU mice showed a significant increase in the Serine 261 phosphorylation of AQP2. This increase in phosphorylation is crucial for the degradation processes of AQP2 causing the decrease of the AQP2 protein levels. We provide here evidence that phosphorylation at Serine 261 is mediated by p38MAPK activation.

We previously demonstrated that p38MAPK could activate miRNAs transcription via ATF1 transcription factor (Ranieri et al., 2024). miR137 is a microRNA, a small non-coding RNA molecule, involved in the regulation of AQP2 gene expression. MicroRNAs typically function by binding to complementary sequences on target messenger RNAs (mRNAs), usually resulting in their silencing through translational repression or target degradation.

Recent studies have started to uncover the relationship between miR137 and AQP2, suggesting that miR137 may influence AQP2 expression and thereby affect kidney function and water balance (Kim et al., 2015; Ranieri et al., 2018; Ranieri, 2019; Ranieri et al., 2024). miR137 may directly target the mRNA of AQP2, leading to its degradation or inhibition of translation. Interestingly we show here that in HU mice miR137 increases resulting in decreased levels of AQP2 protein. Of note, p38MAPK inhibition with SB203580 restores miR137 levels in HU mice compared to Rest mice, demonstrating that this kinase is responsible for miR137 transcription.

This result shows how, by regulating AQP2 levels, miR137 can influence water reabsorption in the collecting ducts of the kidney. Lower levels of AQP2 due to high miR137 activity could lead to reduced water reabsorption and increased urine output. However, we could not measure urinary output in HU mice in this study.

At renal level we have already demonstrated that miR137 levels are increased in parallel with CaSR activation. CaSR stimulation promotes p38MAPK activation able to activate the transcription factor ATF1, which in turn causes an increase in miR137 transcription (Ranieri et al., 2024).

The activation of CaSR is possibly due to an increase in calciuria secondary to an increase in serum calcium concentration, due to bone reabsorption (Rittweger et al., 2009; Bilancio et al., 2013). Unfortunately, because urines were not collected from HU mice, calciuria could not be measured. However, we already demonstrated in these same HU mice that bone from control and HU mice at 4 week had decreased thickness of trabeculae and increasing number of empty lacunae reflecting bone demineralization (Sanesi et al., 2023) which is expected to result in increased calciuria. Increased urinary calcium can activate CaSR which in turn counteracts vasopressin-AQP2 response resulting in reduction of urinary AQP2 excretion (Procino et al., 2012; Valenti et al., 2000) as also observed in HU mice at 4 weeks.

In conclusion, as summarized in the schematic model in Figure 9, this study demonstrates that chronic adaptation to microgravity of mice, simulated by 4 weeks HU suspension, induces a reduced secretion of vasopressin and selective reduction of AQP2 expression mainly due to its degradation, with no change in the expression of other renal AQPs. This response is likely the consequence of the cephalic shift of fluids caused by HU suspension and represents a physiological adaptation to counteract the central hypervolemia.

Materials and methods

Antibodies

AQP2 ((E-2) sc-515770), AQP3 ((C-18) sc-9885) and AQP4 ((C-19) sc-9888) antibodies were purchased from Santa Cruz Biotechnology (Tebu Bio, Milan, Italy). AQP2-pS261 (AQP2 (pSer261) NB100-61100) antibody was from Novus Biologicals (Littleton, CO, United States).

p38MAPK (9212) and phospho-p38 MAPK (Thr180/Tyr182; #9211S) antibodies were obtained from Cell Signaling Technologies Inc., Beverly, MA.

Secondary goat anti-rabbit and mouse antibodies conjugated to horseradish peroxidase (HRP) were obtained from Merck (Merck KGaA, Darmstadt, Germany), whereas secondary donkey anti-goat antibody conjugated to horseradish peroxidase (HRP) was purchased from Santa Cruz Biotechnology (Tebu Bio, Milan, Italy). Secondary goat anti-rabbit Alexa 488 and anti-mouse Alexa 555 conjugate antibodies were from Molecular Probes (Eugene, OR, United States).

Animal models

Hind-limb suspended C57BL6 male and female mice were subjected to the tail suspension technique, according to recommendations by Morey-Holton et al. (2005) and as previously described (Sanesi et al., 2023). Mice were suspended to prevent any contact of the hind limbs with the cage floor, maintaining approximately a 30° head-down tilt. The forelimbs of animals were in contact with the cage bottom to guarantee full access to the entire cage. Each mouse was singly housed, with access to water and regular diet ad libitum (Harlan Teklad, 2019, SDS, England) and maintained under standard conditions on a 12/12 h light/dark cycle. 8-Week-old male and female mice C57BL6 were randomly assigned to two groups: mice kept in control condition (4 weeks Rest, n = 8, four males and four females) and hind-limb unloading suspended mice (4 weeks HU, n = 8, four males and four females) and mice kept in control condition (1 week Rest, n = 7, four males and three females) and hind-limb unloading suspended mice (1 week HU, n = 7, four males and three females). Mice were weighed once a week and at the end of the experimental procedures were euthanized. Both left and right kidney were surgically excised and stored at −80°C until analysis.

This animal interventional study is in accordance with the European Law Implementation of Directive 2010/63/EU and all experimental protocols were reviewed and approved by the Veterinary Department of the Italian Ministry of Health (Project 522- 2016PR).

Serum copeptin measurement

Serum copeptin levels were quantified in this study. To obtain the serum samples, blood was collected, and the tubes were immediately placed on ice and subjected to centrifugation at 1,600 × g for 15 min at 4°C. This centrifugation process facilitated the separation of serum from other blood components. The collected serum

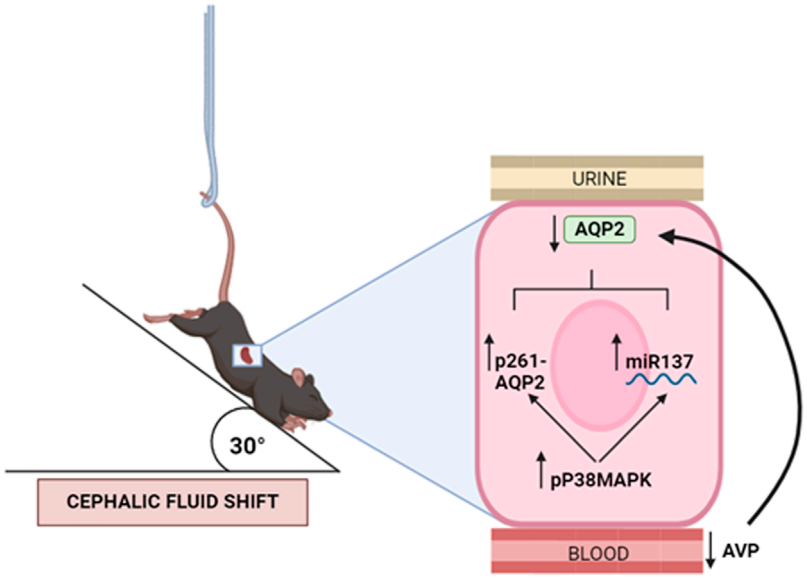

FIGURE 9
Proposed model of kidney mice adaptation to 4 weeks hindlimb suspension (HU). HU suspension is associated with reduced secretion of vasopressin (copeptin) hormone and selective reduction of AQP2 expression, with no change in the expression of other renal AQPs. The AQP2 downregulation occurs through an increased activity of p38MAPK which in turn promotes internalization and degradation via phosphorylation of AQP2 in Ser261 and decreases the AQP2 mRNA translation via miR137.

samples were promptly stored at a temperature of −80°C until they were ready for further analysis.

The levels of Copeptin (CPP) were measured using an ELISA kit (Cloud-Clone Corp., TX, United States). This kit offers high sensitivity and excellent specificity for copeptin detection, with a detection limit lower than 9.6 pg/mL.

Serum Osmolality measurement

Serum Osmolality was measured by using VAPRO® Vapor Pressure Osmometer (Wescor Model 5,520; Wescor Inc., United States).

Tissue preparation

Studies in kidney slices were performed as described (Boone and Deen, 2008). In brief, kidneys were quickly excised and thin traversal slices (500 µm), including cortex and medulla, were obtained using a stereomicroscope. Kidney sections were then equilibrated in a kidney slices buffer (118 mM NaCl, 16 mM HEPES, 17 mM Na-HEPES, 14 mM Glucose, 3.2 mM KCl, 2.5 mM $CaCl_2$, 1.8 mM $MgSO_4$, and 1.8 mM KH_2PO_4, pH 7.4) for 10 min. The kidney slices were maintained at 37°C untreated or treated with 10 µM SB203580 for 30 min. Subsequently, the kidney slices were homogenized in ice-cold kidney slices buffer supplemented with protease (1 mM PMSF, 20 µM leupeptin and 2 µg/mL pepstatin A) and phosphatase (10 mM NaF and 1 mM sodium orthovanadate) inhibitors, using a mini potter. Suspensions were then centrifuged at 12,000 x g for 10 min at 4°C and the supernatants used for Western blotting analysis.

Gel electrophoresis and immunoblotting

60 µg of proteins were separated using 12% stain-free polyacrylamide gels (Bio-Rad Laboratories, Inc., Hercules, CA, United States) under reducing conditions. Protein bands were electrophoretically transferred onto Immobilon-P membranes (Millipore Corporate Headquarters, Billerica, United States) for Western blot analysis. These membranes were blocked in TBS-Tween-20 solution containing 3% bovine serum albumin (BSA) and incubated overnight with primary antibodies. anti-AQP2, anti-pS261AQP2, anti-AQP3, anti-AQP4, anti-p38MAPK, and anti-Pp38MAPK were used at 1:500 dilution.

Immunoreactive bands were detected using secondary antibodies (goat anti-rabbit, goat anti-mouse and donkey anti-goat) conjugated to horseradish peroxidase (HRP), which were obtained from Santa Cruz Biotechnologies (Tebu-Bio, Milan, Italy). Membranes were developed using Clarity Western ECL Substrate with the ChemiDoc System gels (Bio-Rad Laboratories, Milan, Italy).

Obtained bands were normalized to total protein using stain-free technology gels. Densitometry was performed using Image Lab software (Bio-Rad Laboratories, Milan, Italy), and the data were analyzed using GraphPad Prism (GraphPad Software, San Diego, CA, United States).

Isolation of total RNA, reverse transcription, and real-time PCR analysis of mRNA of AQP2 in REST and HU mice

To evaluate the expression level of mRNA of AQP2 in the kidney papillae isolated from REST and HU mouse, real-time

PCR experiments were conducted. Total RNA was extracted from the samples using Trizol method (Thermo Fisher Scientific). Reverse transcription was performed on 2 μg of total RNA using SuperScript Vilo Master Mix (Invitrogen, Life Technologies, Monza, Italy). Real-time PCR amplification was carried out using TaqMan Gene Expression PCR Master Mix with AQP2 assay (Assay ID: Mm00437575_m1), using 18S assays (Assay ID: Hs99999901_s1) as housekeeping gene in the StepOne Real-Time PCR System (Thermo Fisher Scientific, Waltham, MA, United States), setting the thermal cycling conditions as specified by the manufacturer (95°C for 20 s; 40 cycles alternatively at 95°C for 1 s and 60°C for 20 s). Results were quantified as $2^{-\Delta\Delta Ct}$ values, representing the relative expression levels. The calculation of ΔΔCt was based on the following formula: $\Delta\Delta Ct = (Ct_{target}-Ct_{18S})_{HU} - (Ct_{target}-Ct_{18S})_{REST}$.

Isolation of total RNA, reverse transcription, and real-time PCR analysis of miRNA-137 in REST and HU mice

The miRNA-137 levels in the kidney papillae of REST and HU mice were assessed using TaqMan Advanced miRNA Assays (has-miR-137; Assay ID: 477904_mir; Applied Biosystems), which provided highly sensitive and specific quantification of mature miRNA through quantitative PCR. Total RNA was extracted from the samples using Trizol method (Thermo Fisher Scientific). Reverse transcription was performed on 5 ng of total RNA using the TaqMan Advanced miRNA cDNA Synthesis Kit (Applied Biosystems). A calibration line was generated using a synthetic RNA (UUAUUGCUUAAGAAUACGCGUAG) with a 5′-phosphate, synthesized by Applied Biosystems, to accurately evaluate the miR137 content (in ng) in the samples from REST and HU mice by interpolating the miRNA values.

Immunofluorescence

Mouse kidneys were fixed overnight by immersion in 4% (w/v) paraformaldehyde at 4°C, washed in PBS and cryopreserved in 30% (w/v) sucrose in PBS at 4°C for 24 h, and then embedded in paraffin medium. Thin sections (5 μm) were subject to immunofluorescence analysis as follows: after blocking with 1% BSA in PBS for 20 min at room temperature, sections were incubated overnight at 4°C with primary antibodies anti-AQP2 and anti-pS261AQP2. The following day sections were washed three times with PBS and stained with 1:1,000 donkey anti-rabbit Alexa Fluor 488 (Thermo Fisher Scientific, Waltham, MA, United States) or with 1:1,000 anti-mouse Alexa Fluor 555 (Thermo Fisher Scientific, Waltham, MA, United States) for 1 h at room temperature. Next, slides were washed three times with PBS and coverslips were applied onto them, using Mowiol Mounting Medium (Merck KGaA, Darmstadt, Germany). Confocal images were obtained with a confocal laser-scanning fluorescence microscope (Nikon AX R).

Statistical analysis

Statistical analysis was performed using unpaired parametric two-tailed t-test and paired two-tailed t-test for ctrl vs. SB203580 experiments. All values are presented as a means with their corresponding standard error medium (S.E.M.). The difference of $p < 0.05$ was considered statistically significant.

Data availability statement

The raw data supporting the conclusions of this article will be made available by the authors, without undue reservation.

Ethics statement

The animal study was approved by European Law Implementation of Directive 2010/63/EU and all experimental protocols were reviewed and approved by the Veterinary Department of the Italian Ministry of Health (Project 522- 2016PR). The study was conducted in accordance with the local legislation and institutional requirements.

Author contributions

MR: Conceptualization, Data curation, Formal Analysis, Investigation, Methodology, Supervision, Writing – original draft, Writing – review and editing. MV: Data curation, Formal Analysis, Investigation, Methodology, Writing – original draft, Writing – review and editing. GS: Formal Analysis, Investigation, Methodology, Writing – original draft, Writing – review and editing. AF: Data curation, Methodology, Software, Writing – original draft, Writing – review and editing. MD: Data curation, Investigation, Methodology, Writing – original draft, Writing – review and editing. MC: Data curation, Formal Analysis, Writing – original draft, Writing – review and editing. AD: Data curation, Formal Analysis, Writing – original draft, Writing – review and editing. RZ: Data curation, Formal Analysis, Methodology, Writing – original draft, Writing – review and editing. GT: Conceptualization, Formal Analysis, Project administration, Supervision, Writing – original draft, Writing – review and editing. MG: Conceptualization, Data curation, Formal Analysis, Funding acquisition, Methodology, Project administration, Resources, Supervision, Validation, Writing – original draft, Writing – review and editing. GV: Conceptualization, Data curation, Formal Analysis, Funding acquisition, Investigation, Methodology, Project administration, Resources, Supervision, Writing – original draft, Writing – review and editing.

Funding

The author(s) declare that financial support was received for the research and/or publication of this article. This work was supported by the Italian Space Agency (ASI, MARS-PRE Project, Grant No. DC-VUM-2017-006). M.R. is supported financially by POR Puglia FESR FSE 2014-2020 – Asse X - Azione 10.4. – Atto Dirigenziale 162/DIR/2019/00057 del 13/05/2019: Avviso pubblico n. 2/FSE/2019 “Research for Innovation” (REFIN) –

(code 4FC8E072). A.D.M is supported by "Attrazione e Mobilità dei Ricercatori, PON "R&I" 2014–2020, Azione I.2" (code AIM1893457-3, linea 1).

Acknowledgments

The authors thank Mariangela Satalino (MyBiolab, Bari) for the technical support.

Conflict of interest

The authors declare that the research was conducted in the absence of any commercial or financial relationships that could be construed as a potential conflict of interest.

Generative AI statement

The authors declare that no Generative AI was used in the creation of this manuscript.

Publisher's note

Supplementary material

The Supplementary Material for this article can be found online at: https://www.frontiersin.org/articles/10.3389/fphys.2025.1535053/full#supplementary-material

SUPPLEMENTARY FIGURE 1
Expression of AQP3 and AQP4 in 4 weeks HU and REST mice. Kidneys from HU and REST mice were lysed, and immunoblotting experiments were performed using specific antibodies against AQP3 and AQP4. Densitometric analysis of AQP3 and AQP4 bands normalized to the total protein content is reported in the histogram. Data are expressed as mean ± S.E.M. (O.D.). Statistical analysis was done using Unpaired t-test.

References

Barkaszi, I., Ehmann, B., Tölgyesi, B., Balázs, L., and Altbäcker, A. (2022). Are head-down tilt bedrest studies capturing the true nature of spaceflight-induced cognitive changes? A review. *Front. Physiol.* 13, 1008508. doi:10.3389/fphys.2022.1008508

Beysens, D., and Loon, J. (2015). *Generation and applications of extra-terrestrial environments on earth*. Denmark: River Publishers, 1–318.

Bhattacharya, S. K., Chakrabarti, A., and Glover, V. (1998). Stress and water balance: the roles of ANP, AVP and isatin. *Indian J. Exp. Biol.* 36 (12), 1195–1200.

Bilancio, G., Lombardi, C., Pisot, R., Mekjavic, I. B., De Santo, N. G., Luciano, M. G., et al. (2013). Effects of prolonged immobilization on sequential changes in mineral and bone disease parameters. *Am. J. Kidney Dis.* 61 (5), 845–847. doi:10.1053/j.ajkd.2012.10.015

Boone, M., and Deen, P. M. (2008). Physiology and pathophysiology of the vasopressin-regulated renal water reabsorption. *Pflugers Arch.* 456 (6), 1005–1024. doi:10.1007/s00424-008-0498-1

Centrone, M., Ranieri, M., Di Mise, A., D'Agostino, M., Venneri, M., Ferrulli, A., et al. (2022). AQP2 trafficking in health and diseases: an updated overview. *Int. J. Biochem. Cell Biol.* 149, 106261. doi:10.1016/j.biocel.2022.106261

Chung, S. Y., Kim, S. K., Hong, C. W., Oh, K. W., Kim, K. T., Sul, J. G., et al. (2012). The time-dependent alteration of anti-diuretic hormone system in hindlimb unloaded rats. *J. Physiol. Pharmacol.* 63 (1), 87–94.

Convertino, V. A., Doerr, D. F., Eckberg, D. L., Fritsch, J. M., and Vernikos-Danellis, J. (1990). Head-down bed rest impairs vagal baroreflex responses and provokes orthostatic hypotension. *J. Appl. Physiol.* 68 (4), 1458–1464. doi:10.1152/jappl.1990.68.4.1458

Drummer, C., Gerzer, R., Baisch, F., and Heer, M. (2000). Body fluid regulation in micro-gravity differs from that on Earth: an overview. *Pflugers Arch.* 441 (2-3 Suppl. l), R66–R72. doi:10.1007/s004240000335

Drummer, C., Norsk, P., and Heer, M. (2001). Water and sodium balance in space. *Am. J. Kidney Dis.* 38 (3), 684–690. doi:10.1053/ajkd.2001.27765

Fenton, R. A., Moeller, H. B., Hoffert, J. D., Yu, M. J., Nielsen, S., and Knepper, M. A. (2008). Acute regulation of aquaporin-2 phosphorylation at Ser-264 by vasopressin. *Proc. Natl. Acad. Sci. U. S. A.* 105 (8), 3134–3139. doi:10.1073/pnas.0712338105

Globus, R. K., and Morey-Holton, E. (2016). Hindlimb unloading: rodent analog for microgravity. *J. Appl. Physiol.* 120 (10), 1196–1206. doi:10.1152/japplphysiol.00997.2015

Grigoriev, A. I., Morukov, B. V., and Vorobiev, D. V. (1994). Water and electrolyte studies during long-term missions onboard the space stations SALYUT and MIR. *Clin. Investig.* 72 (3), 169–189. doi:10.1007/bf00189308

Heida, J. E., Boesten, L. S. M., Ettema, E. M., Muller Kobold, A. C., Franssen, C. F. M., Gansevoort, R. T., et al. (2017). Comparison of *ex vivo* stability of copeptin and vasopressin. *Clin. Chem. Lab. Med.* 55 (7), 984–992. doi:10.1515/cclm-2016-0559

Hoffert, J. D., Fenton, R. A., Moeller, H. B., Simons, B., Tchapyjnikov, D., McDill, B. W., et al. (2008). Vasopressin-stimulated increase in phosphorylation at Ser269 potentiates plasma membrane retention of aquaporin-2. *J. Biol. Chem.* 283 (36), 24617–24627. doi:10.1074/jbc.M803074200

Hoffert, J. D., Nielsen, J., Yu, M. J., Pisitkun, T., Schleicher, S. M., Nielsen, S., et al. (2007). Dynamics of aquaporin-2 serine-261 phosphorylation in response to short-term vasopressin treatment in collecting duct. *Am. J. Physiol. Ren. Physiol.* 292 (2), F691–F700. doi:10.1152/ajprenal.00284.2006

Hoffert, J. D., Pisitkun, T., Wang, G., Shen, R. F., and Knepper, M. A. (2006). Quantitative phosphoproteomics of vasopressin-sensitive renal cells: regulation of aquaporin-2 phosphorylation at two sites. *Proc. Natl. Acad. Sci. U. S. A.* 103 (18), 7159–7164. doi:10.1073/pnas.0600895103

Isobe, K., Jung, H. J., Yang, C. R., Claxton, J., Sandoval, P., Burg, M. B., et al. (2017). Systems-level identification of PKA-dependent signaling in epithelial cells. *Proc. Natl. Acad. Sci. U. S. A.* 114 (42), E8875–E8884. doi:10.1073/pnas.1709123114

Kharin, A., and Klussmann, E. (2024). Many kinases for controlling the water channel aquaporin-2. *J. Physiol.* 602 (13), 3025–3039. doi:10.1113/jp284100

Kim, J. E., Jung, H. J., Lee, Y. J., and Kwon, T. H. (2015). Vasopressin-regulated miRNAs and AQP2-targeting miRNAs in kidney collecting duct cells. *Am. J. Physiol. Ren. Physiol.* 308 (7), F749–F764. doi:10.1152/ajprenal.00334.2014

Leach, C. S., Alfrey, C. P., Suki, W. N., Leonard, J. I., Rambaut, P. C., Inners, L. D., et al. (1996). Regulation of body fluid compartments during short-term spaceflight. *J. Appl. Physiol.* 81 (1), 105–116. doi:10.1152/jappl.1996.81.1.105

Le Roux, E., De Jong, N. P., Blanc, S., Simon, C., Bessesen, D. H., and Bergouignan, A. (2022). Physiology of physical inactivity, sedentary behaviours and non-exercise activity: insights from the space bedrest model. *J. Physiol.* 600 (5), 1037–1051. doi:10.1113/jp281064

Matsumura, Y., Uchida, S., Rai, T., Sasaki, S., and Marumo, F. (1997). Transcriptional regulation of aquaporin-2 water channel gene by cAMP. *J. Am. Soc. Nephrol.* 8 (6), 861–867. doi:10.1681/asn.v86861

Milstead, J. R., Simske, S. J., and Bateman, T. A. (2004). Spaceflight and hindlimb suspension disuse models in mice. *Biomed. Sci. Instrum.* 40, 105–110.

Moeller, H. B., Olesen, E. T., and Fenton, R. A. (2011). Regulation of the water channel aquaporin-2 by posttranslational modification. *Am. J. Physiol. Ren. Physiol.* 300 (5), F1062–F1073. doi:10.1152/ajprenal.00721.2010

Moore, T. P., and Thornton, W. E. (1987). Space shuttle inflight and postflight fluid shifts measured by leg volume changes. *Aviat. Space Environ. Med.* 58 (9 Pt 2), A91–A96.

Morey, E. R. (1979). Spaceflight and bone turnover: correlation with a new rat model of weightlessness. *BioScience* 29 (3), 168–172. doi:10.2307/1307797

Morey-Holton, E., Globus, R. K., Kaplansky, A., and Durnova, G. (2005). The hindlimb unloading rat model: literature overview, technique update and comparison with space flight data. *Adv. Space Biol. Med.* 10, 7–40. doi:10.1016/s1569-2574(05)10002-1

Morey-Holton, E. R., and Globus, R. K. (2002). Hindlimb unloading rodent model: technical aspects. *J. Appl. Physiol.* 92 (4), 1367–1377. doi:10.1152/japplphysiol.00969.2001

Nedvetsky, P. I., Tabor, V., Tamma, G., Beulshausen, S., Skroblin, P., Kirschner, A., et al. (2010). Reciprocal regulation of aquaporin-2 abundance and degradation by protein kinase A and p38-MAP kinase. *J. Am. Soc. Nephrol.* 21 (10), 1645–1656. doi:10.1681/asn.2009111190

Norsk, P., Christensen, N. J., Bie, P., Gabrielsen, A., Heer, M., and Drummer, C. (2000). Unexpected renal responses in space. *Lancet* 356 (9241), 1577–1578. doi:10.1016/s0140-6736(00)03135-4

Olde Engberink, R. H. G., van Oosten, P. J., Weber, T., Tabury, K., Baatout, S., Siew, K., et al. (2023). The kidney, volume homeostasis and osmoregulation in space: current perspective and knowledge gaps. *NPJ Microgravity* 9 (1), 29. doi:10.1038/s41526-023-00268-1

Procino, G., Mastrofrancesco, L., Tamma, G., Lasorsa, D. R., Ranieri, M., Stringini, G., et al. (2012). Calcium-sensing receptor and aquaporin 2 interplay in hypercalciuria-associated renal concentrating defect in humans. An *in vivo* and *in vitro* study. *PLoS One* 7 (3), e33145. doi:10.1371/journal.pone.0033145

Qaisar, R., Karim, A., and Elmoselhi, A. B. (2020). Muscle unloading: a comparison between spaceflight and ground-based models. *Acta Physiol. (Oxf)* 228 (3), e13431. doi:10.1111/apha.13431

Ranieri, M. (2019). Renal Ca(2+) and water handling in response to calcium sensing receptor signaling: physiopathological aspects and role of CaSR-regulated microRNAs. *Int. J. Mol. Sci.* 20 (21), 5341. doi:10.3390/ijms20215341

Ranieri, M., Angelini, I., D'Agostino, M., Di Mise, A., Centrone, M., Venneri, M., et al. (2024). *In vivo* treatment with calcilytic of CaSR knock-in mice ameliorates renal phenotype reversing downregulation of the vasopressin-AQP2 pathway. *J. Physiol.* 602 (13), 3207–3224. doi:10.1113/jp284233

Ranieri, M., Di Mise, A., Tamma, G., and Valenti, G. (2019). Vasopressin-aquaporin-2 pathway: recent advances in understanding water balance disorders. *F1000Res.* 8. doi:10.12688/f1000research.16654.1

Ranieri, M., Zahedi, K., Tamma, G., Centrone, M., Di Mise, A., Soleimani, M., et al. (2018). CaSR signaling down-regulates AQP2 expression via a novel microRNA pathway in pendrin and NaCl cotransporter knockout mice. *FASEB J.* 32 (4), 2148–2159. doi:10.1096/fj.201700412RR

Rittweger, J., Simunic, B., Bilancio, G., De Santo, N. G., Cirillo, M., Biolo, G., et al. (2009). Bone loss in the lower leg during 35 days of bed rest is predominantly from the cortical compartment. *Bone* 44 (4), 612–618. doi:10.1016/j.bone.2009.01.001

Sanesi, L., Storlino, G., Dicarlo, M., Oranger, A., Zerlotin, R., Pignataro, P., et al. (2023). Time-dependent unloading effects on muscle and bone and involvement of FNDC5/irisin axis. *NPJ Microgravity* 9 (1), 4. doi:10.1038/s41526-023-00251-w

Sullivan, M. J., Hasser, E. M., Moffitt, J. A., Bruno, S. B., and Cunningham, J. T. (2004). Rats exhibit aldosterone-dependent sodium appetite during 24 h hindlimb unloading. *J. Physiol.* 557 (Pt 2), 661–670. doi:10.1113/jphysiol.2004.062265

Tamma, G., Di Mise, A., Ranieri, M., Svelto, M., Pisot, R., Bilancio, G., et al. (2014). A decrease in aquaporin 2 excretion is associated with bed rest induced high calciuria. *J. Transl. Med.* 12, 133. doi:10.1186/1479-5876-12-133

Thornton, W. E., Hedge, V., Coleman, E., Uri, J. J., and Moore, T. P. (1992). Changes in leg volume during microgravity simulation. *Aviat. Space Environ. Med.* 63 (9), 789–794.

Trepiccione, F., Pisitkun, T., Hoffert, J. D., Poulsen, S. B., Capasso, G., Nielsen, S., et al. (2014). Early targets of lithium in rat kidney inner medullary collecting duct include p38 and ERK1/2. *Kidney Int.* 86 (4), 757–767. doi:10.1038/ki.2014.107

Valenti, G., Fraszl, W., Addabbo, F., Tamma, G., Procino, G., Satta, E., et al. (2006). Water immersion is associated with an increase in aquaporin-2 excretion in healthy volunteers. *Biochim. Biophys. Acta* 1758 (8), 1111–1116. doi:10.1016/j.bbamem.2006.03.029

Valenti, G., Laera, A., Pace, G., Aceto, G., Lospalluti, M. L., Penza, R., et al. (2000). Urinary aquaporin 2 and calciuria correlate with the severity of enuresis in children. *J. Am. Soc. Nephrol.* 11 (10), 1873–1881. doi:10.1681/asn.v11101873

Wade, C. E., and Morey-Holton, E. (1998). Alteration of renal function of rats following spaceflight. *Am. J. Physiol.* 275 (4 Pt 2), R1058–R1065. doi:10.1152/ajpregu.1998.275.4.r1058

Watenpaugh, D. E. (2016). Analogs of microgravity: head-down tilt and water immersion. *J. Appl. Physiol.* 120 (8), 904–914. doi:10.1152/japplphysiol.00986.2015

frontiers | Frontiers in Physiology

TYPE Original Research
PUBLISHED 30 May 2025
DOI 10.3389/fphys.2025.1572854

OPEN ACCESS

EDITED BY
Roberto Piacentini,
Catholic University of the Sacred Heart, Italy

REVIEWED BY
Paola Tognini,
Sant'Anna School of Advanced Studies, Italy
Koustubh Vaze,
University of Michigan, United States

*CORRESPONDENCE
Cristina Limatola,
cristina.limatola@uniroma1.it
Giuseppina D'Alessandro,
giuseppina.dalessandro@uniroma1.it

†These authors have contributed equally to this work and share last authorship

RECEIVED 07 February 2025
ACCEPTED 19 May 2025
PUBLISHED 30 May 2025

CITATION
Marrocco F, Khan R, Reccagni A, Lin X, Delli Carpini M, Iebba V, D'Alessandro G and Limatola C (2025) Fecal or bacterial transplantation in mice transfer environment-induced brain plasticity and associated behavioral changes.
Front. Physiol. 16:1572854.
doi: 10.3389/fphys.2025.1572854

Fecal or bacterial transplantation in mice transfer environment-induced brain plasticity and associated behavioral changes

Francesco Marrocco[1], Rizwan Khan[1], Alice Reccagni[1], Xingzi Lin[1], Mary Delli Carpini[1], Valerio Iebba[2], Giuseppina D'Alessandro[1,3]*† and Cristina Limatola[3,4]*†

[1]Department of Physiology and Pharmacology, Sapienza University, Rome, Italy, [2]Gustave Roussy Cancer Campus, ClinicObiome, Villejuif, France, [3]IRCCS Neuromed, Pozzilli, Italy, [4]Laboratory affiliated with Instituto Pasteur, Department of Physiology and Pharmacology, Sapienza University, Rome, Italy

Introduction: Recent studies have shown that lifestyle factors, including diet and environmental stimuli, significantly alter the composition of gut microbiota and the metabolites they produce. Specifically, housing mice in an enriched environment (EE) enhances the production of short-chain fatty acids, which in part mediate the effects of EE on brain plasticity. In this study, we tested the hypothesis that the gut microbial composition of EE-exposed mice could be transplanted into mice housed in a standard environment (SE) to replicate the environmental effects on behavior, gene expression and neurogenesis.

Methods: To test this hypothesis, we transplanted either a specific bacterial mixture or fecal material from EE-housed mice into SE-housed mice.

Results: Our data show that both bacterial and fecal transplants reduce anxiety-like behaviors in mice. Additionally, we observed increased expression of hippocampal neurotrophins and enhanced neurogenesis.

Discussion: These findings support the idea that gut microbiota influence brain functions, including anxiety-like behavior. Further research is necessary to clarify the underlying mechanisms. Moreover, the results suggest that fecal material transplantation (FMT) from individuals with healthy lifestyles may represent a promising strategy for the treatment of mood disorders.

KEYWORDS

enriched environment, fecal material transplantation, animal behavior, neurogenesis, gut-brain axis

1 Introduction

The gut microbiota consists of the microbial community residing in the gastrointestinal tract. These microorganisms are crucial for various biochemical processes, including the digestion of diet-derived fiber (Rosenberg and Zilber-Rosenberg, 2016), which leads to the production of short-chain fatty acids (SCFAs). SCFAs, in turn, influence the growth of other microbes and play a role in modulating both local and peripheral immune functions (Han et al., 2017; Jandhyala, 2015). The composition of the gut microbiota is not static and

undergoes changes from birth, adapting to different stimuli such as diet (Palmer et al., 2007), medications, and physical exercise (Sommer and Bäckhed, 2013). Despite these fluctuations, the adult microbiota remains relatively stable, with approximately 90% of the bacterial population belonging to the Firmicutes and Bacteroidetes phyla (Costello et al., 2009). The dynamic balance between the host and its commensal microbes provides several benefits, including maintaining gut barrier integrity, aiding in food digestion, and storing energy (Rowland et al., 2018). Disruptions to this balance can lead to adverse effects on host homeostasis, contributing to metabolic disorders such as diabetes and obesity (Al Bataineh et al., 2023; Contreras-Rodriguez et al., 2022), as well as neurodevelopmental and psychiatric conditions like autism spectrum disorder, anxiety, and depression (Felice and O'Mahony, 2017; Xu et al., 2021). Recently, fecal material transplantation (FMT) has emerged as a potential therapeutic approach for gut dysbiosis, using fecal material from healthy donors, with promising results observed in both animal models and human trials (Xu et al., 2021). However, the mechanisms underlying these beneficial effects remain poorly understood. Recent studies have explored the impact of housing mice in an enriched environment (EE) on gut microbiota and metabolome composition (Lupori et al., 2022; Marrocco et al., 2022). EE, characterized by enhanced motor, sensory, and social stimuli, has been shown to boost hippocampal neurogenesis, improve learning and memory, and reduce depressive-like behaviors (Chen et al., 2024a). On a molecular level, these changes are linked to increased expression of neurotrophins such as BDNF (Cancedda et al., 2004) and NGF (Birch et al., 2013). Additionally, EE has been associated with higher levels of fecal SCFAs, particularly formate and acetate, and distinct microbial populations compared to mice housed in standard environments (SE). These SCFAs are thought to mediate some of the beneficial effects of EE on the brain (Lupori et al., 2022; Marrocco et al., 2022). In this study, we investigated whether the bacterial strains associated with EE could transfer an "enriched" phenotype to control mice. We also performed FMT from EE-housed mice to control mice to evaluate the effects of the complete gut material—microbes and metabolites—on brain function. Our findings show that both bacterial transplantation and FMT alleviated anxiety-like behavior and increased BDNF expression in the hippocampus. Notably, FMT had more pronounced effects on neurotrophin expression and neurogenesis compared to bacterial transplantation alone. These results provide new evidence that gut microbes, their metabolites, or whole fecal content from EE-exposed mice may offer potential therapeutic strategies to address neuropsychiatric disorders.

2 Materials and methods

2.1 Mice and environmental enrichment protocol

All the experiments conducted were approved by the Italian Ministry of Health (authorization no. 775/2020-PR) under the guidelines of the European Community Council Directive (2010/63/EU) and from Italian D.Lgs 26/2014 for the ethical use of animals in laboratory research. Male C57BL6/N mice, 3 or 4 weeks old, were purchased from Charles River (Calco, Italy). Only male mice were used to avoid possible sex-specific alteration in microbial content (Snigdha et al., 2022). Mice were housed under a 12-h light/dark cycle with animal room's temperature around 20°C–23°C in standard cages (30 cm × 16 cm × 11 cm) with autoclaved drinking water, nesting material composed by strips of paper (Sizzle-pad, Caipet), and standard chow (Altromin, 1310) *ad libitum*. For the EE protocol, at least ten 3-weeks-old mice were raised in a larger cage (36 cm × 54 cm × 19 cm) with different stimuli: two running wheels, tubes, house and plastic objects for 5 weeks, changing tools twice a week respecting the EE setting with different position of tools (Marrocco et al., 2022). Three or two mice were housed in SE cages. In both experimental groups, the bedding materials were changed once a week.

2.2 Stool collection and processing

At the end of the different treatments, fresh stools were collected, frozen, and stored for metagenomic analysis of bacterial composition. Fecal bacterial DNA was extracted with a QIAmp fast DNA Stool mini-kit (51604, QIAGEN) according to the manufacturer's instructions.

2.3 Library preparation and sequencing

Library preparation has been carried out using primer combination Pro341F (CCTACGGGNBGCASCAG) and Pro805R (GACTACNVGGGTATCTAATCC) to amplify the V3-V4 region of 16S rRNA. Subsequently, all samples have been sequenced in 300 paired-end with an Illumina MiSeq platform.

2.4 Bioinformatic analysis

Raw fastq files were analyzed with DADA2 pipeline v.1.14 for quality check and filtering (sequencing errors, denoising, chimerae detection). Filtering parameters were as follows: truncLen = 0, minLen = 100, maxN = 0, maxEE = 2, truncQ = 11, trimLeft = 15. All the other parameters in the DADA2 pipeline for paired-end were left as default. Bioinformatic and statistical analyses on recognized ASV were performed with Python v.3.8.2. Each ASV sequence underwent a nucleotide Blast using the National Center for Biotechnology Information (NCBI) Blast software (ncbi-blast-2.3.0) and the latest NCBI 16 S Microbial Database (https://ftp://ftp.ncbi.nlm.nih.gov/blast/db/). Bacterial species present in blanks (washing and water samples) and not having a biological meaning (environmental, rumen, extra-mammals, food, etc.) were excluded, thus the resulting species were considered for subsequent statistical analyses. The relative species abundances used are available in Supplementary Table 1.

2.5 Statistics and reproducibility

Measurements of α diversity (within sample diversity) such as Richness and Shannon index, were calculated at species level using the SciKit-learn package v1.0.1, starting from raw reads

counts. For beta-diversity, data matrices were first transformed with pseudocount and centered-log-ratio (CLR), then normalized and standardized using QuantileTransformer and StandardScaler methods from Sci-Kit learn package v1.0.1. Normalization using the output_distribution = "normal" option transforms each variable to a Gaussian-like shaped distribution, whilst the standardization results in each normalized variable having a mean of zero and variance of one. Exploratory analysis of β-diversity (between sample diversity) was calculated using the Bray-Curtis measure of dissimilarity and represented in Principal Coordinate Analyses (PcoA), along with methods to compare groups of multivariate sample units (analysis of similarities - ANOSIM, permutational multivariate analysis of variance - PERMANOVA) to assess significance in data points clustering. ANOSIM and PERMANOVA were automatically calculated after 999 permutations, implemented with custom scripts (Python v3.8.2, Seaborn v0.11.2, SciKit-learn v1.0.1). We implemented Partial Least Square Discriminant Analysis (PLS-DA) and the subsequent Variable Importance Plot (VIP) as a supervised analysis wherein the VIP values (order of magnitude) are used to identify the most discriminant bacterial species among the cohorts. Mann–Whitney U test and Kruskal–Wallis test were employed to assess significance for pairwise or multiple comparisons, respectively, considering a P value< =0.05 as significant. Where clearly stated, all P values were corrected for multiple hypothesis testing using a two-stage Benjamini–Hochberg FDR at 10%.

2.6 EE-related bacteria transplantation

All the following lyophilized bacteria administered to mice by oral gavage were obtained from Leibniz-institute DSMZ GMBH: *Bacteroides gallinarum* (DSM18171), *Parasutterella excrementishominis* (DSM21040), *Catabacter hongkongensis* (DSM18959), *Alistipes senegalensis* (DSM25460), *Clostridium Kluyveri* (DSM555). These bacteria were selected from those previously identified in mice reared in an enriched environment (Marrocco et al., 2022). The bacteria were resuspended and activated each time before the administration. Briefly, five different vials each containing a strain were broken under the radial sterilizing field of the Bunsen burner apparatus Each lyophilized strain was resuspended in the anaerobe Wilkins Chalgren medium II (1568, Condalab) according to the manufacturer's procedures (Handling and Safety Information, DSMZ). The amount of bacteria administered via oral gavage was around 6.56 $\boldsymbol{X\,10^8}$ per strain, according to the 600 nm absorbance values measured. To prepare the gut to receive the new bacteria cohort, mice were treated with an antibiotic cocktail in the drinking water for 3 days. The bacterial oral gavages started after 1 day of washout from antibiotics and continued for 4 weeks once a week. Each mouse received 200 µL of bacterial cocktail or vehicle (the same amount of anaerobic medium only).

2.7 Antibiotic pre-treatment

To maximize the bacterial implantation in the gut, an antibiotic cocktail composed of ampicillin (1 mg/mL, ampicillin ready to use, ThermoFisher, J66972-AB), colistin (1 mg/mL, colistin sulfate, PanReac Applichen, 2922,0001) and streptomycin (5 mg/mL, streptomycin sulfate, PanReac Applichen 1852,0100), as previously described (Terrisse et al., 2021) was given to mice for 3 days before the oral gavage treatment of EE-related bacterial or vehicle. Mice subjected to fecal material transplantation were not pre-treated with antibiotics.

2.8 Fecal material transplantation

To prepare the samples for fecal material transplantation (FMT), three pieces of fresh stools from each mouse housed in EE or SE were collected in tubes containing 0.5 mL of PBS. The samples were gently resuspended with an inoculation loop (HS81121C, Merck), and then gently centrifuged (800 g for 3 min) to divide the undigested part from fecal water. To perform FMT we collected 200 µL of fecal water from each animal (donors) and gave the fecal water to receiver mice in a ratio of 1:1.

2.9 Behavioral test

Before testing, the mice were placed in the experimental environments for habituation (>10 min). After each test, the apparatus was carefully cleaned with 50% ethanol. The open field task was performed to study general locomotor activity, anxiety behavior, and willingness to explore after bacteria and fecal material transplantation. Mice were placed on the side of the arena (40 × 40 × 30 cm) The total distance travelled, movement duration and time spent in the center of arena (20 cm × 20 cm) were recorded for each mouse, for 10 min with ANY-MAZE software.

2.10 Immunofluorescence

Mice were sacrificed and intracardially perfused with PBS and PFA 4%. The brains were isolated and then post-fixed in PFA 4% for 24 h, cryopreserved with 30% sucrose, and frozen. Immunofluorescence staining was performed on cryostat sections (10 µm) of the hippocampal dentate gyrus (DG) region (one section every 240 µm, in the range of −1.46 mm to −2.80 mm from Bregma), the entire DG was acquired using a 20x scan slide. The brain sections were incubated for 1 h with 3% goat serum and 0.3% Triton-X-100, in PBS 0.1 M at RT. Sections were then incubated with rabbit anti-DCX (4604, Cell Signaling, USA) diluted in 1% goat serum and 0.1% Triton-X-100, in PBS 0.1 M at 4°C overnight. After washing in PBS, the sections were incubated with secondary antibody (donkey anti-rabbit, Alexafluor, Invitrogen) for 1 h and Hoechst (33342, Molecular Probes) for 5 min, washed and mounted on a microscope slide for the analysis of fluorescence (Eclipse, Nikon). The number DCX + cells in the DG were counted and normalized to the DG area by MetaMorph software.

2.11 RNA extraction and real-time PCR

Total mRNAs were collected from hippocampus of brain sections with RNeasy FFPE kit (73504, QIAGEN) according to

the manufacturer's instructions. The purity and quantity of mRNA was evaluated with Nanodrop One System (Thermo Scientific). One μg of total RNA was reverse transcribed (Mj Mini Thermal Cycler Biorad) using iScriptTM Reverse Transcription Supermix (Biorad) following the manufacturer's protocol: incubation at 25°C for 5 min, reverse transcription at 46°C for 20 min, inactivation 95°C for 1 min. Real-Time PCR (RT-PCR) was performed in a CFx Real-Time PCR System (Biorad) using SsoFastTM EvaGreen Supermix (Biorad) according to the manufacturer's instructions. Specific primer pairs, at a final concentration of 500 nM, were used to measure mRNA levels as follows: glyceraldehyde 3-phosphate dehydrogenase (gapdh) F5′-TTCGCAAAACAAGTTCACCA-3′ and R 5′-TCGTTGTGGTTGTA AATGGAA-3′, brain-derived neurotrophic factor (bdnf) F5′-CCATAAG GACGCGGACTTGTAC-3′ and R 5′-AGACATGTTTGCGGCATCCAGG-3′, nerve growth factor (ngf) F: 5′-ACA CTC TGA TCA CTG CGT TTT TG-3′ and R: 5′-CCT TCT GGG ACA TTG CTA TCT GT-3′, epidermal growth factor (Egf) F5′- AGC ATA CTC AGC GTC ACA GC-3′ and R 5′-GCA GGA CCG GCA CAA GTC-3′R′, vascular endothelial growth factor-a (Vegf-α)F5′-GAT CAT GCG GAT CAA ACC TC-3′, and R 5′-AAT GCT TTC TCC GCT CTG AA-3′. The PCR protocol consisted of 40 cycles of denaturation at 95°C for 30 s and annealing/extension at 58°C for 30 s. Melt curve analysis was performed at the end of every RT-q PCR to confirm the formation of a single PCR product. No template controls were added for each target to exclude possible sample contamination. The comparative threshold cycle (Ct) method was used for quantification analysis. The Ct values from each gene were normalized to the Ct value of Gapdh in the same RNA samples. Relative quantification was performed using the $2^{-\Delta\Delta CT}$ method and expressed as fold changes.

2.12 Statistical analysis

The number of replicates (n) for each experiment and the details of statistical analyses are described in the figure legends or main text. Data are presented as mean ± SEM. Statistical analysis were performed using GraphPad Prism 9 software. Exact p-values are given in the text and multiplicity adjusted p-values are given in the corresponding figures ($^{*}p < 0.05, ^{**}p < 0.01, ^{***}p < 0.001$). Unpaired Student's t-test is used for immunofluorescence analysis, real-time PCR.

3 Results

3.1 Administration of EE-related bacteria affects anxiety-like behavior and neurotrophins expression in mice

We previously demonstrated that housing mice in an EE affects their microbiota and metabolome composition, modulating hippocampal plasticity and gene expression (Marrocco et al., 2022). In particular, we identified a number of bacterial species characterizing the EE housing conditions and correlating with EE-induced changes (Marrocco et al., 2022). Now, we investigated whether treating mice with EE-related bacterial cohorts could affect mice behavior and brain plasticity. At this aim we treated mice with a bacterial consortium composed by *B. gallinarum, Parasutterella excrementihominis, Catabacter hongkongensis* (recently named *Christensenella hongkongensis), A. senegalensis, Clostridium kluyveri,* by oral gavage, once a week for four times. Three days pre-treatment with an antibiotic cocktail was performed to increase colonization of transplanted bacteria (Figure 1a). The fecal microbiota of mice undergoing bacterial transplantation (BT) showed no differences in species diversity (Shannon and inverse Simpson index, Figure 1b) or richness (Observed taxa, BT [n = 5]; C [n = 5] by Mann-Whitney test), when compared to the control group. At difference, the Bray-Curtis dissimilarity distance, employed to quantify beta diversity, showed a significant separation between BT and control groups suggesting that EE-related bacteria induced changes in terms of the composition of gut bacteria community (Figure 1c). Interestingly, the beta diversity metrics are affected by EE-related bacteria administration similarly to what previously reported for EE-housed mice (Marrocco et al., 2022). In addition, we performed Partial Least Square Discriminant Analysis (PLS-DA) and Variable Importance Plot (VIP) analysis to evaluate the colonization of the transplanted species. As shown in Figure 1d among the species highly associated with BT mice, we found that *P. excrementihominis* was the most representative species while none of the other transplanted species changed significantly compared to controls. To evaluate the effects of EE-related BT on anxiety-like behavior in mice, 10 min open field tests were performed. Three days after the last gavage, BT mice showed significant increases of the time spent in the center of the arena (Figure 1e, C [n = 5], 12 ± 3 s; BT [n = 5], 25 ± 4 s,$^{*}p = 0.0498$, Student's t-test) and of the total distance moved (C [n = 4], 19.41 ± 3.06 m; BT [n = 5] 28.6 ± 1.8 m,$^{*}p = 0.0296$, Student's t-test). In accordance, reduced times of immobility (freezing) were observed in BT mice compared to controls (C [n = 4], 47.2 ± 5.6 s; BT [n = 5], 25.4 ± 1.5 s,$^{**}p = 0.0042$, Student's t-test). We also verified that observed changes in behavior were not due to the administration of the antibiotics as shown in Supplementary Figure S1. To further investigate whether BT could modulate hippocampal gene expression, as reported for EE housed mice, quantitative PCR analysis was performed. Data reported in Figure 1f demonstrate an increased level of Bdnf (C [n = 5], 1.01 ± 0.07; BT [n = 4], 1.30 ± 0.08$^{*}p < 0.0272$; Student's t-test), while other neurotrophins were not modified by BT. Similarly, no difference in the number of DCX + positive cells in the dentate gyrus, indicative of new neuronal precursors generation (Figure 1g) was observed upon BT. These data indicate that the administration of EE-related bacteria partially replicates the beneficial effects EE on the brain.

3.2 Transplantation of fecal material from mice housed in EE affects anxiety-like behavior, neurotrophins expression and neurogenesis in receiving mice

As alternative approach to transfer the beneficial effects of EE on brain plasticity and anxiety-like behavior, we investigated the effects of fecal material transplantation from EE housed mice to control SE-housed mice. At this aim, stools were collected from donor mice living either in EE or SE (for at least 4 weeks), transplanted to receiving mice housed in SE by oral gavage (three times a week)

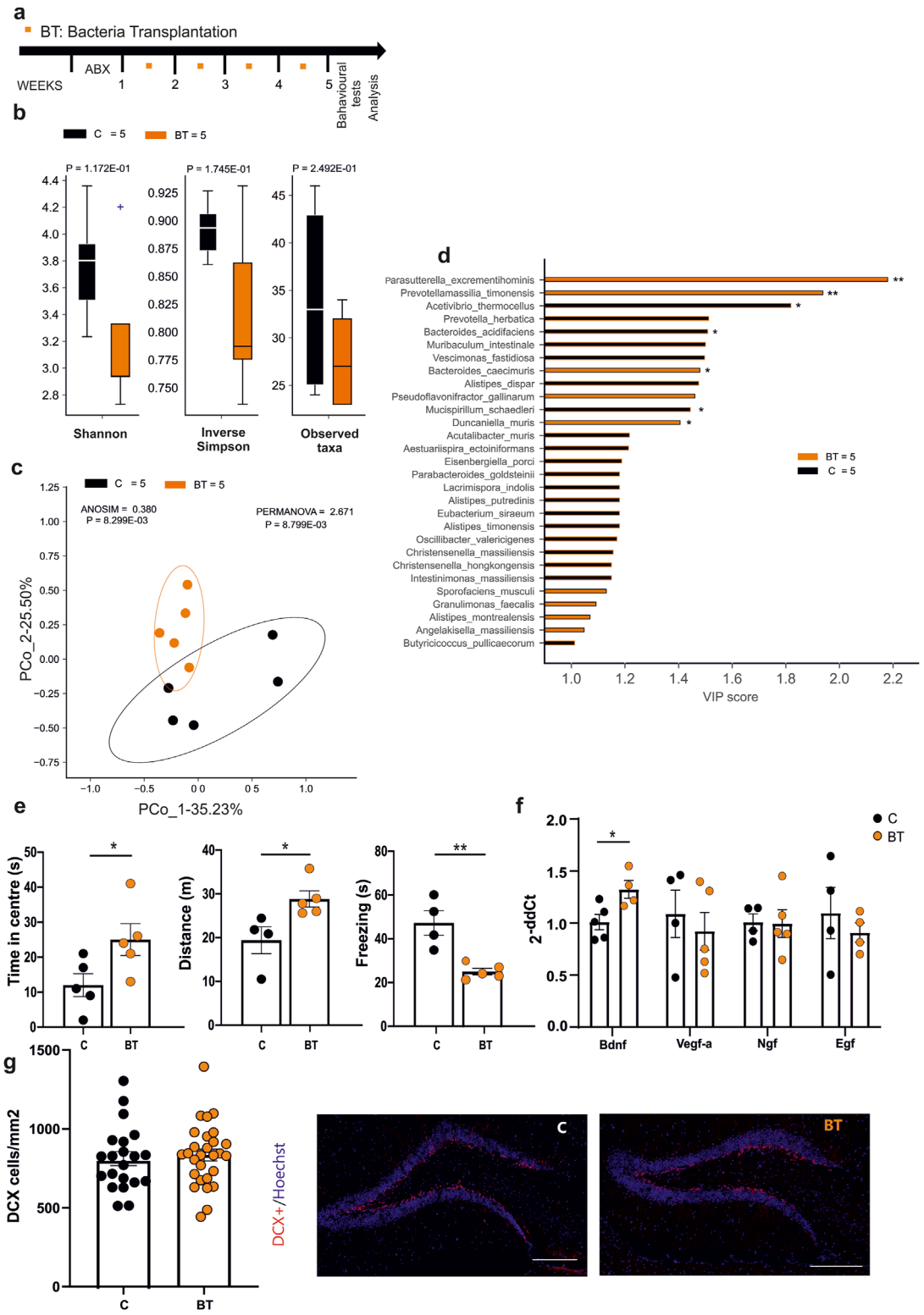

FIGURE 1
(a) Experimental protocol for EE-related Bacteria Transplantation (BT), including antibiotics treatment (3 days) and numbers of oral gavage (orange squares) per week. **(b)** Alpha-diversity (Shannon index, inverse Simpson and observed taxa) showed no differences in both biodiversity and richness metrics after the treatment (C n = 5 and BT n = 5). **(c)** Beta-diversity by the Bray-Curtis dissimilarity distance algorithm showed a significant separation of microbial communities in BT and control mice (C n = 5 and BT n = 5). **(d)** Variable Importance Plot (VIP) showed discriminant species after PLS-DA in descending order of VIP score (bar length), the highest relative abundance depending on the cohort (central bar color) and the lowest one (edge bar color); significant difference after Mann–Whitney U test (non-FDR,*P ≤ 0.05,**P ≤ 0.01;***P ≤ 0.001) between BT (n = 5) and Control (n = 5) groups **(e)** Open field test showed differences in time spent in the center (n = 5 Control and n = 5 BT) of the arena, distance moved (n = 4 Control and n = 5 BT) and time of the freezing episodes (n = 4 Control and n = 5 BT) (*p = 0.0498;*p = 0.0296;**p = 0.0042, by Student's t-test, respectively). **(f)** RT-qPCR
(*Continued*)

FIGURE 1 (Continued)
analysis of hippocampal neurotrophic factors: bar graphs showed increased level of Bdnf ($p < 0.05$ *, Student's t-test, two-tailed) in BT compared to control mice. No differences were found in Vegf-a, NGF, and EGF levels. Circles in the bar graph represent the number of samples (1 hippocampus from one animal) used for gene expression analysis. **(g)** Analysis of the neurogenesis in the hippocampal dentate gyrus (DG) in BT or control mice. Circles in the bar graphs show the total number of DCX + cells divided for total area of DG in mm^2in each slice analyzed (n = 4 Control animals, 21 slices and n = 5 BT animals, 28 slices; ns p = 0.50, by unpaired t-test). Data are presented as mean ±s.e.m. (g right): representative images of mouse hippocampal DG coronal sections (scan slides at ×20 magnification): DCX + cells (red) and nuclei (Hoechst, blue) in control and BT mice (scale bar, 100 μm).

and tested as shown in Figure 2a. Donors are thereafter indicated as SE- or EE-mice and receivers as FMT-SE- or FMT-EE-mice. We first assessed whether donor mice housed in EE showed less anxiety-like behaviour compared to SE donors, and at the end of the experiments we also examined the microbiota composition of both groups. As shown in Supplementary Figure S2, EE donor mice showed less anxiety-like behaviour as well as differences in alpha and beta diversity as previously shown (Marrocco et al., 2022), while PLS-DA VIP analysis partially recapitulated enriched species previously found in EE and SE. At the end of treatments, no significant differences were observed in biodiversity or richness of the fecal microbiota among FMT-SE and FMT-EE mice Figure 2b by Mann-Whitney test. Nevertheless, the Bray-Curtis dissimilarity distance algorithm showed a clear separation (Figure 2c). These data suggest that FMT transfer from mice housed in different environments mainly affects the interactions among microbial communities in the receiving mice. To possibly identify bacterial species distinctive for FMT-EE or FMT-SE cohorts, PLS-DA model and the VIP score were implemented. At least twenty species were distinctive for the EE group, and seven were more significantly enriched in EE, as shown in the pairwise analysis (Figure 2d). Among them *Sporofaciens musculi, Marasmitruncus massiliensis* showed the highest VIP scores possibly being involved in the effects observed. To further evaluate the effect of the different FMT treatments on receiver behavior, the open field tests were performed. The results of the test showed an increased time spent in the center of the arena for the FMT-EE compared to FMT-SE mice (Figure 2e, FMT SE = [n = 5], 30.88 ± 2.07 s; FMT EE = [n = 5], 46.24 ± 6.22 s,$^{*}p = 0.0473$; Student's t-test). No differences in the distance travelled and in freezing behavior were observed between the two groups. We also analyzed the effects of FMT treatment on the expression of neurotrophic factors and on neurogenesis in the hippocampal region. The analysis of gene expression showed significant changes in Bdnf (FMT-SE [n = 3] 1.006 ± 0.080; FMT-EE [n = 3] 20.390 ± 1.874,$^{***}p = 0.0005$), Vegf (FMT-SE [n = 3],1.002 ± 0.040; FMT-EE n = 3, 2.929 ± 0.369,$^{**}p = 0.006$) and Ngf (FMT-SE, [n = 4]; 1.001 ± 0.019; FMT-EE [n = 3],1.081 ± 0.007,$^{*}p = 0.02$ by unpaired t-test) (Figure 2f). In addition, we observed a significant increase of DCX + positive cells in FMT-EE mice compared to FMT-SE, emphasizing the role of gut contents on brain function (FMT SE [n = 59], 266.4 ± 18 cells/mm^2; FMT EE [n = 44], mean 379.1 ± 38.6 cells/mm^2,$^{**}p = 0.0051$; Student's t-test) (Figure 2g). Altogether these data demonstrate that several functions modulated by environmental housing conditions in mice could be transferred to SE housed mice through the fecal content of EE-housed mice.

4 Discussion

It has been described that gut microbiota composition participates in the regulation of host homeostasis and several recent evidence suggest direct and indirect implications of microbes in the modulation of brain microenvironment and functions (Rogers et al., 2016; Sorboni et al., 2022). The use of probiotics reduces the behavioral deficits and restores the microbiota composition in patients with major depressive disorder (MDD) (Huang et al., 2016) alleviating the gastrointestinal and psychiatric symptoms (Johnson et al., 2023). Microbe transplantation from healthy donors reduces memory loss in Alzheimer patients and mice models of the disease (Nassar et al., 2022), while treating mice with microbes identified in AD patients induces endoplasmic reticulum stress (Liu et al., 2023) suggesting a possible role of microbes in disease etiology.

In this work we investigated the bi-directional communication between the gut and the brain in physiologic conditions, focusing our attention on the effect of a healthy lifestyle, modeled by housing mice in an EE. In previous work (Marrocco et al., 2022) we described the specific microbial profile associated with EE housed mice, composed of five bacteria such as *B. gallinarum, P. excrementihominis, Catabacter hongkongensis, A. senegalensis, C. kluyveri*. In this study we further investigated the hypothesis of the involvement of gut microbiota in EE-induced changes in the brain and we observed behavioral, molecular and metagenomic changes upon transfer of bacteria or fecal material. We identify different microbial populations in the two experimental conditions and we wonder whether the oral administration of specific bacteria or fresh fecal material could modify the microbial community in the receivers. We demonstrated that changing the microbiota composition by transferring fecal material or a defined bacterial consortium improved the behavioral outcomes in mice, reducing anxiety-like behavior. The efficacy of fecal material was stronger in comparison with BT, likely suggesting that the two treatments act differently. We cannot exclude differences due to the timing of animal manipulation or to different microbes proliferation in the receivers due to different nature of the gavage content (lyophilized or fresh stool). Studying the effects of BT and FMT on the expression of neurotrophic genes in the hippocampal region, we observed an increase in BDNF gene expression levels in both groups. BDNF represents one of the most common biomarkers (Thornton, 2023) of a healthy brain and lower serum BDNF levels are associated with a higher risk of depressive symptoms in women with cardiovascular disease (Medved et al., 2024). In FMT-treated mice, additional

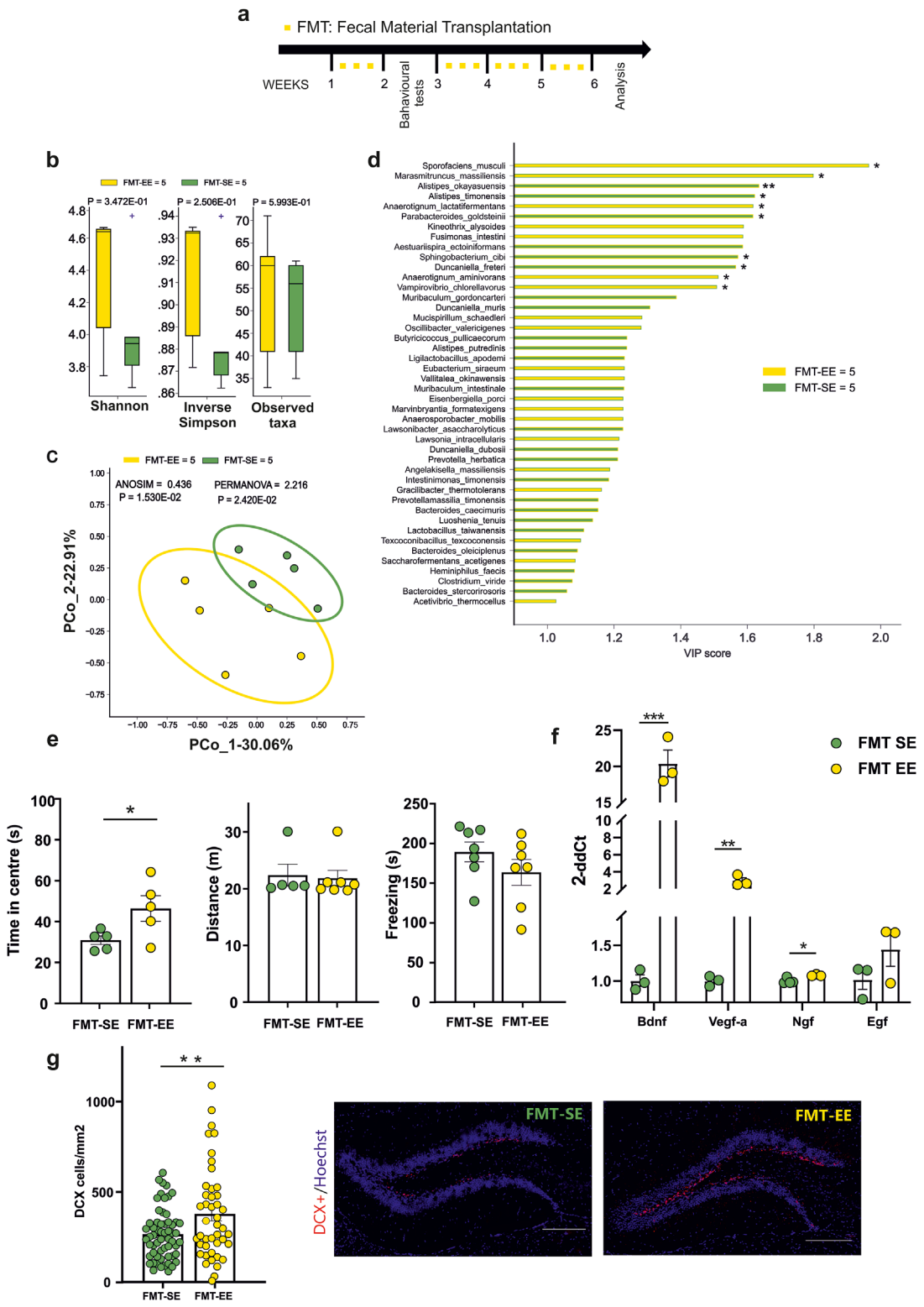

FIGURE 2
(a) Experimental protocol for Fecal Material Transplantation (FMT): oral gavage of fecal content derived from mice reared in an enriched environment (EE) or standard environment (SE) were performed three times a week for four times (yellow squares). The behavioural test were performed after 1 week from treatment **(b)** Alpha- (Shannon, inverse Simpson) and Beta-diversity showed no differences in FMT-SE (n = 5) vs. FMT-EE (n = 5). **(c)** Bray-Curtis distance dissimilarity algorithm showed a significant separation of the microbial cohorts between FMT-SE and FMT-EE groups. **(d)** Variable Importance Plot (VIP) showed discriminant species after PLS-DA in descending order of VIP score (bar length), the highest relative abundance depending on the cohort (central bar color) and the lowest one (edge bar color); significant difference after Mann–Whitney U test (non-FDR,*P ≤ 0.05,**P ≤ 0.01;***P ≤ 0.001) between FMT-SE (n = 5) and FMT-EE (n = 5) groups **(e)** Behavioral tests showed differences in the time spent in the center
(*Continued*)

FIGURE 2 (Continued)
of the arena for FMT-EE (n = 5) compared to FMT-SE mice (n = 5 *p = 0,0473, Student's t-test). **(f)** RT-qPCR analysis of hippocampal neurotrophic factors: an increased level of Bdnf, Vegf-a and Ngf (***p = 0.0005, **p = 0.006, *p < 0.02, Student's t-test, two-tailed) in FMT-EE (n = 3) compared to FMT-SE mice (n = 3-4) was observed. No differences were found in EGF levels between groups. **(g)** The neurogenesis analysis in the dentate gyrus (DG) after FMT from EE or SE mice. Circles in the bar graphs show the total number of DCX + cells divided for total area of DG in mm^2in each slice analyzed (n = 6 FMT-SE, 59 slices and n = 3 FMT-EE animals, 44 slices; **p = 0.0051, by unpaired t-test). Data are presented as mean ±s.e.m (g right). Representative images of hippocampal DG coronal sections stained for DCX + cells (red) and nuclei (Hoechst, blue) in FMT-Se and FMT-EE mice (scale bar, 100 μm). All data are expressed as mean ±s.e.m.

neurotrophins are modulated, with increase of Vegf-a and NGF and higher neurogenesis in the dentate gyrus. The effects on gene expression observed in the FMT group are in line with previous results showing that the administration of SCFAs (formate and acetate) induced changes similar to EE (Marrocco et al., 2022). Moreover, the analysis of fecal bacterial content in BT mice revealed a significant presence of *P. excrementihominis* among all the bacteria administered via oral gavage. This microbe was strongly correlated with formate levels, one of the short-chain fatty acids that play an important role in EE-like changes (Marrocco et al., 2022). However, our data show that other different species were specifically enriched in BT mice after ABX pre-treatment plus inoculation of the bacterial cohort compared to mice receiving only ABX pre-treatment, suggesting that the globally different microbiome (and possibly the relative metabolome) obtained by specific cohort inoculation may be responsible for the differences between the two groups (C vs BT).

The analysis of microbial profile in the EE donor mice partially overlapped the one seen in our previous work; however, the behavioural outcomes of EE group were in line with the literature in terms of anxiety-like behavior, and the microbial profile identified was segregated from SE donor group, highlighting the validation of these mice as donors for the FMT experiments. Note that the alpha diversity of mice receiving fecal material from SE or EE housed mice does not replicate the effects induced by the housing conditions (Marrocco et al., 2022), likely suggesting that FMT-induced effects on host microbiota could hide more subtle effects evoked by transplantation of fecal content from mice housed in different conditions.

The fecal bacteria analysis of FMT partially replicated the segregation of microbial profile observed in the donors; however, we identified some new bacterial strains, such as *Sporofaciens musculi and Anaerotignum lactifermentas* in both EE donors and FMT EE mice. These Gram-positive microbes were isolated for the first time from the caecum of mice and broiler chicken respectively (Rasmussen et al., 2019; Van Der Wielen et al., 2002) and their main metabolic product is acetate. In FMT-EE mice, *Kineothrix alysoides* produces as main metabolites acetate and formate (Haas and Blanchard, 2017) while *Anaerotignum aminovorans* produces acetate as main metabolite (Ueki et al., 2017). Of note, acetate and formate are the metabolites strongly associated with EE and were responsible of the beneficial effects on the central nervous system as observed in our previous work.

In conclusion, we propose that housing mice in an enriched environment leads to profound alterations in the composition of both the microbiota and metabolome. These findings not only highlight the intricate interplay between environmental stimuli and neurobiological processes, but also raise compelling questions about the extent to which external conditions can shape brain function through the gut-brain axis. This insight paves the way for a deeper exploration of how lifestyle and environment may serve as powerful modulators of mental health, potentially offering novel avenues for therapeutic interventions in neurological and psychiatric disorders.

5 Limitations of the study

Considering the differences induced by FMT and BT treatments, we cannot exclude that metabolites present in the fecal water could play additional roles, according to our previous work (Marrocco et al., 2022), and highlighting the presence of different microbial profiles showing the same behavioural outcome in EE mice. In addition, we must consider that oral gavage represents a potentially stressful procedure (Walker et al., 2012) and that this modality of bacteria administration can modify anxiety-like behavior in mice. Further work will be necessary to elucidate the mechanism underlying the effect of EE-induced microbiota on the brain, but here we suggest that enriched environment induces changes in the composition of the microbiota to possibly create different ecological structures (bacteria and metabolome) compared to SE-housed mice, involved in the beneficial effects of the enriched environment in mice.

Data availability statement

The datasets generated and analyzed for this study can be found in the Figshare repository (10.6084/m9.figshare.28369859).

Ethics statement

The animal study was approved by the Italian Ministry of Health (authorization no. 775/2020-PR). The study was conducted in accordance with the local legislation and institutional requirements.

Author contributions

FM: Writing – original draft, Data curation, Investigation. RK: Writing – original draft, Investigation. AR: Writing – original draft, Investigation. XL: Writing – original draft, Investigation. MD: Writing – original draft. VI: Writing – original draft, Data curation. GD'A: Writing – original draft, Conceptualization, Methodology, Supervision. CL: Writing – original draft, Funding acquisition, Project administration, Supervision, Writing – review and editing.

Funding

The author(s) declare that financial support was received for the research and/or publication of this article. This work was supported by Italian Ministry of Health (PNC SALUTE – D3 4 Health – Digital Driven Diagnostics, prognostics and therapeutics for sustainable Healthcare – PNC0001, Spoke 3 Linea tematica 2, CUP B53C22006120001 to CL); Italian Ministry of University and Research (PRIN-2020Z73J5A, PRIN-PNRR-P2022X5ESC to CL); by Associazione Italiana per la Ricerca sul Cancro (AIRC2019-IG23010) to CL; by Italian Ministry of Health Ricerca Corrente to CL.

Conflict of interest

The authors declare that the research was conducted in the absence of any commercial or financial relationships that could be construed as a potential conflict of interest.

The handling editor RP declared a past collaboration with the author(s) CL and GD.

Generative AI statement

The author(s) declare that no Generative AI was used in the creation of this manuscript.

Publisher's note

Supplementary material

The Supplementary Material for this article can be found online at: https://www.frontiersin.org/articles/10.3389/fphys.2025.1572854/full#supplementary-material

References

Al Bataineh, M. T., Künstner, A., Dash, N. R., Alsafar, H. S., Ragab, M., Schmelter, F., et al. (2023). Uncovering the relationship between gut microbial dysbiosis, metabolomics, and dietary intake in type 2 diabetes mellitus and in healthy volunteers: a multi-omics analysis. *Sci. Rep.* 13, 17943. doi:10.1038/s41598-023-45066-7

Birch, A. M., McGarry, N. B., and Kelly, Á. M. (2013). Short-term environmental enrichment, in the absence of exercise, improves memory, and increases NGF concentration, early neuronal survival, and synaptogenesis in the dentate gyrus in a time-dependent manner. *Hippocampus* 23, 437–450. doi:10.1002/hipo.22103

Cancedda, L., Putignano, E., Sale, A., Viegi, A., Berardi, N., and Maffei, L. (2004). Acceleration of visual system development by environmental enrichment. *J. Neurosci.* 24, 4840–4848. doi:10.1523/JNEUROSCI.0845-04.2004

Chen, G., Zhang, Y., Li, R., Jin, L., Hao, K., Rong, J., et al. (2024a). Environmental enrichment attenuates depressive-like behavior in maternal rats by inhibiting neuroinflammation and apoptosis and promoting neuroplasticity. *Neurobiol. Stress* 30, 100624. doi:10.1016/j.ynstr.2024.100624

Chen, Y., Xiao, L., Zhou, M., and Zhang, H. (2024b). The microbiota: a crucial mediator in gut homeostasis and colonization resistance. *Front. Microbiol.* 15, 1417864. doi:10.3389/fmicb.2024.1417864

Contreras-Rodriguez, O., Arnoriaga-Rodríguez, M., Miranda-Olivos, R., Blasco, G., Biarnés, C., Puig, J., et al. (2022). Obesity status and obesity-associated gut dysbiosis effects on hypothalamic structural covariance. *Int. J. Obes.* 46, 30–38. doi:10.1038/s41366-021-00953-9

Costello, E. K., Lauber, C. L., Hamady, M., Fierer, N., Gordon, J. I., and Knight, R. (2009). Bacterial community variation in human body habitats across space and time. *Science* 326, 1694–1697. doi:10.1126/science.1177486

Felice, V. D., and O'Mahony, S. M. (2017). The microbiome and disorders of the central nervous system. *Pharmacol. Biochem. Behav.* 160, 1–13. doi:10.1016/j.pbb.2017.06.016

Haas, K. N., and Blanchard, J. L. (2017). Kineothrix Alysoides, Gen. Nov., Sp. Nov., a saccharolytic butyrate-producer within the family Lachnospiraceae. *Int. J. Syst. Evol. Microbiol.* 67 (2), 402–10. doi:10.1099/ijsem.0.001643

Han, M., Wang, C., Liu, P., Li, D., Li, Y., and Ma, X. (2017). Dietary fiber gap and host gut microbiota. *Protein Pept. Lett.* 24, 388–396. doi:10.2174/0929866524666170220113312

Huang, R., Wang, K., and Hu, J. (2016). Effect of probiotics on depression: a systematic review and meta-analysis of randomized controlled trials. *Nutrients* 8, 483. doi:10.3390/nu8080483

Jandhyala, S. M., Talukdar, R., Subramanyam, C., Vuyyuru, H., Sasikala, M., and Nageshwar Reddy, D. (2015). Role of the normal gut microbiota. *World J. Gastroenterol.* 21, 8787–8803. doi:10.3748/wjg.v21.i29.8787

Johnson, D., Letchumanan, V., Thum, C. C., Thurairajasingam, S., and Lee, L.-H. (2023). A microbial-based approach to mental health: the potential of probiotics in the treatment of depression. *Nutrients* 15, 1382. doi:10.3390/nu15061382

Liu, J., Wu, Q., Wu, Q., Zhong, G., Liang, Y., Gu, Y., et al. (2023). Modulating endoplasmic reticulum stress in APP/PS1 mice by Gomisin B and Osthole in Bushen-Yizhi formula: synergistic effects and therapeutic implications for Alzheimer's disease. *Phytomedicine* 119, 155023. doi:10.1016/j.phymed.2023.155023

Lupori, L., Cornuti, S., Mazziotti, R., Borghi, E., Ottaviano, E., Cas, M. D., et al. (2022). The gut microbiota of environmentally enriched mice regulates visual cortical plasticity. *Cell. Rep.* 38, 110212. doi:10.1016/j.celrep.2021.110212

Marrocco, F., Delli Carpini, M., Garofalo, S., Giampaoli, O., De Felice, E., Di Castro, M. A., et al. (2022). Short-chain fatty acids promote the effect of environmental signals on the gut microbiome and metabolome in mice. *Commun. Biol.* 5, 517. doi:10.1038/s42003-022-03468-9

Medved, S., Salinas, J., Kojis, D., Weinstein, G., Vasan, R. S., Beiser, A., et al. (2024). The association between levels of brain-derived neurotrophic factor and comorbid depression in patients with cardiovascular disease: the Framingham Heart Study. *Psychiatry Clin. Neurosci.* 78, 438–445. doi:10.1111/pcn.13664

Nassar, S. T., Tasha, T., Desai, A., Bajgain, A., Ali, A., Dutta, C., et al. (2022). Fecal microbiota transplantation role in the treatment of alzheimer's disease: a systematic review. *Cureus* 14, e29968. doi:10.7759/cureus.29968

Palmer, C., Bik, E. M., DiGiulio, D. B., Relman, D. A., and Brown, P. O. (2007). Development of the human infant intestinal microbiota. *PLoS Biol.* 5 (7), e177. doi:10.1371/journal.pbio.0050177

Rasmussen, T. S., Streidl, T., Hitch, T. C. A., Wortmann, E., Deptula, P., Hansen, M., et al. (2019). Sporaefaciens Musculi Gen. Nov., Sp. Nov., a novel bacterium isolated from the caecum of an obese mouse. *bioRxiv*. doi:10.1101/2019.12.21.885665

Rogers, G. B., Keating, D. J., Young, R. L., Wong, M. L., Licinio, J., and Wesselingh, S. (2016). From gut dysbiosis to altered brain function and mental illness: mechanisms and pathways. *Mol. Psychiatry* 21 (6), 738–748. doi:10.1038/mp.2016.50

Rosenberg, E., and Zilber-Rosenberg, I. (2016). Microbes drive evolution of animals and plants: the hologenome concept. *mBio* 7 (2), e01395. doi:10.1128/mBio.01395-15

Rowland, I., Gibson, G., Heinken, A., Scott, K., Swann, J., Thiele, I., et al. (2018). Gut microbiota functions: metabolism of nutrients and other food components. *Eur. J. Nutr.* 57, 1–24. doi:10.1007/s00394-017-1445-8

Snigdha, S., Ha, K., Tsai, P., Dinan, T. G., Bartos, J. D., and Shahid, M. (2022). Probiotics: potential novel therapeutics for microbiota-gut-brain axis dysfunction across gender and lifespan. *Pharmacol. Ther.* 231, 107978. doi:10.1016/j.pharmthera.2021.107978

Sommer, F., and Bäckhed, F. (2013). The gut microbiota — masters of host development and physiology. *Nat. Rev. Microbiol.* 11, 227–238. doi:10.1038/nrmicro2974

Sorboni, S. G., Moghaddam, H. S., Jafarzadeh-Esfehani, R., and Soleimanpour, S. (2022). A comprehensive review on the role of the gut microbiome in human neurological disorders. *Clin. Microbiol. Rev.* 35 (1), e0033820. doi:10.1128/CMR.00338-20

Terrisse, S., Derosa, L., Iebba, V., Ghiringhelli, F., Vaz-Luis, I., Kroemer, G., et al. (2021). Intestinal microbiota influences clinical outcome and side effects of early breast cancer treatment. *Cell. Death Differ.* 28, 2778–2796. doi:10.1038/s41418-021-00784-1

Thornton, O. R. (2023). Brain-derived neurotrophic factor (bdnf) in depression: a mini review of clinical and preclinical evidence. *Int. Neuropsychiatr. Dis. J.* 20, 47–56. doi:10.9734/indj/2023/v20i3399

Ueki, A., Goto, K., Ohtaki, Y., Kaku, N., and Ueki, K. (2017). Description of Anaerotignum aminivorans gen. nov., sp. nov., a strictly anaerobic, amino-acid-decomposing bacterium isolated from a methanogenic reactor, and reclassification of Clostridium propionicum, Clostridium neopropionicum and Clostridium lactatifermentans as species of the genus Anaerotignum. *Int. J. Syst. Evol. Microbiol.* 67 (10), 4146–4153. doi:10.1099/ijsem.0.002268

Van Der Wielen, P. W. J. J., Rovers, G. M. L. L., Scheepens, J. M. A., and Biesterveld, S. (2002). Clostridium Lactatifermen Tans Sp. Nov., a lactate-fermenting anaerobe isolated from the caeca of a chicken. *Int. J. Syst. Evol. Microbiol.* 52 (3), 921–25. doi:10.1099/00207713-52-3-921

Walker, M. K., Boberg, J. R., Walsh, M. T., Wolf, V., Trujillo, A., Duke, M. S., et al. (2012). A less stressful alternative to oral gavage for pharmacological and toxicological studies in mice. *Toxicol. Appl. Pharmacol.* 260, 65–69. doi:10.1016/j.taap.2012.01.025

Xu, H.-M., Huang, H.-L., Zhou, Y.-L., Zhao, H.-L., Xu, J., Shou, D.-W., et al. (2021). Fecal microbiota transplantation: a new therapeutic attempt from the gut to the brain. *Gastroenterol. Res. Pract.* 2021, 6699268–6699320. doi:10.1155/2021/6699268

frontiers | Frontiers in Physiology

TYPE Original Research
PUBLISHED 09 June 2025
DOI 10.3389/fphys.2025.1580682

OPEN ACCESS

EDITED BY
Roberto Piacentini,
Catholic University of the Sacred Heart, Italy

REVIEWED BY
Joseph Szule,
Texas A and M University, United States
Javier Durán,
Heidelberg University Hospital, Germany

*CORRESPONDENCE
Maria Giulia Lionetto,
giulia.lionetto@unisalento.it
Maria Elena Giordano,
elena.giordano@unisalento.it

RECEIVED 20 February 2025
ACCEPTED 19 May 2025
PUBLISHED 09 June 2025

CITATION
Giordano ME, Lionetto F and Lionetto MG (2025) Impact of polyethylene terephthalate nanoplastics (PET) on fibroblasts: a study on NIH-3T3 cells.
Front. Physiol. 16:1580682.
doi: 10.3389/fphys.2025.1580682

Impact of polyethylene terephthalate nanoplastics (PET) on fibroblasts: a study on NIH-3T3 cells

Maria Elena Giordano[1]*, Francesca Lionetto[2] and Maria Giulia Lionetto[1,3]*

[1]Department of Biological and Environmental Sciences and Technologies, University of Salento, Lecce, Italy, [2]Department of Engineering for Innovation, University of Salento, Lecce, Italy, [3]NBFC, National Biodiversity Future Center, Palermo, Italy

Plastic pollution has become a major environmental and public health issue due to rising global production. Nanoplastics (NPs) are especially concerning due to their widespread presence and potential health risks. This study aims to determine the impact of the exposure to polyethylene terephthalate (PET) NPs on fibroblast cells using the murine NIH-3T3 cells as experimental model. This is a relevant cellular model for several biological fields of application, including cell migration in wound healing and tissue regeneration. The PET NPs used represented an environmentally realistic PET NPs model since they were produced by a fast top down approach in a process close to the mechanical abrasion of microplastics occurring in the environment. They were characterized by an intrinsic autofluorescence which enables their use in studies of NPs interactions with biological systems without the need for additional fluorescent dyes. Additionally, the Hansen solubility parameters (HSP) of the PET NPs and the culture medium were determined to better understand their interaction. PET NPs were internalized by fibroblasts in a dose-dependent manner, localizing in the cytoplasm. While they caused only a slight reduction in cell viability (within 20% inhibition at 10–100 μg/mL) after 24 h exposure, they significantly impaired fibroblast migration, as demonstrated by the scratch assay, indicating possible interference in tissue repair. The exposure of the cells to PET NPs induced a significant dose-dependent ROS increase suggesting the induction of intracellular oxidative stress as possible mechanisms underlying the observed migration impairment. These findings highlight the potential risks of PET NPs to fibroblasts, emphasizing the need for further research into their impact on cellular functions and mechanisms.

KEYWORDS

wound healing assay, cellular internalization, oxidative stress, cell migration, confocal microscopy, nanoplastics, autofluorescence, hansen solubility parameters

1 Introduction

In recent years plastic pollution has emerged as a critical environmental and public health problem due to plastic production reaching unprecedented levels all over the world (Bidashimwa et al., 2023). Particularly, nanoplastics (NPs)—plastic particles smaller than 1 μm (Gigault et al., 2018), that can arise from the breakdown of larger plastics or be

purposefully manufactured, have gained attention due to their ubiquity across various environmental matrices, raising significant health concerns. Recently, the presence of micro and nanoplastics (MNPs) in human kidney, liver and brain has been confirmed rising concern about bioaccumulation processes (Nihart et al., 2025). MNPs can enter the body through several pathways, including ingestion, inhalation, and dermal contact (Zarus et al., 2021). They have been detected in various food items and drinking water sources (Khan and Jia, 2023). MNPs can originate from various sources, including synthetic fibers and urban dust (Dube and Okuthe, 2023). Dermal contact with MNPs occurs through the use of personal care products containing microbeads, contact with contaminated water, and exposure to airborne MNPs present in the atmosphere that can settle with dust and come into contact with the skin (Abafe et al., 2023). Therefore, the skin may be an important route of MNPs entry into the body (Celebi Sözener et al., 2020). While the skin acts as a barrier, certain conditions may facilitate the penetration of nanoparticles such as skin damage (Larese Filon et al., 2016).

The research on the biological and health related effects of NPs has made significant progress in the last years (Swee-Li Yee et al., 2021) due to the worldwide distribution of this emerging pollutant whose contamination involves all environmental matrices. Particularly, the studies at the cellular level contributed to understanding the molecular and cellular mechanisms underlying the health impact of this emerging pollutants. While there is a growing body of literature examining the impacts of MNPs on various cell types, detailed investigations into their effects on fibroblasts are limited. Fibroblasts play a crucial role in tissue repair, wound healing, and maintaining the extracellular matrix (Plikus et al., 2021). They produce collagen, providing tensile strength and resistance to mechanical stress in tissues (Tracy et al., 2016), remodel the extracellular matrix in response to mechanical signals and its synthesis and degradation (Kendall et al., 2014). Upon injury, fibroblasts become activated and migrate to the wound site, contributing to tissue repair (Kendall et al., 2014). Fibroblasts release cytokines and chemokines, recruiting immune cells and modulating inflammation (Silzle et al., 2003). They also produce Vascular Endothelial Growth Factor (VEGF) and Fibroblast Growth Factors (FGF), promoting endothelial proliferation and blood vessel formation (Ollivier et al., 2000).

The few works available in the literature on the effect of MNPs on fibroblasts have demonstrated that these cells can internalize polystyrene NPs, leading to dose-dependent adverse effects on cellular processes (Peng et al., 2024). These effects vary across different fibroblast cell lines, emphasizing the need for further exploration to understand the implications for human health (Peng et al., 2024). Exposure to polystyrene NPs has been shown to induce significant changes in gene expression and DNA methylation patterns in human dermal fibroblasts, altering the normal cellular functions (Stojkovic et al., 2023). Moreover, aminated polystyrene nanoparticles exhibit dose- and size-dependent cytotoxicity in HFF-2 fibroblasts, with smaller sizes and higher concentrations increasing oxidative stress, apoptosis, and cell cycle arrest (Sadeghinia et al., 2025). Most of the data to date available on the effect of MNPs on fibroblasts refers to polystyrene NPs. Only one study evaluated the impact of environmentally more realistic microplastics of different sizes, sourced from various depths of the Adriatic Sea, on human gingival fibroblasts (hGFs). These microplastics were found to induce inflammatory responses, suggesting that environmental microplastics can affect fibroblast function (Caputi et al., 2022). These results outline the need to expand the research of the effect of MNPs at the cellular levels to other types of plastics materials that can be found in the environment. Due to their extensive production, use, and mismanagement, different micro- and nanosized thermoplastic polymers can be found in the environment, such as polyethylene (PE), polyethylene terephthalate (PET), and polypropylene (PP) (Lionetto et al., 2023).

Research on the cellular effects of polyethylene terephthalate (PET) NPs is currently less extensive compared to studies on other types of NPs, such as polystyrene. While there is a growing body of literature examining the impacts of various NPs on cellular functions, PET-specific studies remain limited. PET is one of the most widely used plastics, found in bottles, textiles, and food packaging (Lionetto et al., 2021; Lionetto et al., 2022). It is a major source of environmental MNPs due to its widespread use and improper disposal. PET degrades slowly, leading to long-term accumulation in ecosystems and increased human exposure through water, food, and air (Lionetto et al., 2021). Therefore, understanding the cellular effects of PET particles is critical due to their widespread presence and persistent nature in the environment.

This study aims to advance understanding of the effects of PET NPs on murine NIH-3T3 fibroblasts, with a focus on cell migration and intracellular redox balance. NIH-3T3 cells represent a versatile fibroblast model widely used in molecular biology, biomedical research, pharmacology, and toxicology (Rahimi et al., 2022), and are particularly suitable for studying migration processes essential to wound healing and tissue regeneration (Giannakopoulos et al., 2023). The PET NPs used in this study were obtained by a fragmentation process close to the mechanical abrasion of microplastics occurring in the environment, according to Lionetto et al. (2022). They were characterized by an intrinsic fluorescence making them useful in the study of NP interaction with biological systems (Lionetto et al., 2022).

2 Materials and methods

2.1 PET nanoplastic production and characterization

Model PET nanoparticles were generated following the method presented in our earlier research (Lionetto et al., 2022), using RT52 PET pellets provided by Invista Resins & Fibers GmbH (Gersthofen, Germany) (Lionetto et al., 2021). This approach employed a top-down mechanical fragmentation technique, which mimicked the natural abrasion of microplastics by sand granules in aquatic environments. The method does not require the use of solvents.

Dynamic light scattering (DLS) measurements were carried out at room temperature using a Malvern Zetamaster Nano-ZS. The measurements were carried out on the diluted suspensions, suitable for light-scattering measurements.

FT-IR analyses allowed the identification of the functional groups present on PET polymer. Fourier transform infrared spectroscopy (FT-IR) was performed with a Jasco 6300 FT-IR 203 spectrometer (JASCO Corporation, Tokyo, Japan). Infrared spectra

were recorded in the wavelength range between 750 cm^{-1} and 3,500 cm^{-1} with 128 scans and 4 cm^{-1} of resolution, by using ATR Pro One X with ZnSe crystal.

The autofluorescence of PET NPs was spectrofluorimetrically characterized in our earlier research (Lionetto et al., 2022). In this work the autofluorescence of PET NPs was assessed by confocal microscopy using a 405 nm laser line of A1 NIKON confocal laser scanning unit (emission filter 425–475 nm) coupled with a NIKON Ti microscope.

2.2 Cell culture and exposure to PET NPs

The effects of PET NPs were assessed on NIH-3T3 fibroblast cell line (ATCC® CRL-1658™) derived from mouse embryos. These cells are widely used in various fields of cell biology research and represent an established fibroblast model for assessing cellular responses to external agents (Boncler et al., 2018; Wagner et al., 2022).

NIH-3T3 cells were cultured in Dulbecco's modified Eagle medium (D-MEM) (EuroClone Paignton-Devon, United Kingdom) supplemented with 10% (v/v) fetal bovine serum, 2 mM L-glutamine, and 100 µg/mL penicillin/streptomycin, in a humidified atmosphere (5% CO_2 in air) at 37°C. For experimental exposure to PET NPs, cells (concentrated 2×10^4 per ml) were seeded in a 96-well plate for 24 h. Thereafter, they were incubated with PET NPs for 24 h at different concentrations (0, 10, 25, 50, and 100 µg/mL). Before incubation with the cells, the dispersion of PET NPs in D-MEM medium was sonicated with a customized protocol using a Bioruptor Plus (Diagenode, Denville, NJ, United States) in order to keep a well dispersed state for the duration of the exposure experiment.

All experiments were performed between passages 3 and 10 of propagation. Every exposure was performed in three replicates.

The selected concentration range (10–100 µg/mL) used in this study is included in the concentrations normally used in *in vitro* studies with PET NPs (Gettings et al., 2024; Aguilar-Guzmán et al., 2022; Zhang et al., 2022; Magrì et al. 2018) to facilitates comparison across different studies and experimental setups in evaluating the biological impacts of PET. A recent study by Leslie et al. (2022)) detected MNPs in human blood at concentrations ranging from 1 to 7 µg/mL, with PET identified as one of the most prevalent plastic components. The range of concentrations used in our study is one order of magnitude higher than the concentration range measured in human blood. This discrepancy is justified by the intrinsic characteristics of *in vitro* studies, where higher concentrations are commonly employed to induce detectable biological effects within short exposure periods. Furthermore, *in vitro* experimental exposure is designed to simulate, over limited timescales, exposure conditions that *in vivo* would occur over much longer durations, potentially leading to accumulation phenomena over time.

2.3 Confocal visualization on living cells

NIH-3T3 cells (concentrated 2×10^4 per ml) were seeded in a tissue culture-treated µ-Slide 4 well (Ibidi GmbH, Gräfelfing, Germany) for 24 h and then they were incubated with PET NPs for 24 h. After incubation cells were washed three times to remove NPs and were visualized by a 405 nm laser line of A1 NIKON confocal laser scanning unit using coupled with a NIKON Ti microscope. Cells were visualized by a Plan Apo 60×1.40 Oil objective (Nikon, Tokyo, Japan).

2.4 Cell viability assessment by MTT test

The effect of PET NP exposure on NIH-3T3 cell viability was assessed using MTT (3-(4,5-dimethylthiazol-2-yl)-2,5-diphenyltetrazolium bromide) test (Sylvester, 2011; Rajabimashhadi et al., 2024). MTT assay is one of the most widely used and well-established methods for assessing cell viability *in vitro*. It is frequently applied in several field of cell research and it is the most prevalent method for assessing cell viability in studies of MNPs (Ferreira et al., 2024). In this regard, the use of the MTT assay in this work allows comparing the cell viability results obtained following exposure to PET NPs with results obtained on other cell types and other NP types.

The test evaluated the mitochondrial NAD(*P*)H-dependent oxidoreductase enzyme activity that can reduce a yellow tetrazolium salt (MTT) to a purple formazan. This in turn accumulated as crystals within healthy cells. The crystals were in turn dissolved with DMSO and the absorbance of the resulting coloured solution was spectrophotometrically analyzed at 570 nm (Cytation 5, BioTek Instruments, Winooski, VT, United States). The relative viability of the cells was calculated by Equation 1:

$$\%\text{Relative viability of cells} = \frac{\text{Treated cells OD}}{\text{Control cells OD}} * 100 \qquad (1)$$

2.5 Wound healing and cell migration assay

The spreading and migration capabilities of 3T3 fibroblasts exposed to PET NPs were measured using a scratch wound assay. First, NIH 3T3 cells were seeded in six-well plates at a density of 5×10^5 cells/well in DMEM, then the cells were incubated at 37°C and 5% CO_2 until they reached a confluence of approximately 80%. Then, an *in vitro* wound model was established by producing a linear scratch across the fibroblast cell layer of the six-well culture plate using a sterile 200 µL pipette tip in a single motion to simulate a wound. Any cellular debris was removed by replacing the medium. Then the cells were exposed to PET NPs 50 µg/mL for 24 h. Images were taken at the same location of each well before and after 24 h by Cytation 5 multimode reader. The wound closure rate was measured using image analysis software ImageJ after downloading the plugin Wound Healing Size Tool (Suarez-Arnedo et al., 2020), that automatically recognizes the size of the scratch wound, corrects the average wound width considering its inclination and quantifies parameters such as area, fraction of wound area, average wound width and width deviation of the wound images.

The wound closure percentage was assessed according to Grada et al. (2017) using Equation 2:

$$\text{Woundclosure}\% = \frac{A_{t=0} - A_{\Delta t}}{A_{t=0}} * 100 \qquad (2)$$

2.6 Intracellular oxidative stress detection

The intracellular oxidative stress was evaluated using the cell-permeant probe sensitive to intracellular reactive species 5-(and-6-)-chloromethyl-2,7-dichlorodihydrofluorescein diacetate acetyl ester (CM-H_2DCFDA) (Ex/Em: 492–495/517–527 nm) (Thermo Fisher Scientific, Waltham, MA, United States). It is a commonly used probe for detecting Reactive Oxygen Species (ROS) formation in cells (King and Oh, 2004; Giordano et al., 2023; Giordano and Lionetto, 2023; Giordano et al., 2020a; Giordano et al., 2020b). Once inside the cell, intracellular esterases cleave the acetate groups of CM-H_2DCFDA, converting it into DCFH, which remains entrapped within the cell. Oxidation of DCFH by intracellular oxidants (via a two-electron process) produces the fluorescent product DCF (Forman et al., 2015). Cells were plated into Corning™ 96-well black/clear bottom plate TC surface for 24 h to allow the cell attachment. Then, the cells were incubated for 24 h with PET NPs in a range of concentrations (0, 10, 25, and 50 μg/mL). Then, they were washed three times to remove residual PET NPs and were charged with CM-H_2DCFDA according to (Giordano et al., 2020a; Giordano et al., 2020b). Briefly the cells were incubated with 5 μM CM-H_2DCFDA for 30 min at 37°C and then washed to remove the extracellular dye. Fluorescence was then measured by Cytation 5™ (BioTek Instruments, Inc., Winooski, VT, United States) multi-mode microplate reader. The results are expressed as percentage variation of the fluorescence intensity with respect to the control and were calculated as follows:

$$\text{Percentage Variation} = \left(\left(FI_{sample} - FI_{control}\right)/FI_{control}\right) \times 100$$

where FI_{sample} is the fluorescence intensity of the test sample, $FI_{control}$ is Fluorescence intensity of the control sample.

In order to assess the intracellular localization of the de-esterified fluorescent probe, the cells charged with CM-H_2DCFDA were also visualized by fluorescent microscopy using the multi-mode microplate reader Cytation 5 using a 40x objective.

2.7 Statistical analysis

All the experiments were performed in triplicate. Statistical tests utilized to evaluate the statistical significance of differences were Student t test, One Way ANOVA, and Dunnett's post-test as indicated in the figures' captions. Data are expressed as mean ± SEM.

3 Results

3.1 PET NPs characterization

As reported in Figure 1A where the DLS intensity-based size distribution is shown (representative of n = 3 independent experiments), the used PET nanoparticles exhibited a bimodal size distribution, with two distinct peaks, suggesting the presence of two populations of particles with different sizes centered at 150 nm and 570 nm. In a previous work of the authors, it was demonstrated that the obtained PET NPs exhibited irregular shapes and surfaces, reflecting characteristics of environmentally occurring secondary NPs formed from the degradation of larger plastic items (Lionetto et al., 2022).

FT-IR spectrum in Figure 1B (representative of n = 3 independent experiments) highlighted the key functional groups of PET. In particular, a strong and prominent peak at 1714 cm^{-1}, typical indicator of the ester carbonyl (C=O) stretching vibration, was observed. Additionally, the peaks at 1,241 cm^{-1} and 1,096 cm^{-1} were related to the C-O stretching vibration in the ester group, due to the aliphatic and aromatic ester, respectively, being a significant feature for identifying ester linkages. The FT-IR spectrum confirmed the preservation of molecular structure of PET NPs without any chemical modification due to the production process.

To better understand the interaction between Dulbecco's modified Eagle medium (D-MEM) supplemented with antibiotic and PET NPs, the Hansen solubility parameters (HSPs) were calculated. HSPs are a set of three parameters, named dispersion or non-polar interaction (δ_D), polar or dipole-dipole interaction (δ_P), and hydrogen bonding interaction (δ_H), as given by Equation 3 (Hansen, 2007):

$$\delta_T^2 = \delta_d^2 + \delta_p^2 + \delta_h^2 \tag{3}$$

These parameters quantify the cohesive energy of a material and predict solubility behavior based on the "like dissolves like" principle. HSPs of PET NPs and D-MEM solution were estimated by the group contribution method by summing the contributions of individual structural groups within a molecule (Greco et al., 2015). This method allows for rapid estimation when experimental data is unavailable. Since D-MEM cell culture medium is a multicomponent solution supplemented with antibiotics, HSPs of the mixture have been calculated using a weighted average of the individual component parameters, i.e., water, salts, sugars, amino acids, vitamins and antibiotic (Hansen, 2007; Yadav et al., 2023; Lionetto et al., 2023) based on their volume fractions Φ_i, as follows (Equation 4):

$$\delta_{mix} = \sum\left(\Phi_i^* \delta_i\right) \tag{4}$$

The obtained Hansen solubility parameters for PET nanoparticles and D-MEM medium are reported in Table 1.

With the HSPs reported in Table 1, a solubility sphere centered at PET HSPs can be drawn with an interaction radius R_0 equal to 5 $(MPa)^{0.5}$ for PET polymer [1], that defines the limit of good solubility or compatibility. To simplify visualization, the 3D sphere is projected as a blue circle area onto three 2D planes in Figure 2, to help assess how close the culture medium lies to the solubility sphere. Since D-MEM falls outside the R_0 radius of PET HSP circle area in all planes (Figure 2), it is energetically unfavorable for it to interact closely with the polymer. This implies that D-MEM medium does not penetrate the PET matrix which cannot swell since swelling of nanoparticles typically requires some degree of solubility.

The laboratory made PET NPs possessed inherent autofluorescence (Lionetto et al., 2022). When excited at 405 nm they expressed a maximum emission at 450 nm. As shown in Figures 3A,B, which presents a representative image of PET NP powder aggregates captured in brightfield (A) and confocal microscopy (B) (from n = 3 independent experiments), PET NPs were clearly visible using confocal microscopy with a 405 nm excitation laser line and a 425–475 nm emission filter. This laser

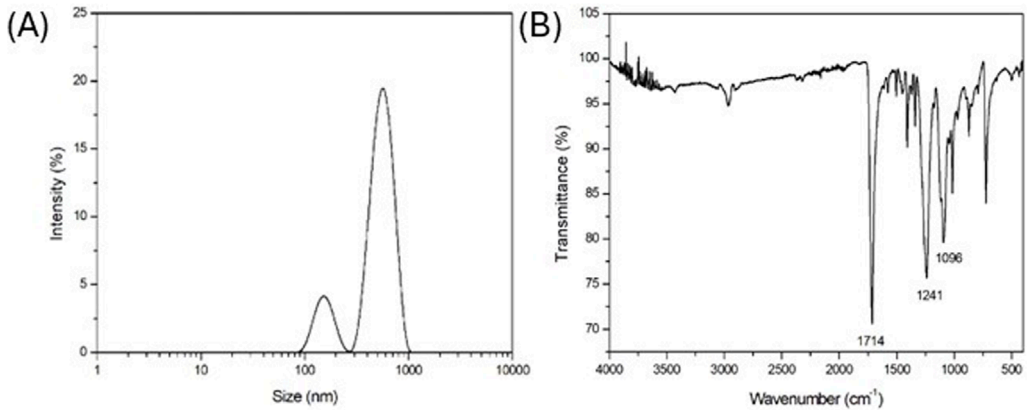

FIGURE 1
(A) DLS intensity-based size distribution (representative of n = 3 independent experiments); **(B)** FT-IR spectrum (representative of n = 3 independent experiments) of laboratory made PET NPs.

TABLE 1 Hansen solubility parameters.

Material	δ_d (MPa)$^{0.5}$	δ_p (MPa)$^{0.5}$	δ_h (MPa)$^{0.5}$	δ_T (MPa)$^{0.5}$
PET	18.2	6.4	6.6	20.4
D-MEM medium	15.5	16.0	42.2	47.7

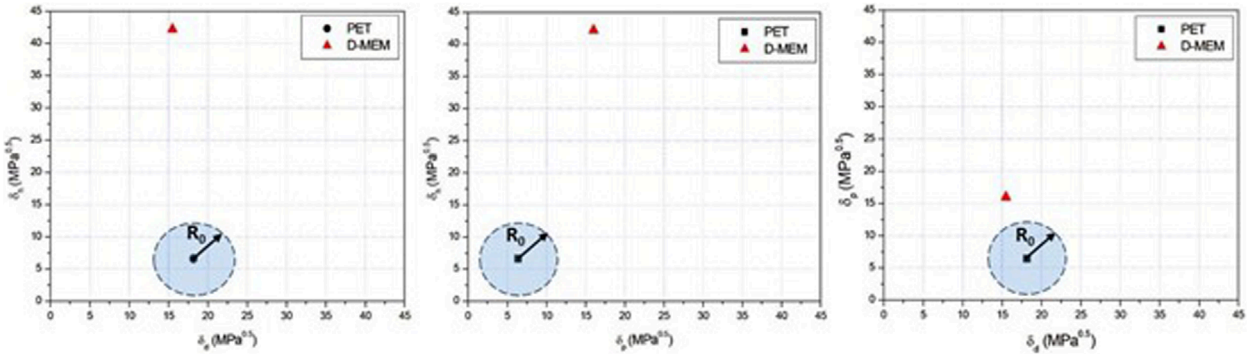

FIGURE 2
Hansen solubility parameter 2D plots for PET and D-MEM medium (representative of n = 3 independent experiments).

line is commonly used in biological research to excite fluorophores with excitation peaks in the near-UV to violet range. This property enables the use of these PET NPs in studies of NPs interactions with biological systems in any fluorescence procedure without the need for additional fluorescent dyes. Moreover, the solvent-free production of these PET NPs offers a key advantage for biological sample applications.

3.2 PET NPs internalization

When 3T3 cells were exposed to PET NPs for 24 h, they showed a cytoplasmatic localization as assessed by confocal microscopy observation on living cells (Figures 4A–E; Supplementary Figure S1, representative images of n = 3 independent experiments), suggesting the ability of PET NPs to be internalized into the cells. The NP internalization appeared dose-dependent in the range of concentrations tested (from 30 μg/mL to 100 μg/mL) (Figure 4E). In particular, at the highest concentration tested we did not observe a proportional increase in the percentage of cells internalizing NPs.

3.3 Cytotoxicity

After demonstrating that PET NPs can be internalized by fibroblasts, we investigated their cellular effects starting with MTT

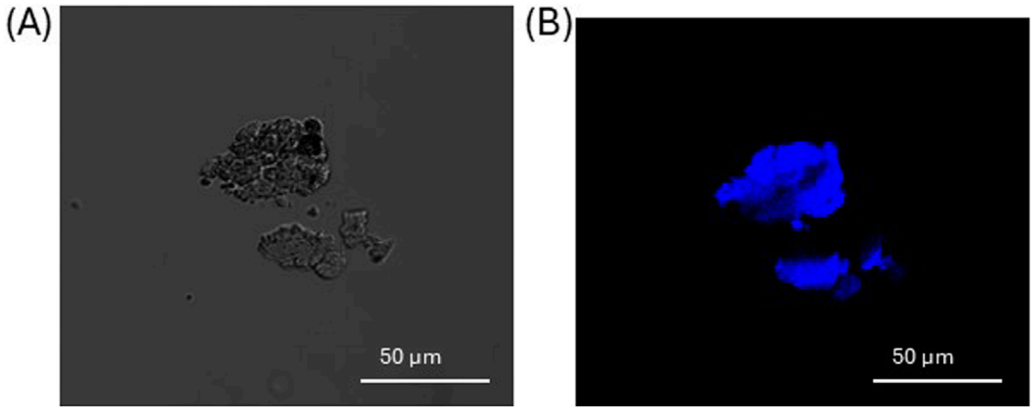

FIGURE 3
Aggregates of PET NPs powder visualized in brightfield **(A)** and confocal microscopy **(B)** by a 405 nm laser line of A1 NIKON confocal laser scanning unit coupled with a NIKON Ti microscope. Objective used 20X. Images representative of n = 3 independent experiments.

test on 3T3 cells exposed to PET NPs for 24 h (concentration range from 10 µg/mL to 100 µg/mL) for the assessment of potential effects on cell viability. Data are expressed as mean ± SEM of three independent experiments. A slightly dose-dependent decline in cell viability was observed (Figure 5). It reached a significant reduction of about 20% at the PET NP concentration of 50 µg/mL. This finding indicates a potential slight cytotoxic effect of PET NPs on NIH-3T3 fibroblasts by interfering with the cellular metabolism. The further increase of the concentration to 100 µg/mL did not produce further increase in the viability reduction. MTT assay measures cellular metabolic activity as an indicator of cell viability, but it may not fully capture other forms of cell stress. A plateau might indicate that metabolic impairment has reached a detectable limit, even if other toxic effects are still occurring.

3.4 Wound healing and cell migration

Fibroblasts are known for their roles in wound healing and cell migration, being essential in the repair and regeneration of tissues following injury (Plikus et al., 2021). In order to assess if any functional interferences in cell migration or mobility were induced in the cells following PET NPs exposure, the scratch wound assay was performed on cells exposed for 24 h to 50 µg/mL PET NPs, the concentration that resulted in the maximum effect of a 20% reduction in vitality in the MTT assay.

As shown in representative Figures 6A–D the exposure of the cells to PET NPs significantly inhibited the migration of the cells and in turn wound closure after scratch. The quantification of the effect (Figure 6E) corresponded to about 60% reduction in the wound closure percentage.

3.5 Oxidative stress

Various studies have shown that NPs can activate oxidative stress pathways, leading to alterations in cellular functions (Kaluç et al., 2024; Wu et al., 2024; Ferrante et al., 2022). Moreover, intracellular reactive oxygen species (ROS) are considered key regulators of cell motility (Huang et al., 2013). To study the mechanisms underlying PET NP induced effects on 3T3 cells, the possible induction of oxidative stress was investigated. The cells where exposed to different concentrations of PET NPs for 24 h and then charged with the cell-permeant ROS sensitive probe CM-H_2DCFDA. As observed by fluorescence microscopy and quantified by spectrofluorimetry (Figure 7), the exposure of the cells induced a significant increase of the fluorescence of the probe compared to control (expressed as percentage variation of the intracellular probe fluorescence). The de-esterified form of CM-H_2DCFDA showed a cytoplasmatic localization as indicated by the diffused intracellular fluorescence observed in the representative images of Figures 7A,B showing control cells and cells exposed to 50 µg/mL PET NP respectively. The fluorescence increase was dose-dependent in the PET NP concentration range tested with a linear increase in the range from 10 µg/mL to 50 µg/mL (Figure 7C). This result suggests that PET NPs exposure was associated with intracellular oxidative stress potentially initiating a cascade of toxicity pathways that could underly the altered cellular function observed.

4 Discussion

Research on the biological and health effects of NPs, particularly at the cellular level, has recently advanced significantly due to their widespread environmental contamination (Yee et al., 2021). However, knowledge gaps remain, limiting a full understanding of NPs effects on human health and ecosystems. Indeed, many studies focus on specific NP types, like polystyrene, which may not reflect the NP environmental diversity, reducing the generalizability of findings (Jayavel et al., 2024; Mahmud et al., 2024; Schröter and Ventura, 2022; Lehner et al., 2019). Additionally, research is often restricted to a few cell types.

The present work contributes to widening the knowledge of the cellular effects of NPs focusing on NIH-3T3 cells as fibroblast cell model and investigating the impact of exposure to PET NPs on key aspects of cell physiology including cell vitality, migration

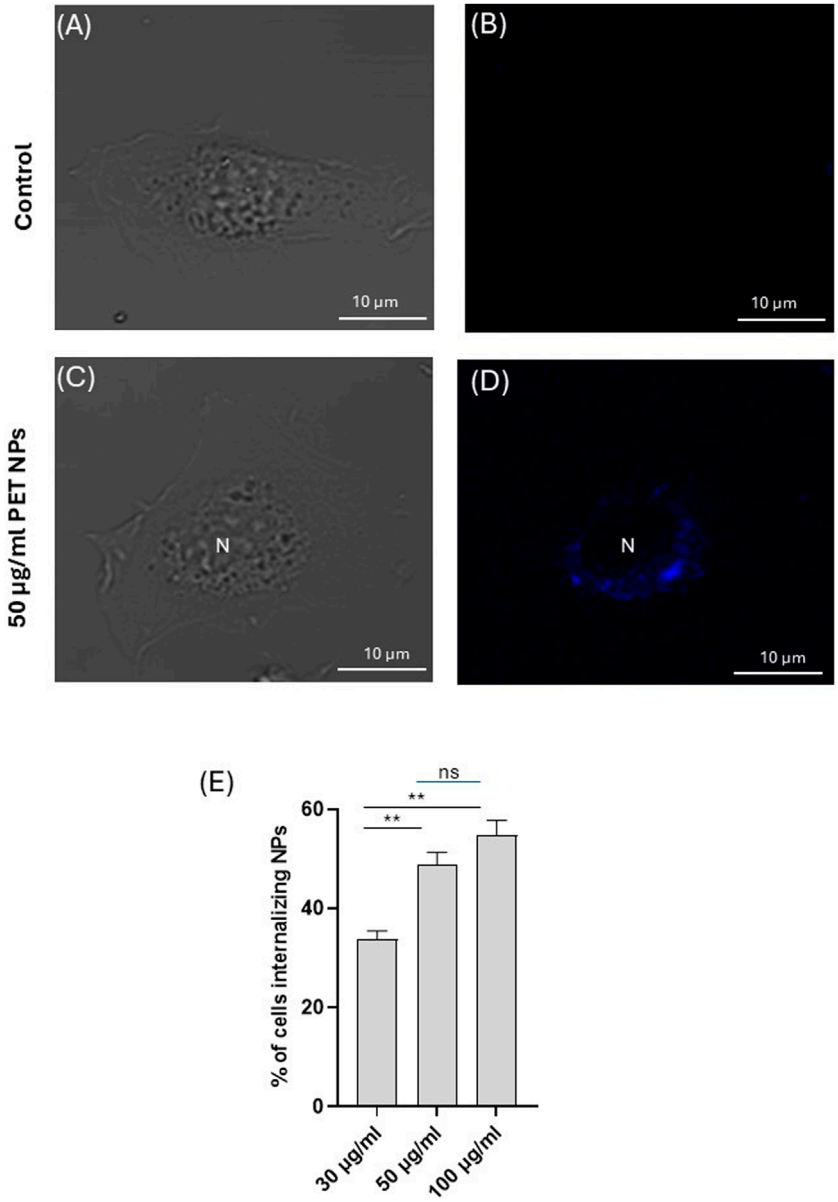

FIGURE 4
Representative image (of n = 3 independent experiments) of a 3T3 fibroblast exposed to PET NPs (50 µg/mL) for 24 h visualized in brightfield **(C)** and confocal microscopy **(D)** by a 405 nm laser line of A1 NIKON confocal laser scanning unit coupled with a NIKON Ti microscope. A control cell **(A,B)** is shown for comparison. Objective used 60X oil immersion. **(E)** % of cells internalizing PET NPs at different NP concentrations (data are expressed as mean ± SEM of three independent experiment).

and redox balance. The cells were exposed to PET NPs obtained by a fragmentation process of PET close to the mechanical abrasion of plastic material occurring in the environment (Lionetto et al., 2022). Compared to previous works mainly based on round-shaped commercial PS NPs, the PET NPs used in this study offer several innovative aspects including their morphology and their intrinsic autofluorescence. They showed a polydisperse size distribution and irregular shapes and surface that closely mimic NPs found in the environment. Moreover, they exhibited intrinsic autofluorescence, eliminating the need for the conjugation with fluorescent dyes and in turn avoiding issues like dye leaching and potential toxicity introduced by the conjugated dyes. The PET NPs used in the present study were characterized by an intrinsic autofluorescence (Lionetto et al., 2022). When excited at 405 nm they expressed a maximum emission at 450 nm. This autofluorescence is attributed to intrinsic fluorescence properties of the polymer ascribable to the presence of aromatic groups in its chemical structure which can absorb photons at specific wavelengths and subsequently re-emit photons at a longer wavelength, generating autofluorescence (Allen et al., 2000; Lionetto et al., 2022). In this work the autofluorescence of PET NPs was assessed by confocal microscopy using a 405 nm laser line of A1 NIKON confocal laser scanning unit (emission filter

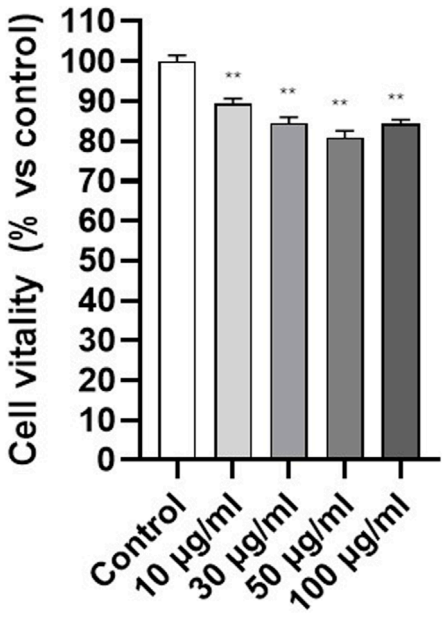

FIGURE 5
Effect of PET NPs exposure (24 h) on 3T3 cell vitality assessed by the MTT test. **P < 0.01 (One Way ANOVA and Dunnett post-test). Data are expressed as mean ± SEM of three independent experiments.

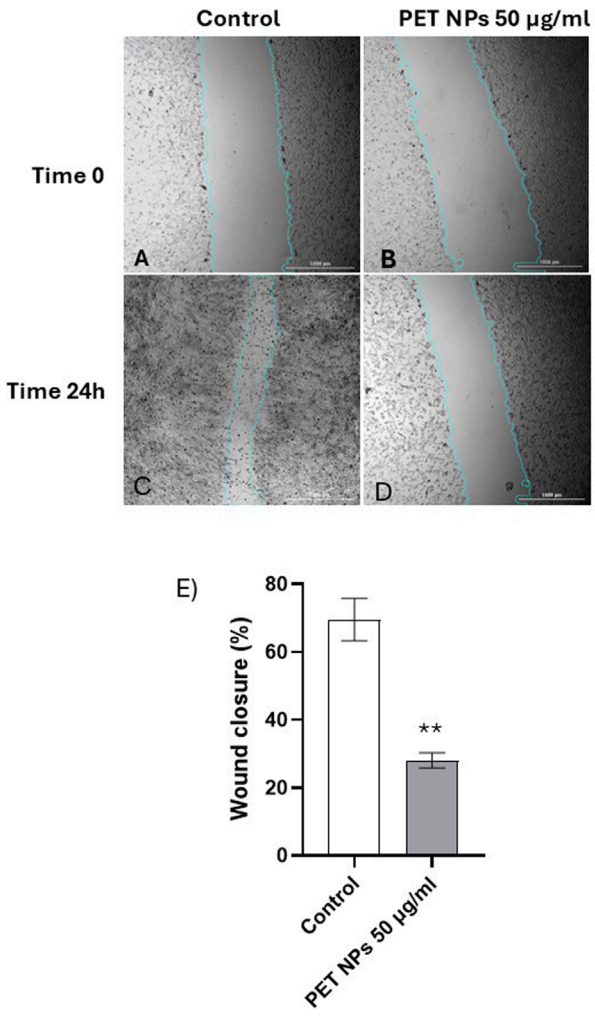

FIGURE 6
(A–E). Representative bright-field images of scratch test on NIH 3T3 cell acquired by the imaging multimode reader Cytation 5 Biotek (obj 4x). **(A)** Control group (t:0 h), **(C)** Control group (t:24 h), **(B)** cells exposed to NPs 100 µg/mL (t:0 h), **(D)** cells exposed to NPs 100 µg/mL (t:24 h). The light blue line was automatically applied by the image analysis software used (see Methods) for recognizing the size of the scratch wound and measure wound closure. **(E)** Wound closure percentage calculated in control and PET NPs (50 µg/mL) exposed cells for 24 h **P < 0.01 (Student t test). Data are expressed as mean ± SEM of three independent experiments.

425–475 nm) coupled with a NIKON Ti microscope, demonstrating that the spectral properties of PET NPs make them suitable for spectrofluorimetry and fluorescence microscopy applications since they showed an excitation and emission peak compatible with the commercially available UV/violet light source and microscope's filters and detectors.

We detected the internalization of PET NPs into 3T3 fibroblasts after 24 h exposure. The internalized PET NPs showed a cytoplasmatic distribution as can be assessed by merging brightfield and fluorescence images acquired by confocal microscopy. The internalization was dose-dependent. This result agrees with our previous data demonstrating the ability of these PET NPs to be internalized in another cell model represented by hemocytes of the bioindicator species *Mytilus galloprovincialis* under *in vitro* study (Lionetto et al., 2022). The internalization of NPs has been widely demonstrated for polystyrene NPs in several cell types, including rat basophilic leukemia cells (RBL-2H3) (Liu et al., 2021), human lung epithelial cells A549 (Xu et al., 2019), THP-1 cells from a human monocytic leukemia cell line (Liu et al., 2024), gastric epithelial (GES-1) cells (Ding et al., 2021), and human induced pluripotent stem cells (hiPSCs). It is known that polystyrene NPs can be internalized into cells through various pathways, including passive membrane transport and active endocytosis (Hua and Wang, 2022; Jeong et al., 2022) (Liu et al., 2021). Smaller particles (e.g., 50 nm) were internalized more efficiently than larger ones (e.g., 500 nm) (Liu et al., 2021) (Liu et al., 2024). The passive membrane penetration is due to the partition of polystyrene NPs in the water-phospholipid system thanks to hydrophobic interactions and Van der Waals' forces as assessed on model membranes (Liu et al., 2021). On the other hand, NPs endocytosis pathways included clathrin-mediated, caveolin-mediated, and micropinocytosis (Liu et al., 2021; Ding et al., 2021) (Liu et al., 2024). Compared to the studies on polystyrene NPs, the available data on cellular internalization of PET NP is limited. To the best of our knowledge only a few studies investigated PET NPs cellular internalization. Magrì et al. (2018) demonstrated PET nanoparticle (NP) internalization into endolysosomes of Caco-2 intestinal cells at concentrations similar to the concentrations used in this study. Rodríguez-Hernández et al. (2019) and Aguilar-Guzmán et al. (2022) observed PET NP uptake in RAW macrophages, while Zhang et al. (2022) reported endocytotic uptake in A549 pulmonary cells after 24 h. In our experimental model we observed a cytoplasmatic distribution of PET NPs allowing to hypothesize an endocytotic pathway as a possible NPs uptake mechanism. However, the contribution

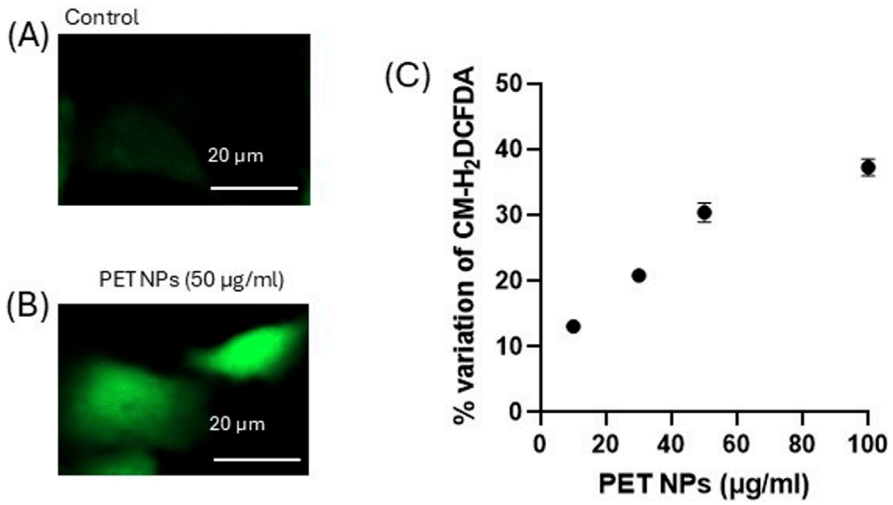

FIGURE 7
(A,B) Representative fluorescence microscopy images (of n = 3 independent experiments) of control and PET NP exposed (24 h) 3T3 cells charged with the ROS sensitive probe CM-H_2DCFDA for the intracellular ROS assessment; **(C)** % variation of the fluorescence intensity of 3T3 cells exposed for 24 h to increasing concentrations of PET NPs and then charged with CM-H_2DCFDA. **P < 0.01 (One Way ANOVA and Dunnett post-test). Data are expressed as mean ± SEM of three independent experiments.

of different internalization mechanisms cannot be excluded according to the heterogeneous dimensions and shape of the NPs used in the study. Indeed, both the size and shape of NPs significantly influence their internalization into cells (Liu et al., 2021; Agarwal et al., 2013) (Xu et al., 2019). Our results demonstrated for the first time fibroblasts were able to incorporate PET NPs within a short time period of exposure in a dose-dependent manner. However, based on the current results, we are not yet able to determine the precise subcellular localization of NPs. Future studies will be necessary to accurately identify the subcellular localization and to in deep characterize the internalization mechanisms of PET NPs into the cells, including a size-resolved analysis of the uptake.

Once assessed the internalization, we investigated potential cellular effects. PET NPs slightly but significantly decreased cell viability after 24 h exposure reaching the maximum effect of 20% viability inhibition at 50 µg/mL. This result agrees with data obtained by Zhang et al. (2022) on A549 cells using commercial PET NPs sized from 164 to 190 nm in a similar concentration range. However, we observed PET NPs able to interfere with an important cellular function in fibroblast physiology represented by cell migration and wound healing. The *in vitro* experimental model used to mimic aspects of wound repair was the so-called scratch test, which involves creating a scratch in the cell monolayer and observing and quantifying how cells migrate to close the gap. While the scratch test is valuable for studying cell migration, it does not fully replicate the complexity of *in vivo* wound healing, which involves multiple tissue layers, immune responses, and other physiological factors. Instead, the scratch test primarily evaluates cellular behaviours such as cell migration (how cells move to cover the scratch area) and cell proliferation (how cells proliferate to fill the wound area) (Grada et al., 2017; Suarez-Arnedo et al., 2020). About 60% reduction in the gap closure percentage of 3T3 cells was assessed by scratch test. Fibroblast migration is a complex, highly regulated process essential for wound healing, tissue repair, and development. This process involves coordinated events, including cytoskeletal reorganization, cell adhesion dynamics, and extracellular matrix (ECM) interactions (Tschumperlin, 2013). Obtained results suggest possible direct or indirect interference of PET NPs with the mechanisms underlying fibroblast migration and their involvement in wound healing. Alterations in cell migration induced by NPs exposure have been previously demonstrated in other cell types and the effects appeared cell type and NP specific. Polystyrene NPs inhibited the migration and invasion of human trophoblast cells by disrupting the ROCK1 pathway, triggering autophagy, and degrading the key transcription factor SOX2 (Wan et al., 2024). In astrocytes derived from neural stem cells, both polystyrene nano- and microplastics modify the expression of genes involved in cell migration, suggesting that these particles can affect cellular motility (Marcellus et al., 2024). In addition, polyethylene NPs enhanced the migration potential of the cells through mechanisms involving Epithelial–Mesenchymal Transition and, in turn, raising concern for possible role in carcinogenesis (Traversa et al., 2024).

Intracellular reactive oxygen species (ROS) are considered key regulators of cell motility (Huang et al., 2013). They are known to exert a dual role, promoting migration at low concentrations but inhibiting cell motility when excessively produced, disrupting cytoskeletal integrity, adhesion turnover, and mitochondrial function (Huang et al., 2013; Dunagan and Rao, 2009). The ROS effects on cell motility are highly context-dependent, influenced by the type of cells and the specific oxidative stress conditions (Huang et al., 2013; Dunagan and Rao, 2009) (P. Xu et al., 2020). In fibroblasts, it has been demonstrated that modulating reactive oxygen species (ROS) levels plays a crucial role in regulating wound healing (Janda et al., 2016) and that excess intracellular ROS can impair fibroblast migration (Fujiwara et al., 2019; Loo and Halliwell, 2012). In our experimental model, using the cell

permeant dichlorofluorescein diacetate probe (CM-H_2DCFDA), we demonstrated that PET NPs significantly increased the ROS intracellular contents, which in turn suggested the induction of an oxidative stress condition in 3T3 cells. The effect was dose-dependent with a linear increase in the concentration range 10–50 μg/mL and a saturating behaviour at the highest concentration tested of 100 μg/mL. The saturating behavior could be ascribed to the fact that the cellular uptake of NPs may be limited by the endocytic capacity of the cell. Previous studies on other cellular models demonstrated that endocytosis of nanoparticles shows saturation with increased concentration and time (Sun et al., 2022). Once this capacity is saturated, it is possible that no further NPs are internalized and no further increase in cellular effects can be observed. Moreover, the exocytosis of internalized PET NPs should also be considered in this process and could contribute to determining the observed plateau. Recent studies on polystyrene NPs have documented NPs exocytosis in different cell types (Liu et al., 2023; Han and Ryu, 2022). Further research is required to address this aspect.

The marked dose-response ROS increase observed in our experimental cell model suggests that oxidative stress induction could represent an early step in the cascade of events induced by PET NPs exposure earlier to more integrated endpoints. The effects detected on 3T3 fibroblast confirm evidence obtained from other cell types such as primary human nasal epithelial cells (Annangi et al., 2023), where an increase of the intracellular ROS concentration following PET NPs exposure was associated to the alteration of mitochondrial membrane functionality. Increases ROS production and consequent oxidative stress induced by PET NPs have also been detected in *Saccharomyces cerevisiae* (Kaluç et al., 2024), and primary nasal epithelial cells (HNEpCs) (Annangi et al., 2023). As regards possible mechanisms to explain the PET induced intracellular increase of ROS concentration and in turn oxidative stress in 3T3 fibroblasts, we can hypothesize possible alteration in the mitochondrial functions since mitochondrial respiratory chain is a primary source of intracellular ROS. It is known that dysfunction in mitochondria leads to increased ROS production (Murphy, 2013). Mitochondria can respond in turn to elevated ROS levels by further increasing their own ROS production, a process known as ROS-induced ROS release (Brady et al., 2006). Moreover, PET NPs induced alterations in the antioxidant defence of the cells could be another possible mechanism contributing to the enhanced ROS concentration in our experimental model. It is known that NPs can significantly alter the activity of antioxidant enzymes across various cell types and organisms (Z. Liu et al., 2020; Babaei et al., 2022; Polo et al., 2024). Although most of the information available on this aspect arises from studies on polystyrene NPs, these effects could also be involved in the PET NPs oxidative stress induction.

Overall, the integrated analysis of scratch test and ROS data suggests that PET NPs induced ROS production could interfere with cell migration in 3T3 cells, possibly representing an underlying early toxicity mechanism. Although future studies will be addressed to clarify this issue, the present work for the first time demonstrated PET NPs able to impair cell migration in fibroblasts with implication in wound healing in association with induced ROS increase.

5 Conclusion

This study analyzes the effects of PET NPs on fibroblasts cells using the NIH-3T3 murine model. The PET NPs used, produced through a top-down approach, closely resemble environmental NPs and exhibit intrinsic autofluorescence, facilitating NP interaction studies without the need for additional fluorescent labels. Furthermore, the determination of the Hansen solubility parameters of the PET NPs and culture medium provides valuable insights into PET NPs interaction behavior, contributing to a deeper understanding of NPs behavior in biological systems.

PET NPs can be internalized by fibroblasts and localize in the cytoplasm in a dose-dependent manner. They induce a slightly dose-dependent decrease in cell viability within 20% inhibition in the concentration range used (10–100 μg/mL) but a more marked oxidative stress due to increase intracellular ROS concentration which could be a key mechanism of toxic effect inside the cell. PET NP exposure impaired fibroblast migration, as observed in a wound healing assay suggesting potential interference with tissue repair and wound healing. Overall, this study underscores the potential hazards of PET NPs on fibroblasts, which play a crucial role in wound healing and tissue maintenance. The observed oxidative stress and impaired migration suggest that PET NPs may exert negative effect on fibroblasts, warranting further investigation into their interference and underlying mechanisms.

Data availability statement

The raw data supporting the conclusions of this article will be made available by the authors, without undue reservation.

Ethics statement

Ethical approval was not required for the studies on animals in accordance with the local legislation and institutional requirements because only commercially available established cell lines were used.

Author contributions

MG: Conceptualization, Data curation, Formal Analysis, Investigation, Methodology, Software, Writing – original draft, Writing – review and editing. FL: Conceptualization, Data curation, Funding acquisition, Investigation, Methodology, Project administration, Resources, Software, Validation, Writing – original draft, Writing – review and editing. ML: Conceptualization, Data curation, Funding acquisition, Investigation, Project administration, Resources, Supervision, Validation, Writing – original draft, Writing – review and editing.

Funding

The author(s) declare that financial support was received for the research and/or publication of this article. This study was partially funded by the REFIN—Research for Innovation

project "NANOPLASTIC," project no. EF42B557, within the POR PUGLIA FESR-FSE 2014/2020 framework and by NBFC (National Biodiversity Future Center) funded by European Union NextGenerationEU, PNRR, project n. CN00000033, CUP: F87G22000290001.

Acknowledgments

We thank the BIOforIU infrastructure at the Department of Biological and Environmental Sciences and Technologies of the University of Salento.

Conflict of interest

The authors declare that the research was conducted in the absence of any commercial or financial relationships that could be construed as a potential conflict of interest.

The author(s) declared that they were an editorial board member of Frontiers, at the time of submission. This had no impact on the peer review process and the final decision.

Generative AI statement

The author(s) declare that no Generative AI was used in the creation of this manuscript.

Publisher's note

Supplementary material

The Supplementary Material for this article can be found online at: https://www.frontiersin.org/articles/10.3389/fphys.2025.1580682/full#supplementary-material

References

Abafe, O. A., Harrad, S., and Abdallah, M. A.-E. (2023). Novel insights into the dermal bioaccessibility and human exposure to brominated flame retardant additives in microplastics. *Environ. Sci. and Technol.* 57 (29), 10554–10562. doi:10.1021/acs.est.3c01894

Agarwal, R., Singh, V., Jurney, P., Shi, L., Sreenivasan, S. V., and Roy, K. (2013). Mammalian cells preferentially internalize hydrogel nanodiscs over nanorods and use shape-specific uptake mechanisms. *Proc. Natl. Acad. Sci. U. S. A.* 110 (43), 17247–17252. doi:10.1073/pnas.1305000110

Aguilar-Guzmán, J. C., Bejtka, K., Fontana, M., Valsami-Jones, E., Villezcas, A. M., Vazquez-Duhalt, R., et al. (2022). Polyethylene terephthalate nanoparticles effect on RAW 264.7 macrophage cells. *Microplast. Nanoplast.* 2 (1), 9. doi:10.1186/s43591-022-00027-1

Allen, N. S., Rivalle, G., Edge, M., Roberts, I., and Fagerburg, D. R. (2000). Characterisation and identification of fluorescent hydroxylated terephthalate species in the thermal and UV degradation of poly (ethylene-co-1, 4-cyclohexanedimethylene terephthalate)(PECT). *Polym. Degrad. Stab.* 67, 325–334.

Annangi, B., Villacorta, A., Vela, L., Tavakolpournegari, A., Marcos, R., and Hernández, A. (2023). Effects of true-to-life PET nanoplastics using primary human nasal epithelial cells. *Environ. Toxicol. Pharmacol.* 100, 104140. doi:10.1016/j.etap.2023.104140

Babaei, A. A., Rafiee, M., Khodagholi, F., Ahmadpour, E., and Amereh, F. (2022). Nanoplastics-induced oxidative stress, antioxidant defense, and physiological response in exposed Wistar albino rats. *Environ. Sci. Pollut. Res.* 29 (8), 11332–11344. doi:10.1007/s11356-021-15920-0

Bidashimwa, D., Hoke, T., Huynh, T. B., Narkpitaks, N., Priyonugroho, K., Ha, T. T., et al. (2023). Plastic pollution: how can the global health community fight the growing problem? In *BMJ Glob. Health* 8. e012140. doi:10.1136/bmjgh-2023-012140

Boncler, M., Lukasiak, M., Dastych, J., Golanski, J., and Cezary, W. (2018). Differentiated mitochondrial function in mouse 3T3 fibroblasts and human epithelial or endothelial cells in response to chemical exposure. *Basic Clin. Pharmacol. Toxicol.* 124, 199–210. doi:10.1111/bcpt.13117

Brady, N. R., Hamacher-Brady, A., Westerhoff, H. V., and Gottlieb, R. A. (2006). A wave of reactive oxygen species (ROS)-Induced ROS release in a Sea of excitable mitochondria. *Https//Home.Liebertpub.Com/Ars* 8 (9–10), 1651–1665. doi:10.1089/ARS.2006.8.1651

Caputi, S., Diomede, F., Lanuti, P., Marconi, G. D., Di Carlo, P., Sinjari, B., et al. (2022). Microplastics affect the inflammation pathway in human gingival fibroblasts: a study in the Adriatic Sea. *Int. J. Environ. Res. Public Health* 19 (13), 7782. doi:10.3390/ijerph19137782

Celebi Sözener, Z., Cevhertas, L., Nadeau, K., Akdis, M., and Akdis, C. A. (2020). Environmental factors in epithelial barrier dysfunction. *J. Allergy Clin. Immunol.* 145 (6), 1517–1528. doi:10.1016/j.jaci.2020.04.024

Ding, Y., Zhang, R., Li, B., Du, Y., Li, J., Tong, X., et al. (2021). Tissue distribution of polystyrene nanoplastics in mice and their entry, transport, and cytotoxicity to GES-1 cells. *Environ. Pollut.* 280, 116974. doi:10.1016/j.envpol.2021.116974

Dube, E., and Okuthe, G. E. (2023). Plastics and micro/nano-plastics (MNPs) in the environment: occurrence, impact, and toxicity. *Int. J. Environ. Res. Public Health* 20 (17), 6667. doi:10.3390/ijerph20176667

Dunagan, M., and Rao, R. K. (2009). Oxidative stress attenuates epithelial differentiation and accelerates cell migration in caco-2 cells. *FASEB J.* 23 (S1), 979.1. doi:10.1096/FASEBJ.23.1_SUPPLEMENT.979.1

Ferrante, M. C., Monnolo, A., Del Piano, F., Mattace Raso, G., and Meli, R. (2022). The pressing issue of micro- and nanoplastic contamination: profiling the reproductive alterations mediated by oxidative stress. *Antioxidants* 11 (2), 193. doi:10.3390/antiox11020193

Ferreira, R. O. G., Nag, R., Gowen, A., and Xu, J. L. (2024). Deciphering the cytotoxicity of micro- and nanoplastics in Caco-2 cells through meta-analysis and machine learning. *Environ. Pollut.* 362, 124971. doi:10.1016/j.envpol.2024.124971

Forman, H. J., Augusto, O., Brigelius-Flohe, R., Dennery, P. A., Kalyanaraman, B., Ischiropoulos, H., et al. (2015). Even free radicals should follow some rules: a Guide to free radical research terminology and methodology. *Free Radic. Biol. Med.* 78, 233–235. doi:10.1016/J.FREERADBIOMED.2014.10.504

Fujiwara, T., Dohi, T., Maan, Z. N., Rustad, K. C., Kwon, S. H., Padmanabhan, J., et al. (2019). Age-associated intracellular superoxide dismutase deficiency potentiates dermal fibroblast dysfunction during wound healing. *Exp. Dermatol.* 28 (4), 485–492. doi:10.1111/EXD.13404

Gettings, S. M., Timbury, W., Dmochowska, A., Sharma, R., McGonigle, R., MacKenzie, L. E., et al. (2024). Polyethylene terephthalate (PET) micro- and nanoplastic particles affect the mitochondrial efficiency of human brain vascular pericytes without inducing oxidative stress. *NanoImpact*. 34, 100508. doi:10.1016/j.impact.2024.100508

Giannakopoulos, E., Katopodi, A., Rallis, M., Politopoulos, K., and Alexandratou, E. (2023). The effects of low power laser light at 661 nm on wound healing in a scratch assay fibroblast model. *Lasers Med. Sci.* 38 (27), 27. doi:10.1007/s10103-022-03670-5

Gigault, J., Halle, A. T., Baudrimont, M., Pascal, P. Y., Gauffre, F., Phi, T. L., et al. (2018). Current opinion: what is a nanoplastic? *Environ. Pollut.* 235, 1030–1034. doi:10.1016/j.envpol.2018.01.024

Giordano, M. E., Caricato, R., and Lionetto, M. G. (2020a). Concentration dependence of the antioxidant and prooxidant activity of trolox in hela cells: involvement in the induction of apoptotic volume decrease. *Antioxidants* 9 (11), 1058–1112. doi:10.3390/antiox9111058

Giordano, M. E., Caricato, R., Verri, T., and Lionetto, M. G. (2020b). The colon epithelium as a target for the intracellular antioxidant activity of hydroxytyrosol: a study on rat colon explants. *J. Funct. Foods* 64, 103604. doi:10.1016/j.jff.2019.103604

Giordano, M. E., and Lionetto, M. G. (2023). Intracellular redox behavior of quercetin and resveratrol singly and in mixtures. *Molecules* 28 (12), 4682. doi:10.3390/MOLECULES28124682

Giordano, M. E., Udayan, G., Guascito, M. R., De Bartolomeo, A. R., Carlino, A., Conte, M., et al. (2023). Apoptotic volume decrease (AVD) in A549 cells exposed to water-soluble fraction of particulate matter (PM10). *Front. Physiol.* 14, 1218687. doi:10.3389/fphys.2023.1218687

Grada, A., Otero-Vinas, M., Prieto-Castrillo, F., Obagi, Z., and Falanga, V. (2017). Research techniques made simple: analysis of collective cell migration using the wound healing assay. *J. Invest. Dermatol.* 137 (2), e11–e16. doi:10.1016/j.jid.2016.11.020

Greco, A., Lionetto, F., and Maffezzoli, A. (2015). Processing and characterization of amorphous polyethylene terephthalate fibers for the alignment of carbon nanofillers in thermosetting resins. *Polym. Compos.* 36 (6), 1096–1103. doi:10.1002/PC.23366

Han, S. W., and Ryu, K. Y. (2022). Increased clearance of non-biodegradable polystyrene nanoplastics by exocytosis through inhibition of retrograde intracellular transport. *J. Hazard. Mater.* 439, 129576. doi:10.1016/j.jhazmat.2022.129576

Hansen, C. M. (2007). *Hansen solubility parameters a User's Handbook*. Second Edition.

Hua, X., and Wang, D. (2022). Cellular uptake, transport, and organelle response after exposure to microplastics and nanoplastics: current knowledge and perspectives for environmental and health risks. *Cell. Uptake, Transp. Organelle Response After Expo. Microplast. Nanoplast. Curr. Knowl. Perspect. Environ. Health Risks* 260, 12. doi:10.1007/s44169-022-00013-x

Huang, J.-S., Cho, C.-Y., Hong, C.-C., Yan, M.-D., Hsieh, M.-C., Lay, J.-D., et al. (2013). Oxidative stress enhances Axl-mediated cell migration through an Akt1/Rac1-dependent mechanism. *Free Radic. Biol. Med.* 65, 1246–1256. doi:10.1016/j.freeradbiomed.2013.09.011

Janda, J., Nfonsam, V., Calienes, F., Sligh, J. E., and Jandova, J. (2016). Modulation of ROS levels in fibroblasts by altering mitochondria regulates the process of wound healing. *Arch. Dermatol. Res.* 308 (4), 239–248. doi:10.1007/s00403-016-1628-9

Jayavel, S., Govindaraju, B., Michael, J. R., and Viswanathan, B. (2024). Impacts of micro and nanoplastics on human health. *Bull. Natl. Res. Centre* 48 (1), 110. doi:10.1186/s42269-024-01268-1

Jeong, H., Kim, W., Choi, D., Heo, J., Han, U., Jung, S. Y., et al. (2022). Potential threats of nanoplastic accumulation in human induced pluripotent stem cells. *Chem. Eng. J.* 427, 131841. doi:10.1016/j.cej.2021.131841

Kaluç, N., Çötelli, E. L., Tuncay, S., and Thomas, P. B. (2024). Polyethylene terephthalate nanoplastics cause oxidative stress induced cell death in *Saccharomyces cerevisiae*. *J. Environ. Sci. Health, Part A* 59 (4), 180–188. doi:10.1080/10934529.2024.2345026

Kendall, R. T., Feghali-Bostwick, C. A., Murray, L. A., Ltd, M., and Seta, F. (2014). Fibroblasts in fibrosis: novel roles and mediators. *Front. Pharmacol.* 5, 123. doi:10.3389/fphar.2014.00123

Khan, A., and Jia, Z. (2023). Recent insights into uptake, toxicity, and molecular targets of microplastics and nanoplastics relevant to human health impacts. *iScience*. doi:10.1016/j.isci.2023.106061

King, B. A., and Oh, D. H. (2004). Spatial control of reactive oxygen species formation in fibroblasts using two-photon excitation. *Photochem. Photobiol.* 80, 1–6. doi:10.1562/2004-03-01-RA-093.1

Larese Filon, F., Bello, D., Cherrie, J. W., Sleeuwenhoek, A., Spaan, S., and Brouwer, D. H. (2016). Occupational dermal exposure to nanoparticles and nano-enabled products: Part I—factors affecting skin absorption. *Int. J. Hyg. Environ. Health* 219 (6), 536–544. doi:10.1016/j.ijheh.2016.05.009

Lehner, R., Weder, C., Petri-Fink, A., and Rothen-Rutishauser, B. (2019). Emergence of nanoplastic in the environment and possible impact on human health. *Environ. Sci. and Technol.* 53 (4), 1748–1765. doi:10.1021/acs.est.8b05512

Leslie, H. A., van Velzen, M. J. M., Brandsma, S. H., Vethaak, A. D., Garcia-Vallejo, J. J., and Lamoree, M. H. (2022). Discovery and quantification of plastic particle pollution in human blood. *Environ. Int.* 163, 107199. doi:10.1016/j.envint.2022.107199

Lionetto, F., Esposito Corcione, C., Messa, F., Perrone, S., Salomone, A., and Maffezzoli, A. (2023). The sorption of amoxicillin on engineered polyethylene terephthalate microplastics. *J. Polym. Environ.* 31, 1383–1397. doi:10.1007/s10924-022-02690-0

Lionetto, F., Esposito Corcione, C., Rizzo, A., Maffezzoli, A., and Ramanavicius, A. (2021). Production and characterization of polyethylene terephthalate nanoparticles. *Polym. (Basel).* 13, 3745. doi:10.3390/polym13213745

Lionetto, F., Lionetto, M. G., Mele, C., Corcione, C. E., Bagheri, S., Udayan, G., et al. (2022). Autofluorescence of model polyethylene terephthalate nanoplastics for cell interaction studies. *Nanomaterials* 12 (9), 1560. doi:10.3390/nano12091560

Liu, L., Xu, K., Zhang, B., Ye, Y., Zhang, Q., and Jiang, W. (2021). Cellular internalization and release of polystyrene microplastics and nanoplastics. *Sci. Total Environ.* 779, 146523. doi:10.1016/j.scitotenv.2021.146523

Liu, Y. Y., Liu, J., Wu, H., Zhang, Q., Tang, X. R., Li, D., et al. (2023). Endocytosis, distribution, and exocytosis of polystyrene nanoparticles in human lung cells. *Nanomaterials* 13 (1), 84. doi:10.3390/NANO13010084/S1

Liu, Z., Huang, Y., Jiao, Y., Chen, Q., Wu, D., Yu, P., et al. (2020). Polystyrene nanoplastic induces ROS production and affects the MAPK-HIF-1/NFkB-mediated antioxidant system in *Daphnia pulex*. *Aquat. Toxicol.* 220, 105420. doi:10.1016/j.aquatox.2020.105420

Liu, Z., Wang, G., Sheng, C., Zheng, Y., Tang, D., Zhang, Y., et al. (2024). Intracellular protein adsorption behavior and biological effects of polystyrene nanoplastics in THP-1 cells. *Environ. Sci. and Technol.* 58 (6), 2652–2661. doi:10.1021/acs.est.3c05493

Loo, A. E. K., and Halliwell, B. (2012). Effects of hydrogen peroxide in a keratinocyte-fibroblast co-culture model of wound healing. *Biochem. Biophys. Res. Commun.* 423 (2), 253–258. doi:10.1016/j.bbrc.2012.05.100

Magrì, D., Sánchez-Moreno, P., Caputo, G., Gatto, F., Veronesi, M., Bardi, G., et al. (2018). Laser ablation as a versatile Tool to mimic polyethylene terephthalate nanoplastic pollutants: characterization and toxicology assessment. *ACS Nano* 12 (8), 7690–7700. doi:10.1021/acsnano.8b01331

Mahmud, F., Sarker, D. B., Jocelyn, J. A., and Sang, Q. X. A. (2024). Molecular and cellular effects of microplastics and nanoplastics: focus on inflammation and senescence. *Cells* 13 (21), 1788. doi:10.3390/cells13211788

Marcellus, K. A., Bugiel, S., Nunnikhoven, A., Curran, I., and Gill, S. S. (2024). Polystyrene nano- and microplastic particles induce an inflammatory gene expression profile in rat neural stem cell-derived astrocytes *in vitro*. *Nanomaterials* 14 (5), 429. doi:10.3390/nano14050429

Murphy, M. P. (2013). Mitochondrial dysfunction indirectly elevates ROS production by the endoplasmic reticulum. *Cell Metab.* 18 (2), 145–146. doi:10.1016/j.cmet.2013.07.006

Nihart, A. J., Garcia, M. A., El Hayek, E., Liu, R., Olewine, M., Kingston, J. D., et al. (2025). Bioaccumulation of microplastics in decedent human brains. *Nat. Med.* 31, 1114–1119. doi:10.1038/s41591-024-03453-1

Ollivier, V., Chabbat, J., Herbert, J. M., Hakim, J., and De Prost, D. (2000). Vascular endothelial growth factor production by fibroblasts in response to factor VIIa binding to tissue factor involves thrombin and factor Xa. *Arterioscler., Thromb., Vasc. Biol.* 20 (5), 1374–1381. doi:10.1161/01.atv.20.5.1374

Peng, M., Félix, R. C., Canário, A. V. M., and Power, D. M. (2024). The physiological effect of polystyrene nanoplastic particles on fish and human fibroblasts. *Sci. Total Environ.* 914, 169979. doi:10.1016/j.scitotenv.2024.169979

Plikus, M. V., Wang, X., Sinha, S., Forte, E., Thompson, S. M., Herzog, E. L., et al. (2021). Fibroblasts: origins, definitions, and functions in health and disease. *Cell* 184 (15), 3852–3872. doi:10.1016/j.cell.2021.06.024

Polo, G., Lionetto, F., Giordano, M. E., and Lionetto, M. G. (2024). Interaction of micro- and nanoplastics with enzymes: the case of carbonic anhydrase. *Int. J. Mol. Sci.* 25 (17), 9716. doi:10.3390/ijms25179716

Rahimi, A. M., Cai, M., and Hoyer-Fender, S. (2022). Heterogeneity of the NIH3T3 fibroblast cell line. *Cells* 11, 2677. doi:10.3390/cells11172677

Rajabimashhadi, Z., Gallo, N., Russo, F., Ghiyami, S., Mele, C., Giordano, M. E., et al. (2024). Production and physico-chemical characterization of nano-sized collagen from equine tendon. *Int. J. Biol. Macromol.* 277, 134220. doi:10.1016/j.ijbiomac.2024.134220

Rodríguez-Hernández, A. G., Muñoz-Tabares, J. A., Aguilar-Guzmán, J. C., and Vazquez-Duhalt, R. (2019). A novel and simple method for polyethylene terephthalate (PET) nanoparticle production. *Environ. Sci. Nano* 6 (7), 2031–2036. doi:10.1039/C9EN00365G

Sadeghinia, H., Hanachi, P., Ramezani, R., and Karbalaei, S. (2025). Toxic effects of polystyrene nanoplastics on MDA-MB-231 breast cancer and HFF-2 normal fibroblast cells: viability, cell death, cell cycle and antioxidant enzyme activity. *Environ. Sci. Eur.* 37, 1. doi:10.1186/s12302-024-01026-0

Schröter, L., and Ventura, N. (2022). Nanoplastic toxicity: insights and challenges from experimental model systems. *Small* 18 (31), e2201680. doi:10.1002/SMLL.202201680

Silzle, T., Randolph, G. J., Kreutz, M., and Kunz-Schughart, L. A. (2003). The fibroblast: sentinel cell and local immune modulator in tumor tissue. *Int. J. Cancer* 108, 173–180. doi:10.1002/ijc.11542

Stojkovic, M., Ortuño Guzmán, F. M., Han, D., Stojkovic, P., Dopazo, J., and Stankovic, K. M. (2023). Polystyrene nanoplastics affect transcriptomic and epigenomic signatures of human fibroblasts and derived induced pluripotent stem cells: implications for human health. *Environ. Pollut. (Barking, Essex)* 1987, 120849. doi:10.1016/J.ENVPOL.2022.120849

Suarez-Arnedo, A., Torres, F., Id, F., Clavijo, C., Arbelá Ez, P., Cruz, J. C., et al. (2020). An image J plugin for the high throughput image analysis of *in vitro* scratch wound healing assays. *PLoS One* 15, e0232565. doi:10.1371/journal.pone.0232565

Sun, W., Tian, Y., Wang, Z., Zhang, H., and Zheng, A. (2022). The study of cyclosporin A nanocrystals uptake and transport across an intestinal epithelial cell model. *Polymers* 14 (10), 1975. doi:10.3390/POLYM14101975

Swee-Li Yee, M., Hii, L.-W., King Looi, C., Lim, W.-M., Wong, S.-F., Kok, Y.-Y., et al. (2021). Impact of microplastics and nanoplastics on human health. *Nanomater. (Basel).* 11, 496. doi:10.3390/nano11020496

Sylvester, P. W. (2011). "Optimization of the tetrazolium dye (MTT) colorimetric assay for cellular growth and viability," in *Drug design and discovery: methods and*

protocols. Editor S. D. Satyanarayanajois (Totowa, NJ: Humana Press), 157–168. doi:10.1007/978-1-61779-012-6_9

Tracy, L. E., Minasian, R. A., and Caterson, E. J. (2016). Extracellular matrix and dermal fibroblast function in the healing wound. *Adv. Wound Care* 5 (3), 119–136. doi:10.1089/WOUND.2014.0561

Traversa, A., Mari, E., Pontecorvi, P., Gerini, G., Romano, E., Megiorni, F., et al. (2024). Polyethylene micro/nanoplastics exposure induces epithelial–mesenchymal transition in human bronchial and alveolar epithelial cells. *Int. J. Mol. Sci.* 25 (18), 10168. doi:10.3390/ijms251810168

Tschumperlin, D. J. (2013). Fibroblasts and the ground they walk on. *Physiology* 28 (6), 380–390. doi:10.1152/physiol.00024.2013

Wagner, G., Sievers, L., Tiburcy, M., Zimmermann, W. H., Kollmar, O., Schmalz, G., et al. (2022). Impact of immunosuppressive drugs on fibroblasts: an *in vitro* study. *J. Clin. Med.* 11, 3107. doi:10.3390/jcm11113107

Wan, S., Wang, X., Chen, W., Xu, Z., Zhao, J., Huang, W., et al. (2024). Polystyrene nanoplastics activate autophagy and suppress trophoblast cell migration/invasion and migrasome formation to induce miscarriage. *ACS Nano* 18 (4), 3733–3751. doi:10.1021/acsnano.3c11734

Wu, Q., Liu, C., Liu, D., Wang, Y., Qi, H., Liu, X., et al. (2024). Polystyrene nanoplastics-induced lung apoptosis and ferroptosis via ROS-dependent endoplasmic reticulum stress. *Sci. Total Environ.* 912, 169260. doi:10.1016/j.scitotenv.2023.169260

Xu, M., Halimu, G., Zhang, Q., Song, Y., Fu, X., Li, Y., et al. (2019). Internalization and toxicity: a preliminary study of effects of nanoplastic particles on human lung epithelial cell. *Sci. Total Environ.* 694, 133794. doi:10.1016/j.scitotenv.2019.133794

Xu, P., Xue, Y. N., Ji, H. H., Tan, C., and Guo, S. (2020). H2O2-induced oxidative stress disrupts mitochondrial functions and impairs migratory potential of human epidermal melanocytes. *Exp. Dermatol.* 29 (8), 733–741. doi:10.1111/EXD.14134

Yadav, D., Savjani, J., Savjani, K., and Shah, H. (2023). Exploring potential coformer screening techniques based on experimental and virtual strategies in the manufacturing of pharmaceutical cocrystal of efavirenz. *J. Pharm. Innovation* 18 (3), 1128–1144. doi:10.1007/S12247-022-09704-3/TABLES/6

Yee, M. S. L., Hii, L. W., Looi, C. K., Lim, W. M., Wong, S. F., Kok, Y. Y., et al. (2021). Impact of microplastics and nanoplastics on human health. *Nanomaterials* 11 (2), 496. doi:10.3390/NANO11020496

Zarus, G. M., Muianga, C., Hunter, C. M., and Pappas, R. S. (2021). A review of data for quantifying human exposures to micro and nanoplastics and potential health risks. *Sci. Total Environ.* 756, 144010. doi:10.1016/j.scitotenv.2020.144010

Zhang, H., Zhang, S., Duan, Z., and Wang, L. (2022). Pulmonary toxicology assessment of polyethylene terephthalate nanoplastic particles *in vitro*. *Environ. Int.* 162, 107177. doi:10.1016/j.envint.2022.107177

frontiers | Frontiers in Physiology

TYPE Review
PUBLISHED 26 June 2025
DOI 10.3389/fphys.2025.1618330

OPEN ACCESS

EDITED BY
Roberto Piacentini,
Catholic University of the Sacred Heart, Italy

REVIEWED BY
Nicolau Beckmann,
Novartis Institutes for BioMedical Research, Switzerland
Fabrizia Cesca,
University of Trieste, Italy

*CORRESPONDENCE
Barbara Bettegazzi,
bettegazzi.barbara@hsr.it

RECEIVED 25 April 2025
ACCEPTED 16 June 2025
PUBLISHED 26 June 2025

CITATION
Porcari C, Cattaneo S, Crippa L, Simonato M and Bettegazzi B (2025) Exploring the diversity of biological processes regulated by glial cell line-derived neurotrophic factor, a pleiotropic molecule with therapeutic potential. *Front. Physiol.* 16:1618330. doi: 10.3389/fphys.2025.1618330

Exploring the diversity of biological processes regulated by glial cell line-derived neurotrophic factor, a pleiotropic molecule with therapeutic potential

Cristina Porcari[1,2], Stefano Cattaneo[3], Lucia Crippa[4], Michele Simonato[1,2] and Barbara Bettegazzi[2,4]*

[1]Department of Neuroscience and Rehabilitation, Section of Pharmacology, University of Ferrara, Ferrara, Italy, [2]Division of Neuroscience, IRCCS Ospedale San Raffaele, Milan, Italy, [3]IRCCS Neuromed, Pozzili, Italy, [4]Università Vita-Salute San Raffaele, Milan, Italy

Glial cell line–derived neurotrophic factor (GDNF) is a potent trophic factor essential for neuronal survival and function. Encoded by the GDNF gene, its mature protein arises from specific post-translational modifications and is secreted through distinct isoform-dependent pathways. Once released, GDNF binds to its receptors, GFRα1 and RET, activating downstream signaling cascades that regulate cell growth, differentiation, and survival. In the central nervous system, GDNF exerts protective effects on dopaminergic neurons—highlighted in Parkinson's disease research—and shows promise for modulating schizophrenia, depression, and addiction. Beyond dopaminergic pathways, GDNF influences synaptic plasticity in hippocampal neurons and supports GABAergic function. Glial cells also produce and respond to GDNF: astrocyte-derived GDNF can promote neuroprotection but also modulate microglial state and neuroinflammation. Other cell sources, such as pericytes and endothelial cells, contribute to GDNF levels, impacting blood-brain and blood-nerve barrier permeability. Peripherally, GDNF is critical for sympathetic and parasympathetic neuron development, somatic sensory neuron maintenance, and motor neuron reinnervation at the neuromuscular junction. Finally, GDNF has been recently implicated in tumour biology, underscoring its multifaceted role at the interface between beneficial and detrimental effects. Clinically, its therapeutic potential is being explored in different diseases, including neurodegenerative disorders and epilepsy. In this review, we will explore various aspects of GDNF biology and then focus our attention to the physiological mechanisms of GDNF-regulated processes in the central and peripheral nervous system, concluding with a brief perspective related to its therapeutic potential for central nervous system disorders. A deeper knowledge of the mechanisms regulating GDNF secretion and signaling, particularly the cellular source and the specificity of the GDNF-engaged intracellular signaling pathways, could

be helpful to develop more precise therapeutic strategies for different CNS diseases.

KEYWORDS

GDNF (glial cell line-derived neurotrophic factor), GDNF secretion, GDNF signaling, astrocytic GDNF, GDNF physiological functions, GDNF role in the CNS

1 Introduction

GDNF, the glial cell line-derived neurotrophic factor, is a neurotrophic factor involved in fundamental physiological processes in the central nervous system (CNS) and periphery. GDNF can elicit a variety of cellular responses, involved in several key processes, including neuronal survival, neurite outgrowth, and synaptogenesis. Beyond its role in development, GDNF exerts a significant neuroprotective role in different pathophysiological conditions, including neuroinflammatory and neurodegenerative diseases, but also some psychiatric disorders and addiction. The clinical potential of GDNF has been evident since its discovery in the nineties, nonetheless, the possibility to exploit this molecule in therapy has not yet fulfilled its promise. Indeed, the lack of knowledge of certain aspects of GDNF biology has slowed the progress of GDNF-based therapies. In this review, we focused on a wide assessment of the current knowledge about GDNF and its role in different physiological processes, highlighting the therapeutic opportunities arising from this knowledge.

1.1 The glial cell line–derived neurotrophic factor (GDNF)

The glial cell line-derived neurotrophic factor belongs to the GDNF family ligands (GFLs), which also include persephin, neurturin, and artemin (Airaksinen and Saarma, 2002). In physiological conditions, GDNF is expressed in soft tissue, testis, kidney, adrenal gland, parathyroid gland, placenta, gastrointestinal tract, spinal cord, and in different areas of the brain (The Human Protein Atlas - https://www.proteinatlas.org/ENSG00000168621-GDNF/tissue). Neurotrophic factors are proteins that support neuronal survival, cell proliferation, and differentiation. Additionally, they function as neurocytokines, facilitating communication between neurons and target tissues. GFLs members exert their function through binding as homodimers to the tyrosine kinase receptor Rearranged during Transfection (RET). In turn, RET activation occurs only if the GFL is bound to a member of the GDNF-family receptor-α (GFRα) receptors, which are anchored to the plasma membrane via a glycosyl phosphatidylinositol (GPI) linker, lacking transmembrane and intracellular domains (Airaksinen and Saarma, 2002). The intracellular pathways activated by all GFLs play a crucial role in promoting neuronal development and survival. Moreover, GDNF was initially isolated from rat glial cell lines and identified as a neurotrophic factor able to enhance dopamine uptake in midbrain dopaminergic neurons (Lin et al., 1993). The neuroprotective effect of GDNF has attracted significant interest from the scientific community for its potential use in treating neurodegenerative diseases (see below).

1.1.1 GDNF, from the gene to the mature protein

The human GDNF gene is located on chromosome 5 (5p13.2), it is 12 kb-long and consists of six exons. An alternative splicing occurring at the level of the third exon gives rise to two conserved alternative isoforms: a full-length transcript, the pre-α-pro-GDNF, and a shorter version of the transcript, lacking 78 bp in the sequence encoding the pro region, named pre-β-pro-GDNF (Schaar et al., 1994; Cristina et al., 1995). This results in a 26 amino-acid difference in the pro region of the pre- α-pro-GDNF and pre- β-pro-GDNF (Figure 1 – upper panel). Both isoforms, however, lead to the same 134 amino-acid-long mature GDNF protein, since the proteolytic cleavage site that is crucial to obtain the mature protein is encoded in exon II, which is not affected by the alternative splicing (Cristina et al., 1995). The protein maturation process starts soon after synthesis, with the pre-sequence-mediated localization of the protein in the endoplasmic reticulum. The protein folds, disulfide (S-S) bonds are formed, and dimerization occurs. GDNF is also modified by N-linked glycosylation. After that, GDNF undergoes proteolytic processing into its mature form. The proteases that are involved in the processing of pro-GDNF to mature GDNF are furin, PACE4, and the following protein convertases: PC5A, PC5B, and PC7 (Lonka-Nevalaita et al., 2010). From a structural point of view, GDNF is characterized by a topological knot formed by three cysteines (Eigenbrot and Gerber, 1997), which makes it a distant member of the transforming growth factor-β (TGF-β) family. GDNF features two finger-like structures that play a role in its interaction with GFRα. The site where the protein undergoes post-translational modification through N-glycosylation is situated near one of these finger-like structures. Although this modification is not critical for receptor binding and activation, it is necessary for the proper folding and processing of GDNF in mammalian cells (Piccinini et al., 2013).

1.2 GDNF secretion

GDNF is a secreted protein, synthesized as a precursor protein (pre-pro-GDNF). Both the presence of the pro-domain and of the cysteine residues are important for secretion, that is strongly reduced in their absence (Oh-hashi et al., 2009; Piccinini et al., 2013). As mentioned before, in humans and rodents, GDNF is present in two splice isoforms, the pre-α-pro-GDNF and pre-β-pro-GDNF, that differ for a 26 amino-acid deletion in the pro domain of the β isoform. A study conducted in PC-6.3 cells showed distinct subcellular localizations for these two isoforms under normal conditions and after neuronal stimulation (Lonka-Nevalaita et al., 2010). Pre-α-pro-GDNF is primarily found in the Golgi complex and gradually progresses through the secretory pathway after stimulation. On the other hand, pre-β-pro-GDNF is mainly located in secretory vesicles and moves more quickly

10.3389/fphys.2025.1618330

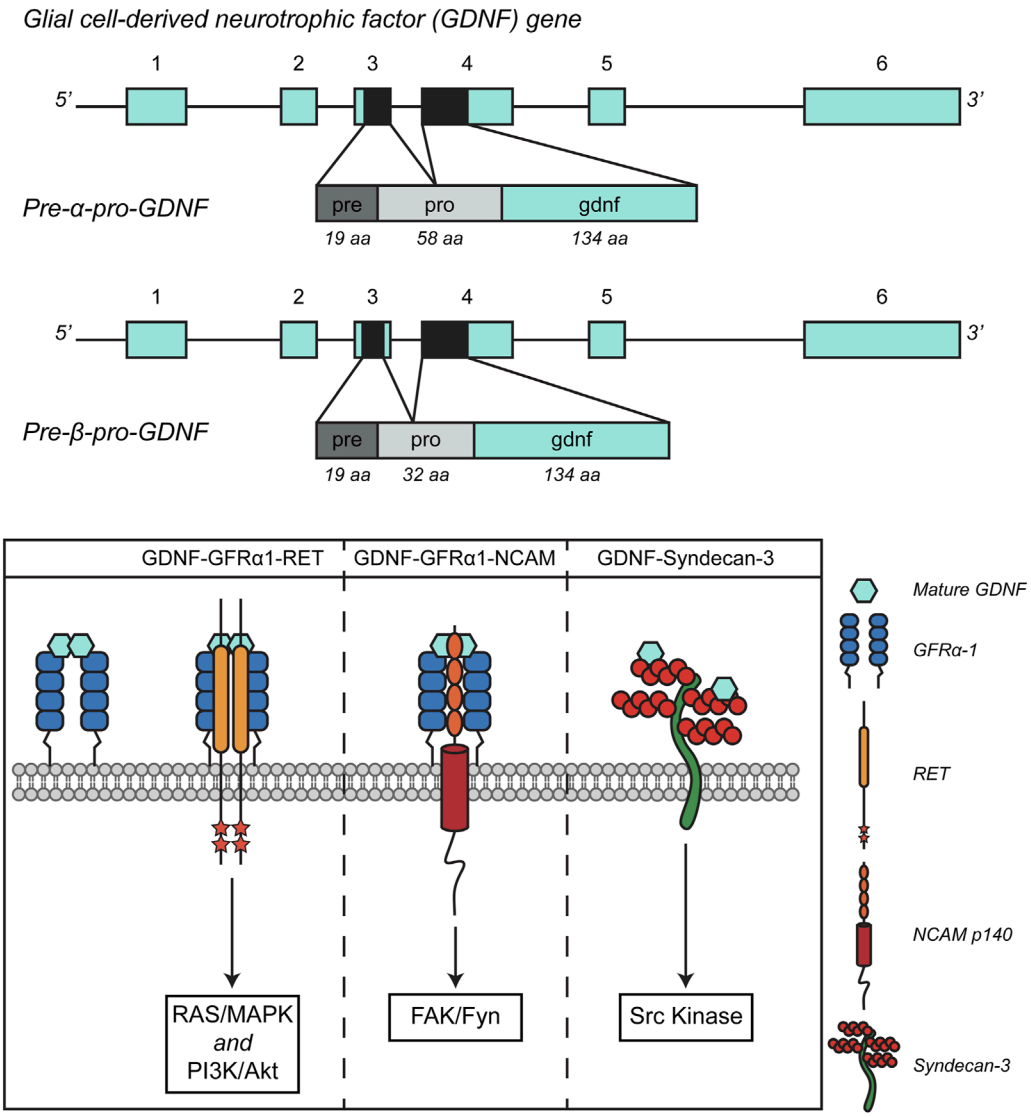

FIGURE 1
Schematic representation of GDNF splicing isoforms (A) and signaling pathways. Adapted from (Penttinen et al., 2018, Front. Neurol., CC BY 4.0).

through the secretory pathway upon stimulation. The presence of both the α and β isoforms in secretory granules is confirmed by the co-localisation with the Rab3A and Rab27A markers. However, only pre-β-pro-GDNF shows strong co-localization with Secretogranin II, indicating its presence in the vesicles of the regulated secretory pathway, whereas pre-α-pro-GDNF shows less co-localization. Additionally, upon stimulation with potassium chloride, only the secretion of the mature GDNF form derived from the β precursor protein is increased (Lonka-Nevalaita et al., 2010). A potential reason for the difference between pre-α-pro-GDNF and pre-β-pro-GDNF could be that pre-α-pro-GDNF is less efficiently sorted into secretory granules at the trans-Golgi network, accounting for the higher presence of the α precursor in the Golgi region. Due to this inefficient sorting, some pre-α-pro-GDNF may also enter the constitutive secretion pathway.

1.3 GDNF signaling pathways

As previously mentioned, GFLs exert their trophic action through the activation of the RET receptor, but this interaction requires the presence of the co-receptor GFRα. Notably, there are four GFRα proteins capable of interacting with GFLs: GFRα1, GFRα2, GFRα3, and GFRα4, with GDNF binding preferentially to GFRα1 and with lower affinity to GFRα2, as demonstrated in mice studies (Cacalano et al., 1998). GDNF acts as a homodimer, stabilized by the formation of a disulfide bond. The GDNF-GFRα1 complex increases the affinity for the RET receptor and once bound, it triggers the dimerization of the RET receptor and the transphosphorylation of tyrosine residues in its intracellular portion, thereby activating intracellular signaling. Like other tyrosine-kinase receptors, the outcome of the GDNF-GFRα1-RET interaction is the engagement of signaling effectors that include

the Ras/MAP kinase, PI3 kinase/AKT, and phospholipase C-γ (PLCγ) pathways (Ibanez, 2013).

Focusing on the subcellular organization of this interaction, GFRα1 is located on the outer leaflet of the plasma membrane via the GPI anchor, residing in detergent-insoluble, sphingolipid- and cholesterol-rich membrane microdomains known as lipid rafts (Tansey et al., 2000; Paratcha et al., 2001). In the context of GDNF signaling, it has been observed that, for efficient downstream signaling and maximal GDNF-mediated bioactivity, RET must be recruited to these lipid rafts by GFRα1. Additionally, activated RET interacts with Src family kynases (SFKs) only when it is localized within these microdomains (Tansey et al., 2000). In the absence of SFKs recruitment, a decrease in the activation of AKT and MAPK pathways is observed, highlighting the crucial role of Src activity for optimal GDNF-mediated neuronal survival and neurite outgrowth (Encinas et al., 2001). The intensity of RET engagement by GDNF can then be modulated by its localization inside or outside lipid rafts, as well as by the ability of GFRα to function in soluble form, the so-called "trans" signaling (Tansey et al., 2000; Paratcha et al., 2001).

The observation that GDNF and GFRα are widely expressed even in the absence of co-expressed RET suggests that the neurotrophic factor might exert its functions through alternative, RET-independent signaling systems (Trupp et al., 1997). GDNF can indeed interact with the Neural Cell Adhesion Molecule (NCAM), a cell surface glycoprotein crucial for neural development and plasticity. NCAM plays a key role in cell-cell adhesion, neuron growth, and migration during brain development. In addition to its ability to facilitate cellular interaction, NCAM, in conjunction with GFRα receptors, has been found to act as a RET-independent signaling receptor for GFLs. This interaction helps to explain the tissue distribution of GFRα proteins. Specifically, it has been demonstrated that GFRα can form a complex with NCAM, particularly with the p140NCAM isoform, at the cell surface. This interaction results in enhanced binding of GDNF and reduced homophilic interactions between NCAM molecules (Paratcha et al., 2003). The binding of GDNF activates Src-like kinase Fyn and focal adhesion kinase (FAK) in the cytoplasm, ultimately stimulating Schwann cell migration and promoting axonal growth in hippocampal and cortical neurons (Paratcha et al., 2003). GDNF can also act independently of both RET and NCAM. During development, GDNF and GFRα promote the differentiation of ventral precursors into GABAergic cells, enhancing their neuronal morphology and motility–see below (Pozas and Ibáñez, 2005). Moreover, all GFLs except persephin, when immobilized and bound to the extracellular matrix, interact with a transmembrane heparan sulphate proteoglycan named Syndecan-3. The interaction between GFLs and Syndecan-3 causes the activation of Src kinase and is crucial for promoting neurite outgrowth and cell spreading. Specifically, the GDNF-syndecan-3 interaction enhances the migration of cortical neurons (Bespalov et al., 2011). GDNF signaling pathways are summarized in Figure 1 – lower panel.

2 The role of GDNF in biological processes

GDNF is extensively distributed across both the CNS and peripheral tissues. In either physiological or pathological conditions, it can be produced and secreted by a variety of cell types, including neurons, glial cells such as astrocytes, Schwann cells, and oligodendrocytes, as well as by motor neurons and skeletal muscle cells (Henderson et al., 1994). Additionally, GDNF signaling is involved in the normal development and shaping of the ureteric bud in the kidneys, and it is also secreted by Sertoli cells within the testis, playing a role in self-renewal and proliferation of spermatogonial stem cell (Costantini, 2010). The crucial role of GDNF signaling in development is highlighted by the fact that mice deficient in RET, GDNF, or GFRα do not survive after birth, displaying kidney agenesis and a lack of many parasympathetic and enteric neurons. While mice lacking other GFLs or co-receptors are viable and fertile, the ones missing NRTN or GFRα2 show similar deficits in enteric and parasympathetic innervation.

2.1 Functions of GDNF in the CNS

2.1.1 GDNF in neurons

GDNF expression increases during embryonic development of the CNS, decreasing instead in adulthood, when it remains restricted to specific brain areas such as the cortex, hippocampus, striatum, Substantia nigra, thalamus, cerebellum, and spinal cord (Hellmich et al., 1996; Mogi et al., 2001).

2.1.1.1 Dopaminergic neurons

Since its initial isolation, GDNF has been regarded as a potential therapeutic neurotrophic factor playing a role in the development of Substantia nigra (SN) Dopaminergic (DA) neurons (Lin et al., 1993). In spite of its name, GDNF is not physiologically expressed in glial cells of the murine nervous system, but rather in neurons, particularly in parvalbumin-positive (PV+) interneurons, cholinergic and somatostatin-positive interneurons in the striatum, as demonstrated in transgenic mice with the lacZ cassette at the GDNF locus (Pascual et al., 2008; Gonzalez-Reyes et al., 2012; Hidalgo-Figueroa et al., 2012). The pre-α-pro-GDNF isoform appears to be the predominant isoform in the dopaminergic system, particularly in the striatum and substantia nigra (Airavaara et al., 2011). In healthy adult human brains, GDNF mRNA levels are typically low; however, they have been found to increase under pathological conditions such as Parkinson's disease, not only in neurons but also in astrocytes, microglia, and macrophages (Nakagawa et al., 2005; Bäckman et al., 2006; Azevedo et al., 2020).

GDNF principal receptors, GFRα1 and RET, mRNA and protein have been found to be expressed in rodent midbrain DA neurons from early embryonic development through to adulthood (Trupp et al., 1997; Golden et al., 1999; Airaksinen and Saarma, 2002). Several studies on rodent models have investigated the role of GDNF, GFRα1, and RET in the midbrain dopaminergic system. In rat and mouse models of Parkinson's disease, a transient increase followed by a decline in GFRα1 and RET mRNA levels was observed in the substantia nigra after 6-hydroxydopamine (6-OHDA) exposure (Marco et al., 2002). A similar reduction in RET receptor levels was reported in the striatum following 1-methyl-4-phenyl-1,2,3,6-tetrahydropyridine (MPTP) treatment (Hirata and Kiuchi, 2007), with both studies linking decreased GFRα1 and RET expression to the loss of tyrosine hydroxylase (TH)-positive dopaminergic neurons in the midbrain and their

diminished innervation of the striatum (Hirata and Kiuchi, 2007). GDNF injection during the postnatal period has been shown to have a protective effect on the survival of substantia nigra (SN) dopaminergic neurons, while transgenic models overexpressing GDNF exhibit increased dopamine levels and striatal innervation (Burke, 2004; Kumar et al., 2015). However, GDNF and GFRα1 knockout mice die shortly after birth without evident alterations in the dopaminergic system. In contrast, RET deficiency leads to a progressive loss of SN dopaminergic neurons in aging mice (Kramer et al., 2007). Moreover, in a recently published study, the disruption of the *gdnf* gene in zebrafish embryos, utilizing CRISPR/Cas9 gene editing, resulted in a significant reduction (~20%) of dopaminergic neurons in specific diencephalic clusters. This decrease was associated with altered expression of key transcription factors, including *otpb* and *lmx1b.1*, which are critical for dopaminergic neuron differentiation. Additionally, gdnf-deficient zebrafish exhibited impaired locomotor activity at 7 days post-fertilization and increased susceptibility to neurotoxic insults. These findings suggest that GDNF plays a conserved and essential role in the early development and functional maintenance of dopaminergic neurons (Wong et al., 2021). On the other hand, constitutive RET activation caused by a missense Meth918Thr mutation in the receptor results in an increased number of dopaminergic neurons in the SN and greater resistance to neurotoxins such as MPTP and 6-OHDA (Mijatovic et al., 2011). Moreover, conditional deletion studies of GDNF and RET have produced conflicting results regarding their necessity for neuronal survival in adulthood, suggesting the presence of compensatory mechanisms or alternative ligands (Pascual et al., 2008; Kopra et al., 2017). Several questions remain open, including the identity of the essential ligand for RET in the midbrain and the intracellular signaling pathways involved in neuronal survival.

2.1.1.2 Hippocampal neurons

GDNF and its receptors, GFRα1 and NCAM, are expressed in hippocampal neurons during embryonic and early postnatal development, with GFRa1 localized at both pre- and post-synaptic sites, while NCAM is restricted to presynaptic terminals (Ledda, 2007). In hippocampal neuron cultures, GDNF enhances synapse formation, and the interaction of GFRα1-coated beads with neurons in the presence of soluble GDNF can induce ectopic presynaptic sites, demonstrating an instructive role of GDNF/GFRα1 signaling in synaptogenesis (Ledda, 2007), a process that partially relies on NCAM at presynaptic terminals. *In vivo*, mutant mice with reduced GDNF levels exhibit impaired presynaptic maturation and a decreased number of presynaptic sites during hippocampal development, further supporting the role of GDNF in synaptic assembly (Bonafina et al., 2019). Furthermore, utilizing crystallography and electron microscopy, it has been identified a decameric assembly comprising two GFRα1 pentamers bridged by five GDNF dimers. This configuration facilitates synaptic adhesion by forming complexes that bridge adjacent cell membranes. Further experiments demonstrated that the presence of the RET receptor and heparan sulfate can inhibit the formation of this adhesion complex by competing for the same binding interfaces (Bonafina et al., 2019). These findings suggest a dual role for GFRα1: promoting synaptic adhesion independently of RET and engaging in RET-mediated trophic signaling. This dual functionality provides insights into the molecular mechanisms underlying neuronal connectivity and the modulation of synaptic structures (Bonafina et al., 2019).

Additionally, GDNF/GFRα1 signaling is critical for the structural and functional integration of adult-born granule cells into preexisting hippocampal circuits. Conditional GFRα1 knockout mice display deficits in behavioural pattern separation, a function linked to adult neurogenesis. Notably, physical activity enhances GDNF expression in the dentate gyrus, promoting GFRα1-dependent CREB activation and dendritic maturation. These findings highlight GDNF/GFRα1 signaling as a key regulator of both developmental and adult hippocampal plasticity, orchestrating synaptogenesis and the incorporation of new neurons into functional circuits (Bonafina et al., 2019). Recently, it has also been demonstrated that elevated levels of GDNF enhance GABAergic inhibitory inputs onto pyramidal neurons in the CA1 region of the hippocampus (Mikroulis et al., 2022). This effect is mediated through the activation of the RET receptor pathway, facilitated by the co-receptor GFRα1. Notably, the other GDNF receptors, namely as NCAM or Syndecan3, are not implicated in this process. The study also demonstrated similar enhancements in inhibitory synaptic transmission in human hippocampal slices obtained from epilepsy patients. These findings suggest that GDNF's ability to strengthen inhibitory signaling may contribute to its observed seizure-suppressant effects in various epilepsy models (Paolone et al., 2019; Wahlberg et al., 2020; Mikroulis et al., 2022).

2.1.1.3 Serotonergic neurons

Recent research has revealed significant interactions of GDNF with the serotonergic (5-HT) system. Serotonergic neurons of the raphe nuclei express GDNF receptors, particularly GFRα1 and RET, suggesting direct responsiveness to GDNF (Okaty et al., 2015; 2020; Huang et al., 2019; Ren et al., 2019). The effect of GDNF on the brain 5-HT system is controversial, with some studies showing positive effects on brain 5-HT (Pertusa et al., 2008; Naumenko et al., 2013), and others reporting little or no effect (Hudson et al., 1995; Mijatovic et al., 2007). On the other hand, serotonin increases GDNF expression and secretion from C6 rat glioma cells, acting predominantly via 5-HT2A receptors (Hisaoka et al., 2004; Tsuchioka et al., 2008). While moderate increases in GDNF enhance serotonin neuron number, serotonergic gene expression, and 5-HT levels, excessive GDNF leads to a decrease in serotonergic neurons differentiation (Menegola et al., 2004). This nonlinear relationship may explain previous conflicting reports on GDNF's effects on the serotonergic system.

Human data with antidepressants provide indirect evidence of a connection between GDNF and the serotonergic system. Acute or chronic administration of antidepressants increasing the levels of synaptic serotonin (such as tricyclic antidepressants, tetracyclic antidepressants, and serotonin-selective reuptake inhibitors) is indeed able to increase GDNF expression both in cell culture (Mercier et al., 2004; Hisaoka et al., 2007; Golan et al., 2011; Kajitani et al., 2012; Hisaoka-Nakashima et al., 2015; 2019; Abe et al., 2019) and in serum of patients with depression (Zhang et al., 2008). Preclinical data show that animals exposed to chronic unpredictable stress exhibit depression-like behavior and decreased GDNF expression in the hippocampus, that is reverted by chronic tricyclic antidepressant treatment (Uchida et al., 2011; Liu Q. et al.,

2012). In addition, GDNF may be decreased in the peripheral blood of patients with major depressive disorder (Takebayashi et al., 2006; Lin and Tseng, 2015; Sharma et al., 2016).

These findings suggest that the modulation of GDNF production may be a component of the therapeutic effect of antidepressants and that the fine-tuning of the serotonergic system by GDNF could be implied in the mechanisms of development of neuropsychiatric disorders. This nuanced relationship positions GDNF as a key neurotrophic factor beyond its classical dopaminergic role, critically involved in serotonergic system regulation (Popova et al., 2017).

2.1.1.4 GDNF and neurogenesis

Glial cell line-derived neurotrophic factor (GDNF) plays a multifaceted role in neurogenesis, influencing neural progenitor proliferation, migration, and differentiation across developmental and adult stages. GDNF has been recognized as a chemoattractant and differentiation signal for neuronal precursors, particularly in the subventricular zone and rostral migratory stream (Paratcha et al., 2006), where it modulates key signaling pathways, including RET/GFRα1 and PI3K/Akt, enhancing neurogenic output and synaptic integration (Airaksinen and Saarma, 2002).

In the forebrain, inhibitory GABAergic interneurons originate in the ventral telencephalon and migrate tangentially to reach the developing cortex, hippocampus, and olfactory bulb (Bartolini et al., 2013). The ganglionic eminences serve as temporary neurogenic regions, with the medial and caudal ganglionic eminences (MGE and CGE) generating most cortical GABAergic neurons, whereas the lateral ganglionic eminence (LGE) primarily contributes interneurons to the olfactory bulb. Both GDNF and its co-receptor GFRα1 are expressed in the MGE and along the migratory routes of GABAergic neurons (Pozas and Ibáñez, 2005), where GDNF facilitates differentiation and functions as a chemoattractant (Pozas and Ibáñez, 2005; Paratcha et al., 2006). These effects depend on GFRα1 but not on NCAM or RET, and the addition of soluble GFRα1 to MGE cultures enhances differentiation and migration even in cells lacking endogenous GFRα1 (Perrinjaquet et al., 2011). Moreover, syndecan-3 has been proposed as an alternative GDNF receptor in MGE-derived GABAergic neurons, independently of GFRα1 (Bespalov et al., 2011). Mice deficient in GFRα1 exhibit reduced migration of GABAergic neurons, leading to a lower number of inhibitory neurons in the cortex and hippocampus at birth (Pozas and Ibáñez, 2005), as well as disrupted integration of parvalbumin-expressing neurons and altered social behaviors linked to increased cortical excitability (Canty et al., 2009), a phenomenon consistent with certain autism models (Tabuchi et al., 2007). GFRα1 signaling is also crucial for olfactory system development, as its loss results in deficits in multiple GABAergic interneuron populations in the olfactory bulb, along with impairments in neurogenesis, migration, and sensory axon growth (Marks et al., 2012).

In stroke models, direct GDNF infusion significantly increases neurogenesis in the striatum (Kobayashi et al., 2006), while in the hippocampus, GDNF and its receptor GFRα1 are essential for proper integration of adult-born granule neurons (Bonafina et al., 2019). Following ischemia and traumatic brain injury, expression of various growth factors is increased and modulates neurogenesis, NSPC biology, and striatum connectivity (Christie and Turnley, 2013; Bacigaluppi et al., 2020; Butti et al., 2022). More recently, the neurogenic efficacy of GDNF has been harnessed through biomaterial-based delivery systems that enhance spinal cord repair and remyelination (Liu et al., 2024). Transplanting mesenchymal stem cells engineered to overexpress GDNF significantly improves neuroregenerative outcomes following ischemic or traumatic injury (Salgado et al., 2015; Chiavellini et al., 2022). This therapeutic strategy offers promising avenues in treating neurodegenerative disorders highlighting GDNF not only as a neuroprotective factor but also as a potent pro-neurogenic agent with promising translational potential in regenerative therapies.

2.1.1.5 GDNF and neuroplasticity

Neuroplasticity, the ability of the central nervous system to promote neurogenesis and renew connections, is influenced by different psychological, environmental and physiological factors, often involving the synthesis and secretion of neurotrophins (Kempermann et al., 2018).

For example, several recent studies highlight that engaging in regular physical exercise, whether aerobic or strength-based, can enhance cognitive function and promote neuroplasticity through different mechanisms (De Sousa Fernandes et al., 2020). Aerobic exercise primarily boosts glutamatergic signaling and neurotrophic factors like BDNF and CREB, while resistance training engages pathways involving PKCα and inflammatory cytokines, while it has been shown that both kinds of exercise share as a common outcome the upregulation of GDNF in plantaris myofibers (Gyorkos and Spitsbergen, 2014; Rabelo et al., 2017; Vilela et al., 2017). GDNF likely plays a central role in mediating the cognitive benefits of exercise by promoting hippocampal remodelling and resilience to age-related neural decline (Vilela et al., 2017). In young adult mice, voluntary exercise increases levels of GDNF and BDNF in the dentate gyrus (DG) (Cotman and Berchtold, 2002; Farmer et al., 2004). This upregulation correlates with enhanced dendritic growth and complexity in newly generated granule cells, suggesting a role for these factors in mediating activity-dependent neuronal integration. Notably, the effects of exercise on granule cells maturation seems to be dependent on GFRα1, the co-receptor for GDNF. Mechanistically, GDNF/GFRα1 signaling may act through the activation of the transcription factor CREB, which is known to regulate activity-dependent dendritic development (Jagasia et al., 2009). *In vitro* stimulation of DG-derived neural stem cell cultures with GDNF lead to phosphorylation of both CREB and Erk1/2, confirming that GDNF directly activates this signaling cascade in differentiating neurons (Bonafina et al., 2019).

2.1.2 GDNF in glial cells

As discussed above, GDNF is almost exclusively expressed by neurons in physiological conditions in the CNS (Pochon et al., 1997; Hidalgo-Figueroa et al., 2012), although its transcript can also be found in other cell types (Schaar et al., 1994). However, in various diseases, its expression in the brain changes over time, and other cell populations may become new reservoirs of GDNF production. Thus, in the following section, we will focus on the role of glia-derived GDNF.

2.1.2.1 GDNF in astrocytes

A growing body of evidence is pointing at a fundamental role of astrocyte-derived GDNF, which contributes to neuroprotection by modulating synaptic function, reducing oxidative stress, and

promoting neuronal survival. Studies on primary astrocytic culture highlighted that inflammatory stimuli distinctly regulate GDNF and Neuregulin-1 (NRG-1) in rodent astrocytes and microglia, with LPS treatment significantly increasing GDNF expression in astrocytes (Bresjanac and Antauer, 2000; Iravani et al., 2012; Kronenberg et al., 2019; Merienne et al., 2019). However, inflammatory stimuli are not the only ones able to impact GDNF expression. In an *in vitro* model of ischemia, utilizing neuron-glia and astrocyte cortical cultures subjected to oxygen and glucose deprivation, astrocyte-GDNF emerged as one of the released factors that mediated neuroprotection, elicited by high-frequency repetitive magnetic stimulation (Gava-Junior et al., 2023). Cinnamon and its metabolite sodium benzoate (NaB) can upregulate GDNF in human astrocytes. Oral administration of NaB and cinnamon increased astrocytic expression of GDNF in a model of PD *in vivo*, conferring neuroprotection of TH neurons of the *Substantia Nigra Pars Compacta*. However, this effect was absent in astrocyte-specific GDNF knockout mice (GDNFΔastro) (Patel et al., 2019). In another PD model, Gemfibrozil, a lipid-lowering drug approved by the FDA, has been shown to stimulate astrocytic GDNF, protecting dopaminergic neurons, through a PPARα-dependent pathway. Interestingly, Gemfibrozil was not effective in GDNFΔastro mice lacking GDNF, specifically in astrocytes (Gottschalk et al., 2021). Reactive astrocytes in Parkinson's disease models also exhibit neurotrophic functions, with Nestin-positive astrocytes expressing GDNF (Chen et al., 2006). Furthermore, astrocytic GDNF mitigates cognitive decline post-anesthesia by improving hippocampal synaptic plasticity (Lin et al., 2024).

Conversely, exposure to di-(2-ethylhexyl) phthalate (DEHP), an environmental endocrine-disrupting compound used in food packages, medical devices, office supplies, and children's toys, reduces the secretion of GDNF, interfering with the estrogen pathway, by downregulating the ERK/c-fos signaling in astrocytes (Wang et al., 2021). Excessive GDNF levels have been linked to astrocyte proliferation and potential gliomagenesis via the GFRα1/RET/MAPK/pCREB/LOXL2 axis (Wang et al., 2022). Finally, chronic overexpression of GDNF in brain astrocytes in a transgenic mouse model appears to have a detrimental influence on nigrostriatal dopamine metabolism and neurotransmission (Sotoyama et al., 2017).

2.1.2.2 GDNF in microglial cells

GDNF produced by activated microglia and macrophages can aid in the repair of CNS injuries. In a model of spinal cord injury, LPS-induced macrophage activation enhanced GDNF expression at lesion sites, promoting functional recovery of the spinal cord by sustaining a neurotrophic environment, while mitigating oxidative stress (Hashimoto et al., 2005). GDNF mRNA was also upregulated a few hours post-injury, in a model of mechanical injury in the mouse striatum, with brain macrophages as the primary source, establishing a critical link between GDNF expression and dopaminergic neuron protection (Liberatore et al., 1997). Microglia, which persist long after injury, contribute significantly to neurotrophic support, predominantly secreting GDNF and BDNF. This immune-mediated neurotrophic environment facilitates dopaminergic axonal sprouting and tissue repair, particularly in neurodegenerative contexts such as PD (Batchelor et al., 1999; 2002). Notably, sprouting dopaminergic fibers associate closely with neurotrophic factor-expressing microglia, exploiting them as structural support to navigate toward lesion edges (Batchelor et al., 2002). NG2-positive and Iba1-positive cells in the substantia nigra express GDNF and it has been shown that they are localized close to surviving TH-positive neurons in the *Substantia Nigra Pars Compacta*, suggesting a neuroprotective role for these cells in dopaminergic neuron survival (Kitamura et al., 2010). Moreover, experiments on BV2 cells have shown that GDNF exerts an anti-inflammatory effect by decreasing the release of pro-inflammatory cytokines such as TNF-α, TGF-β, IL-1β, and IL-12β in a model of inflammation induced by amyloid beta. This study highlights the involvement of the Hippo/YAP signaling pathway in this process (Qing et al., 2020). These findings collectively highlight the interplay between immune cells and neurotrophic factors in CNS repair.

2.1.2.3 GDNF and neuroinflammation

GDNF has long been recognized for its pivotal role in promoting axonal growth and neuronal regeneration, particularly within the peripheral nervous system (Lee et al., 2016). However, emerging evidence underscores its potent anti-inflammatory effects, highlighting its critical role in modulating neuroinflammation in several neurological diseases (Bido et al., 2024; Dingledine et al., 2024). Neuroinflammation is a complex process involving immune cell activation, vascular modulation, and alterations of resident cells, namely astrocytes and microglia. It can have both beneficial and detrimental effects on brain pathologies (Simonato et al., 2006; DiSabato et al., 2016).

A key aspect of this response is mediated by pattern recognition receptors (PRRs), which detect pathogen- and damage-associated molecular patterns (PAMPs and DAMPs), leading to immune cell activation (Iravani et al., 2012; Singh et al., 2022). Recent studies have shown that neurotrophic factors, including BDNF, NGF, and GDNF, play a crucial role in regulating neuroinflammatory pathways (Rocha et al., 2012; Guarino et al., 2022). Among these, GDNF is expressed by both astrocytes and microglia in pathological conditions, with astrocyte-secreted GDNF exerting a strong inhibitory effect on microglial activation, thereby mitigating neuroinflammation. GDNF can modulate the activation of microglia after Zymosan A (yeast-derived immune stimulant) treatment. It has been shown that the effect is dependent on GFRα1 and neutralization of GDNF or GFRα1, as well as GDNF silencing in astrocyte cultures, abolishes its regulatory effects, confirming that GDNF binding to the microglial GFRα1 receptor initiates intracellular signaling cascades responsible for suppressing microglial activation (Rocha et al., 2012).

In hippocampal astrocytes, GDNF/GFRα1 signaling contributes to neuroprotection by regulating immune responses. The upregulation of GDNF and its receptor GFRα-1 in hippocampal neurons and astrocytes enhances resilience against thrombin-induced neurotoxicity, known mechanisms to activate microglia, and induce neuronal death (Yun et al., 2020). Recently, it has been highlighted that astrocytic Sterile Alpha and TIR Motif Containing 1 (SARM1), which plays a critical role in axonal degeneration and inflammation in Multiple Sclerosis (MS), promotes neuroinflammation and axonal demyelination by suppressing GDNF expression. Moreover, pharmacological reduction of GDNF worsened disease progression, reinforcing its

neuroprotective function and therapeutic potential in MS (Jin et al., 2022). Beyond microglial regulation, GDNF modulates immune responses through GFL receptors, which are also expressed in immune cells. Activation of these receptors leads to the suppression of immune cell activity and the regulation of pro-inflammatory mediator release (Vargas-Leal et al., 2005).

2.1.3 GDNF from other cell sources in the CNS

Besides the already discussed cell types, GDNF has been identified in less abundant cellular components, in particular endothelial cells and pericytes, where it can act as a modulator of Blood-Brain-Barrier (BBB) and Blood-Nerve-Barrier (BNB) (Sharma et al., 2022). The BBB is a protective membrane that regulates molecular exchange between the bloodstream and neural tissue. Brain endothelial cells strictly limit the entry of molecules, particularly harmful ones, into the brain parenchyma. Indeed, a major challenge in CNS drug development is determining whether drug candidates can effectively cross the BBB. In recent years, several BBB and BNB models have been proposed, and Trans Endothelial Electrical Resistance (TEER) has been used as a key measure of barrier integrity, with values of 500 $\Omega \times cm^2$ or higher indicating an intact BBB and values of 150 $\Omega \times cm^2$ or higher indicating an intact BNB (Yosef and Ubogu, 2013). Studies have shown that GDNF strengthens the BBB by increasing tight junction protein expression, such as claudin-5, leading to elevated TEER values in various models, including porcine BBB and human brain microvascular endothelial cells (Igarashi et al., 1999; Shimizu et al., 2011; Kanjanasirirat et al., 2024). Similar effects were also demonstrated for BNB, where it was shown that MAPK signaling was essential for GDNF-mediated BNB TEER increase (Dong and Ubogu, 2018).

Finally, oligodendrocytes have been shown to produce and secrete GDNF. In particular, differentiated oligodendrocytes were identified as a source of GDNF, which can activate distinct intracellular pathways in neurons (Wilkins et al., 2003). In particular, decreased release of GDNF by these cells has been linked with neurodegeneration in a model of Multiple system atrophy (Ubhi et al., 2010).

2.2 Functions of GDNF in the peripheral nervous system

Initially identified for its role in dopaminergic neuron survival, GDNF is a crucial neurotrophic factor that supports the survival, maintenance, and regeneration of neurons in the peripheral nervous system (PNS). GDNF influences the development and function of peripheral neurons, including sensory, motor, and autonomic neuronal cells. It is produced by Schwann cells, muscle cells, and target tissues, creating a supportive microenvironment for nerve regeneration following injury. GDNF enhances axonal growth, promotes remyelination, and prevents neuronal apoptosis.

2.2.1 Development of sympathetic and parasympathetic neurons

Four ganglia in the cranial region host postganglionic parasympathetic neurons: the ciliary, sphenopalatine, submandibular, and otic ganglia. In newborn mice lacking RET, GFRα1, or GDNF, the otic and sphenopalatine ganglia are not present, indicating that the GDNF signaling through the GFRα1-RET receptor complex is critical for the development of these parasympathetic neurons during embryogenesis. Indeed, at embryonic day 12, these ganglia are already missing, and their neuronal precursors exhibit defects in migration and proliferation. Therefore, GDNF signaling through GFRα1–RET is necessary for the migration and proliferation of specific parasympathetic neuronal precursors in the early stages of embryonic development (Enomoto et al., 2000).

2.2.2 Somatic sensory neurons

Although *in vitro* studies showed that GFLs can support specific subpopulations of primary sensory neurons, their precise physiological functions *in vivo* remain largely unclear. Before birth, the survival of numerous primary sensory neurons in the petrosal ganglion relies on target-derived GDNF and BDNF (Erickson et al., 2001). These visceral chemoafferent neurons, which innervate the carotid body, play a role in the regulation of breathing. Indeed, mice lacking GDNF or RET exhibit respiratory disturbances, and mutations in these genes have been associated with congenital central hypoventilation syndrome (Manié et al., 2001).

2.2.3 Enteric neurons

Enteric neurons and ganglia originate from vagal and sacral neural crest cells, which migrate from the neural tube to the gut wall. Within the gut, they initially move in a rostrocaudal direction before transitioning from superficial to deeper layers. Following migration, these cells proliferate and differentiate to form the enteric plexus. In this context, GDNF/RET signaling is fundamental for the migration, proliferation, and survival of enteric neural crest cells (ENCCs) during the development of the enteric nervous system (Obermayr et al., 2013; Nagy and Goldstein, 2017). GDNF is secreted by mesodermal cells of the gut mesenchyme (Young et al., 2001), as well as by intestinal smooth muscle and epithelial cells in some pathological conditions (Xiao et al., 2014; Meir et al., 2015; Le Berre-Scoul et al., 2017). RET is expressed by ENCCs, while its co-receptor GFRα1 is required for efficient signaling. Studies in mice have demonstrated that the loss of function in GDNF, RET, or GFRα1 results in the complete absence of the enteric nervous system, underscoring the critical role of this pathway in gut innervation (Schuchardt et al., 1994; Moore et al., 1996; Cacalano et al., 1998). Experimental studies have shown that GDNF functions as a potent chemoattractant, reliably directing ENCC migration *in vitro* and in *ex vivo* explants (Natarajan et al., 2002; Wang et al., 2010). Overexpression or systemic administration of GDNF enhances ENCC proliferation and migration, increasing their numbers within the gut. However, while GDNF plays a crucial role in supporting the survival and neurogenesis of neuronal-fated ENCCs, it does not independently induce neural fate determination. Instead, it acts as a permissive factor, allowing the differentiation of ENCCs into specific neuronal subtypes at appropriate developmental stages (Wang et al., 2010). Recent studies also showed that GDNF supports intestinal barrier maturation and protects against inflammation-induced damage in inflammatory bowel disease (IBD). This finding highlights the role of enteric glial cells as a key source of GDNF, showing that its secretion enhances barrier function and prevents inflammatory breakdown, underscoring the importance of these cells in intestinal homeostasis (Meir et al., 2015; 2021). Collectively,

these findings highlight the indispensable role of GDNF/RET signaling in enteric nervous system development, regulating ENCC migration, proliferation, and differentiation while ensuring the formation of functionally diverse neuronal populations.

2.2.4 Motor neurons

GDNF plays a crucial role in motor neuron survival and development (Henderson et al., 1994; Oppenheim et al., 1995). While it promotes motor neuron viability *in vitro*, studies in knockout mice have demonstrated that the absence of GDNF or its receptor RET results in a significant loss of lumbar spinal motor neurons at birth, particularly affecting γ-motor neurons that innervate intrafusal muscle spindles (Moore et al., 1996; Sánchez et al., 1996; Gould et al., 2008; Bonanomi et al., 2012). This indicates that GDNF-dependent RET activation is essential for early motor neuron development, acting through the co-receptor GFRα1 (Gould et al., 2008). However, RET signaling does not appear necessary for motor neuron survival in adulthood but contributes to neuromuscular junction (NMJ) maintenance and muscle innervation. Evidence suggests that amyloid precursor protein (APP)-regulated GDNF expression is crucial for NMJ integrity and muscle function (Stanga et al., 2016).

Interestingly, altered GDNF levels have been observed in muscle biopsies and cerebrospinal fluid samples from ALS patients, suggesting its involvement in the disease (Yamamoto et al., 1999; Stanga et al., 2018). While its precise role in the pathology remains unclear, the GDNF/RET pathway may contribute to neuroprotection, as indicated by studies on the ALS drug Edaravone, which appears to exert its neuroprotective effects through this signaling axis (Li et al., 2022). Conversely, recent findings suggest that inhibiting RET tyrosine kinase activity could enhance retrograde transport in motor neurons (Rhymes et al., 2022), and its interaction with p75 may even promote apoptosis under certain conditions (Donnelly et al., 2018), highlighting the complexity of RET signaling in motor neuron health and disease.

2.2.5 GDNF delivery for regenerative medicine

GDNF plays a critical neurotrophic role in the regeneration of the peripheral nervous system, especially in supporting motor neuron survival, promoting axonal outgrowth, and enabling target muscle reinnervation after injury. GDNF delivery has been shown to protect motor neurons from apoptosis, stimulate robust axonal regeneration, and improve reinnervation of muscle targets, ultimately restoring neuromuscular function (Cintron-Colon et al., 2022). Recent studies highlight that timed delivery of GDNF enhances long-distance axonal regeneration and functional recovery in severe injury models like ventral root avulsion (Eggers et al., 2020a; 2020b). Sustained GDNF expression via viral vectors or hydrogels promotes neuromuscular junction repair and muscle fiber preservation, especially when delivered locally to the nerve or muscle (Kokai et al., 2011; Cintron-Colon et al., 2022). Furthermore, GDNF combined with biomaterial scaffolds such as nerve conduits or engineered Schwann cell grafts has shown enhanced reinnervation efficiency and reduced denervation-induced muscle atrophy (Zhang et al., 2009; Carvalho et al., 2021), although some contrasting results on the GDNF release and dosage are emerging (Kong et al., 2021). Altogether, these findings establish GDNF as a pivotal factor in peripheral nerve repair strategies, supporting both the neural and the muscular components of regeneration.

2.3 Function of GDNF outside the nervous system

Outside the nervous system, GDNF is essential for kidney morphogenesis by mediating reciprocal inductive signaling between the nephrogenic mesenchyme and the ureteric bud (Sariola and Saarma, 2003). GDNF, expressed in the mesenchyme, binds to RET and GFRα1 on the ureteric bud, promoting its branching and nephron formation (Suvanto et al., 1996; Sainio et al., 1997). Knockout studies of GDNF, RET, or GFRα1 result in severe renal defects, highlighting their critical role (Pichel et al., 1996; Saarma and Sariola, 1999). Factors such as heparan sulfate proteoglycans and transcription factors like Pax2 and Eya1 further regulate GDNF expression and function in kidney development (Brophy et al., 2001).

GDNF is secreted by Sertoli cells and plays a crucial role in regulating spermatogenesis through paracrine signaling. RET and GFRα1 are expressed in undifferentiated spermatogonia, which include spermatogenic stem cells. GDNF dosage is critical for stem cell balance: reduced levels lead to excessive differentiation and depletion, while overexpression causes undifferentiated spermatogonia clustering and infertility (reviewed in (Parekh et al., 2019).

2.3.1 GDNF and tumors

GDNF and its receptors play a crucial role in various cancers by influencing cell proliferation, migration, and invasion. In neuroendocrine tumors, GDNF is highly expressed in growth hormone-secreting pituitary adenomas but absent in most other pituitary tumors, suggesting a potential link to growth hormone signaling (Japo´n et al., 2002). RET activation by GDNF regulates somatotroph populations via the p53 apoptotic pathway, with Pit-1 transcription factor mediating this effect (Shewchuk et al., 2006; Cañibano et al., 2007). In pancreatic cancer, GDNF and its receptors are widely expressed, promoting tumor proliferation, invasion, and perineural infiltration through integrin β1 and matrix metalloprotease-9 (MMP-9) upregulation (Okada et al., 2003; Liu H. et al., 2012). Similarly, gliomas exhibit elevated GDNF levels, which enhance migration via the MAPK and JNK pathways and confer chemoresistance, while Growth Arrest Specific 1, a protein that is structurally homologous with the GFRα receptors, blocks this process by inhibiting RET signaling (Song and Moon, 2006; Domínguez-Monzón et al., 2009; Ng et al., 2009). In colorectal cancer, GDNF activates the RET/GFRα1 complex, enhancing β1 integrin expression and increasing VEGF-VEGFR-mediated migration through p38, PI3K/Akt, and HIF1α pathways (Huang et al., 2014). Breast cancer cells also express RET and GFRα1, responding to both autocrine and paracrine GDNF signaling (Neve et al., 2006; Esseghir et al., 2007; Kang et al., 2009). Testicular cancer is associated with GDNF overexpression, promoting invasive seminoma behavior (Sariola and Meng 2003; Ferranti et al., 2012). In melanoma, GDNF-driven RET activation correlates with malignancy, significantly enhancing proliferation

and invasion through phosphorylated Tyr905 in human melanoma cells (Kato et al., 1998; 2007; Narita et al., 2009; Ohshima et al., 2010).

Collectively, these findings underscore the oncogenic potential of GDNF signaling across multiple cancer types. The GDNF-RET axis functions as a double-edged sword that requires precise regulation to achieve therapeutic benefits. In certain oncological diseases, inhibiting this axis may be advantageous, while enhancing it could be vital for the survival of neurons in various neurological disorders. In the final chapter, we will concentrate on the latter therapeutic approach.

3 Challenges and future directions

3.1 Future directions in the elucidation of GDNF biology

Looking at the complex biology of GDNF (Figure 2), there are still several areas where our understanding remains incomplete. While we know some transcription factors [e.g., EGR1, CREB - (Liu et al., 2020; Marks et al., 2023)] that can induce GDNF expression, the full regulatory network controlling its expression in different tissues and under different physiological or pathological conditions is not well mapped and we still do not completely understand how GDNF expression is modulated in response to injury, inflammation, or neurodegeneration. From the signaling point of view, the biological relevance and downstream effects of the engagement of RET-independent pathways are still being explored, to define if they are compensatory, redundant or used to generate specialized signals.

The same can be said regarding context-dependent signaling, with specific responses, occurring most likely due to differences in receptor expression, co-signaling molecules, or epigenetic state of the cells, that still need to be clarified. For example, GDNF role in normal homeostasis of mature neurons, especially in the adult brain and peripheral autonomic system, is not well defined, while its role in pathology has been more characterized. GDNF interacts or overlaps with other neurotrophic factors like NGF, BDNF and Neurturin, but the functional cross-talk, synergy, or competition among these factors is still not fully understood. Finally, the mechanisms of secretion, diffusion, and gradient formation of GDNF *in vivo* remain technically hard to measure and model. Understanding GDNF distribution, degradation and turnover will be essential for both biology and therapeutic design.

3.2 Clinical potential of GDNF

Since its identification, GDNF, along with other GFLs, has sparked significant interest in the scientific community for its potential as a therapeutic agent in treating various neurological disorders. Multiple pre-clinical studies demonstrated that GDNF delivery supports the long-term motor neuron survival and axon regeneration following peripheral nerve injury in both newborn and adult mice (Hottinger et al., 2000; Eggers et al., 2019; Cintron-Colon et al., 2022). Additionally, GDNF has been found to have a potent analgesic effect in neuropathic pain models (Boucher et al., 2000) and to facilitate sensory axon regeneration into the spinal cord after dorsal root injury, thereby restoring sensory function (Ramer et al., 2000).

GDNF has also emerged as a potential antiepileptic candidate. GDNF and its receptor are expressed in the pyramidal and granule cells of the hippocampus, and a link has been found between the neurotrophic factor levels and epilepsy, since locally increasing GDNF levels in the temporal lobe can suppress epileptic activity (Kanter-Schlifke et al., 2007; Nanobashvili et al., 2019; Paolone et al., 2019).

In experimental models of focal ischemia, administering exogenous GDNF before or immediately after anoxia has been shown to reduce ischemic brain injury. Specifically, GDNF appears to mitigate excitotoxic neuronal death through an ERK-dependent pathway, making early administration crucial in the treatment of stroke (Wang et al., 1997).

The involvement of GDNF in regulating dopaminergic neuronal plasticity has shown promise in influencing the biochemical adaptation processes and the rewarding effects associated with drug addiction, suggesting its potential application in the treatment of substance or alcohol abuse (Messer et al., 2000; Ford et al., 2023).

Given its vital role in promoting the survival of dopaminergic neurons, GDNF has also demonstrated its ability to prevent neurotoxin-induced death of dopamine neurons and to facilitate functional recovery in various animal models of Parkinson's disease (Kearns and Gash, 1995; Tomac et al., 1995; Airaksinen and Saarma, 2002; Barker et al., 2020). These findings paved the way for the transition to clinical studies. Initial Phase I and II trials using direct intraventricular or intraputaminal infusion of GDNF (Kordower et al., 1999; Gill et al., 2003; Nutt et al., 2003; Love et al., 2005; Slevin et al., 2005) showed promising motor improvements and good safety profiles. However, a larger placebo-controlled Phase II trial (Lang et al., 2006) failed to show significant clinical benefit, raising concerns about inconsistent delivery and variable efficacy. More recent efforts in PD have focused on using convection-enhanced delivery (CED) systems (Barua et al., 2013; Taylor et al., 2013; Whone et al., 2019) and gene therapy vectors [e.g., AAV2-GDNF - (Rocco et al., 2022; Heiss et al., 2024)] to improve distribution and achieve sustained expression in the putamen of treated patients. These trials have shown better target coverage and encouraging biomarker responses (increased [18F]-DOPA uptake), but clinical improvements (and particularly systemic motor score improvements) remain modest or variable (Barker et al., 2020), underscoring the limitations that still need to be overcome to fully exploit GDNF therapeutic potential.

3.3 Current limitations of GDNF as a therapeutic molecule

Despite encouraging preclinical results, clinical translation remains complex due to issues related to optimal dosing, delivery methods, and long-term safety. Nonetheless, GDNF continues to be a promising candidate for the development of novel neurorestorative therapies. One of the primary challenges is effective delivery to target tissues, particularly the central nervous system, due to the BBB. Direct intracerebral administration, while bypassing the BBB, is highly invasive and may result in uneven distribution and local tissue damage. Furthermore, one of the biggest challenges is

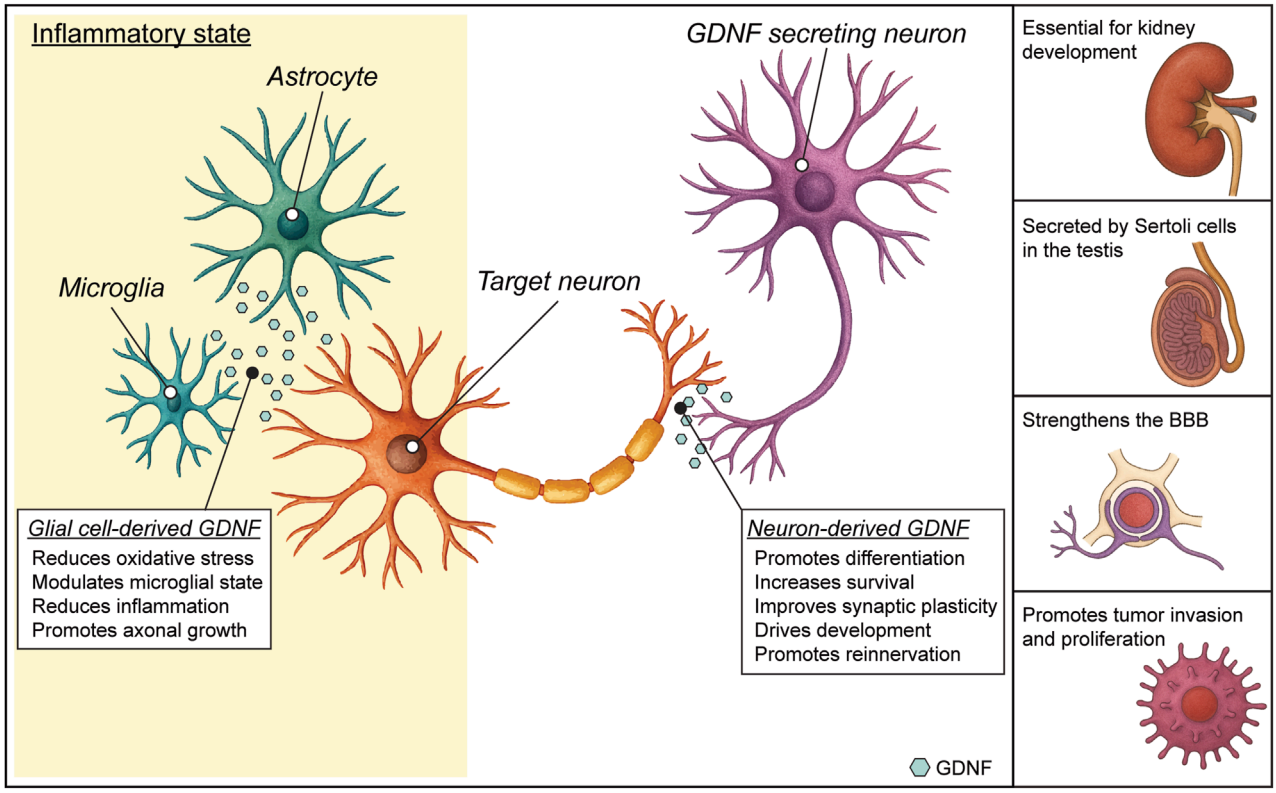

FIGURE 2
Glial cell line-derived neurotrophic factor (GDNF) functions. In the healthy nervous system, GDNF expression is mainly neuronal. The engagement of GDNF receptors in the neuronal membrane by GDNF binding triggers an intracellular signaling cascade that promotes different effects, such as survival and differentiation. In diseased states, GDNF can also be expressed by glial cells. Glial GDNF expression can promote neuroprotection, neuronal survival and modulate astrocyte and microglial activation, but sustained GDNF overexpression can lead to adverse effects. Outside the CNS (lateral panel), GDNF has fundamental roles in kidney morphogenesis, spermatogenesis in testis and maintenance of the blood brain barrier. GDNF can also have a role in inducing proliferation of certain tumors (see text).

indeed optimization of the dose of GDNF, which is complicated by its narrow therapeutic window. Indeed, low doses may be insufficient to elicit a neuroprotective or neurorestorative effect, while high doses can lead to adverse physiological changes. For instance, in preclinical models, excessive GDNF has been shown to cause ectopic or abnormal sprouting of dopaminergic fibres, especially in the striatum, which may disrupt normal circuitry (Georgievska, 2002; Marshall, 2023). It can also downregulate tyrosine hydroxylase, a key enzyme in dopamine synthesis, thereby paradoxically impairing dopaminergic signaling over time. Short half-life and rapid degradation in the extracellular space further limit its efficacy when delivered exogenously. In addition, variability in patient response and limited efficacy observed in clinical trials in Parkinson's disease highlight the need for improved delivery platforms, such as gene therapy or controlled-release systems. Finally, concerns regarding long-term safety, immune responses, and potential off-target effects pose additional hurdles that must be addressed before GDNF can be widely adopted in therapeutic settings.

Another layer of complexity is the temporal aspect: GDNF's effects may vary depending on the stage of disease progression, meaning that timing and duration of treatment are just as critical as dose magnitude. Chronic overexpression—such as in some preclinical gene therapy approaches—may lead to long-term dysregulation of neuronal homeostasis or immune activation.

Finally, inter-individual variability—due to differences in GDNF receptor (RET and GFRα1) expression levels, regional pathology, or genetic background—further complicates standardized dosing protocols, making personalized approaches potentially necessary for safe and effective use.

4 Conclusion

GDNF has long been studied for its neuroprotective effects, however, it also has broader physiological roles that still need elucidation. GDNF is indeed critical for the development, survival, and maintenance of dopaminergic, sympathetic, parasympathetic, and enteric neurons, and it plays essential roles in organ systems such as the kidney, testis, and gastrointestinal tract. Its involvement in tissue regeneration and modulation of inflammatory responses underscores its broader impact on homeostasis. Finally, the diversity of GDNF signaling pathways makes it a rich model for exploring ligand-receptor dynamics, signal integration, and cell-type specificity. In this review we explored GDNF's endogenous functions—beyond its therapeutic potential—providing insight into

its fundamental role as a neurotrophic factor in neural and non-neural systems, reframing GDNF as a multifaceted regulator of physiological function, rather than solely as a neurotrophic therapeutic.

Author contributions

CP: Writing – original draft, writing - review and editing. SC: Writing – original draft, Writing – review and editing, Conceptualization. LC: Writing – original draft. MS: Funding acquisition, Supervision, Writing – review and editing. BB: Conceptualization, Formal Analysis, Supervision, Writing – original draft, Writing – review and editing.

Funding

The author(s) declare that financial support was received for the research and/or publication of this article. Experiments performed in our laboratory were supported by a grant from the European Union's Horizon 2020 Work Programme (call H2020-FETOPEN-2018-2020) under grant agreement 964712 (PRIME).

Conflict of interest

The authors declare that the research was conducted in the absence of any commercial or financial relationships that could be construed as a potential conflict of interest.

Generative AI statement

The author(s) declare that Generative AI was used in the creation of this manuscript. To generate the cartoons of neuron and astrocyte in Figure 2

Publisher's note

All claims expressed in this article are solely those of the authors and do not necessarily represent those of their affiliated organizations, or those of the publisher, the editors and the reviewers. Any product that may be evaluated in this article, or claim that may be made by its manufacturer, is not guaranteed or endorsed by the publisher.

References

Abe, H., Kajitani, N., Okada-Tsuchioka, M., Omori, W., Yatsumoto, M., and Takebayashi, M. (2019). Antidepressant amitriptyline-induced matrix metalloproteinase-9 activation is mediated by src family tyrosine kinase, which leads to glial cell line-derived neurotrophic factor mRNA expression in rat astroglial cells. *Neuropsychopharm Rep.* 39, 156–163. doi:10.1002/npr2.12055

Airaksinen, M. S., and Saarma, M. (2002). The GDNF family: signalling, biological functions and therapeutic value. *Nat. Rev. Neurosci.* 3, 383–394. doi:10.1038/nrn812

Airavaara, M., Pletnikova, O., Doyle, M. E., Zhang, Y. E., Troncoso, J. C., and Liu, Q. R. (2011). Identification of novel GDNF isoforms and cis-antisense GDNFOS gene and their regulation in human middle temporal gyrus of alzheimer disease. *J. Biol. Chem.* 286, 45093–45102. doi:10.1074/jbc.M111.310250

Azevedo, M. D., Sander, S., and Tenenbaum, L. (2020). GDNF, a neuron-derived factor upregulated in glial cells during disease. *J. Clin. Med.* 9, 456. doi:10.3390/jcm9020456

Bacigaluppi, M., Sferruzza, G., Butti, E., Ottoboni, L., and Martino, G. (2020). Endogenous neural precursor cells in health and disease. *Brain Res.* 1730, 146619. doi:10.1016/j.brainres.2019.146619

Bäckman, C. M., Shan, L., Zhang, Y. J., Hoffer, B. J., Leonard, S., Troncoso, J. C., et al. (2006). Gene expression patterns for GDNF and its receptors in the human putamen affected by Parkinson's disease: a real-time PCR study. *Mol. Cell. Endocrinol.* 252, 160–166. doi:10.1016/j.mce.2006.03.013

Barker, R. A., Björklund, A., Gash, D. M., Whone, A., Van Laar, A., Kordower, J. H., et al. (2020). GDNF and parkinson's disease: where next? A summary from a recent workshop. *JPD* 10, 875–891. doi:10.3233/JPD-202004

Bartolini, G., Ciceri, G., and Marín, O. (2013). Integration of GABAergic interneurons into cortical cell assemblies: lessons from embryos and adults. *Neuron* 79, 849–864. doi:10.1016/j.neuron.2013.08.014

Barua, N. U., Woolley, M., Bienemann, A. S., Johnson, D. E., Lewis, O., Wyatt, M. J., et al. (2013). Intermittent convection-enhanced delivery to the brain through a novel transcutaneous bone-anchored port. *J. Neurosci. Methods* 214, 223–232. doi:10.1016/j.jneumeth.2013.02.007

Batchelor, P. E., Liberatore, G. T., Wong, J. Y. F., Porritt, M. J., Frerichs, F., Donnan, G. A., et al. (1999). Activated macrophages and microglia induce dopaminergic sprouting in the injured striatum and express brain-derived neurotrophic factor and glial cell line-derived neurotrophic factor. *J. Neurosci.* 19, 1708–1716. doi:10.1523/JNEUROSCI.19-05-01708.1999

Batchelor, P. E., Porritt, M. J., Martinello, P., Parish, C. L., Liberatore, G. T., Donnan, G. A., et al. (2002). Macrophages and microglia produce local trophic gradients that stimulate axonal sprouting toward but not beyond the wound edge. *Mol. Cell Neurosci.* 21, 436–453. doi:10.1006/mcne.2002.1185

Bespalov, M. M., Sidorova, Y. A., Tumova, S., Ahonen-Bishopp, A., Magalhães, A. C., Kulesskiy, E., et al. (2011). Heparan sulfate proteoglycan syndecan-3 is a novel receptor for GDNF, neurturin, and artemin. *J. Cell Biol.* 192, 153–169. doi:10.1083/jcb.201009136

Bido, S., Nannoni, M., Muggeo, S., Gambarè, D., Ruffini, G., Bellini, E., et al. (2024). Microglia-specific IL-10 gene delivery inhibits neuroinflammation and neurodegeneration in a mouse model of Parkinson's disease. *Sci. Transl. Med.* 16, eadm8563. doi:10.1126/scitranslmed.adm8563

Bonafina, A., Trinchero, M. F., Ríos, A. S., Bekinschtein, P., Schinder, A. F., Paratcha, G., et al. (2019). GDNF and GFRα1 are required for proper integration of adult-born hippocampal neurons. *Cell Rep.* 29, 4308–4319.e4. doi:10.1016/j.celrep.2019.11.100

Bonanomi, D., Chivatakarn, O., Bai, G., Abdesselem, H., Lettieri, K., Marquardt, T., et al. (2012). Ret is a multifunctional coreceptor that integrates Diffusible- and contact-axon guidance signals. *Cell* 148, 568–582. doi:10.1016/j.cell.2012.01.024

Boucher, T. J., Okuse, K., Bennett, D. L. H., Munson, J. B., Wood, J. N., and McMahon, S. B. (2000). Potent analgesic effects of GDNF in neuropathic pain states. *Science* 290, 124–127. doi:10.1126/science.290.5489.124

Bresjanac, M., and Antauer, G. (2000). Reactive astrocytes of the quinolinic acid-lesioned rat striatum express GFRalpha1 as well as GDNF *in vivo*. *Exp. Neurol.* 164, 53–59. doi:10.1006/exnr.2000.7416

Brophy, P. D., Ostrom, L., Lang, K. M., and Dressler, G. R. (2001). Regulation of ureteric bud outgrowth by Pax2-dependent activation of the glial derived neurotrophic factor gene. *Development* 128, 4747–4756. doi:10.1242/dev.128.23.4747

Burke, R. E. (2004). Ontogenic cell death in the nigrostriatal system. *Cell Tissue Res.* 318, 63–72. doi:10.1007/s00441-004-0908-4

Butti, E., Cattaneo, S., Bacigaluppi, M., Cambiaghi, M., Scotti, G. M., Brambilla, E., et al. (2022). Neural precursor cells tune striatal connectivity through the release of IGFBPL1. *Nat. Commun.* 13, 7579. doi:10.1038/s41467-022-35341-y

Cacalano, G., Fariñas, I., Wang, L.-C., Hagler, K., Forgie, A., Moore, M., et al. (1998). GFRalpha1 is an essential receptor component for GDNF in the developing nervous system and kidney. *Neuron* 21, 53–62. doi:10.1016/S0896-6273(00)80514-0

Cañibano, C., Rodriguez, N. L., Saez, C., Tovar, S., Garcia-Lavandeira, M., Borrello, M. G., et al. (2007). The dependence receptor ret induces apoptosis in somatotrophs through a Pit-1/p53 pathway, preventing tumor growth. *EMBO J.* 26, 2015–2028. doi:10.1038/sj.emboj.7601636

Canty, A. J., Dietze, J., Harvey, M., Enomoto, H., Milbrandt, J., and Ibáñez, C. F. (2009). Regionalized loss of parvalbumin interneurons in the cerebral cortex of mice with deficits in GFRalpha1 signaling. *J. Neurosci.* 29, 10695–10705. doi:10.1523/JNEUROSCI.2658-09.2009

Carvalho, C. R., Chang, W., Silva-Correia, J., Reis, R. L., Oliveira, J. M., and Kohn, J. (2021). Engineering silk fibroin-based nerve conduit with neurotrophic factors for proximal protection after peripheral nerve injury. *Adv. Healthc. Mater.* 10, 2000753. doi:10.1002/adhm.202000753

Chen, L.-W., Zhang, J.-P., Kwok-Yan Shum, D., and Chan, Y.-S. (2006). Localization of nerve growth factor, neurotrophin-3, and glial cell line-derived neurotrophic factor in nestin-expressing reactive astrocytes in the caudate-putamen of 1-methyl-4-phenyl-1,2,3,6-tetrahydropyridine-treated C57/Bl mice. *J. Comp. Neurol.* 497, 898–909. doi:10.1002/cne.21014

Chiavellini, P., Canatelli-Mallat, M., Lehmann, M., Goya, R. G., and Morel, G. R. (2022). Therapeutic potential of glial cell line-derived neurotrophic factor and cell reprogramming for hippocampal-related neurological disorders. *Neural Regen. Res.* 17, 469–476. doi:10.4103/1673-5374.320966

Christie, K., and Turnley, A. (2013). Regulation of endogenous neural stem/progenitor cells for neural repair - factors that promote neurogenesis and gliogenesis in the normal and damaged brain. *Front. Cell. Neurosci.* 6, 70. doi:10.3389/fncel.2012.00070

Cintron-Colon, A., Almeida-Alves, G., VanGyseghem, J., and Spitsbergen, J. (2022). GDNF to the rescue: GDNF delivery effects on motor neurons and nerves, and muscle re-innervation after peripheral nerve injuries. *Neural Regen. Res.* 17, 748–753. doi:10.4103/1673-5374.322446

Costantini, F. (2010). GDNF/ret signaling and renal branching morphogenesis: from mesenchymal signals to epithelial cell behaviors. *Organogenesis* 6, 252–262. doi:10.4161/org.6.4.12680

Cotman, C. W., and Berchtold, N. C. (2002). Exercise: a behavioral intervention to enhance brain health and plasticity. *Trends Neurosci.* 25 (6), 295–301. doi:10.1016/s0166-2236(02)02143-4

Cristina, N., Chatellard-Causse, C., Manier, M., and Feuerstein, C. (1995). GDNF: existence of a second transcript in the brain. *Mol. Brain Res.* 32, 354–357. doi:10.1016/0169-328X(95)00103-Y

De Sousa Fernandes, M. S., Ordônio, T. F., Santos, G. C. J., Santos, L. E. R., Calazans, C. T., Gomes, D. A., et al. (2020). Effects of physical exercise on neuroplasticity and brain function: a systematic review in human and animal studies. *Neural Plast.* 2020, 8856621–21. doi:10.1155/2020/8856621

Dingledine, R., Varvel, N. H., Ravizza, T., and Vezzani, A. (2024). "Neuroinflammation in epilepsy: cellular and molecular mechanisms," in *Jasper's basic mechanisms of the epilepsies*. Editors J. L. Noebels, M. Avoli, M. A. Rogawski, A. Vezzani, and A. V. Delgado-Escueta (New York: Oxford University Press). Available online at: http://www.ncbi.nlm.nih.gov/books/NBK609862/ (Accessed March 29, 2025).

DiSabato, D. J., Quan, N., and Godbout, J. P. (2016). Neuroinflammation: the devil is in the details. *J. Neurochem.* 139, 136–153. doi:10.1111/jnc.13607

Domínguez-Monzón, G., Benítez, J. A., Vergara, P., Lorenzana, R., and Segovia, J. (2009). Gas1 inhibits cell proliferation and induces apoptosis of human primary gliomas in the absence of shh. *Int. J. Dev. Neurosci.* 27, 305–313. doi:10.1016/j.ijdevneu.2009.03.009

Dong, C., and Ubogu, E. E. (2018). GDNF enhances human blood-nerve barrier function *in vitro via* MAPK signaling pathways. *Tissue Barriers* 6, 1–22. doi:10.1080/21688370.2018.1546537

Donnelly, C. R., Gabreski, N. A., Suh, E. B., Chowdhury, M., and Pierchala, B. A. (2018). Non-canonical ret signaling augments p75-mediated cell death in developing sympathetic neurons. *J. Cell Biol.* 217, 3237–3253. doi:10.1083/jcb.201703120

Eggers, R., De Winter, F., Hoyng, S. A., Hoeben, R. C., Malessy, M. J. A., Tannemaat, M. R., et al. (2019). Timed GDNF gene therapy using an immune-evasive gene switch promotes long distance axon regeneration. *Brain* 142, 295–311. doi:10.1093/brain/awy340

Eggers, R., de Winter, F., Smit, L., Luimens, M., Muir, E. M., Bradbury, E. J., et al. (2020a). Combining timed GDNF and ChABC gene therapy to promote long-distance regeneration following ventral root avulsion and repair. *FASEB J.* 34, 10605–10622. doi:10.1096/fj.202000559R

Eggers, R., De Winter, F., Tannemaat, M. R., Malessy, M. J. A., and Verhaagen, J. (2020b). GDNF gene therapy to repair the injured peripheral nerve. *Front. Bioeng. Biotechnol.* 8, 583184. doi:10.3389/fbioe.2020.583184

Eigenbrot, C., and Gerber, N. (1997). X-ray structure of glial cell-derived neurotrophic factor at 1.9 A resolution and implications for receptor binding. *Nat. Struct. Mol. Biol.* 4, 435–438. doi:10.1038/nsb0697-435

Encinas, M., Tansey, M. G., Tsui-Pierchala, B. A., Comella, J. X., Milbrandt, J., and Johnson, E. M. (2001). c-Src is required for glial cell line-derived neurotrophic factor (GDNF) family ligand-mediated neuronal survival *via* a Phosphatidylinositol-3 kinase (PI-3K)-Dependent pathway. *J. Neurosci.* 21, 1464–1472. doi:10.1523/JNEUROSCI.21-05-01464.2001

Enomoto, H., Heuckeroth, R. O., Golden, J. P., Johnson, E. M., and Milbrandt, J. (2000). Development of cranial parasympathetic ganglia requires sequential actions of GDNF and neurturin. *Development* 127, 4877–4889. doi:10.1242/dev.127.22.4877

Erickson, J. T., Brosenitsch, T. A., and Katz, D. M. (2001). Brain-derived neurotrophic factor and glial cell line-derived neurotrophic factor are required simultaneously for survival of dopaminergic primary sensory neurons *in vivo*. *J. Neurosci.* 21, 581–589. doi:10.1523/JNEUROSCI.21-02-00581.2001

Esseghir, S., Todd, S. K., Hunt, T., Poulsom, R., Plaza-Menacho, I., Reis-Filho, J. S., et al. (2007). A role for glial cell-derived neurotrophic factor-induced expression by inflammatory cytokines and RET/GFRα1 receptor up-regulation in breast cancer. *Cancer Res.* 67, 11732–11741. doi:10.1158/0008-5472.CAN-07-2343

Farmer, J., Zhao, X., van Praag, H., Wodtke, K., Gage, F. H., and Christie, B. R. (2004). Effects of voluntary exercise on synaptic plasticity and gene expression in the dentate gyrus of adult male Sprague-Dawley rats *in vivo*. *Neuroscience*. 124 (1), 71–79. doi:10.1016/j.neuroscience.2003.09.029

Ferranti, F., Muciaccia, B., Ricci, G., Dovere, L., Canipari, R., Magliocca, F., et al. (2012). Glial cell line-derived neurotrophic factor promotes invasive behaviour in testicular seminoma cells. *Int. J. Androl.* 35, 758–768. doi:10.1111/j.1365-2605.2012.01267.x

Ford, M. M., George, B. E., Van Laar, V. S., Holleran, K. M., Naidoo, J., Hadaczek, P., et al. (2023). GDNF gene therapy for alcohol use disorder in Male non-human Primates. *Nat. Med.* 29, 2030–2040. doi:10.1038/s41591-023-02463-9

Gava-Junior, G., Ferreira, S. A., Roque, C., Mendes-Oliveira, J., Serrenho, I., Pinto, N., et al. (2023). High-frequency repetitive magnetic stimulation rescues ischemia-injured neurons through modulation of glial-derived neurotrophic factor present in the astrocyte's secretome. *J. Neurochem.* 164, 813–828. doi:10.1111/jnc.15740

Georgievska, B., Kirik, D., and Björklund, A. (2002). Aberrant sprouting and downregulation of tyrosine hydroxylase in lesioned nigrostriatal dopamine neurons induced by long-lasting overexpression of glial cell line derived neurotrophic factor in the striatum by lentiviral gene transfer. *Exp. Neurol.* 177, 461–474. doi:10.1006/exnr.2002.8006

Gill, S. S., Patel, N. K., Hotton, G. R., O'Sullivan, K., McCarter, R., Bunnage, M., et al. (2003). Direct brain infusion of glial cell line–derived neurotrophic factor in parkinson disease. *Nat. Med.* 9, 589–595. doi:10.1038/nm850

Golan, M., Schreiber, G., and Avissar, S. (2011). Antidepressants elevate GDNF expression and release from C_6 glioma cells in a β-arrestin1-dependent, CREB interactive pathway. *Int. J. Neuropsychopharm.* 14, 1289–1300. doi:10.1017/S1461145710001550

Golden, J. P., Demaro, J. A., Osborne, P. A., Milbrandt, J., and Johnson, E. M. (1999). Expression of neurturin, GDNF, and GDNF family-receptor mRNA in the developing and mature mouse. *Exp. Neurol.* 158, 504–528. doi:10.1006/exnr.1999.7127

Gonzalez-Reyes, L. E., Verbitsky, M., Blesa, J., Jackson-Lewis, V., Paredes, D., Tillack, K., et al. (2012). Sonic hedgehog maintains cellular and neurochemical homeostasis in the adult nigrostriatal circuit. *Neuron* 75, 306–319. doi:10.1016/j.neuron.2012.05.018

Gottschalk, C. G., Jana, M., Roy, A., Patel, D. R., and Pahan, K. (2021). Gemfibrozil protects dopaminergic neurons in a mouse model of parkinson's disease *via* PPARα-Dependent astrocytic GDNF pathway. *J. Neurosci.* 41, 2287–2300. doi:10.1523/JNEUROSCI.3018-19.2021

Gould, T. W., Yonemura, S., Oppenheim, R. W., Ohmori, S., and Enomoto, H. (2008). The neurotrophic effects of glial cell line-derived neurotrophic factor on spinal motoneurons are restricted to fusimotor subtypes. *J. Neurosci.* 28, 2131–2146. doi:10.1523/JNEUROSCI.5185-07.2008

Guarino, A., Bettegazzi, B., Aziz, N., Barbieri, M., Bochicchio, D., Crippa, L., et al. (2022). Low-dose 7,8-Dihydroxyflavone administration after status epilepticus prevents epilepsy development. *Neurotherapeutics* 19, 1951–1965. doi:10.1007/s13311-022-01299-4

Gyorkos, A. M., and Spitsbergen, J. M. (2014). GDNF content and NMJ morphology are altered in recruited muscles following high-speed and resistance wheel training. *Physiol. Rep.* 2, e00235. doi:10.1002/phy2.235

Hashimoto, M., Nitta, A., Fukumitsu, H., Nomoto, H., Shen, L., and Furukawa, S. (2005). Inflammation-induced GDNF improves locomotor function after spinal cord injury. *NeuroReport* 16, 99–102. doi:10.1097/00001756-200502080-00004

Heiss, J. D., Ray-Chaudhury, A., Kleiner, D. E., Ehrlich, D. J., Scott, G., Edwards, N. A., et al. (2024). Persistent GDNF expression 45 months after putaminal infusion of AAV2- *GDNF* in a patient with parkinson's disease. *Mov. Disord.* 39, 1412–1417. doi:10.1002/mds.29820

Hellmich, H. L., Kos, L., Cho, E. S., Mahon, K. A., and Zimmer, A. (1996). Embryonic expression of glial cell-line derived neurotrophic factor (GDNF) suggests multiple developmental roles in neural differentiation and epithelial-mesenchymal interactions. *Mech. Dev.* 54, 95–105. doi:10.1016/0925-4773(95)00464-5

Henderson, C. E., Phillips, H. S., Pollock, R. A., Davies, A. M., Lemeulle, C., Armanini, M., et al. (1994). GDNF: a potent survival factor for motoneurons present in peripheral nerve and muscle. *Science* 266, 1062–1064. doi:10.1126/science.7973664

Hidalgo-Figueroa, M., Bonilla, S., Gutiérrez, F., Pascual, A., and López-Barneo, J. (2012). GDNF is predominantly expressed in the PV+ neostriatal interneuronal ensemble in normal mouse and after injury of the nigrostriatal pathway. *J. Neurosci.* 32, 864–872. doi:10.1523/JNEUROSCI.2693-11.2012

Hirata, Y., and Kiuchi, K. (2007). Rapid down-regulation of ret following exposure of dopaminergic neurons to neurotoxins. *J. Neurochem.* 102, 1606–1613. doi:10.1111/j.1471-4159.2007.04695.x

Hisaoka, K., Nishida, A., Takebayashi, M., Koda, T., Yamawaki, S., and Nakata, Y. (2004). Serotonin increases glial cell line-derived neurotrophic factor release in rat C6 glioblastoma cells. *Brain Res.* 1002, 167–170. doi:10.1016/j.brainres.2004.01.009

Hisaoka, K., Takebayashi, M., Tsuchioka, M., Maeda, N., Nakata, Y., and Yamawaki, S. (2007). Antidepressants increase glial cell line-derived neurotrophic factor production through monoamine-independent activation of protein tyrosine kinase and extracellular signal-regulated kinase in glial cells. *J. Pharmacol. Exp. Ther.* 321, 148–157. doi:10.1124/jpet.106.116558

Hisaoka-Nakashima, K., Miyano, K., Matsumoto, C., Kajitani, N., Abe, H., Okada-Tsuchioka, M., et al. (2015). Tricyclic antidepressant amitriptyline-induced glial cell line-derived neurotrophic factor production involves pertussis toxin-sensitive Gαi/o activation in astroglial cells. *J. Biol. Chem.* 290, 13678–13691. doi:10.1074/jbc.M114.622415

Hisaoka-Nakashima, K., Taki, S., Watanabe, S., Nakamura, Y., Nakata, Y., and Morioka, N. (2019). Mirtazapine increases glial cell line-derived neurotrophic factor production through lysophosphatidic acid 1 receptor-mediated extracellular signal-regulated kinase signaling in astrocytes. *Eur. J. Pharmacol.* 860, 172539. doi:10.1016/j.ejphar.2019.172539

Hottinger, A. F., Azzouz, M., Déglon, N., Aebischer, P., and Zurn, A. D. (2000). Complete and long-term rescue of lesioned adult motoneurons by lentiviral-mediated expression of glial cell line-derived neurotrophic factor in the facial nucleus. *J. Neurosci.* 20, 5587–5593. doi:10.1523/JNEUROSCI.20-15-05587.2000

Huang, K. W., Ochandarena, N. E., Philson, A. C., Hyun, M., Birnbaum, J. E., Cicconet, M., et al. (2019). Molecular and anatomical organization of the dorsal raphe nucleus. *eLife* 8, e46464. doi:10.7554/eLife.46464

Huang, S. M., Chen, T. S., Chiu, C. M., Chang, L. K., Liao, K. F., Tan, H. M., et al. (2014). GDNF increases cell motility in human Colon cancer through VEGF-VEGFR1 interaction. *Endocrine-Related Cancer* 21, 73–84. doi:10.1530/ERC-13-0351

Hudson, J., Granholm, A.-C., Gerhardt, G. A., Henry, M. A., Hoffman, A., Biddle, P., et al. (1995). Glial cell line-derived neurotrophic factor augments midbrain dopaminergic circuits *in vivo*. *Brain Res. Bull.* 36, 425–432. doi:10.1016/0361-9230(94)00224-O

Ibanez, C. F. (2013). Structure and physiology of the RET receptor tyrosine kinase. *Cold Spring Harb. Perspect. Biol.* 5, a009134. doi:10.1101/cshperspect.a009134

Igarashi, Y., Utsumi, H., Chiba, H., Yamada-Sasamori, Y., Tobioka, H., Kamimura, Y., et al. (1999). Glial cell line-derived neurotrophic factor induces barrier function of endothelial cells forming the blood–brain barrier. *Biochem. Biophysical Res. Commun.* 261, 108–112. doi:10.1006/bbrc.1999.0992

Iravani, M. M., Sadeghian, M., Leung, C. C. M., Jenner, P., and Rose, S. (2012). Lipopolysaccharide-induced nigral inflammation leads to increased IL-1β tissue content and expression of astrocytic glial cell line-derived neurotrophic factor. *Neurosci. Lett.* 510, 138–142. doi:10.1016/j.neulet.2012.01.022

Jagasia, R., Steib, K., Englberger, E., Herold, S., Faus-Kessler, T., Saxe, M., et al. (2009). GABA-cAMP response element-binding protein signaling regulates maturation and survival of newly generated neurons in the adult hippocampus. *J. Neurosci.* 29, 7966–7977. doi:10.1523/JNEUROSCI.1054-09.2009

Japo´n, M. A., Japo´n, J., Urbano, A. G., Saéz, C. S., Segura, D. I., Cerro, A. L., et al. (2002). Glial-derived neurotropic factor and RET gene expression in normal human anterior pituitary cell types and in pituitary tumors. *J. Clin. Endo-crinol Metab.* 87, 1879–1884. doi:10.1210/jcem.87.4.8383

Jin, L., Zhang, J., Hua, X., Xu, X., Li, J., Wang, J., et al. (2022). Astrocytic SARM1 promotes neuroinflammation and axonal demyelination in experimental autoimmune encephalomyelitis through inhibiting GDNF signaling. *Cell Death Dis.* 13, 759–13. doi:10.1038/s41419-022-05202-z

Kajitani, N., Hisaoka-Nakashima, K., Morioka, N., Okada-Tsuchioka, M., Kaneko, M., Kasai, M., et al. (2012). Antidepressant acts on astrocytes leading to an increase in the expression of neurotrophic/growth factors: differential regulation of FGF-2 by noradrenaline. *PLoS ONE* 7, e51197. doi:10.1371/journal.pone.0051197

Kang, J., Perry, J. K., Pandey, V., Fielder, G. C., Mei, B., Qian, P. X., et al. (2009). Artemin is oncogenic for human mammary carcinoma cells. *Oncogene* 28, 2034–2045. doi:10.1038/onc.2009.66

Kanjanasirirat, P., Saengsawang, W., Ketsawatsomkron, P., Asavapanumas, N., Borwornpinyo, S., Soodvilai, S., et al. (2024). GDNF and cAMP significantly enhance *in vitro* blood-brain barrier integrity in a humanized tricellular transwell model. *Heliyon* 10, e39343. doi:10.1016/j.heliyon.2024.e39343

Kanter-Schlifke, I., Georgievska, B., Kirik, D., and Kokaia, M. (2007). Seizure suppression by GDNF gene therapy in animal models of epilepsy. *Mol. Ther.* 15, 1106–1113. doi:10.1038/sj.mt.6300148

Kato, M., Ohgami, N., Kawamoto, Y., Tsuzuki, T., Hossain, K., Yanagishita, T., et al. (2007). Protective effect of hyperpigmented skin on UV-mediated cutaneous cancer development. *J. Investigative Dermatology* 127, 1244–1249. doi:10.1038/sj.jid.5700659

Kato, M., Takahashi, M., Akhand, A. A., Liu, W., Dai, Y., Shimizu, S., et al. (1998). Transgenic mouse model for skin malignant melanoma. *Oncogene* 17, 1885–1888. doi:10.1038/sj.onc.1202077

Kearns, C. M., and Gash, D. M. (1995). GDNF protects nigral dopamine neurons against 6-hydroxydopamine *in vivo*. *Brain Res.* 672, 104–111. doi:10.1016/0006-8993(94)01366-P

Kempermann, G., Gage, F. H., Aigner, L., Song, H., Curtis, M. A., Thuret, S., et al. (2018). Human adult neurogenesis: evidence and remaining questions. *Cell Stem Cell* 23, 25–30. doi:10.1016/j.stem.2018.04.004

Kitamura, Y., Inden, M., Minamino, H., Abe, M., Takata, K., and Taniguchi, T. (2010). The 6-hydroxydopamine-induced nigrostriatal neurodegeneration produces microglia-like NG2 glial cells in the rat substantia nigra. *Glia* 58, 1686–1700. doi:10.1002/glia.21040

Kobayashi, T., Ahlenius, H., Thored, P., Kobayashi, R., Kokaia, Z., and Lindvall, O. (2006). Intracerebral infusion of glial cell line-derived neurotrophic factor promotes striatal neurogenesis after stroke in adult rats. *Stroke* 37, 2361–2367. doi:10.1161/01.STR.0000236025.44089.e1

Kokai, L. E., Bourbeau, D., Weber, D., McAtee, J., and Marra, K. G. (2011). Sustained growth factor delivery promotes axonal regeneration in long gap peripheral nerve repair. *Tissue Eng. Part A* 17, 1263–1275. doi:10.1089/ten.tea.2010.0507

Kong, Y., Shi, W., Zhang, D., Jiang, X., Kuss, M., Liu, B., et al. (2021). Injectable, antioxidative, and neurotrophic factor-deliverable hydrogel for peripheral nerve regeneration and neuropathic pain relief. *Appl. Mater. Today* 24, 101090. doi:10.1016/j.apmt.2021.101090

Kopra, J. J., Panhelainen, A., Af Bjerkén, S., Porokuokka, L. L., Varendi, K., Olfat, S., et al. (2017). Dampened amphetamine-stimulated behavior and altered dopamine transporter function in the absence of brain GDNF. *J. Neurosci.* 37, 1581–1590. doi:10.1523/JNEUROSCI.1673-16.2016

Kordower, J. H., Palfi, S., Chen, E.-Y., Ma, S. Y., Sendera, T., Cochran, E. J., et al. (1999). Clinicopathological findings following intraventricular glial-derived neurotrophic factor treatment in a patient with Parkinson's disease. *Ann. Neurol.* 46, 419–424. doi:10.1002/1531-8249(199909)46:3<419::AID-ANA21>3.0.CO;2-Q

Kramer, E. R., Aron, L., Ramakers, G. M. J., Seitz, S., Zhuang, X., Beyer, K., et al. (2007). Absence of ret signaling in mice causes progressive and late degeneration of the nigrostriatal system. *PLoS Biol.* 5, e39–e628. doi:10.1371/journal.pbio.0050039

Kronenberg, J., Merkel, L., Heckers, S., Gudi, V., Schwab, M. H., and Stangel, M. (2019). Investigation of Neuregulin-1 and glial cell-derived neurotrophic factor in rodent astrocytes and microglia. *J. Mol. Neurosci.* 67, 484–493. doi:10.1007/s12031-019-1258-8

Kumar, A., Kopra, J., Varendi, K., Porokuokka, L. L., Panhelainen, A., Kuure, S., et al. (2015). GDNF overexpression from the native locus reveals its role in the nigrostriatal dopaminergic system function. *PLoS Genet.* 11, e1005710. doi:10.1371/journal.pgen.1005710

Lang, A. E., Gill, S., Patel, N. K., Lozano, A., Nutt, J. G., Penn, R., et al. (2006). Randomized controlled trial of intraputamenal glial cell line–derived neurotrophic factor infusion in parkinson disease. *Ann. Neurology* 59, 459–466. doi:10.1002/ana.20737

Le Berre-Scoul, C., Chevalier, J., Oleynikova, E., Cossais, F., Talon, S., Neunlist, M., et al. (2017). A novel enteric neuron-glia coculture system reveals the role of glia in neuronal development. *J. Physiol.* 595, 583–598. doi:10.1113/JP271989

Ledda, F. (2007). Ligand-induced cell adhesion as a new mechanism to promote synapse formation. *Cell Adhesion Migr.* 1, 137–139. doi:10.4161/cam.1.3.4985

Lee, J., Hyeon, S. J., Im, H., Ryu, H., Kim, Y., and Ryu, H. (2016). Astrocytes and microglia as non-cell autonomous players in the pathogenesis of ALS. *Exp. Neurobiol.* 25, 233–240. doi:10.5607/en.2016.25.5.233

Li, Q., Feng, Y., Xue, Y., Zhan, X., Fu, Y., Gui, G., et al. (2022). Edaravone activates the GDNF/RET neurotrophic signaling pathway and protects mRNA-induced motor neurons from iPS cells. *Mol. Neurodegener.* 17, 8. doi:10.1186/s13024-021-00510-y

Liberatore, G. T., Wong, J. Y., Porritt, M. J., Donnan, G. A., and Howells, D. W. (1997). Expression of glial cell line-derived neurotrophic factor (GDNF) mRNA following mechanical injury to mouse striatum. *Neuroreport* 8, 3097–3101. doi:10.1097/00001756-199709290-00018

Lin, L.-F. H., Doherty, D. H., Lile, J. D., Bektesh, S., and Collins, F. (1993). GDNF: a glial cell line-derived neurotrophic factor for midbrain dopaminergic neurons. *Science* 260, 1130–1132. doi:10.1126/science.8493557

Lin, P.-Y., and Tseng, P.-T. (2015). Decreased glial cell line-derived neurotrophic factor levels in patients with depression: a meta-analytic study. *J. Psychiatric Res.* 63, 20–27. doi:10.1016/j.jpsychires.2015.02.004

Lin, X., Ren, P., Xue, Z., Liu, X., Cao, Y., Li, T., et al. (2024). Astrocytic GDNF ameliorates anesthesia and surgery-induced cognitive impairment by promoting hippocampal synaptic plasticity in aged mice. *Neurochem. Int.* 177, 105765. doi:10.1016/j.neuint.2024.105765

Liu, H., Li, X., Xu, Q., Lv, S., Li, J., and Ma, Q. (2012a). Role of glial cell line-derived neurotrophic factor in perineural invasion of pancreatic cancer. *Biochimica Biophysica Acta - Rev. Cancer* 1826, 112–120. doi:10.1016/j.bbcan.2012.03.010

Liu, J., Yan, R., Wang, B., Chen, S., Hong, H., Liu, C., et al. (2024). Decellularized extracellular matrix enriched with GDNF enhances neurogenesis and remyelination for improved motor recovery after spinal cord injury. *Acta Biomater.* 180, 308–322. doi:10.1016/j.actbio.2024.04.015

Liu, Q., Zhu, H.-Y., Li, B., Wang, Y.-Q., Yu, J., and Wu, G.-C. (2012b). Chronic clomipramine treatment restores hippocampal expression of glial cell line-derived neurotrophic factor in a rat model of depression. *J. Affect. Disord.* 141, 367–372. doi:10.1016/j.jad.2012.03.018

Liu, X.-F., Tang, C.-X., Zhang, L., Tong, S.-Y., Wang, Y., Abdulrahman, A. A., et al. (2020). Down-regulated CUEDC2 increases GDNF expression by stabilizing CREB through reducing its ubiquitination in glioma. *Neurochem. Res.* 45, 2915–2925. doi:10.1007/s11064-020-03140-w

Lonka-Nevalaita, L., Lume, M., Leppänen, S., Jokitalo, E., Peränen, J., and Saarma, M. (2010). Characterization of the intracellular localization, processing, and secretion of two glial cell line-derived neurotrophic factor splice isoforms. *J. Neurosci.* 30, 11403–11413. doi:10.1523/JNEUROSCI.5888-09.2010

Love, S., Plaha, P., Patel, N. K., Hotton, G. R., Brooks, D. J., and Gill, S. S. (2005). Glial cell line–derived neurotrophic factor induces neuronal sprouting in human brain. *Nat. Med.* 11, 703–704. doi:10.1038/nm0705-703

Manié, S., Santoro, M., Fusco, A., and Billaud, M. (2001). The RET receptor: function in development and dysfunction in congenital malformation. *Trends Genet.* 17, 580–589. doi:10.1016/S0168-9525(01)02420-9

Marco, S., Saura, J., Prez-Navarro, E., Mart, M. J., Tolosa, E., and Alberch, J. (2002). Regulation of c-Ret, GFRα1, and GFRα2 in the substantia nigra pars compacta in a rat model of Parkinson's disease. *J. Neurobiol.* 52, 343–351. doi:10.1002/neu.10082

Marks, B. A., Pipia, I. M., Mukai, C., Horibata, S., Rice, E. J., Danko, C. G., et al. (2023). GDNF-RET signaling and EGR1 form a positive feedback loop that promotes tamoxifen resistance *via* cyclin D1. *BMC Cancer* 23, 138. doi:10.1186/s12885-023-10559-1

Marks, C., Belluscio, L., and Ibáñez, C. F. (2012). Critical role of GFRα1 in the development and function of the main olfactory system. *J. Neurosci.* 32, 17306–17320. doi:10.1523/JNEUROSCI.1522-12.2012

Marshall, P. (2023). Finding an optimal level of GDNF overexpression: insights from dopamine cycling. *Cell Mol. Neurobiol.* 43, 3179–3189. doi:10.1007/s10571-023-01375-z

Meir, M., Flemming, S., Burkard, N., Bergauer, L., Metzger, M., Germer, C.-T., et al. (2015). Glial cell line-derived neurotrophic factor promotes barrier maturation and wound healing in intestinal epithelial cells *in vitro*. *Am. J. Physiology-Gastrointestinal Liver Physiology* 309, G613–G624. doi:10.1152/ajpgi.00357.2014

Meir, M., Kannapin, F., Diefenbacher, M., Ghoreishi, Y., Kollmann, C., Flemming, S., et al. (2021). Intestinal epithelial barrier maturation by enteric glial cells is GDNF-dependent. *Int. J. Mol. Sci.* 22, 1887. doi:10.3390/ijms22041887

Menegola, E., Broccia, M. L., Di Renzo, F., Massa, V., and Giavini, E. (2004). Effects of excess and deprivation of serotonin on *in vitro* neuronal differentiation. *Vitro Cell Dev. Biol. Anim.* 40, 52–56. doi:10.1290/1543-706X(2004)40<52:EOEADO>2.0.CO;2

Mercier, G., Lennon, A. M., Renouf, B., Dessouroux, A., Ramaugé, M., Courtin, F., et al. (2004). MAP kinase activation by fluoxetine and its relation to gene expression in cultured rat astrocytes. *JMN* 24, 207–216. doi:10.1385/JMN:24:2:207

Merienne, N., Meunier, C., Schneider, A., Seguin, J., Nair, S. S., Rocher, A. B., et al. (2019). Cell-type-specific gene expression profiling in adult mouse brain reveals normal and disease-state signatures. *Cell Rep.* 26, 2477–2493.e9. doi:10.1016/j.celrep.2019.02.003

Messer, C. J., Eisch, A. J., Carlezon, W. A., Whisler, K., Shen, L., Wolf, D. H., et al. (2000). Role for GDNF in biochemical and behavioral adaptations to drugs of abuse. *Neuron* 26, 247–257. doi:10.1016/S0896-6273(00)81154-X

Mijatovic, J., Airavaara, M., Planken, A., Auvinen, P., Raasmaja, A., Piepponen, T. P., et al. (2007). Constitutive ret activity in Knock-In multiple endocrine neoplasia type B mice induces profound elevation of brain dopamine concentration *via* enhanced synthesis and increases the number of TH-Positive cells in the substantia nigra. *J. Neurosci.* 27, 4799–4809. doi:10.1523/JNEUROSCI.5647-06.2007

Mijatovic, J., Piltonen, M., Alberton, P., Männistö, P. T., Saarma, M., and Piepponen, T. P. (2011). Constitutive ret signaling is protective for dopaminergic cell bodies but not for axonal terminals. *Neurobiol. Aging* 32, 1486–1494. doi:10.1016/j.neurobiolaging.2009.08.009

Mikroulis, A., Waloschková, E., Bengzon, J., Woldbye, D., Pinborg, L. H., Jespersen, B., et al. (2022). GDNF increases inhibitory synaptic drive on principal neurons in the hippocampus *via* activation of the ret pathway. *IJMS* 23, 13190. doi:10.3390/ijms232113190

Mogi, M., Togari, A., Kondo, T., Mizuno, Y., Kogure, O., Kuno, S., et al. (2001). Glial cell line-derived neurotrophic factor in the substantia nigra from control and parkinsonian brains. *Neurosci. Lett.* 300, 179–181. doi:10.1016/S0304-3940(01)01577-4

Moore, M. W., Klein, R. D., Fariñas, I., Sauer, H., Armanini, M., Phillips, H., et al. (1996). Renal and neuronal abnormalities in mice lacking GDNF. *Nature* 382, 76–79. doi:10.1038/382076a0

Nagy, N., and Goldstein, A. M. (2017). Enteric nervous system development: a crest cell's journey from neural tube to Colon. *Seminars Cell and Dev. Biol.* 66, 94–106. doi:10.1016/j.semcdb.2017.01.006

Nakagawa, T., Yabe, T., and Schwartz, J. P. (2005). Gene expression profiles of reactive astrocytes cultured from dopamine-depleted striatum. *Neurobiol. Dis.* 20, 275–282. doi:10.1016/j.nbd.2005.03.009

Nanobashvili, A., Melin, E., Emerich, D., Tornøe, J., Simonato, M., Wahlberg, L., et al. (2019). Unilateral *ex vivo* gene therapy by GDNF in epileptic rats. *Gene Ther.* 26, 65–74. doi:10.1038/s41434-018-0050-7

Narita, N., Tanemura, A., Murali, R., Scolyer, R. A., Huang, S., Arigami, T., et al. (2009). Functional RET G691S polymorphism in cutaneous malignant melanoma. *Oncogene* 28, 3058–3068. doi:10.1038/onc.2009.164

Natarajan, D., Marcos-Gutierrez, C., Pachnis, V., and de Graaff, E. (2002). Requirement of signalling by receptor tyrosine kinase RET for the directed migration of enteric nervous system progenitor cells during Mammalian embryogenesis. *Development* 129, 5151–5160. doi:10.1242/dev.129.22.5151

Naumenko, V. S., Bazovkina, D. V., Semenova, A. A., Tsybko, A. S., Il'chibaeva, T. V., Kondaurova, E. M., et al. (2013). Effect of glial cell line-derived neurotrophic factor on behavior and key members of the brain serotonin system in mouse strains genetically predisposed to behavioral disorders. *J Neurosci. Res.* 91, 1628–1638. doi:10.1002/jnr.23286

Neve, R. M., Chin, K., Fridlyand, J., Yeh, J., Baehner, F. L., Fevr, T., et al. (2006). A collection of breast cancer cell lines for the study of functionally distinct cancer subtypes. *Cancer Cell* 10, 515–527. doi:10.1016/j.ccr.2006.10.008

Ng, W. H., Wan, G. Q., Peng, Z. N., and Too, H. P. (2009). Glial cell-line derived neurotrophic factor (GDNF) family of ligands confer chemoresistance in a ligand-specific fashion in malignant gliomas. *J. Clin. Neurosci.* 16, 427–436. doi:10.1016/j.jocn.2008.06.002

Nutt, J. G., Burchiel, K. J., Comella, C. L., Jankovic, J., Lang, A. E., Laws, E. R., et al. (2003). Randomized, double-blind trial of glial cell line-derived neurotrophic factor (GDNF) in PD. *Neurology* 60, 69–73. doi:10.1212/WNL.60.1.69

Obermayr, F., Hotta, R., Enomoto, H., and Young, H. M. (2013). Development and developmental disorders of the enteric nervous system. *Nat. Rev. Gastroenterol. Hepatol.* 10, 43–57. doi:10.1038/nrgastro.2012.234

Oh-hashi, K., Ito, M., Tanaka, T., Hirata, Y., and Kiuchi, K. (2009). Biosynthesis, processing, and secretion of glial cell line-derived neurotrophic factor in astroglial cells. *Mol. Cell Biochem.* 323, 1–7. doi:10.1007/s11010-008-9958-3

Ohshima, Y., Yajima, I., Takeda, K., Iida, M., Kumasaka, M., Matsumoto, Y., et al. (2010). c-RET molecule in malignant melanoma from oncogenic RET-Carrying transgenic mice and human cell lines. *PLoS ONE* 5, e10279. doi:10.1371/journal.pone.0010279

Okada, Y., Eibl, G., Duffy, J. P., Reber, H. A., and Hines, O. J. (2003). Glial cell-derived neurotrophic factor upregulates the expression and activation of matrix metalloproteinase-9 in human pancreatic cancer. *Surgery* 134, 293–299. doi:10.1067/msy.2003.239

Okaty, B. W., Freret, M. E., Rood, B. D., Brust, R. D., Hennessy, M. L., deBairos, D., et al. (2015). Multi-scale molecular deconstruction of the serotonin neuron system. *Neuron* 88, 774–791. doi:10.1016/j.neuron.2015.10.007

Okaty, B. W., Sturrock, N., Escobedo Lozoya, Y., Chang, Y., Senft, R. A., Lyon, K. A., et al. (2020). A single-cell transcriptomic and anatomic atlas of mouse dorsal raphe Pet1 neurons. *eLife* 9, e55523. doi:10.7554/eLife.55523

Oppenheim, R. W., Houenou, L. J., Johnson, J. E., Lin, L.-F. H., Li, L., Lo, A. C., et al. (1995). Developing motor neurons rescued from programmed and axotomy-induced cell death by GDNF. *Nature* 373, 344–346. doi:10.1038/373344a0

Paolone, G., Falcicchia, C., Lovisari, F., Kokaia, M., Bell, W. J., Fradet, T., et al. (2019). Long-term, targeted delivery of GDNF from encapsulated cells is neuroprotective and reduces seizures in the pilocarpine model of epilepsy. *J. Neurosci.* 39, 2144–2156. doi:10.1523/JNEUROSCI.0435-18.2018

Paratcha, G., Ibáñez, C. F., and Ledda, F. (2006). GDNF is a chemoattractant factor for neuronal precursor cells in the rostral migratory stream. *Mol. Cell. Neurosci.* 31, 505–514. doi:10.1016/j.mcn.2005.11.007

Paratcha, G., Ledda, F., Baars, L., Coulpier, M., Besset, V., Anders, J., et al. (2001). Released GFRalpha1 potentiates downstream signaling, neuronal survival, and differentiation *via* a novel mechanism of recruitment of c-Ret to lipid rafts. *Neuron* 29, 171–184. doi:10.1016/S0896-6273(01)00188-X

Paratcha, G., Ledda, F., and Ibáñez, C. F. (2003). The neural cell adhesion molecule NCAM is an alternative signaling receptor for GDNF family ligands. *Cell* 113, 867–879. doi:10.1016/S0092-8674(03)00435-5

Parekh, P. A., Garcia, T. X., and Hofmann, M.-C. (2019). Regulation of GDNF expression in sertoli cells. 157, R95, R107. doi:10.1530/REP-18-0239

Pascual, A., Hidalgo-Figueroa, M., Piruat, J. I., Pintado, C. O., Gómez-Díaz, R., and López-Barneo, J. (2008). Absolute requirement of GDNF for adult catecholaminergic neuron survival. *Nat. Neurosci.* 11, 755–761. doi:10.1038/nn.2136

Patel, D., Jana, A., Roy, A., and Pahan, K. (2019). Cinnamon and its metabolite protect the nigrostriatum in a mouse model of parkinson's disease *via* astrocytic GDNF. *J. Neuroimmune Pharmacol.* 14, 503–518. doi:10.1007/s11481-019-09855-0

Penttinen, A.-M., Parkkinen, I., Voutilainen, M. H., Koskela, M., Bäck, S., Their, A., et al. (2018). Pre-α-pro-GDNF and Pre-β-pro-GDNF isoforms are neuroprotective in the 6-hydroxydopamine rat model of parkinson's disease. *Front. Neurol.* 9, 457. doi:10.3389/fneur.2018.00457

Perrinjaquet, M., Sjöstrand, D., Moliner, A., Zechel, S., Lamballe, F., Maina, F., et al. (2011). MET signaling in GABAergic neuronal precursors of the medial ganglionic eminence restricts GDNF activity in cells that express GFRα1 and a new transmembrane receptor partner. *J. Cell Sci.* 124, 2797–2805. doi:10.1242/jcs.083717

Pertusa, M., García-Matas, S., Mammeri, H., Adell, A., Rodrigo, T., Mallet, J., et al. (2008). Expression of GDNF transgene in astrocytes improves cognitive deficits in aged rats. *Neurobiol. Aging* 29, 1366–1379. doi:10.1016/j.neurobiolaging.2007.02.026

Piccinini, E., Kalkkinen, N., Saarma, M., and Runeberg-Roos, P. (2013). Glial cell line-derived neurotrophic factor: characterization of Mammalian posttranslational modifications. *Ann. Med.* 45, 66–73. doi:10.3109/07853890.2012.663927

Pichel, J. G., Shen, L., Sheng, H. Z., Granholm, A. C., Drago, J., Grinberg, A., et al. (1996). Defects in enteric innervation and kidney development in mice lacking GDNF. *Nature* 382, 73–76. doi:10.1038/382073a0

Pochon, N. a.-M., Menoud, A., Tseng, J. L., Zurn, A. D., and Aebischer, P. (1997). Neuronal GDNF expression in the adult rat nervous system identified by *in situ* hybridization. *Eur. J. Neurosci.* 9, 463–471. doi:10.1111/j.1460-9568.1997.tb01623.x

Popova, N. K., Ilchibaeva, T. V., and Naumenko, V. S. (2017). Neurotrophic factors (BDNF and GDNF) and the serotonergic system of the brain. *Biochem. Mosc.* 82, 308–317. doi:10.1134/S0006297917030099

Pozas, E., and Ibáñez, C. F. (2005). GDNF and GFRalpha1 promote differentiation and tangential migration of cortical GABAergic neurons. *Neuron* 45, 701–713. doi:10.1016/j.neuron.2005.01.043

Qing, J., Liu, X., Wu, Q., Zhou, M., Zhang, Y., Mazhar, M., et al. (2020). Hippo/YAP pathway plays a critical role in effect of GDNF against Aβ-Induced inflammation in microglial cells. *DNA Cell Biol.* 39, 1064–1071. doi:10.1089/dna.2019.5308

Rabelo, P. C. R., Horta, N. A. C., Cordeiro, L. M. S., Poletini, M. O., Coimbra, C. C., Szawka, R. E., et al. (2017). Intrinsic exercise capacity in rats influences dopamine neuroplasticity induced by physical training. *J. Appl. Physiology* 123, 1721–1729. doi:10.1152/japplphysiol.00506.2017

Ramer, M. S., Priestley, J. V., and McMahon, S. B. (2000). Functional regeneration of sensory axons into the adult spinal cord. *Nature* 403, 312–316. doi:10.1038/35002084

Ren, J., Isakova, A., Friedmann, D., Zeng, J., Grutzner, S. M., Pun, A., et al. (2019). Single-cell transcriptomes and whole-brain projections of serotonin neurons in the mouse dorsal and median raphe nuclei. *eLife* 8, e49424. doi:10.7554/eLife.49424

Rhymes, E. R., Tosolini, A. P., Fellows, A. D., Mahy, W., McDonald, N. Q., and Schiavo, G. (2022). Bimodal regulation of axonal transport by the GDNF-RET signalling axis in healthy and diseased motor neurons. *Cell Death Dis.* 13, 584–11. doi:10.1038/s41419-022-05031-0

Rocco, M. T., Akhter, A. S., Ehrlich, D. J., Scott, G. C., Lungu, C., Munjal, V., et al. (2022). Long-term safety of MRI-Guided administration of AAV2-GDNF and gadoteridol in the putamen of individuals with Parkinson's disease. *Mol. Ther.* 30, 3632–3638. doi:10.1016/j.ymthe.2022.08.003

Rocha, S. M., Cristovão, A. C., Campos, F. L., Fonseca, C. P., and Baltazar, G. (2012). Astrocyte-derived GDNF is a potent inhibitor of microglial activation. *Neurobiol. Dis.* 47, 407–415. doi:10.1016/j.nbd.2012.04.014

Saarma, M., and Sariola, H. (1999). Other neurotrophic factors: glial cell line-derived neurotrophic factor (GDNF). *Microsc. Res. Tech.* 45, 292–302. doi:10.1002/(SICI)1097-0029(19990515/01)45:4/5<292::AID-JEMT13>3.0.CO;2-8

Sainio, K., Suvanto, P., Davies, J., Wartiovaara, J., Wartiovaara, K., Saarma, M., et al. (1997). Glial-cell-line-derived neurotrophic factor is required for bud initiation from ureteric epithelium. *Development* 124, 4077–4087. doi:10.1242/dev.124.20.4077

Salgado, A. J., Sousa, J. C., Costa, B. M., Pires, A. O., Mateus-Pinheiro, A., Teixeira, F. G., et al. (2015). Mesenchymal stem cells secretome as a modulator of the neurogenic niche: basic insights and therapeutic opportunities. *Front. Cell. Neurosci.* 9, 249. doi:10.3389/fncel.2015.00249

Sánchez, M. P., Silos-Santiago, I., Frisén, J., He, B., Lira, S. A., and Barbacid, M. (1996). Renal agenesis and the absence of enteric neurons in mice lacking GDNF. *Nature* 382, 70–73. doi:10.1038/382070a0

Sariola, H., and Saarma, M. (2003). Novel functions and signalling pathways for GDNF. *J. Cell Sci.* 116, 3855–3862. doi:10.1242/jcs.00786

Sariola, H., and Meng, X. (2003). GDNF-induced seminomatous tumours in mouse–an experimental model for human seminomas?. *APMIS* 111 (1), 192–196. doi:10.1034/j.1600-0463.2003.11101231.x

Schaar, D. G., Sieber, B.-A., Sherwood, A. C., Dean, D., Mendoza, G., Ramakrishnan, L., et al. (1994). Multiple astrocyte transcripts encode nigral trophic factors in rat and human. *Exp. Neurol.* 130, 387–393. doi:10.1006/exnr.1994.1218

Schuchardt, A., D'Agati, V., Larsson-Blomberg, L., Costantini, F., and Pachnis, V. (1994). Defects in the kidney and enteric nervous system of mice lacking the tyrosine kinase receptor ret. *Nature* 367, 380–383. doi:10.1038/367380a0

Sharma, A. N., Da Costa E Silva, B. F. B., Soares, J. C., Carvalho, A. F., and Quevedo, J. (2016). Role of trophic factors GDNF, IGF-1 and VEGF in major depressive disorder: a comprehensive review of human studies. *J. Affect. Disord.* 197, 9–20. doi:10.1016/j.jad.2016.02.067

Sharma, K., Zhang, Y., Paudel, K. R., Kachelmeier, A., Hansbro, P. M., and Shi, X. (2022). The emerging role of Pericyte-Derived extracellular vesicles in vascular and neurological health. *Cells* 11, 3108. doi:10.3390/cells11193108

Shewchuk, B. M., Ho, Y., Liebhaber, S. A., and Cooke, N. E. (2006). A single base difference between Pit-1 binding sites at the hGH promoter and locus control region specifies distinct Pit-1 conformations and functions. *Mol. Cell. Biol.* 26, 6535–6546. doi:10.1128/mcb.00267-06

Shimizu, F., Sano, Y., Abe, M., Maeda, T., Ohtsuki, S., Terasaki, T., et al. (2011). Peripheral nerve pericytes modify the blood–nerve barrier function and tight junctional molecules through the secretion of various soluble factors. *J. Cell. Physiology* 226, 255–266. doi:10.1002/jcp.22337

Simonato, M., Tongiorgi, E., and Kokaia, M. (2006). Angels and demons: neurotrophic factors and epilepsy. *Trends Pharmacol. Sci.* 27, 631–638. doi:10.1016/j.tips.2006.10.002

Singh, S., Sahu, K., Singh, C., and Singh, A. (2022). Lipopolysaccharide induced altered signaling pathways in various neurological disorders. *Naunyn Schmiedeb. Arch. Pharmacol.* 395, 285–294. doi:10.1007/s00210-021-02198-9

Slevin, J. T., Gerhardt, G. A., Smith, C. D., Gash, D. M., Kryscio, R., and Young, B. (2005). Improvement of bilateral motor functions in patients with parkinson disease through the unilateral intraputaminal infusion of glial cell Line—Derived neurotrophic factor. *J. Neurosurg.* 102, 216–222. doi:10.3171/jns.2005.102.2.0216

Song, H., and Moon, A. (2006). Glial cell-derived neurotrophic factor (GDNF) promotes low-grade Hs683 glioma cell migration through JNK, ERK-1/2 and p38 MAPK signaling pathways. *Neurosci. Res.* 56, 29–38. doi:10.1016/j.neures.2006.04.019

Sotoyama, H., Iwakura, Y., Oda, K., Sasaoka, T., Takei, N., Kakita, A., et al. (2017). Striatal hypodopamine phenotypes found in transgenic mice that overexpress glial cell line-derived neurotrophic factor. *Neurosci. Lett.* 654, 99–106. doi:10.1016/j.neulet.2017.06.005

Stanga, S., Brambilla, L., Tasiaux, B., Dang, A. H., Ivanoiu, A., Octave, J.-N., et al. (2018). A role for GDNF and soluble APP as biomarkers of amyotrophic lateral sclerosis pathophysiology. *Front. Neurol.* 9, 384. doi:10.3389/fneur.2018.00384

Stanga, S., Zanou, N., Audouard, E., Tasiaux, B., Contino, S., Vandermeulen, G., et al. (2016). APP-Dependent glial cell line-derived neurotrophic factor gene expression drives neuromuscular junction formation. *FASEB J.* 30, 1696–1711. doi:10.1096/fj.15-278739

Suvanto, P., Hiltunen, J. O., Arumäe, U., Moshnyakov, M., Sariola, H., Sainio, K., et al. (1996). Localization of glial cell line-derived neurotrophic factor (GDNF) mRNA in embryonic rat by *in situ* hybridization. *Eur. J. Neurosci.* 8, 816–822. doi:10.1111/j.1460-9568.1996.tb01267.x

Tabuchi, K., Blundell, J., Etherton, M. R., Hammer, R. E., Liu, X., Powell, C. M., et al. (2007). A Neuroligin-3 mutation implicated in autism increases inhibitory synaptic transmission in mice. *Science* 318, 71–76. doi:10.1126/science.1146221

Takebayashi, M., Hisaoka, K., Nishida, A., Tsuchioka, M., Miyoshi, I., Kozuru, T., et al. (2006). Decreased levels of whole blood glial cell line-derived neurotrophic factor (GDNF) in remitted patients with mood disorders. *Int. J. Neuropsychopharm.* 9, 607–612. doi:10.1017/S1461145705006085

Tansey, M. G., Baloh, R. H., Milbrandt, J., and Johnson, E. M. (2000). GFRalpha-mediated localization of RET to lipid rafts is required for effective downstream signaling, differentiation, and neuronal survival. *Neuron* 25, 611–623. doi:10.1016/S0896-6273(00)81064-8

Taylor, H., Barua, N., Bienemann, A., Wyatt, M., Castrique, E., Foster, R., et al. (2013). Clearance and toxicity of recombinant methionyl human glial cell line-derived neurotrophic factor (r-metHu GDNF) following acute convection-enhanced delivery into the striatum. *PLoS ONE* 8, e56186. doi:10.1371/journal.pone.0056186

Tomac, A., Lindqvist, E., Lin, L.-F. H., Ögren, S. O., Young, D., Hoffer, B. J., et al. (1995). Protection and repair of the nigrostriatal dopaminergic system by GDNF *in vivo*. *Nature* 373, 335–339. doi:10.1038/373335a0

Trupp, M., Belluardo, N., Funakoshi, H., and Ibáñez, C. F. (1997). Complementary and overlapping expression of glial cell line-derived neurotrophic factor (GDNF), c-ret proto-oncogene, and GDNF Receptor-α indicates multiple mechanisms of trophic actions in the adult rat CNS. *J. Neurosci.* 17, 3554–3567. doi:10.1523/JNEUROSCI.17-10-03554.1997

Tsuchioka, M., Takebayashi, M., Hisaoka, K., Maeda, N., and Nakata, Y. (2008). Serotonin (5-HT) induces glial cell line-derived neurotrophic factor (GDNF) mRNA expression *via* the transactivation of fibroblast growth factor receptor 2 (FGFR2) in rat C6 glioma cells. *J. Neurochem.* 106, 244–257. doi:10.1111/j.1471-4159.2008.05357.x

Ubhi, K., Rockenstein, E., Mante, M., Inglis, C., Adame, A., Patrick, C., et al. (2010). Neurodegeneration in a transgenic mouse model of multiple system atrophy is associated with altered expression of oligodendroglial-derived neurotrophic factors. *J. Neurosci.* 30, 6236–6246. doi:10.1523/JNEUROSCI.0567-10.2010

Uchida, S., Hara, K., Kobayashi, A., Otsuki, K., Yamagata, H., Hobara, T., et al. (2011). Epigenetic status of gdnf in the ventral striatum determines susceptibility and adaptation to daily stressful events. *Neuron* 69, 359–372. doi:10.1016/j.neuron.2010.12.023

Vargas-Leal, V., Bruno, R., Derfuss, T., Krumbholz, M., Hohlfeld, R., and Meinl, E. (2005). Expression and function of glial cell line-derived neurotrophic factor family

ligands and their receptors on human immune cells. *J. Immunol.* 175, 2301–2308. doi:10.4049/jimmunol.175.4.2301

Vilela, T. C., Muller, A. P., Damiani, A. P., Macan, T. P., Da Silva, S., Canteiro, P. B., et al. (2017). Strength and aerobic exercises improve spatial memory in aging rats through stimulating distinct neuroplasticity mechanisms. *Mol. Neurobiol.* 54, 7928–7937. doi:10.1007/s12035-016-0272-x

Wahlberg, L. U., Emerich, D. F., Kordower, J. H., Bell, W., Fradet, T., and Paolone, G. (2020). Long-term, stable, targeted biodelivery and efficacy of GDNF from encapsulated cells in the rat and goettingen miniature pig brain. *Curr. Res. Pharmacol. Drug Discov.* 1, 19–29. doi:10.1016/j.crphar.2020.04.001

Wang, H., Hughes, I., Planer, W., Parsadanian, A., Grider, J. R., Vohra, B. P. S., et al. (2010). The timing and location of glial cell line-derived neurotrophic factor expression determine enteric nervous system structure and function. *J. Neurosci.* 30, 1523–1538. doi:10.1523/JNEUROSCI.3861-09.2010

Wang, J., Li, X., Wang, C., Li, Y., Wang, J., Fang, R., et al. (2021). Exposure to di-(2-ethylhexyl) phthalate reduces secretion of GDNF *via* interfering with estrogen pathway and downregulating ERK/c-fos signaling pathway in astrocytes. *Food Chem. Toxicol.* 158, 112592. doi:10.1016/j.fct.2021.112592

Wang, M., Han, X., Zha, W., Wang, X., Liu, L., Li, Z., et al. (2022). GDNF promotes astrocyte abnormal proliferation and migration through the GFRα1/RET/MAPK/pCREB/LOXL2 signaling axis. *Mol. Neurobiol.* 59, 6321–6340. doi:10.1007/s12035-022-02978-1

Wang, Y., Lin, S.-Z., Chiou, A.-L., Williams, L. R., and Hoffer, B. J. (1997). Glial cell line-derived neurotrophic factor protects against ischemia-induced injury in the cerebral cortex. *J. Neurosci.* 17, 4341–4348. doi:10.1523/JNEUROSCI.17-11-04341.1997

Whone, A. L., Boca, M., Luz, M., Woolley, M., Mooney, L., Dharia, S., et al. (2019). Extended treatment with glial cell line-derived neurotrophic factor in parkinson's disease. *JPD* 9, 301–313. doi:10.3233/JPD-191576

Wilkins, A., Majed, H., Layfield, R., Compston, A., and Chandran, S. (2003). Oligodendrocytes promote neuronal survival and axonal length by distinct intracellular mechanisms: a novel role for oligodendrocyte-derived glial cell line-derived neurotrophic factor. *J. Neurosci.* 23, 4967–4974. doi:10.1523/JNEUROSCI.23-12-04967.2003

Wong, C. E. D., Hua, K., Monis, S., Saxena, V., Norazit, A., Noor, S. M., et al. (2021). Gdnf affects early diencephalic dopaminergic neuron development through regulation of differentiation-associated transcription factors in zebrafish. *J. Neurochem.* 156, 481–498. doi:10.1111/jnc.15108

Xiao, W., Wang, W., Chen, W., Sun, L., Li, X., Zhang, C., et al. (2014). GDNF is involved in the barrier-inducing effect of enteric glial cells on intestinal epithelial cells under acute ischemia reperfusion stimulation. *Mol. Neurobiol.* 50, 274–289. doi:10.1007/s12035-014-8730-9

Yamamoto, M., Mitsuma, N., Inukai, A., Ito, Y., Li, M., Mitsuma, T., et al. (1999). Expression of GDNF and GDNFR-α mRNAs in muscles of patients with motor neuron diseases. *Neurochem. Res.* 24, 785–790. doi:10.1023/A:1020739831778

Yosef, N., and Ubogu, E. E. (2013). An immortalized human blood-nerve barrier endothelial cell line for *in vitro* permeability studies. *Cell Mol. Neurobiol.* 33, 175–186. doi:10.1007/s10571-012-9882-7

Young, H. M., Hearn, C. J., Farlie, P. G., Canty, A. J., Thomas, P. Q., and Newgreen, D. F. (2001). GDNF is a chemoattractant for enteric neural cells. *Dev. Biol.* 229, 503–516. doi:10.1006/dbio.2000.0100

Yun, D., Jeon, M.-T., Kim, H.-J., Moon, G. J., Lee, S., Ha, C. M., et al. (2020). Induction of GDNF and GFRα-1 following AAV1-Rheb(S16H) administration in the hippocampus *in vivo*. *Exp. Neurobiol.* 29, 164–175. doi:10.5607/en19075

Zhang, L., Ma, Z., Smith, G. M., Wen, X., Pressman, Y., Wood, P. M., et al. (2009). GDNF-enhanced axonal regeneration and myelination following spinal cord injury is mediated by primary effects on neurons. *Glia* 57, 1178–1191. doi:10.1002/glia.20840

Zhang, X., Zhang, Z., Xie, C., Xi, G., Zhou, H., Zhang, Y., et al. (2008). Effect of treatment on serum glial cell line-derived neurotrophic factor in depressed patients. *Prog. Neuro-Psychopharmacology Biol. Psychiatry* 32, 886–890. doi:10.1016/j.pnpbp.2008.01.004

Glossary

GDNF	Glial cell line-derived neurotrophic factor
GFLs	GDNF Family Ligands
RET	Rearranged during Transfection
GFRα1	GDNF Family Receptor alpha 1
GPI	Glycosylphosphatidylinositol
TGF-β	Transforming Growth Factor beta
PC5A/5B/7, PACE4, Furin	Proprotein Convertases
pre-α/β-pro-GDNF	Alternative precursor isoforms
PI3K	Phosphoinositide 3-kinase
AKT	Protein kinase B
MAPK	Mitogen-Activated Protein Kinase
JNK	c-Jun N-terminal Kinase
Erk1/2	Extracellular signal-regulated kinases 1/2
CREB	cAMP Response Element-Binding Protein
PLCγ	Phospholipase C gamma
SFKs	Src Family Kinases
NCAM	Neural Cell Adhesion Molecule
FAK	Focal Adhesion Kinase
PC-6.3	PC-6.3 cells
Rab3A/Rab27A	Ras-related proteins
ER	Endoplasmic Reticulum
SN	Substantia Nigra
DA neurons	Dopaminergic neurons
TH	Tyrosine hydroxylase
PV+	Parvalbumin-positive
6-OHDA	6-Hydroxydopamine
MPTP	1-Methyl-4-phenyl-1,2,3,6-tetrahydropyridine
CNS	Central Nervous System
PNS	Peripheral Nervous System
ECM	Extracellular Matrix
BDNF	Brain-Derived Neurotrophic Factor
NGF	Nerve Growth Factor
CREB	cAMP response element-binding protein
PKCα	Protein Kinase C alpha
DG	Dentate Gyrus
NRG-1	Neuregulin-1
OGD	Oxygen-glucose deprivation
NaB	Sodium Benzoate
PD	Parkinson's Disease
PPARα	Peroxisome proliferator-activated receptor α
DEHP	Di-(2-ethylhexyl) phthalate
LOXL2	Lysyl oxidase-like 2
NG2	Neural/glial antigen 2
Iba1	Ionized calcium-binding adapter molecule 1
TNF-α	Tumor Necrosis Factor alpha
IL-1β	Interleukin-1 beta
IL-12β	Interleukin-12 beta
YAP	Yes-associated protein
PRRs	Pattern Recognition Receptors
PAMPs	Pathogen-associated molecular patterns
DAMPs	Damage-associated molecular patterns
MS	Multiple Sclerosis
SARM1	Sterile Alpha and TIR Motif Containing 1
BV2	BV2 cell line
Zymosan A	Yeast-derived immune stimulant

frontiers | Frontiers in Physiology

TYPE Original Research
PUBLISHED 08 August 2025
DOI 10.3389/fphys.2025.1662171

OPEN ACCESS

EDITED BY
Damiana Leo,
University of Mons, Belgium

REVIEWED BY
Danqing Yang,
Helmholtz Association of German Research Centres (HZ), Germany
Julien P. Dupuis,
Institut National de la Santé et de la Recherche Médicale (INSERM), France
Lisa Mapelli,
University of Pavia, Italy

*CORRESPONDENCE
Roberto Piacentini,
roberto.piacentini@unicatt.it

†These authors have contributed equally to this work

RECEIVED 08 July 2025
ACCEPTED 29 July 2025
PUBLISHED 08 August 2025

CITATION
Cannata B, Sposito L, Albini M, Aceto G, Puliatti G, Lazzarino G, Ripoli C, Tropea MR, Puzzo D, Piacentini R and Grassi C (2025) Functional deletion of α7 nicotinic acetylcholine receptor impairs Ca^{2+}-dependent glutamatergic synaptic transmission by affecting both presynaptic and postsynaptic protein expression and function.
Front. Physiol. 16:1662171.
doi: 10.3389/fphys.2025.1662171

Functional deletion of α7 nicotinic acetylcholine receptor impairs Ca^{2+}-dependent glutamatergic synaptic transmission by affecting both presynaptic and postsynaptic protein expression and function

Beatrice Cannata[1,2†], Laura Sposito[1†], Martina Albini[1], Giuseppe Aceto[1,2], Giulia Puliatti[1], Giacomo Lazzarino[3,4], Cristian Ripoli[1,2], Maria Rosaria Tropea[5], Daniela Puzzo[5,6], Roberto Piacentini[1,2]* and Claudio Grassi[1,2]

[1]Department of Neuroscience, Università Cattolica del Sacro Cuore, Rome, Italy, [2]Fondazione Policlinico Universitario A. Gemelli IRCCS, Rome, Italy, [3]Departmental Faculty of Medicine, UniCamillus - Saint Camillus International University of Health Sciences, Rome, Italy, [4]IRCCS San Camillo Hospital, Venice, Italy, [5]Department of Biomedical and Biotechnological Sciences, University of Catania, Catania, Italy, [6]Oasi Research Institute-IRCCS, Troina, Italy

Alpha7 nicotinic acetylcholine receptors (α7-nAChRs) are ionotropic, Ca^{2+}-permeable receptors highly expressed in brain regions involved in memory formation, such as the hippocampus. Their activation induces cation influx and neuronal depolarization, which in turn promotes glutamate release—highlighting a crucial interplay between cholinergic and glutamatergic signaling in the healthy brain. Interestingly, the genetic deletion of α7-nAChRs in mice (α7-KO mice) leads to an Alzheimer's disease (AD)-like phenotype characterized by aberrant amyloid-β accumulation, tau phosphorylation, and neuroinflammation in aged (>12 months) mice. However, glutamatergic transmission in these mice prior to the onset of the AD-like phenotype has been poorly investigated. We thus studied molecular and functional properties of glutamatergic transmission in 4–6-months-old α7-KO mice, representing a prodromal phase of the AD-like neuropathology. We found that hippocampal CA1 neurons in brain slices from α7-KO mice showed a reduced frequency of the spontaneous excitatory post-synaptic currents (sEPSCs) compared to those of wild-type (WT) mice. On the contrary, the amplitude of sEPSCs was not affected, although in α7-KO neurons these currents displayed a longer rise time than in wild-type. CA1 neurons from α7-KO mice also exhibited a significantly smaller evoked NMDA currents than WT neurons, whereas AMPA currents were unaffected. From a molecular point of view, hippocampal neurons of α7-KO mice exhibited an increased expression of the pre-synaptic protein Synapsin-1 and of the NMDA subunits GluN2A and GluN2B, but no modifications in the expression of AMPA receptor subunits (GluA1 and GluA2) were found. Importantly, selective re-expression of the α7-nAChRs in neurons of α7-KO

mice restored the evoked NMDA current amplitude and the rise time of sEPSCs, but it did not rescue the frequency of sEPSCs, thus suggesting that post-synaptic integrity depends on neuronal α7-nAChRs.

KEYWORDS

α7 nAChRs, NMDA, AMPA, hippocampus, glutamate, acethylcholine

Introduction

Alzheimer's disease (AD) is the most common neurodegenerative disorder and the leading cause of dementia, accounting for at least two-thirds of cases in individuals aged 65 and older worldwide (Kumar et al., 2025). Characterized by an insidious onset and progressive decline in behavioral and cognitive functions, AD significantly impairs daily functioning. Several studies have identified amyloid-β (Aβ) and hyperphosphorylated tau (pTau) proteins as key contributors to AD pathology due to their accumulation in insoluble aggregates and soluble oligomeric forms, with the latter considered primarily responsible for early synaptic failure (Selkoe, 2002; Spires-Jones and Hyman, 2014), especially at hippocampal level (Henstridge et al., 2019).

Although glutamatergic transmission is primarily affected in both early and late stages of AD (Zott and Konnerth, 2023), a loss of function of nicotinic acetylcholine receptors (nAChRs) — particularly the homopentameric α7 isoform, which is the most abundant subtype expressed in the mammalian hippocampus—has also been hypothesized to contribute to AD pathogenesis (Ferreira-Vieira T et al., 2016; Parri et al., 2011; Wu et al., 2010; Yakel, 2012; Rao et al., 2022). Indeed, an important cross-talk between cholinergic and glutamatergic transmission has been reported (Francis, 2003). The ionotropic α7-nAChR promotes Ca^{2+} influx, regulating activation of several kinases and gene transcription (Abraham et al., 2025), and leading to membrane depolarization and enhanced glutamatergic excitatory signaling by triggering glutamate release from presynaptic terminals. This process contributes to synaptic plasticity, such as long-term potentiation (LTP) at CA3-CA1 synapse, and memory formation (Cheng and Yakel, 2015). Notably, mice lacking α7-nAChRs (α7-KO) develop an age-dependent AD-like phenotype, with accumulation of AD hallmarks, neuroinflammation, and hippocampal synaptic plasticity and memory deficits starting from about 12 months of age (Tropea et al., 2021). However, glutamatergic transmission in these mice prior to the onset of the AD-like phenotype remains poorly understood. Based on these premises we aimed to investigate molecular and functional basis of glutamatergic transmission in α7-KO mice aged 4–6 months, corresponding to a prodromal phase of the AD-like neuropathology. In addition, we employed AAV-mediated gene re-expression to selectively restore neuronal α7-nAChR expression in α7-KO mice, in order to dissect its causal role in the glutamatergic deficits exhibited by this genetic model.

Materials and methods

Animal models and ethics approval

We used wild type (WT, C57BL/6; RRID: IMSR_JAX:000664) and α7-KO mice (B6.129S7-Chrna7^{tm1Bay}/J; RRID: IMSR_JAX:003232) purchased from The Jackson Laboratory. Colonies were established in the animal house of Università Cattolica del Sacro Cuore. Housing conditions were controlled maintaining stable hygrometric and thermic conditions (50%; 21°C ± 1°C) on 12 h light/dark cycle with *ad libitum* access to food and water. Mice were used at 4–6 months of age, and were sex balanced. All animal procedures were approved by the Ethics Committee of Università Cattolica and Italian Ministry of Health (authorization n. 944/2021-PR) and were fully compliant with Italian Ministry of Health guidelines (Legislative Decree No. 116/1992) and European Union (Directive No. 2010/63/EU) legislations on animal research. All experiments were conducted to minimize animal suffering.

Primary cultures of hippocampal neurons

Primary cultures of neurons were prepared from hippocampi of wild-type (WT) E18 C57BL/6 and B6.129S7-CHRNA7 (α7-KO) mice, as previously described (Tropea et al., 2021; Piacentini et al., 2017; Li Puma et al., 2022). Briefly, brain tissues were gently dissected in Phosphate Buffered Saline (PBS) at 4°C and then incubated for 10 min at 37°C in PBS containing trypsin–ethylenediaminetetraacetic acid 0.025%/0.01% w/v (Trypsin-EDTA, Biochrom AG, Berlin, Germany). After trypsin inactivation through fetal bovine serum (FBS), tissues were centrifugated and resuspended in the dissociation medium, consisting of minimum essential medium (MEM, Biochrom) supplemented with 1% FBS, 2 mM glutamine, 25 mM glucose, and 1% penicillin–streptomycin-neomycin antibiotic mixture (PSN, Thermo Fisher Scientific, Waltham, MA). Tissues were mechanically dissociated with a fire-polished Pasteur pipette at room temperature (RT) and then centrifuged at 235 × g for 10 min at RT. Cells were resuspended in the previously described medium added with 5% horse serum and 5% FBS and plated on poly-L-lysine (0.1 mg/mL, Sigma, St. Louis, MO)-pre-coated 20-mm coverslips (10^5 cells/well) for confocal Ca^{2+} imaging and on 35-mm six-well plates (10^6 cells/well) for High-Performance Liquid Chromatography (HPLC) and Western blot (WB) analyses. After 24 h from seeding (1 day *in vitro*), the culture medium was replaced with a fresh medium

consisting of 96.5% Neurobasal medium (Thermo), 2% B-27 (Thermo), 2 mM glutamine and 1% PSN; after another 72 h (4 days *in vitro*), this medium was replaced with a glutamine-free version of the same medium, and the cells were grown for 10 more days before carrying-out experiments. Cell cultures were incubated in a 5% CO_2 humidified incubator at 37°C.

Organotypic hippocampal brain slices preparation

Hippocampal organotypic slice cultures were prepared from WT P4-8 C57BL/6 mice using a McIllwain tissue chopper, employing at least four mice for each preparation. Slices (300 µm) were placed on semi-porous membranes (Merck Millipore, No. PCIMORG50, Burlington, MA, United States) fed by tissue medium made of MEM (Thermo) supplemented with 30 µM HEPES, 5.8 mM $NaHCO_3$, 26.6 mM D-glucose, 2.5% ascorbic acid, 0.5 mg/mL insulin, 20% horse serum (Thermo), 2 mM $MgSO_4$, 1 mM $CaCl_2$. Slices were incubated at 36°C in 5% CO_2.

Plasmid design and viral vector assembly for CHRNA7 overexpression or silencing

In order to overexpress CHRNA7 we used the purchased plasmid Addgene #62276. To generate plasmids capable of overexpressing CHRNA7 selectively in neurons, the CHRNA7 coding sequence from plasmid Addgene #62276 was amplified by PCR and inserted into two in-house pAAV2 viral backbones, containing the hSyn promoter as well as mRuby2 gene reporter, using Gibson Assembly (Gibson Assembly Master Mix, New England Biolabs, Ipswich, MA, United States). All restriction enzymes were purchased from New England Biolabs. In this way, we generated pAAV-hSyn-CHRNA7-mRuby2. Sequence verification was performed by Sanger sequencing. Data were analyzed using SeqScape Software (Applied Biosystems, Foster City, CA, United States), supported by SnapGene (GSL Biotech, Boston, MA, United States).

For the silencing of endogenous CHRNA7, we inserted a home-made CHRNA7-targeting shRNA sequence under the hSyn promoter into pAAV2 viral backbone using Gibson Assembly. The final constructs, carrying mRuby2 as a reporter, was named pscAAV [shRNA]-hSyn>{CHRNA7_shRNA}-hSyn > mRuby2, and allows the silencing selectively in neurons.

Finally, both the overexpression and silencing plasmids were turned into adeno-associated viral vector by InnovaVector s.r.l. (Pozzuoli, Italy), generating the following constructs:

- AAV2-PHP.eB-hSyn > CHRNA7-mRuby2
- AAV2-PHP.eB-hSyn > shRNA_CHRNA7-hSyn > mRuby2

Viral infections

Ex vivo. Hippocampal organotypic slices from WT mice were infected 2 h after preparation with AAV2-PhP.eB-hSyn > shRNA_CHRNA7-hSyn > mRuby2 at a concentration of 2.8×10^{10} gc/slice. Slices were studied 1 week after the infection.

In vivo. Three-month old α7-KO mice were anesthetized (80–100 mg/kg ketamine + 5–10 mg/mL xylazine) and placed in the stereotaxic frame. AAV2-PhP.eB-hSyn > CHRNA7-mRuby2 vector was inoculated in the dorsal hippocampus at the following coordinates (2 µL/region): dorsal CA1: 2.1 AP, ±1.8 ML, – 1.5 DV; dorsal CA2: 2.1 AP, ±2.2 ML, – 1.9 DV; and dorsal CA3: 2.1 AP, ±2 ML, – 2.1 DV. At the end of the procedure, the surgical wound was sutured, and the animals were administered with saline solution (200 µL/mouse) via intramuscular injection. Three weeks after the injections, mice were sacrificed by cervical dislocation and their brain collected for WB analysis or electrophysiological experiments.

Confocal Ca^{2+} imaging

To perform Ca^{2+} imaging, cultures of WT and α7-KO neurons were incubated for 30 min at 37°C with 2.5 µM Fluo-4-AM (Thermo), a Ca^{2+} sensitive fluorescent dye, in Tyrode's solution. This solution consisted of 150 mM NaCl, 10 mM glucose, 10 mM HEPES, 4 mM KCl, 2 mM $CaCl_2$ and 1 mM $MgCl_2$, and its pH was adjusted to 7.4 with NaOH. Cells were then maintained in fresh Tyrode's solution at RT for 20 min to allow dye de-esterification. Intracellular Ca^{2+} transients were elicited after cell depolarization obtained by exposing Fluo-4-AM-loaded cells to 50 mM KCl for 10 s. Fluo-4 was excited at 488 nm and its emission signal was collected between 500 and 550 nm with an inverted laser scanning confocal system Leica TCS-SP5 (Wetzlar, Germany). The amplitude of each Ca^{2+} signal was estimated in a semi-quantitative way by the following formula: $\Delta F/F = (F_t - F_{pre})/(F_{pre} - F_{bgnd})$, where F_t is the mean of fluorescence intensities measured in a region of interest (ROI) drawn around each cell body at a given time (t); F_{pre} is the basal fluorescence intensity in this ROI estimated as mean value of fluorescence during 20-s prior KCl exposure; F_{bgnd} is background fluorescence intensity measured in an area lacking dye-filled cells.

High-performance liquid chromatography (HPLC)

For HPLC measurements, primary cultures of WT and α7-KO neurons were stimulated with 50 mM KCl for 30 s in Tyrode's solution. After this treatment, supernatants were collected and treated as already done in (Piacentini et al., 2017; Li Puma et al., 2022; Puliatti et al., 2023). Tyrode's solution was withdrawn from each well and deproteinized according to (Tavazzi et al., 2005). Briefly, supernatant samples were transferred to an Eppendorf tube equipped with a filtering membrane of 3 KDa cut-off (Nanosep® Centrifugal Devices, Pall Gelman Laboratory, Ann Arbor, MI, United States) and centrifuged at 10,500 × g for 15 min at 4 °C. The protein-free ultrafiltrate samples were analyzed by HPLC to determine extracellular glutamate concentrations released by neurons in culture media, by using an automated pre-column derivatization protocol, with a mixture of 25 mmol/L orthophthalaldehyde (OPA), 1% 3-methylpropionic acid (MPA) and 237.5 mmol/L sodium borate, pH 9.8, as described by Lazzarino et al. (2022). The HPLC apparatus consisted of a Surveyor HPLC System (Thermo Fisher Italia, Rodano, Milan, Italy) and a highly sensitive photodiode array detector, equipped with a 5 cm

light path flow cell, set up between 200 and 400 nm wavelength for acquisition of chromatographic runs. Data were acquired and analyzed by ChromQuest® software package, version 5.0 provided by the HPLC manufacturer. Assignment and calculation of derivatized-glutamate levels in culture media were carried out at 338 nm wavelengths by comparing retention times and areas of peaks with those of chromatographic runs of freshly prepared ultra-pure standard containing known glutamate concentrations. In each cell culture (WT and α7-KO) the total amount of proteins was determined according to the Bradford method (Bradford, 1976). Glutamate levels in culture media were normalized for the total cell protein concentrations and expressed as nmol/mg of proteins.

Protein isolation and western blot analysis

Cells cultures, hippocampal organotypic slices, and hippocampi were lysed in RIPA buffer, supplemented with 1 mM phenylmethylsulfonyl fluoride (PMSF), sodium fluoride (NaF), sodium orthovanadate (Na_3VO_4), and protease inhibitor (PI) mixture. Then, they were sonicated and centrifuged at 13,000 × g for 20 min at 4°C. The supernatants were collected, and their protein concentration was assessed by BCA Assay Kit (Thermo). For each sample, an equivalent amount of protein (30 µg) was loaded onto 8%–12% tris-glycine polyacrylamide gel for electrophoresis separation. Proteins were then electroblotted onto nitrocellulose membranes and blocked with 5% non-fat dry milk in tris-buffered saline containing 0.1% Tween-20 for 1 h at RT. Membranes were incubated overnight at 4°C with a combination of the following primary antibodies (all diluted 1:1,000): rabbit anti-nicotinic acetylcholine receptor alpha 7 (#ab216485, Abcam), rabbit anti-Synapsin-1 (#5297, Cell Signaling Technology, Danvers, MA, United States), mouse anti-Synaptophysin (#ab8049, Abcam), mouse anti-GluA1 (#MAB2263, Merck Millipore), mouse anti-GluA2 (#30–0300, Invitrogen), mouse anti-NMDAR2B (#610417, BD Biosciences, Franklin Lakes, NJ, United States), rabbit anti-NMDAR2A (#07–632, Merck Millipore), rabbit anti-Homer1 (#PA5-21487, Invitrogen), rabbit anti-SNAP25 (#5309, Cell Signaling). Mouse anti-GAPDH [1D4] (#A85382, Antibodies.com, Cambridge, United Kingdom) was used as loading control. Membranes were then incubated with appropriate secondary horseradish peroxidase-conjugated (HRP) antibodies diluted at 1:5,000 (anti-rabbit #7074, anti-mouse #7076; Cell Signaling) for 1 h at RT. Visualization was performed with WESTAR ECL (Cyanagen, Bologna, Italy), using UVItec Cambridge Alliance. Molecular weights for immunoblot analysis were determined through Precision Plus Protein™ Standards (BioRad, Hercules, CA). Densitometric analysis was carried out with UVItec software. Experiments were repeated at least three times. Original uncropped gel and/or Western blot analysis are available upon reasonable request.

Immunohistochemistry

Immunofluorescence analyses were performed on coronal sections (40 µm thick) of perfused brains from α7-KO mice infected with the viral vector AAV2-PhP.eB-hSyn > CHRNA7-mRuby2 in the left hemisphere, whereas the contralateral one was used as an internal control. The slices were incubated for 15 min with DAPI (0.5 µg/mL) and the sections were mounted on glass slides and coverslipped with ProLong Gold antifade reagent. Confocal stacks of images were acquired with a confocal laser scanning system Nikon A1MP, detecting the reporter gene mRuby2 and DAPI signals.

Electrophysiological recordings

Electrophysiological analyses were performed on *ex vivo* hippocampal slices as previously described by (Mainardi et al., 2017). For both evoked and spontaneous excitatory post-synaptic current (EPSC) recordings, neurons were voltage-clamped at −70 mV, and for evoked currents electrical stimuli were delivered to the Schaffer collaterals. To determine the stimulus intensity for evoked EPSCs, input–output curves were first generated to identify the maximal response amplitude. Subsequent recordings were conducted using stimulation intensity corresponding to 30% of the maximal response. To assess the AMPA/NMDA current ratio, stimuli of identical intensity were delivered at holding potentials of −70 mV and +40 mV, respectively, at a frequency of 0.05 Hz. For spontaneous EPSC (sEPSC) recordings, neurons were held at −70 mV throughout the acquisition. Recordings were obtained using a Digidata 1440A Series interface and pClamp 10 software (Molecular Devices). Signals were filtered at 1 kHz, digitized at 10 kHz, and analyzed offline using pClamp 10. AMPA receptor-mediated EPSC amplitude was defined as the difference between the peak response and baseline. NMDA receptor-mediated EPSC amplitude was measured as the current amplitude 50 m after the response onset. For sEPSC frequency analysis, a detection template was generated using the "Event Detection/Create Template" function, as described in (Ripoli et al., 2013). sEPSCs were then detected using the "Event Detection/Template Search" function, with a template match threshold set to 3.5. Results were manually inspected to eliminate false positives. For amplitude analysis, all waveforms detected in a single recording were averaged, and the mean amplitude was calculated. For the kinetic analysis of spontaneous excitatory postsynaptic currents (sEPSCs), only clearly isolated, non-overlapping events were analyzed. Events showing temporal overlap or occurring within bursts were excluded, as they could artificially prolong rise time measurements. Event detection and selection were performed using defined thresholds, ensuring that only clean, individual sEPSCs with stable baselines and smooth rising phases were included in the analysis.

Statistics

Statistical comparisons and analyses were carried out with SigmaPlot software 14.0. Data samples were subjected to normal distribution assay and then expressed as mean ± standard error of the mean (SEM). For statistical comparisons we used one of the following tests: two-tailed Student's t-test and one-way ANOVA with Bonferroni's or Dunnet's *post hoc* tests. The Mann–Whitney (Wilcoxon) nonparametric statistic was used when experimental data were fewer than 10 observations. The level of significance (p) was set at 0.05.

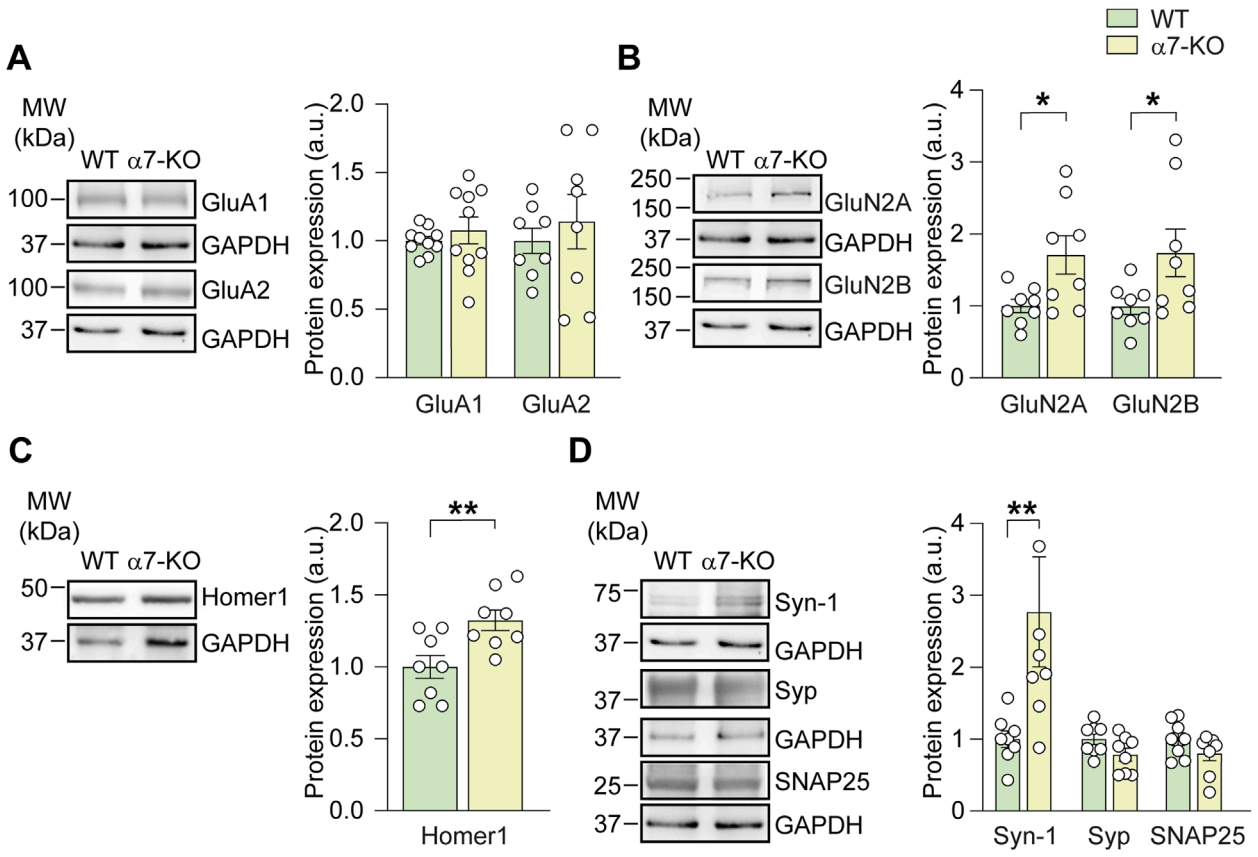

FIGURE 1
Lack of α7-nAChRs impairs the expression of pre- and post-synaptic proteins. Bar graphs and respective representative WB analysis carried out on hippocampal lysates of WT and α7-KO mice, detecting the expression of: **(A)** AMPA subunits (GluA1, n = 10/group, and GluA2, n = 8/group); **(B)** NMDA subunits (GluN2A, n = 8/group, and GluN2B, n = 8/group); **(C)** Homer1, n = 8/group; **(D)** Synapsin-1, n = 8/group, Synaptophysin, n = 8/group, and SNAP25, n = 8 WT and n = 7 α7-KO. GAPDH was used as loading control, statistical significance was assessed by Student's t-test. *p < 0.05, **p < 0.01.

Results

Functional deletion of α7 nicotinic acetylcholine receptor alters NMDA receptor expression

To investigate the role of the α7-nAChR in neuronal communication, we first analyzed the expression of proteins typically associated with synaptic transmission in hippocampi of young α7-KO mice (4–6 months old) compared to wild-type (WT, C57BL/6) controls. The use of young animals is based on evidence that this age may represent a prodromal phase of neurodegenerative processes. Indeed, previous studies have shown that older α7-KO mice (12 months and above) exhibit an AD-like phenotype, including aberrant Aβ and hyperphosphorylated tau accumulation, impaired LTP at CA3–CA1 synapses and memory deficits (Cheng and Yakel, 2015).

We performed Western blot analysis on hippocampal lysates from α7-KO and WT mice, focusing on AMPA and NMDA receptor subunits, the post-synaptic scaffold protein Homer-1, and presynaptic markers such as synapsin-1 and synaptophysin. AMPA receptor subunits GluA1 and GluA2 were similarly expressed in both genotypes (Figure 1A). In contrast, the NMDA receptor subunits GluN2A and GluN2B were significantly upregulated in the hippocampi of α7-KO mice compared to those of WT controls. Specifically, GluN2B expression increased from 1.00 ± 0.12 in WT to 1.75 ± 0.35 in α7-KO mice (+75%; p = 0.049; Figure 1B). Similar results were observed for GluN2A, which showed a 71% increase in α7-KO mice (from 1.00 ± 0.12 to 1.71 ± 0.28; p = 0.024; Figure 1B).

Interestingly, α7-KO mice also exhibited increased expression of the scaffold post-synaptic protein Homer1 b/c that was 33% ± 8% higher than in WT mice (p = 0.009; Figure 1C). This scaffold protein, belonging to the post-synaptic density (PSD) family, is known to i) interact with mGluR1-5 receptors, regulating their trafficking from the cytoplasm to the plasma membrane, and ii) cluster with GluN2B (Gao et al., 2013). We also found that functional deletion of α7-nAChR resulted in a significant increase in synapsin-1 expression, rising from 1.00 ± 0.16 in WT mice to 2.55 ± 0.75 in the hippocampi of α7-KO mice (p = 0.0064), whereas no differences were found for synaptophysin and SNAP25 (Figure 1D).

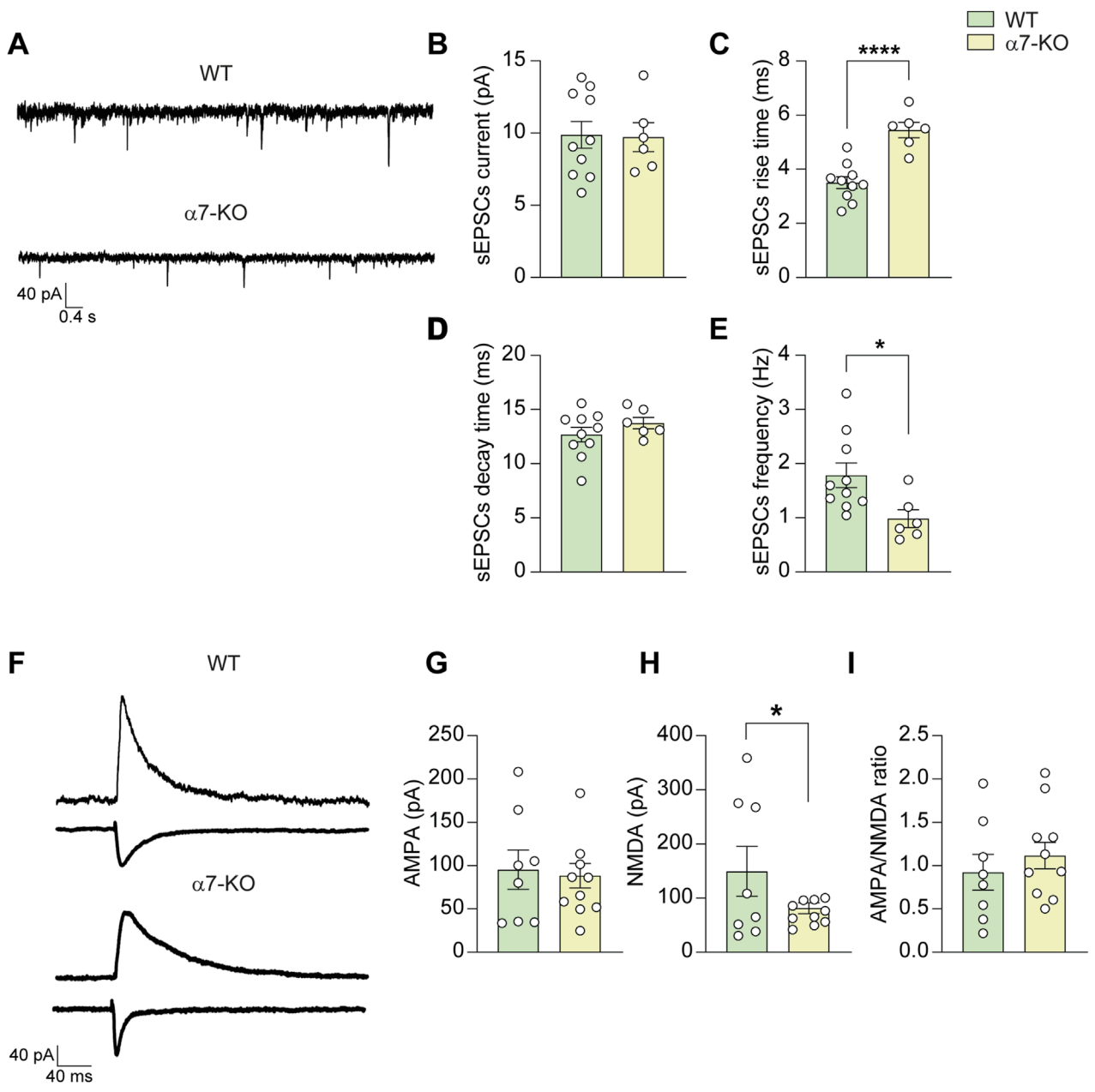

FIGURE 2
CA1 hippocampal α7-KO neurons exhibit altered synaptic transmission. **(A)** Representative traces of sEPSCs recorded in CA1 neurons (WT, top trace; α7-KO, bottom trace). **(B)** Bar graph representing the mean amplitude of sEPSCs carried out as in **(A)** (n = 10 WT; n = 6 α7-KO). **(C)** Bar graph representing the mean rise and **(D)** decay times of sEPSCs recorded as in **(A)**. **(E)** Bar graph representing the mean frequency of sEPSCs recorded as in **(A)**. **(F)** Representative AMPA and NMDA evoked currents in WT and α7-KO CA1 hippocampal neurons. Stimulation artifacts were removed for clarity. **(G–I)** Bar graphs showing the mean amplitudes of AMPA **(G)** and NMDA **(H)** currents, as well as the and AMPA/NMDA ratio **(I)** (n = 7 WT and n = 10 α7-KO for all graphs). Statistical significance was assessed by Student's t-test. *$p < 0.05$, ****$p < 0.0001$.

Hippocampal neurons from α7-KO mice exhibit altered synaptic transmission

We then wondered whether the observed difference in synaptic protein expression in the hippocampus of α7-KO mice correlated with functional alterations in neuronal communication. To address this issue, we performed patch-clamp experiments on CA1 hippocampal pyramidal neurons in brain slices obtained from 4 to 6 months-old WT and α7-KO mice.

Spontaneous excitatory post-synaptic currents (sEPSCs, recorded at a holding potential of −70 mV) exhibited similar amplitudes between WT and α7-KO mice (9.9 ± 1.0 vs. 9.7 ± 1.1 pA, n = 10 and 6, respectively; Figures 2A,B). However, the kinetics of sEPSCs were altered. The rise time (i.e., time to peak) was significantly longer in α7-KO neurons than in WT (5.4 ± 0.3 vs. 3.5 ± 0.2 m, respectively; $p < 0.0001$; Figure 2C) whereas the decay time was similar for the two genotypes (13.9 ± 0.5 and 12.7 ± 0.7 m in α7-KO and WT, respectively; $p = 0.28$; Figure 2D). We also

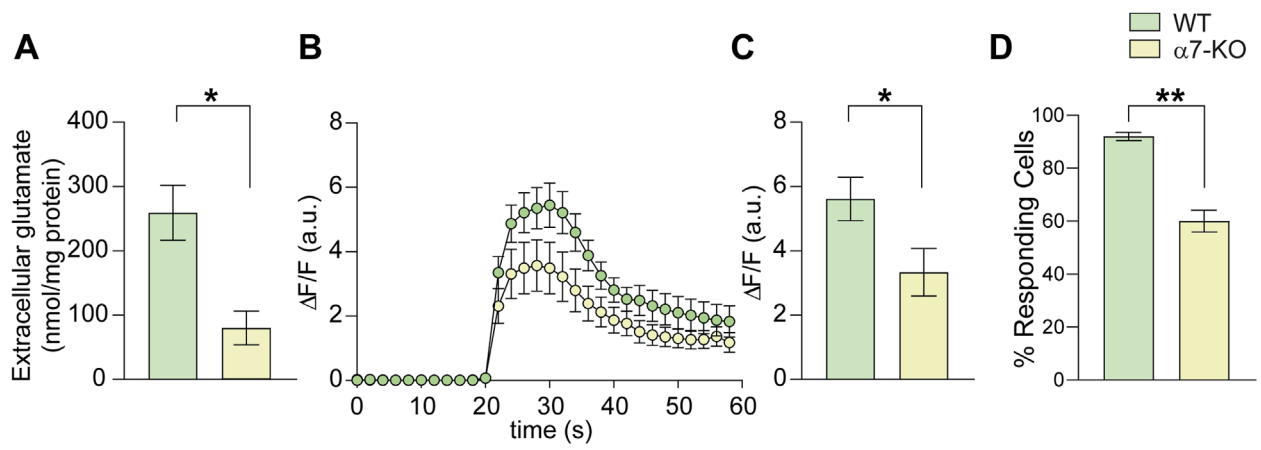

FIGURE 3
Lack of α7-nAChRs affects glutamate release and Ca^{2+} transients in hippocampal neurons. **(A)** Bar graph representing the mean amount of glutamate released extracellularly by cultured WT and α7-KO hippocampal neurons stimulated with KCl 50 mM for 30 s (n = 5 WT and n = 4 α7-KO; *p < 0.05 assessed by Mann-Whitney test). **(B)** Time course of intracellular Ca^{2+} transients elicited by 10 s KCl 50 mM stimulation in WT and α7-KO hippocampal neurons. (n = 42 for WT and n = 31 for α7-KO). **(C)** Bar graph representing the mean amplitude of intracellular Ca^{2+} transients in WT and α7-KO hippocampal neurons triggered by KCl 50 mM for 10 s and recorded for 1 min *p < 0.05 assessed by Student's t-test. **(D)** Bar graph representing the percentage of responding WT and α7-KO neurons stimulated with KCl 50 mM for 10 s **p < 0.01 assessed by Student's t-test.

observed a marked decrease in sEPSC frequency in α7-KO neurons, that was 0.97 ± 0.19 Hz vs. 1.78 ± 0.24 Hz in WT (p = 0.02, assessed by Student's t-test; Figures 2A,E).

Evoked AMPA and NMDA currents were also examined: AMPA currents in CA1 neurons were not significantly different between WT and α7-KO mice (95.3 ± 24.3 pA and 82.2 ± 25.9 pA, respectively; Figures 2F,G) whereas NMDA currents in α7-KO mice were significantly smaller (73.2 ± 16.2 pA in α7-KO CA1 neurons vs. 163.6 ± 54.6 pA in WT, p = 0.050 Figures 2F,H). However, the AMPA/NMDA ratio differences between WT neurons (0.92 ± 0.22) and α7-KO ones (1.14 ± 0.24) did not reach statistical significance (p = 0.164; Figures 2F,I).

Functional deletion of α7-nAChRs affects depolarization-induced glutamate release from hippocampal neurons

To determine whether α7-nAChR deletion affects glutamate release from hippocampal neurons in addition to altering NMDA receptor expression, we performed HPLC experiments to quantify glutamate levels in the culture medium of WT and α7-KO primary hippocampal neurons following 30-s exposure to 50 mM KCl in Tyrode's solution. This stimulus is indeed known to determine cell depolarization. We found that the glutamate released from α7-KO neurons was significantly smaller than that released from WT ones (80.1 vs. 259.2 nmol/mg protein; p = 0.012; n = 4 independent experiments; Figure 3A). This was associated with reduced Ca^{2+} influx upon depolarization, as evidenced by the maximum amplitude of intracellular calcium transients that was, in terms of ΔF/F, 5.6 ± 0.7 in WT vs. 3.3 ± 0.8 (p = 0.027) α7-KO neurons (Figures 3B,C). Moreover, the percentage of cells responding to depolarizing stimulus with a Ca^{2+} increase was reduced in the α7-KO cultures, decreasing from 92% ± 5% in WT neurons to 60% ± 11% in α7-KO neurons (p = 0.005, Figure 3D).

Selective re-expression of neuronal α7-nAChRs rescues the post-synaptic alterations observed in α7-KO mice

Organotypic hippocampal slices obtained from WT mice and treated with AAV2-PHP.eB-hSyn > shRNA_CHRNA7-hSyn > mRuby2 (α7KO-neuro), which selectively silences neuronal α7-nAChRs, exhibited a 52% ± 15% reduction in α7-nAChR protein levels, as measured by WB (p = 0.011 vs. non-silenced WT; Supplementary Figure S1A,B). After, we selectively re-expressed α7-nAChRs in hippocampal neurons of α7-KO mice using an AAV2-PHP.eB-hSyn > CHRNA7-mRuby2 vector (α7KI-neuro model). This model allowed us to determine the specific role of neuronal α7-nAChRs in the post-synaptic modifications observed in the KO mice. Three weeks after the intra-hippocampal injection hippocampal neurons exhibit expression of mRuby2-conjugated α7-nAChRs (Figures 4A,B). No differences were found in terms of sEPSCs frequency between α7-KO and α7KI-neuro neurons (Figures 4C,D). On the contrary, the rise time of sEPSCs, that is considered a post-synaptic parameter, was restored by the specific re-expression of neuronal α7-nAChRs. Indeed, in α7KI-neuro neurons it was 4.0 ± 0.5 (p = 0.05 vs. α7-KO; Figure 4E). Also, the NMDA current amplitude, that was smaller in α7-KO neurons, was restored by the re-expression of the receptor, returning to a value of 169.2 ± 31.5 (p = 0.015 vs. α7-KO; Figures 4F,G).

Discussion

Alpha7-nicotinic acetylcholine receptor (α7-nAChR) is a homopentameric receptor for acetylcholine highly expressed in brain areas fundamental to memory and cognition, such as the amygdala and the hippocampus (Letsinger et al., 2022), mainly on pyramidal neurons. From a functional point of view, activation of α7-nAChRs induces cell depolarization and modulates both

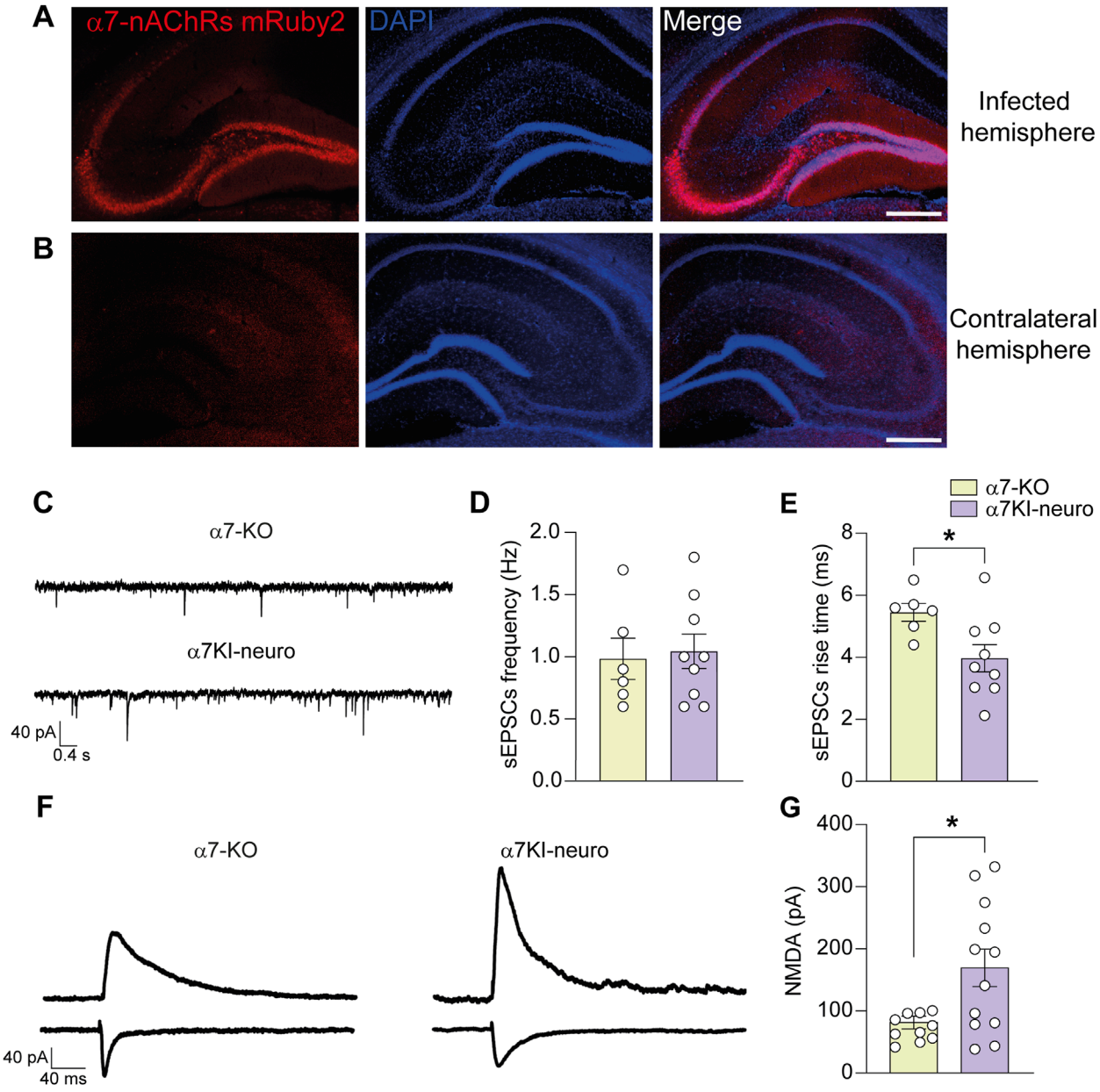

FIGURE 4
Neuronal α7-nAChR is involved in the functional post-synaptic modification of α7-KO model. **(A,B)** Representative immunofluorescence images carried out on α7-KO animals infected with the viral vector AAV2-PhP.eB-hSyn > CHRNA7-mRuby2. The mRuby2 reporter gene is detected in the infected hemisphere **(A)** while is absent in the contralateral one **(B)**; scale bar: 100 μm. **(C)** Representative traces of sEPSCs recorded in CA1 neurons from α7-KO hippocampus (top trace) and α7KI-neuro one (bottom trace). **(D)** Bar graphs representing the mean frequency of sEPSCs recorded as in **(C)** (n = 6 for α7-KO and n = 9 for α7KI-neuro). **(E)** Bar graphs representing the mean rise time of sEPSCs as shown in **(C)** (n = 6 for α7-KO and n = 9 for α7KI-neuro). **(F)** Representative NMDA evoked currents in α7-KO (left) and α7KI-neuro (right) CA1 hippocampal neurons. Stimulation artifacts were removed for clarity. **(G)** Bar graphs showing the mean NMDA currents recorded in CA1 neurons from α7-KO slices (n = 10) and α7KI-neuro ones (n = 12). Statistical significance was assessed by Student's t-test. *$p < 0.05$.

cholinergic and glutamatergic transmission by influencing pre- and post-synaptic mechanisms, thereby affecting neurotransmitter release and post-synaptic currents. The high Ca^{2+} permeability of α7-nAChR strongly impacts on gene transcription, especially at neuronal level. Given the importance of α7 receptor activity, its dysfunction may lead to several illnesses. For example, reduced α7-nAChR function is associated with schizophrenia, as the expression of α7-nAChR is decreased in hippocampus and other brain regions of schizophrenic patients (Freund et al., 2016). Moreover, stimulation of nicotinic acetylcholine α7 receptors with specific agonists rescue schizophrenia-like cognitive impairments in rodents (Potasiewicz et al., 2017). These receptors play also a crucial role in hippocampal synaptic plasticity (e.g., LTP at CA3-CA1 synapse) by regulating the release of glutamate. Aβ42 has

been reported to act as α7-nAChR agonist thus regulating synaptic plasticity in healthy brain (Hascup and Hascup, 2016). Deletion of α7-nAChR function has been proposed to trigger aberrant Aβ accumulation and the onset of an AD-like pathology (Tropea et al., 2021). Indeed, α7-KO mice older than 12 months exhibited increased Aβ levels, associated to tau hyperphosphorylation, neuronal loss and astrogliosis, all representing molecular hallmarks of the disease (Tropea et al., 2021).

Based on these findings, we investigated whether α7-KO mice, at an age of 4–6 months likely representing a prodromal phase of the disease, already show early signs of glutamatergic dysfunction at hippocampal level.

Even if at this age no accumulation of Aβ and pTau was observed, hippocampal neurons of α7-KO mice exhibited altered expression of pre- and post-synaptic proteins, including synapsin-1 and the NMDA receptor subunits GluN2A and GluN2B, along with the post-synaptic scaffold protein Homer-1, that were increased. These molecular changes were associated with significant alterations of the electrophysiological properties of the CA1 pyramidal neurons, including the frequency of spontaneous EPSCs, the time to peak of these currents, and the amplitude of evoked glutamate-mediated NMDA currents. Conversely, no significant changes were observed in AMPA receptor-mediated transmission, at both molecular and functional levels. The prodromic stage of the AD pathology is also characterized by alteration of calcium dynamics, which contributes to disrupted function of glutamatergic transmission. Accordingly, we found that α7-KO neurons also exhibited altered depolarization-induced Ca^{2+}-transients and reduced glutamate release.

In neurons, ionotropic glutamate receptors and nAChRs are actually colocalized and functionally interdependent (Stone et al., 2021). Specifically, the formation of nAChR and NMDA receptor complexes promoting glutamate release have been reported by Li and colleagues (Li et al., 2012). This interaction is further supported by the regulation of protein trafficking including subunits of glutamate receptors carried out by α7-nAChRs (Puddifoot et al., 2015). The activation of α7-nAChRs can also modify the subunit composition as well as cellular distribution of both NMDA and non-NMDA receptors, leading to altered neuronal excitability (Stone et al., 2021). The discrepancy between the increased expression of NMDA subunits and the reduced amplitude of NMDA currents might be due to not fully functional NMDARs, thus not allowing proper cation permeability, as suggested by previous literature reports demonstrating a functional interaction between the α7-nAChRs and NMDAR expression and function (Abraham et al., 2025). Alternatively, NMDARs might be retained in the cytosol, thus precluding their functional insertion in the plasma membrane. At the same time we also can explain the reduced frequency of sEPSCs with the increased expression of synapsin-1 and the decreased depolarization-induced Ca^{2+} entry in neurons. Indeed, synapsin is known to bind synaptic vesicles to actin filaments in the cytoskeleton thus increasing the "reserve" pool. We hypothesize that: i) synapsin overexpression increases the reserve pool and reduces the readily releasable pool; ii) the reduction in intracellular Ca^{2+} transient amplitude following neuronal depolarization may also limit CaMKII-mediated synapsin phosphorylation, leading to reduced number of SVs at the presynaptic terminal, thus affecting spontaneous vesicular release.

In 2013, Lin and colleagues studied the age-dependent modification of NMDA receptor subunits observed at cortical level by α7-KO mice. In particular, they reported that the major differences respect to WT mice were observed in the first 2 months of age (8–56 days postnatal). In line with Lin et al.'s findings, we found that at 5 months of age NR2B expression in the cortex of α7-KO mice is slightly, though not significantly, reduced (Supplementary Figure S2). In contrast, NR2B expression in the hippocampus of the same animals is increased.

Given that α7-nAChRs are expressed in both neurons and astrocytes (Fontana et al., 2023), we sought to dissect the specific contribution of neuronal α7 receptors to the observed alterations in glutamatergic transmission by focusing on electrophysiological readouts. By a specific adeno-associated viral (AAV) vector-based silencing system, we found that in WT mice, neuronal α7-nAChR accounted for half of the total receptors, supporting the rationale underlying our study of a key contribution of neuronal α7-nAChRs in the alteration of glutamatergic synaptic transmission. We thus employed an AAV vector engineered to selectively re-express α7-nAChRs in hippocampal neurons of α7-KO mice. This was achieved by driving CHRNA7 expression under the control of the neuron-specific human synapsin promoter (α7KI-neuro).

Following hippocampal AAV injection, we found that the re-expression of neuronal α7-nAChRs was sufficient to rescue post-synaptic alterations, but not presynaptic ones. Specifically, 3 weeks post-AAV injection, CA1 pyramidal neurons of α7KI-neuro mice displayed normalized NMDA receptor-mediated current amplitude and restored rise time of spontaneous EPSCs. However, the decreased frequency of sEPSCs remained unchanged, indicating that the presynaptic deficits were not rescued by neuronal α7-nAChR expression alone.

In conclusion, our findings suggest that the functional loss of α7-nAChRs disrupts glutamatergic transmission through distinct mechanisms acting at pre- and post-synaptic levels, with neuronal receptors playing a pivotal role in maintaining post-synaptic integrity. This highlights the complexity of α7-nAChR signaling in the hippocampus and supports the idea that early synaptic dysfunction in AD may arise from the disruption of cholinergic-glutamatergic cross-talk well before overt neurodegeneration occurs. Disentangling the cell-type-specific contributions of α7-nAChRs could therefore open new routes for targeting prodromal synaptic failure in AD and refining therapeutic strategies aimed at preserving circuit function in the early stages of the disease.

Data availability statement

The raw data supporting the conclusions of this article will be made available by the authors, without undue reservation.

Ethics statement

The animal study was approved by Ethics Committee of Università Cattolica and Italian Ministry of Health (authorization n. 944/2021-PR). The study was conducted in accordance with the local legislation and institutional requirements.

Author contributions

BC: Data curation, Formal Analysis, Investigation, Methodology, Writing – original draft. LS: Data curation, Formal Analysis, Investigation, Writing – original draft, Methodology. MA: Data curation, Formal Analysis, Investigation, Methodology, Writing – original draft. GA: Data curation, Formal Analysis, Investigation, Methodology, Writing – original draft. GP: Data curation, Investigation, Methodology, Writing – original draft, Formal Analysis. GL: Investigation, Writing – original draft, Data curation, Methodology. CR: Investigation, Writing – original draft, Conceptualization, Writing – review and editing. MT: Writing – original draft, Formal Analysis, Investigation. DP: Funding acquisition, Writing – original draft, Writing – review and editing. RP: Conceptualization, Writing – original draft, Writing – review and editing, Data curation, Formal Analysis, Investigation, Supervision. CG: Conceptualization, Funding acquisition, Project administration, Writing – original draft, Writing – review and editing.

Funding

The author(s) declare that financial support was received for the research and/or publication of this article. This work was supported by the Italian Ministry of University and Research (MIUR) funds PRIN2020 "2020AMLXHH" to CG and DP. Università Cattolica del Sacro Cuore contributed to the funding of this research project and its publication.

Acknowledgments

We would like to acknowledge the contribution of G-STeP Facilities (Electrophysiology and Microscopy) of Fondazione Policlinico Universitario "A. Gemelli" IRCCS for synaptic transmission studies and confocal analyses. We would like to acknowledge Dr. Pietro Renna from Università Cattolica for his technical assistance in the development of the AAV-based vector for the selective silencing and expression of α7-nAChRs.

Conflict of interest

The authors declare that the research was conducted in the absence of any commercial or financial relationships that could be construed as a potential conflict of interest.

The author(s) declared that they were an editorial board member of Frontiers, at the time of submission. This had no impact on the peer review process and the final decision.

Generative AI statement

The author(s) declare that no Generative AI was used in the creation of this manuscript.

Publisher's note

Supplementary material

The Supplementary Material for this article can be found online at: https://www.frontiersin.org/articles/10.3389/fphys.2025.1662171/full#supplementary-material

References

Abraham, S. M., Suresh, S., and Komal, P. (2025). Targeting neuronal Alpha7 nicotinic acetylcholine receptor upregulation in age-related neurological disorders. *Cell Mol. Neurobiol.* 45 (1), 70. doi:10.1007/s10571-025-01586-6

Bradford, M. M. (1976). A rapid and sensitive method for the quantitation of microgram quantities of protein utilizing the principle of protein-dye binding. *Anal. Biochem.* 72 (1-2), 248–254. doi:10.1016/0003-2697(76)90527-3

Cheng, Q., and Yakel, J. L. (2015). The effect of α7 nicotinic receptor activation on glutamatergic transmission in the hippocampus. *Biochem. Pharmacol.* 97 (4), 439–444. doi:10.1016/j.bcp.2015.07.015

Ferreira-Vieira T, H., Guimaraes I, M., Silva F, R., and Ribeiro F, M. (2016). Alzheimer's disease: targeting the cholinergic system. *Curr. Neuropharmacol.* 14 (1), 101–115. doi:10.2174/1570159X13666150716165726

Fontana, I. C., Kumar, A., and Nordberg, A. (2023). The role of astrocytic α7 nicotinic acetylcholine receptors in alzheimer disease. *Nat. Rev. Neurol.* 19 (5), 278–288. doi:10.1038/s41582-023-00792-4

Francis, P. T. (2003). Glutamatergic systems in Alzheimer's disease. *Int. J. Geriatr. Psychiatry* 18 (Suppl. 1), S15–S21. doi:10.1002/gps.934

Freund, R. K., Graw, S., Choo, K. S., Stevens, K. E., Leonard, S., and Dell'Acqua, M. L. (2016). Genetic knockout of the α7 nicotinic acetylcholine receptor gene alters hippocampal long-term potentiation in a background strain-dependent manner. *Neurosci. Lett.* 627, 1–6. doi:10.1016/j.neulet.2016.05.043

Gao, C., Tronson, N. C., and Radulovic, J. (2013). Modulation of behavior by scaffolding proteins of the post-synaptic density. *Neurobiol. Learn Mem.* 105, 3–12. doi:10.1016/j.nlm.2013.04.014

Hascup, K. N., and Hascup, E. R. (2016). Soluble Amyloid-β42 stimulates glutamate release through activation of the α7 nicotinic acetylcholine receptor. *J. Alzheimers Dis. Jad.* 53 (1), 337–347. doi:10.3233/JAD-160041

Henstridge, C. M., Hyman, B. T., and Spires-Jones, T. L. (2019). Beyond the neuron–cellular interactions early in alzheimer disease pathogenesis. *Nat. Rev. Neurosci.* 20 (2), 94–108. doi:10.1038/s41583-018-0113-1

Kumar, A., Sidhu, J., Lui, F., and Tsao, J. W. (2025). Alzheimer disease.

Lazzarino, G., Di Pietro, V., Rinaudo, M., Nagy, Z., Barnes, N. M., Bruce, L., et al. (2022). ILB®, a low molecular weight dextran sulphate, restores glutamate homeostasis, amino acid metabolism and neurocognitive functions in a rat model of severe traumatic brain injury. *Int. J. Mol. Sci.* 23 (15), 8460. doi:10.3390/ijms23158460

Letsinger, A. C., Gu, Z., and Yakel, J. L. (2022). α7 nicotinic acetylcholine receptors in the hippocampal circuit: taming complexity. *Trends Neurosci.* 45 (2), 145–157. doi:10.1016/j.tins.2021.11.006

Li, S., Li, Z., Pei, L., Le, A. D., and Liu, F. (2012). The α7nACh–NMDA receptor complex is involved in cue-induced reinstatement of nicotine seeking. *J. Exp. Med.* 209 (12), 2141–2147. doi:10.1084/jem.20121270

Li Puma, D. D., Ripoli, C., Puliatti, G., Pastore, F., Lazzarino, G., Tavazzi, B., et al. (2022). Extracellular tau oligomers affect extracellular glutamate handling by astrocytes through downregulation of GLT-1 expression and impairment of NKA1A2 function. *Neuropathol. Appl. Neurobiol.* 48 (5), e12811. doi:10.1111/nan.12811

Mainardi, M., Spinelli, M., Scala, F., Mattera, A., Fusco, S., D'Ascenzo, M., et al. (2017). Loss of leptin-induced modulation of hippocampal synaptic trasmission and signal transduction in high-fat diet-fed mice. *Front. Cell Neurosci.* 11, 225. doi:10.3389/fncel.2017.00225

Parri, H. R., Hernandez, C. M., and Dineley, K. T. (2011). Research update: alpha7 nicotinic acetylcholine receptor mechanisms in Alzheimer's disease. *Biochem. Pharmacol.* 82 (8), 931–942. doi:10.1016/j.bcp.2011.06.039

Piacentini, R., Li Puma, D. D., Mainardi, M., Lazzarino, G., Tavazzi, B., Arancio, O., et al. (2017). Reduced gliotransmitter release from astrocytes mediates tau-induced synaptic dysfunction in cultured hippocampal neurons. *GLIA* 65 (8), 1302–1316. doi:10.1002/glia.23163

Potasiewicz, A., Nikiforuk, A., Hołuj, M., and Popik, P. (2017). Stimulation of nicotinic acetylcholine alpha7 receptors rescue schizophrenia-like cognitive impairments in rats. *J. Psychopharmacol. (Oxf)* 31 (2), 260–271. doi:10.1177/0269881116675509

Puddifoot, C. A., Wu, M., Sung, R. J., and Joiner, W. J. (2015). Ly6h regulates trafficking of Alpha7 nicotinic acetylcholine receptors and nicotine-induced potentiation of glutamatergic signaling. *J. Neurosci.* 35 (8), 3420–3430. doi:10.1523/JNEUROSCI.3630-14.2015

Puliatti, G., Li Puma, D. D., Aceto, G., Lazzarino, G., Acquarone, E., Mangione, R., et al. (2023). Intracellular accumulation of tau oligomers in astrocytes and their synaptotoxic action rely on amyloid precursor protein intracellular Domain-dependent expression of Glypican-4. *Prog. Neurobiol.* 227, 102482. doi:10.1016/j.pneurobio.2023.102482

Rao, Y. L., Ganaraja, B., Murlimanju, B. V., Joy, T., Krishnamurthy, A., and Agrawal, A. (2022). Hippocampus and its involvement in Alzheimer's disease: a review. *3 Biotech.* 12 (2), 55. doi:10.1007/s13205-022-03123-4

Ripoli, C., Piacentini, R., Riccardi, E., Leone, L., Li Puma, D. D., Bitan, G., et al. (2013). Effects of different amyloid β-protein analogues on synaptic function. *Neurobiol. Aging* 34 (4), 1032–1044. doi:10.1016/j.neurobiolaging.2012.06.027

Selkoe, D. J. (2002). Alzheimer's disease is a synaptic failure. *Science* 298 (5594), 789–791. doi:10.1126/science.1074069

Spires-Jones, T. L., and Hyman, B. T. (2014). The intersection of amyloid beta and tau at synapses in alzheimer's disease. *Neuron* 82 (4), 756–771. doi:10.1016/j.neuron.2014.05.004

Stone, T. W. (2021). Relationships and interactions between ionotropic glutamate receptors and nicotinic receptors in the CNS. *Neuroscience* 468, 321–365. doi:10.1016/j.neuroscience.2021.06.007

Tavazzi, B., Lazzarino, G., Leone, P., Amorini, A. M., Bellia, F., Janson, C. G., et al. (2005). Simultaneous high performance liquid chromatographic separation of purines, pyrimidines, N-acetylated amino acids, and dicarboxylic acids for the chemical diagnosis of inborn errors of metabolism. *Clin. Biochem.* 38 (11), 997–1008. doi:10.1016/j.clinbiochem.2005.08.002

Tropea, M. R., Li Puma, D. D., Melone, M., Gulisano, W., Arancio, O., Grassi, C., et al. (2021). Genetic deletion of α7 nicotinic acetylcholine receptors induces an age-dependent Alzheimer's disease-like pathology. *Prog. Neurobiol.* 206, 102154. doi:10.1016/j.pneurobio.2021.102154

Wu, J., Ishikawa, M., Zhang, J., and Hashimoto, K. (2010). Brain imaging of nicotinic receptors in alzheimer's disease. *Int. J. Alzheimers Dis.* 2010, 548913–11. doi:10.4061/2010/548913

Yakel, J. L. (2012). Nicotinic ACh receptors in the hippocampus: role in excitability and plasticity. *Nicotine Tob. Res.* 14 (11), 1249–1257. doi:10.1093/ntr/nts091

Zott, B., and Konnerth, A. (2023). Impairments of glutamatergic synaptic transmission in Alzheimer's disease. *Semin. Cell Dev. Biol.* 139, 24–34. doi:10.1016/j.semcdb.2022.03.013

frontiers | Frontiers in Physiology

TYPE Original Research
PUBLISHED 24 September 2025
DOI 10.3389/fphys.2025.1625137

OPEN ACCESS

EDITED BY
Roberto Piacentini,
Catholic University of the Sacred Heart, Italy

REVIEWED BY
Myriam Catalano,
Sapienza University of Rome, Italy
Fabrizio Vecchio,
University of eCampus, Italy

*CORRESPONDENCE
F. Deriu,
deriuf@uniss.it

‡These authors have contributed equally to this work

RECEIVED 08 May 2025
ACCEPTED 29 August 2025
PUBLISHED 24 September 2025
CORRECTED 10 October 2025

CITATION
Loi N, Ginatempo F, Zeroual M, Ventura L, Cano A, Oneto C, Ortu P, Piras MR and Deriu F (2025) A new index of cortical plasticity induced by paired associative stimulation to describe cognitive status in aged healthy subjects.
Front. Physiol. 16:1625137.
doi: 10.3389/fphys.2025.1625137

A new index of cortical plasticity induced by paired associative stimulation to describe cognitive status in aged healthy subjects

Nicola Loi[1,2‡], Francesca Ginatempo[2‡], Mohammed Zeroual[2], Lucia Ventura[1,2], Antonella Cano[1,2], Carmen Oneto[2], Paola Ortu[3], Maria Rita Piras[3] and Franca Deriu [2,4*]

[1]Azienda Ospedaliero Universitaria di Sassari, Sassari, Italy, [2]Department of Biomedical Sciences, University of Sassari, Sassari, Italy, [3]National Research Council – Institute for Genetics and Biomedical Research, Sassari, Italy, [4]Unit of Endocrinology, Nutritional and Metabolic Disorders, Azienda Ospedaliero Universitaria di Sassari, Sassari, Italy

Introduction: Cortical plasticity is a key factor for cognitive skills, and paired associative stimulation (PAS) is useful to study it in humans. Currently, due to the number of non-responders to PAS and discrepancies in the post-PAS time-points assessed, a plasticity index describing PAS effects and correlating it to cognitive status is lacking. Therefore, this study investigated which PAS index better discriminates between responders (RRs) and non-responders (NRs) and correlates with cognitive status.

Methods: Seventy-six healthy aged subjects (67.0 ± 7.2 y.o., 35 males) were enrolled. The Montreal Cognitive Assessment (MoCA), the Mini-Mental State Examination (MMSE), and the Addenbrooke's Cognitive Assessment (ACER) were used to assess cognitive status. Motor-evoked potentials (MEPs) were recorded from the first dorsal interosseous muscle at baseline and after 0, 10, 20, and 30 min from PAS, pairing peripheral median nerve stimulation with a transcranial magnetic stimulation stimulus over the left primary motor cortex. MEP amplitude was used to calculate the grand average (GrA), which is the mostused PAS plasticity index, along with two newly introduced indexes: the curve concavity (CC) and the pre- vs. post-PAS difference (PPPD). CC described the curve shape of the PAS effects, while PPPD calculated the significant differences between the baseline and post-PAS MEP amplitude.

Results: CC demonstrated good consistency as PAS-plasticity index with high odds ratios and sensibility in the discrimination of responsiveness to PAS; PPPD had higher specificity in the identification of RRs. Only the MoCA score was significantly higher ($p = 0.006$) in RRs than in NRs when the two groups were discriminated according to CC, and it significantly correlated with CC ($p = 0.013$).

Discussion: In conclusion, CC may represent a potential PAS-plasticity index to describe the cortical plasticity and cognitive status in humans, with a possible practical application in patients with cognitive impairment.

KEYWORDS

transcranial magnetic stimulation, paired associative stimulation, cognitive skills, aged subjects, paired associative stimulation responsiveness

1 Introduction

Synaptic plasticity is a physiological mechanism in which activity-dependent modifications of the strength or efficacy of synaptic transmissions occur after exogenous or endogenous stimulation (Citri and Malenka, 2008). This mechanism is crucial to adapt to environmental changes, and it is the basis for learning phenomena (Kandel et al., 2014). Among several types of synaptic plastic changes, long-term potentiation (LTP) is a key mechanism that is able to strengthen specifically stimulated synaptic connections, requiring high-frequency stimulation and near-synchronous activation of both pre- and post-synaptic neurons (Malenka and Bear, 2004; Kandel et al., 2014).

In humans, LTP at the cortical level can be studied through a transcranial magnetic stimulation (TMS) protocol named paired associative stimulation (PAS) (Stefan et al., 2000; 2002; Carson and Kennedy, 2013). PAS is administered by pairing electrical stimulation (ES) of the peripheral nerve afference followed by a TMS stimulus over the primary motor cortex (M1), for 100–200 times, determining a rapidly evolving (<30 min) and long-lasting (>60 min) increase in cortical excitability assessed through motor-evoked potentials (MEPs) (Stefan et al., 2000; 2002). This increase in excitability is because of the LTP-like mechanism (Stefan et al., 2000; Wolters et al., 2003), which depends on the enhanced strength of the connections between the primary somatosensory cortex (S1) and the excitatory interneurons within M1 (Stefan et al., 2000; 2002; Ridding and Taylor, 2001). Several studies demonstrated that PAS improves motor learning in healthy subjects as well as in pathological conditions (Ziemann et al., 2004; Wessel et al., 2015). However, there is no evidence demonstrating a significant correlation between PAS-related gain and cognitive status in healthy subjects (Schättin et al., 2018; Minkova et al., 2019).

In the last 24 years, several studies have used PAS effects as a clinical parameter for studying cortical plasticity, with conflicting results obtained when dealing with patients with cognitive decline (Battaglia et al., 2007; Terranova et al., 2013; Lahr et al., 2016; Minkova et al., 2019; Di Lorenzo et al., 2020; Meder et al., 2021). Some studies found differences in PAS effects between cognitively impaired patients and healthy controls (Battaglia et al., 2007; Terranova et al., 2013; Di Lorenzo et al., 2020), while others failed to detect any significant effect (Lahr et al., 2016; Minkova et al., 2019; Meder et al., 2021). These conflicting results could be because of the different experimental procedures used. In fact, some studies observed PAS effects at only one time point after PAS administration (Tecchio et al., 2008; Fathi et al., 2010), while others observed the effects at two (Cirillo et al., 2009; Singh et al., 2014; Lahr et al., 2016; Schättin et al., 2018; Meder et al., 2021) or even more than two time points after PAS delivery (Müller-Dahlhaus et al., 2008; Terranova et al., 2013; Bhandari et al., 2018; Minkova et al., 2019).

Another factor that affects PAS results is the subjects' responsiveness to the PAS protocol. It has been observed that PAS elicited the expected effects in 60% or less of the participants (Karabanov et al., 2016; Lahr et al., 2016; Minkova et al., 2019), and it depends on the subjects' inter- and intra-variability due to circadian fluctuations, time of the day (Sale et al., 2007), alertness (Kamke et al., 2012), attentional state (Stefan et al., 2004), stimulation intensity (Müller-Dahlhaus et al., 2008), genetic traits (Cheeran et al., 2008), cortical thickness (List et al., 2013), and microstructural properties of the white matter (Klöppel et al., 2008). This variable response to the PAS protocol limits its use as a tool that can be correlated with the subject's cognitive status, especially in aged people and patients with cognitive decline. For this reason, it is necessary to determine a plasticity index that is able to describe the whole PAS effects, including all the time points, and discriminate between responders (RRs) and non-responders (NRs) to PAS. In the literature, the most-used PAS-plasticity index is the grand average (GrA) (Wolters et al., 2005; Müller-Dahlhaus et al., 2008; Lahr et al., 2016; Minkova et al., 2019), which is the average of the post-PAS MEP amplitudes. More studies tried to relate GrA with the cognitive status in humans, but no significant correlation was found (Schättin et al., 2018; Minkova et al., 2019), raising the question of whether it is the most suitable PAS-plasticity index.

Therefore, we aimed to identify PAS-plasticity indexes that are able to describe the PAS effect across several time points and correlate it with the cognitive status. For this reason, two PAS-plasticity indexes were defined as the curve concavity (CC) and the pre- vs. post-PAS difference (PPPD), and these indexes were compared with the GrA.

Both CC and PPPD were established considering that the plasticity effect is a long-lasting phenomenon that is recordable at different time points after PAS administration. This consideration differs from several works that identified the responsivity to the PAS protocol based on the increase in the MEP amplitude at only one time point after PAS, which could be the result of changes in the cortical excitability rather than the synaptic plasticity phenomenon (Malenka and Bear, 2004; Kandel et al., 2014). In this light, the mean MEP amplitudes at each time point were used to determine the curve, and its concavity was used as a PAS-plasticity index. In addition, the PPPD, which was determined when at least two post-PAS time points showed a significant increase in MEP amplitude compared to that at baseline, was taken as another PAS-plasticity index. Both CC and PPPD were used to discriminate between RRs and NRs to the PAS protocol.

Finally, we verified whether these PAS-plasticity indexes correlated with cognitive status. In the perspective of clinical application of these indexes in patients with cognitive decline, the study involved a group of aged, healthy subjects since it has been demonstrated that cognitive decline is an age-related feature and can occur even before the older age threshold (Murman, 2015).

2 Methods

2.1 Participants

Seventy-six healthy, aged subjects (mean age 67.0 ± 7.2; range: 50 years–89 years old; 35 males), all right-handed according to the Oldfield inventory scale, participated in the study. According to the age range (10 years), the sample consisted of the following age groups: 50–59 = 13 subjects, 60–69 = 35 subjects, 70–79 = 24 subjects, and 80–89 = 4 subjects. Informed written consent was obtained from all the subjects. The experimental procedures were approved by the Local Ethics Committee (Sardinia Ethics Committee Prot. PG/2023/5172, 06/04/2023) and were conducted in accordance with the guidelines of the Declaration of Helsinki. None of the participants had a history and/or current

signs/symptoms of neurological and/or psychiatric diseases, and none used psychotropic drugs (neuroleptics and anticonvulsive medications). The exclusion criteria followed the TMS safety guidelines (Rossi et al., 2021). Subjects were seated in a comfortable chair, and they were asked to stay relaxed but alert during the recordings, which were performed in a quiet room.

2.2 Cognitive evaluation

The cognitive status was evaluated using standardized neuropsychological tests including the Montreal Cognitive Assessment (MoCA) (Nasreddine et al., 2005), the Addenbrooke's Cognitive Examination revised (ACE-R) (Mioshi et al., 2006), and the Mini-Mental State Examination (MMSE) (Folstein et al., 1975). Moreover, subcategory scores of MoCA and ACE-R were also used as variables. MoCA included the assessment of visuo-spatial abilities, executive functions, language, orientation, attention, and memory (raw scores). ACE-R included the assessment of orientation, memory, verbal fluency, language, and visuo-spatial abilities. Tests were administered and analyzed by expert neuropsychologists. Raw values were corrected for age and education level.

2.3 Electromyography (EMG)

Surface electromyography (EMG) was recorded from the first dorsal interosseous (FDI) muscle using 9-mm-diameter Ag–AgCl surface electrodes. The active electrode was placed over the muscle belly, the reference electrode was placed over the metacarpophalangeal joint of the second finger, and the ground electrode was placed over the forearm (Ginatempo et al., 2022). EMG signals were recorded (D360 amplifier, Digitimer Ltd., Welwyn Garden City, UK), amplified (1,000 times), filtered (bandpass 3 Hz–3,000 Hz), and sampled at 5 kHz using a 1,401 power analog-to-digital converter and Signal 6 software (Cambridge Electronic Design, Cambridge, UK).

2.4 Transcranial magnetic stimulation (TMS)

TMS was performed using a 70-mm figure-of-eight coil connected to a Magstim 200 stimulator through a BiStim module (Magstim Co., Whitland and Dyfed, UK). The optimal stimulation site for the right FDI muscle was carefully identified and then marked with a soft-tip pen on the scalp to maintain the same coil position throughout the experiments. The handle of the coil was pointed posteriorly and laterally, at approximately 45° to the interhemispheric line (Rossini et al., 2015). The resting motor threshold (RMT) was measured as the lowest TMS intensity that is able to elicit MEPs of 0.05 mV in the relaxed muscle in at least five out of 10 consecutive trials. RMT was expressed as a percentage of the maximum stimulator output (MSO). The test stimulus intensity was set at 120% of RMT.

2.5 Paired associative stimulation (PAS)

Experiments were performed in the afternoon (between 15:00 and 17:00). The PAS intervention was administered by pairing 200 electrical stimulation (ES) of the right median nerve with TMS over the left hand M1 using inter-stimulus intervals of 25 ms at 0.25 Hz (Stefan et al., 2000; 2002) lasting for approximately 13 min. ES was delivered to the right median nerve at the wrist through a pair of cup electrodes (cathode distal) connected to a current stimulator (model DS7; Digitimer Ltd). Single square-wave pulses (0.2-ms duration) were delivered, and the stimulus intensity was set at three times the perceptive threshold (PT). TMS was delivered over the left hand M1 using a stimulus intensity at 110% of RMT.

Fifteen MEPs were collected from the resting FDI before (baseline) and immediately (T0), 10 (T10), 20 (T20), and 30 (T30) minutes after PAS administration based on previous studies that showed the strongest PAS effect in this time-window (Wischnewski and Schutter, 2016). During PAS stimulation, subjects were asked to mentally count the stimuli to maintain attention. Effects of PAS were measured as MEPs' peak-to-peak amplitude collected at each tested time interval. PAS-plasticity indexes were determined comparing the ratio of the post-PAS MEPs at each time-point with baseline MEPs.

2.6 Data analysis

Responsiveness to PAS was determined using GrA, CC, and PPPD. Since PPPD is not a continuous variable, only GrA and CC were used as PAS plasticity indexes for the correlation analysis with the scores in the cognitive batteries (MMSE, ACE-R, and MoCA) and their subcategories. Each subject was categorized as RR or NR according to the three PAS plasticity index criteria. They were divided into RR and NR based on the GrA. The CC criterion reclassified the same subjects differently, and the PPPD criterion applied its own way of grouping them, ensuring that the same 76 subjects were categorized as RR or NR on three separate occasions according to the three PAS plasticity index criteria.

GrA was calculated as the mean value of the MEP amplitude ratios calculated at each post-PAS time point (post-PAS time point/baseline) (Müller-Dahlhaus et al., 2008). Subjects were categorized as RRs when GrA >1 (Figure 1A) and as NRs when GrA <1 (Figure 1B).

The MEP amplitude curve was used to determine CC, which was obtained using the polynomial function of the curve ($y = ax^2 + bx + c$), where the "a" coefficient expresses the concavity of the curve. The curve function was built from the raw MEP amplitudes collected throughout the five time points (baseline, T0, T10, T20, and T30) using the Excel polynomial function (Office 365 pro plus, Microsoft Corporation, Redmond, USA). A negative a value (negative concavity) identified RRs (Figure 1C), while a positive a value (positive concavity) identified NRs (Figure 1D).

PPPD identified RRs when post-PAS raw MEP amplitudes were significantly higher than those of baseline MEP in at least two out of the four post-PAS MEPs (T0, T10, T20, and T30) (Figure 1E); otherwise, they were identified as NRs (Figure 1F). To describe responsiveness through PPPD, paired Student's t-test was used to compare the means of baseline MEP amplitudes with the means of

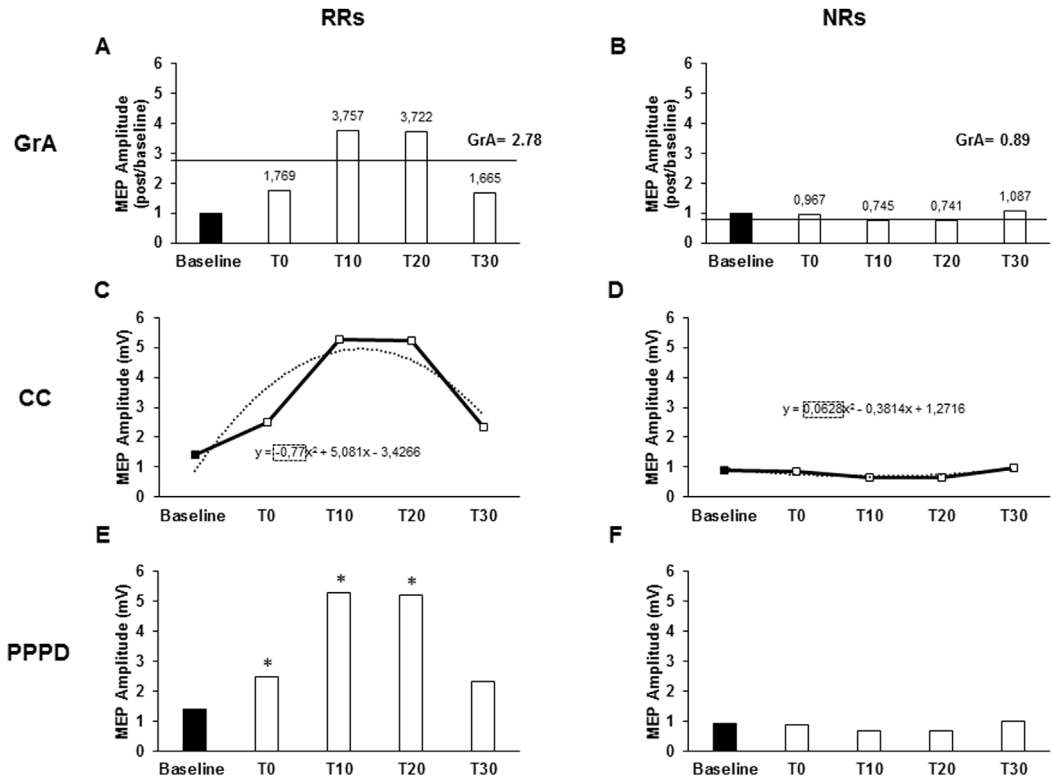

FIGURE 1
Responsiveness characteristics when using the grand average (GrA), curve concavity (CC), or pre- vs. post-PAS difference (PPPD) as PAS plasticity indexes. The charts describe the responsiveness of two representative subjects of a non-responder (NR) and a responder (RR) to the PAS protocol, assessed as the MEP amplitude at baseline and after 0 (T0), 10 (T10), 20 (T20), and 30 (T30) minutes from PAS delivery. Continued lines identify GrA of the post-PAS time point MEPs; GrA was calculated as the mean value of the MEP amplitude ratios calculated at each post-PAS time point (post-PAS time point/baseline). GrA >1 identified an RR **(A)**, while GrA <1 identified an NR **(B)**. Dashed lines identify the CC. CC was obtained using the polynomial function of the curve (y = ax2 + bx + c), where the "a" coefficient expresses the concavity of the curve. The curve function was built from the raw MEP amplitudes collected throughout the five time points. CC <0 identified a RR **(C)**, while CC >0 identified a NR **(D)**. In the PPPD, asterisks identify those time points where MEPs were significantly higher than baseline MEPs; PPPD identified RRs when post-PAS raw MEP amplitudes were significantly higher than baseline MEPs in at least two out of the four post-PAS MEPs **(E)**; if less than two time points were higher than the baseline, it determined NRs **(F)**. *$p < 0.05$.

each post-PAS time point. Since PPPD is a categorical variable, it was not used in the correlation analysis.

2.7 Statistical analysis

Statistical analysis was performed with SPSS 26 software (SPSS Inc., Chicago, IL, USA). The analysis of variance (ANOVA) and planned *post hoc* t-test with Bonferroni correction for multiple comparisons were used. Compound symmetry was evaluated with Mauchly's test, and Greenhouse–Geisser correction was performed when required. Results were considered statistically significant when the p-value was <0.05. A preliminary descriptive analysis was performed to evaluate the presence of outliers in all the variables (raw amplitude MEPs, MEP ratios, CC, GrA values, and MoCA, ACE-R and MMSE scores). Subjects were considered outliers when they exhibited extreme values for all TMS and/or all cognitive variables, which led to their exclusion from further analysis.

Moreover, to understand if cortical excitability could describe MoCA scores, we used a linear regression model with MoCA as the dependent variable and baseline MEP and RMT as the independent variables.

2.7.1 Evaluation of PAS effects

Repeated-measure (RM) ANOVA was used to assess PAS effects using MEP amplitude as a variable with time (baseline, T0, T10, T20, and T30) as the within-subject factor. Moreover, to assess if the PAS effect was present within the groups of RRs and NRs, RM-ANOVA was separately performed for RRs and NRs, using MEP amplitude as a variable with time (baseline, T0, T10, T20, and T30) as the within-subject factor. Responsiveness was detected using GrA as the PAS plasticity index.

2.7.2 Evaluation of the characteristics of the PAS plasticity indexes

To assess the goodness of fit between the modeled curve derived from the CC and the individual data points obtained at each time interval, a goodness of fit analysis using curve estimation regression on all raw MEP values (used to construct the CC curve) was performed for each subject. In this analysis, the dependent variable was MEP amplitude, and the independent variable was the MEP

trial number at each time point (baseline, T0, T10, T20, and T30). Model fit was evaluated using the mean R^2 across the subjects and the root-mean-squared error (RMSE).

To understand if RRs and NRs were different regarding cortical excitability, once we determined the RR and NR groups based on each PAS-plasticity index (GrA, CC, and PPPD), one-way ANOVA with variables RMT and MEP at baseline was performed separately with the index (GrA, CC, and PPPD) as the between-subject factor. Chi-square analysis was carried out to assess whether a significant difference was present between the rate of RRs and NRs when discriminated with the three PAS-plasticity indexes (GrA, CC, and PPPD). The intra-class correlation coefficient (ICC) was calculated to assess the individual consistency of CC in describing the PAS plasticity effect in comparison to GrA. Inter-rater reliability analysis was conducted using a two-way mixed-effects model with a consistency type. In this context, the two indices—CC and GrA—were treated as "raters" for the ICC calculation. It is important to note that these indices do not represent repeated measurements of the same variable, but rather that of two distinct metrics.

A contingency model was used to calculate the likelihood of CC and PPPD in the identification of RRs. GrA, which represents the commonly used PAS plasticity index in the literature (Wolters et al., 2005; Müller-Dahlhaus et al., 2008; Lahr et al., 2016; Minkova et al., 2019), was compared to CC and PPPD regarding the responsiveness discrimination, calculating the odds ratios (ORs).

The contingency model of the receiver operating characteristic (ROC) (Zweig and Campbell, 1993) was used to calculate the sensibility and specificity in the PAS responsiveness characterization of CC and PPPD. GrA, which represents the commonly used PAS plasticity index in the literature (Wolters et al., 2005; Müller-Dahlhaus et al., 2008; Lahr et al., 2016; Minkova et al., 2019), was used as the reference value. A 2 x 2 contingency table was determined using GrA as the PAS plasticity index reference and comparing CC and PPPD in sensibility and specificity in the discrimination of responsiveness. True RRs were defined when both the GrA and CC/PPPD indexes described a plastic effect; on the contrary, true NRs were defined when both GrA and CC/PPPD indexes did not individuate a PAS effect. False RRs were defined as the subjects who were RRs for the CC/PPPD index but not for the reference index, i.e., GrA; false NRs were defined as the subjects who were RRs for the reference index (GrA), but not for CC/PPPD. Sensibility [true RRs/(true RRs + false NRs)] and specificity [true NRs/(true NRs + false RRs)] were then calculated. In this light, sensibility describes the amount of wrongly considered NRs by the new indexes compared to the GrA; while, specificity describes the number of wrongly considered RRs by the new indexes compared to the GrA. False RRs and false NRs were not excluded by the following analyses.

Furthermore, in order to assess the robustness of sensibility and specificity of CC and PPPD as indexes discriminating between RRs and NRs, the same contingency table was developed in a reduced sample (70%) (Babyak, 2004).

2.7.3 Assessment of the influence of gender and age on the neurophysiological tests and the PAS-plasticity indexes

To evaluate the effect of gender in cognitive tests (MMSE, ACE-R, and MoCA) and PAS plasticity indexes (GrA and CC), a one-way ANOVA was performed, while PPPD differences in gender frequency were assessed through chi-square analysis. To evaluate the influence of age on PAS effects and cognitive status, Spearman's bivariate correlation analysis was performed to correlate age with cognitive scores (MMSE, ACE-R, and MoCA) and PAS plasticity indexes (GrA and CC), while for PPPD, a one-way ANOVA was used with index as a factor.

2.7.4 Evaluation of the influence of responsiveness to the PAS protocol on the cognitive status

To assess if cognitive scores were different between RRs and NRs, a one-way ANOVA was separately performed for each cognitive test (MMSE, ACE-R, and MoCA) and their subcategories using the PAS plasticity indexes as a factor (GrA, CC, and PPPD).

Moreover, a Bayesian one-way ANOVA was performed to better understand differences between RRs and NRs in the cognitive scores based on the frequentist approach. The Bayesian factor (BF) was used, according to the Bayesian information criterion (BIC), to probabilistically test the null hypothesis (H0), i.e., no difference between RRs and NRs, while a significant difference between RRs and NRs identified the alternative hypothesis (H1). BF values were interpreted as follows: BF up to 0.33, evidence for H0; BF between 0.33 and 3.0, no evidence; and BF >3.0, evidence for H1. The strength of the evidence (anecdotal, moderate, strong, very strong, and extreme) was also appraised according to the same guidelines by Lee and Wagenmakers (2014)

2.8 Assessment of the correlation between PAS plasticity indexes and cognitive status

To select the appropriate test for the correlation analysis, the normality of the variable distributions was assessed using the Kolmogorov–Smirnov (K–S) and Shapiro–Wilk (S–W) tests. Variables were classified as non-normally distributed when both tests showed significant results ($p < 0.05$). Correlation analysis was conducted between cognitive scores (MoCA, ACE-R, and MMSE) and PAS plasticity indexes (GrA and CC).

3 Results

3.1 Evaluation of the PAS effects

When considering data from all participants, statistical analysis demonstrated a significant PAS effect at all time points tested. In particular, RM-one-way ANOVA showed a significant effect of time ($F_{4,72} = 10.617$, $p < 0.001$, $\eta^2p = 0.130$), and Bonferroni's *post hoc* analysis highlighted an increase in MEP amplitude compared to that at baseline at T0 ($p = 0.040$), T10 ($p < 0.001$), T20 ($p < 0.001$), and T30 ($p < 0.001$) (Figure 2A). When considering only the RR group for GrA categorization, RM-ANOVA detected a significant effect of time ($F_{4,49} = 16.468$, $p < 0.001$; $\eta^2p = 0.248$), and *post hoc* analysis found that baseline MEP was significantly lower than MEPs at T0 ($p = 0.003$), T10 ($p < 0.001$), T20 ($p < 0.001$), and T30 ($p < 0.001$) (Figure 2B). On the other hand, when focusing the analysis on the NR group, the effect of time was again detected ($F_{4,19} = 3.744$, $p = 0.031$; $\eta^2p = 0.212$), but *post hoc* analysis found that baseline

MEP was significantly higher than that at T20 ($p = 0.003$), but not different when compared to that at T0 ($p = 0.100$), T10 ($p = 0.072$), and T30 ($p = 0.261$) (Figure 2C). When evaluating the RR group for CC categorization, the RM-ANOVA found significant effect of time ($F_{4,44} = 14.107$, $p < 0.001$; $\eta^2p = 0.243$), and *post hoc* analysis found that the baseline MEP was significantly lower than MEPs at T0 ($p = 0.002$), T10 ($p < 0.001$), T20 ($p < 0.001$), and T30 ($p = 0.001$) (Figure 2D). When assessing NRs, a significant PAS effect was detected ($F_{4,24} = 4.690$, $p = 0.002$; $\eta^2p = 0.148$), but *post hoc* analysis found no significant differences between baseline MEP and post-PAS time-points (all $p > 0.05$) (Figure 2E). Finally, when using PPPD as the discrimination PAS-index, a significant PAS effect for RRs was found (F 4.36 = 16.707, $p < 0.001$; $\eta^2p = 0.300$). *Post hoc* analysis found that baseline MEP was significantly lower than MEPs at T0 ($p = 0.003$), T10 ($p < 0.001$), T20 ($p < 0.001$), and T30 ($p < 0.001$) (Figure 2F); however, when considering NRs for PPPD PAS-index, no significant PAS effect was detected ($F_{4,32} = 1.741$, $p = 0.145$; $\eta^2p = 0.052$) (Figure 2G).

3.2 Evaluation of the characteristics of the PAS plasticity indexes

The curve estimate regression assessing the CC goodness of fit showed an R^2 of 0.212, with a mean RMSE of 0.674 mV. Linear regression analysis determined a significant goodness of fit between the modeled curve derived from both GrA and CC and the individual data obtained by the single time points (GrA: $F_{5,76} = 61.855$, $p < 0.001$; CC: $F_{5,76} = 50{,}367.553$, $p < 0.001$). When considering GrA, each independent variable significantly influenced it (baseline: standard $\beta = -0.655$, $t71 = -10.380$, $p < 0.001$; T0: standard $\beta = -0.380$, $t71 = 4.194$, $p < 0.001$; T10: standard $\beta = -0.229$, $t71 = 2.357$, $p = 0.021$; T20: standard $\beta = -0.188$, $t71 = 1.587$, $p = 0.117$; T30: standard $\beta = 0.410$, $t71 = 4.677$, $p < 0.001$), with the residual mean < 0.001 and a standard deviation of the residual of 0.454. When assessing CC, each independent variable significantly influenced the dependent one (baseline: standard $\beta = 0.390$, $t71 = 159.457$, $p < 0.001$; T0: standard $\beta = -0.436$, $t71 = 127.950$, $p < 0.001$; T10: standard $\beta = -0.924$, $t71 = 246.332$, $p < 0.001$; T20: standard $\beta = -0.487$, $t71 = 105.845$, $p < 0.001$; T30: standard $\beta = 0.937$, $t71 = 273.573$, $p < 0.001$), with the residual mean <0.001 and a standard deviation of the residual of 0.003.

The responsiveness rates and mean values of RMT and baseline MEPs for RRs and NRs groups based on each PAS plasticity index and the characteristics of the participants are shown in Table 1. Using GrA as the PAS plasticity index, 53 subjects (69.7%) were classified as RRs, and 23 subjects (30.3%) were classified as NRs. With CC, 48 subjects (63.2%) were identified as RRs, and 28 (36.8%) were identified as NRs, while PPPD classified 40 subjects (52.6%) as RRs and 36 (47.4%) as NRs. Seventeen subjects (22.4%) were consistently classified as RRs across all three indices, and 32 (42.1%) were consistently identified as NRs. Discrepancies in the responsiveness classification were observed between GrA and CC in five subjects (6.6%), between GrA and PPPD in 13 subjects (17.1%), and between CC and PPPD in eight subjects (10.5%). Linear regression modeling was utilized to evaluate the cortical excitability's influence on MoCA and ACE-R scores, and it showed non-significant results (MoCA: $F_{2,74} = 0.549$, $p = 0.580$; ACE-R: $F_{2,74} = 0.827$, $p = 0.441$). This finding ruled out that cortical excitability could have influenced the results. One-way ANOVA failed to detect any significant difference in RMT and baseline MEP between RRs and NRs. In particular, one-way ANOVA showed non-significant effect of index when considering CC (RMT: $F_{1,75} = 0.489$, $p = 0.487$, $\eta^2p = 0.007$; baseline MEP: $F_{1,75} = 1.229$, $p = 0.271$, $\eta^2p = 0.016$), GrA (RMT: $F_{1,75} = 0.122$, $p = 0.727$, $\eta^2p = 0.002$; baseline MEP: $F_{1,75} = 0.345$, $p = 0.558$, $\eta^2p = 0.005$), and PPPD (RMT: $F_{1,75} = 0.510$, $p = 0.477$, $\eta^2p = 0.007$; baseline MEP: $F_{1,75} = 2.079$, $p = 0.153$, $\eta^2p = 0.027$). Chi-square analysis found that the RR rate was significantly higher than that of NRs when using GrA ($X^2_{1,76} = 11.842$, $p = 0.001$, $\varphi = 0.395$) and CC ($X^2_{1,76} = 5.263$, $p = 0.022$, $\varphi = 0.266$) as the PAS plasticity indexes, but it was not the same for PPPD ($X^2_{1,76} = 0.212$, $p = 0.646$, $\varphi = 0.053$).

ICC analysis found good consistency of CC, compared to GrA, in the description of the PAS-plasticity effect (ICC = 0.672, $p < 0.001$).

ORs to determine the likelihood to discriminate responsiveness, compared to GrA, found no differences between GrA and CC (OR = 0.744, $p = 0.391$); meanwhile, PPPD had significantly less likelihood to discriminate responsiveness than GrA (OR = 0.482, $p = 0.032$).

A contingency model using GrA as the reference index showed that CC had a sensibility ratio of 0.81 and a specificity of 0.63 in responsiveness discrimination, while PPPD demonstrated a sensibility ratio of 0.74 and a specificity of 1.0 (Table 2).

When assessing the robustness of sensibility and specificity scores on a total of 54 selected subjects (70% of the whole sample), CC confirmed a good robustness for sensibility, while PPPD demonstrated good robustness for specificity. In fact, when using CC as the classification index, with GrA as the reference index, 35 subjects were considered as RRs and 19 as NRs. With this categorization, the sensibility accounted was 0.80, while the specificity was 0.20. When using PPPD as the index in comparison with GrA, the analysis showed that 31 subjects were considered as RRs and 23 as NRs, with a sensibility of 0.82 and a specificity of 1.00.

3.3 Assessment of the influence of gender and age on the neurophysiological tests and the PAS-plasticity indexes

Statistical analysis failed to detect any significant effect of gender on cognitive test scores (MMSE: $F_{1,75} = 0.723$, $p = 0.398$, $\eta^2p = 0.010$; ACE-R: $F_{1,75} = 2.701$, $p = 0.105$, $\eta^2p = 0.035$; MoCA: $F_{1,75} = 0.290$, $p = 0.765$, $\eta^2p = 0.001$) and on PAS plasticity indexes (GrA: $F_{1,75} < 0.00$, $p = 0.994$, $\eta^2p < 0.001$; CC: $F_{1,75} = 1.145$, $p = 0.288$, $\eta^2p = 0.015$; PPPD: $X^2_{1,76} = 0.211$, $p = 0.646$, $\varphi = 0.075$). Spearman's analysis found no significant correlation between age and PAS plasticity indexes (GrA: $r = 0.044$, $p = 0.079$ and CC: $r = -0.069$, $p = 0.551$). When assessing the neuropsychological scores, MoCA and MMSE were not significantly correlated with age (MMSE: $r = 0.082$, $p = 0.479$; MoCA: $r = 0.033$, $p = 0.776$), while ACE-R showed a significant positive correlation with age ($r = 0.370$, $p = 0.001$). One-way ANOVA evaluation of age differences between RRs and NRs, using PPPD as the discriminating factor, found no significant difference ($F_{1,75} = 0.006$, $p = 0.939$).

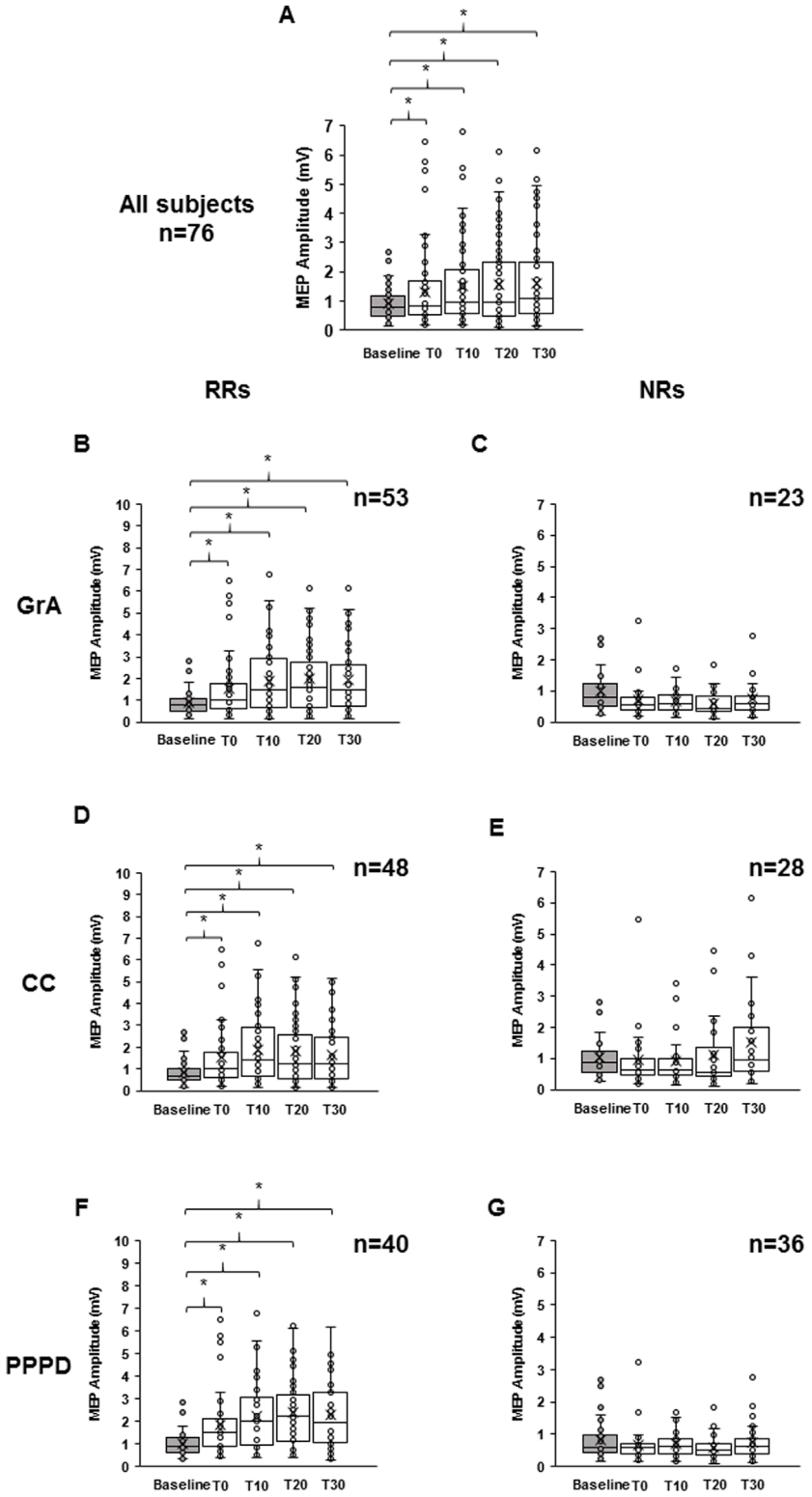

FIGURE 2
Effect of paired associative stimulation (PAS) on motor-evoked potentials (MEPs). The boxplots show MEP raw amplitudes at the different time points assessed: baseline (gray color), immediately after (T0), and after 10 min (T10), 20 min (T20), and 30 min (T30) from PAS delivery, for the all subjects **(A)**, for the responders **(B)**, and for the non-responders **(C)** to the PAS protocol. Responsiveness was determined using the grand average **(B, C)**, curve concavity **(D, E)**, and post-PAS difference **(F, G)**. The continuous line in the boxplots represents the median value, while the ' × ' symbol represents the mean value of the group. Dots represent individual data. *$p < 0.05$.

TABLE 1 Responsivity distribution and mean values of demographic features, baseline MEP, and RMT between RRs and NRs.

Plasticity indexes		CC	GrA	PPPD
Responsiveness (n)	RRs	48	53	40
	NRs	28	23	36
Age	RRs	67.4 ± 6.9	67.2 ± 7.4	67.1 ± 8.0
	NRs	66.5 ± 7.8	66.8 ± 6.7	67.0 ± 6.3
	p (ANOVA)	0.620	0.839	0.939
Sex	RRs	29 F–19 M	30 F–23 M	23 F–17 M
	NRs	12 F–16 M	11 F–12 M	18 F–18 M
	p (X2)	0.138	0.481	0.512
RMT (%MSO)	RRs	44.6 ± 7.7	45.1 ± 8.3	44.4 ± 8.1
	NRs	46.0 ± 9.7	44.6 ± 8.5	45.8 ± 8.9
	p (ANOVA)	0.487	0.727	0.477
Baseline MEP (mV)	RRs	0.9 ± 0.6	0.9 ± 0.5	1.0 ± 0.6
	NRs	1.0 ± 0.6	1.0 ± 0.7	0.8 ± 0.6
	p(ANOVA)	*0.271*	*0.558*	*0.153*

CC, curve concavity; GrA, grand average; PPPD, pre- vs. post-PAS difference; RRs, responders; NRs; non-responders; M, male; F female; RMT, resting motor threshold; %MSO, percentage of the maximum stimulator output; MEP, motor-evoked potential; *p(ANOVA)*, *p* value of the one-way ANOVA; $p(X^2)$, *p* value of the chi-square test; *p < 0.05. Error measurement is represented by ± standard deviation.

TABLE 2 Contingency table for subjects' responsiveness to the PAS protocol when using CC or PPPD as the PAS plasticity index.

	Responsiveness to PAS	GrA	
		RRs	NRs
CC	RRs	42	6
	NRs	10	17
	Sensibility	42/(42 + 10) = 0.81	
	Specificity	17/(17 + 6) = 0.74	
PPPD	RRs	40	0
	NRs	13	23
	Sensibility	40/(40 + 13) = 0.75	
	Specificity	23/(23 + 0) = 1.0	

For both CC and PPPD panels: the top-left value identifies real RRs, the top-right value identifies false RRs, the bottom-left value identifies false NRs, and the bottom-right value identifies real NRs. Sensibility is calculated as [true RRs/(true RRs + false NRs)], while specificity is calculated as [true NRs/(true NRs + false RRs)].
GrA, grand average; RRs, responders; NRs, non-responders; CC, curve concavity; PPPD, pre- vs. post-PAS difference in MEP amplitude over at least two time-points.

3.4 Evaluation of the influence of responsiveness to the PAS protocol on the cognitive status

Table 3 shows the mean values of the MMSE, ACE-R, and MoCA scores for the RR and NR groups based on each PAS-plasticity index. One-way ANOVA showed that MMSE and ACE-R scores were not significantly different between RRs and NRs when considering GrA (MMSE: $F_{1,75} = 0.870$, $p = 0.354$, $\eta^2p = 0.012$; ACE-R: $F_{1,75} = 0.764$, $p = 0.385$, $\eta^2p = 0.010$), CC (MMSE: $F_{1,75} = 1.232$, $p = 0.271$, $\eta^2p = 0.016$; ACE-R: $F_{1,75} = 3.315$, $p = 0.073$; $\eta^2p = 0.043$), and PPPD (MMSE: $F_{1,75} = 0.175$, $p = 0.677$, $\eta^2p = 0.002$; ACE-R: $F_{1,75} = 0.469$, $p = 0.496$, $\eta^2p = 0.006$). A non-significant difference in the MoCA score was found between RRs and NRs for GrA ($F_{1,75} = 0.234$, $p = 0.630$, $\eta^2p = 0.003$) and PPPD ($F_{1,75} = 1.699$, $p = 0.196$, $\eta^2p = 0.022$); conversely, RRs showed a higher MoCA score than NRs when CC was used as the PAS-plasticity index ($F_{1,75} = 7.963$, $p = 0.006$, $\eta^2p = 0.097$) (Figure 3).

Analysis of the subcategories of MoCA and ACE-R showed a significant difference between RRs and NRs for the three PAS indexes (GrA, CC, and PPPD) in the MoCA and ACE-R subcategory of memory, but it was only when CC was used as the discriminative index (MoCA: $F_{1,75} = 4.559$, $p = 0.036$, $\eta^2p = 0.058$; ACE-R: $F_{1,75} = 7.212$, $p = 0.009$, $\eta^2p = 0.089$) (Table 3).

Bayesian analysis confirmed the ANOVA results. In fact, when using GrA and PPPD as the discriminative PAS plasticity indexes, BF always showed moderate evidence to accept the null hypothesis (GrA: MMSE BF = 0.139, MoCA BF = 0.101, ACE-R BF = 0.114; PPPD: MMSE BF = 0.099, MoCA BF = 0.207, ACE-R BF = 0.114); when using CC, it showed moderate evidence for acceptance of the null hypothesis for MMSE (BF = 0.165), anecdotal evidence for acceptance of the null hypothesis for ACE-R (BF = 0.499), but moderate evidence for acceptance of the alternative hypothesis for MoCA (BF = 3.794). The same results have been found for the cognitive subcategories: moderate evidence for acceptance of the null hypothesis when using both GrA and PPPD for all subcategories; meanwhile, when using CC, the memory subcategory of ACE-R showed anecdotal evidence for acceptance of the alternative hypothesis (BF = 2.709), and the memory subcategory of MoCA showed anecdotal evidence for acceptance of the null hypothesis (BF = 0.804); the other subcategories of ACE-R and MoCA showed moderate evidence for acceptance of the null hypothesis.

Table 4 reports demographic, neurophysiological and cognitive values divided by sample and responsiveness to the PAS protocol.

3.5 Assessment of the correlation between PAS plasticity indexes and cognitive status

Normality tests indicated that the variables included in the correlation analysis were not normally distributed: GrA (K–S = 0.167, $p < 0.001$; S–W = 0.840, $p < 0.001$), CC (K–S = 0.191, $p < 0.001$; S–W = 0.861, $p < 0.001$), MMSE (K–S = 0.193, $p < 0.001$; S–W = 0.918, $p < 0.001$), MoCA (K–S = 0.099, $p = 0.063$; S–W = 0.973, $p = 0.104$), and ACE-R (K–S = 0.103, $p = 0.045$; S–W = 0.968, $p = 0.055$). Consequently, Spearman's rank test was applied. Spearman's correlation analysis detected a significant

TABLE 3 Mean values and statistical differences of the Mini-Mental State Examination, Addenbrooke's Cognitive Examination revised, and Montreal Cognitive Assessment between RRs and NRs.

Cognitive score		GrA			CC			PPPD		
Cognitive test	Categories	RRs	NRs	*p*	RRs	NRs	*p*	RRs	NRs	*p*
MMSE		28.9 ± 1.0	29.1 ± 1.1	*0.354*	29.1 ± 1.1	28.8 ± 1.1	*0.271*	28.9 ± 1.0	29.0 ± 1.1	*0.677*
ACE-R	Total score	95.5 ± 4.7	94.5 ± 4.7	*0.385*	95.6 ± 3.8	93.9 ± 5.1	*0.106*	95.5 ± 5.1	94.8 ± 4.2	*0.496*
	Orientation	18.0 ± 0.3	18.0 ± 0.2	*0.783*	18.0 ± 0.2	18.0 ± 0.2	*0.216*	18.0 ± 0.3	18.1 ± 0.2	*0.435*
	Memory	23.7 ± 2.9	22.4 ± 4.1	*0.122*	24.0 ± 2.6	22.0 ± 4.0	*0.009**	23.5 ± 2.9	23.1 ± 3.8	*0.604*
	Verbal fluency	11.7 ± 2.0	11.9 ± 1.7	*0.635*	11.6 ± 2.1	12.0 ± 1.6	*0.353*	11.7 ± 2.0	11.9 ± 1.8	*0.644*
	Language	26.2 ± 1.0	26.3 ± 0.7	*0.745*	26.2 ± 0.9	26.4 ± 0.9	*0.319*	26.2 ± 1.1	26.3 ± 0.7	*0.609*
	Visuo-spatial	15.4 ± 1.3	15.4 ± 1.1	*0.993*	15.5 ± 1.3	15.3 ± 1.2	*0.595*	15.6 ± 1.2	15.3 ± 1.3	*0.300*
MoCA	Total score	26.3 ± 2.5	26.0 ± 2.5	*0.630*	26.8 ± 2.4	25.2 ± 2.3	*0.006**	26.6 ± 2.4	25.8 ± 2.5	*0.196*
	Visuo-spatial	3.6 ± 0.6	3.8 ± 0.4	*0.201*	3.7 ± 0.7	3.6 ± 0.5	*0.615*	3.7 ± 0.7	3.7 ± 0.5	*0.814*
	Executive functions	3.5 ± 0.6	3.4 ± 0.75	*0.608*	3.5 ± 0.6	3.4 ± 0.8	*0.636*	3.5 ± 0.6	3.4 ± 0.7	*0.531*
	Language	5.6 ± 0.6	5.6 ± 0.7	*0.889*	5.7 ± 0.6	5.4 ± 0.8	*0.120*	5.6 ± 0.7	5.5 ± 0.7	*0.649*
	Orientation	6.0 ± 0.27	6.0 ± 0.1	*0.477*	6.0 ± 0.3	6.0 ± 0.1	*0.392*	6.0 ± 0.3	6.0 ± 0.1	*0.328*
	Attention	5.6 ± 0.6	5.6 ± 0.6	*0.764*	5.7 ± 0.6	5.5 ± 0.6	*0.183*	5.7 ± 0.6	5.6 ± 0.6	*0.492*
	Memory	2.6 ± 1.6	2.2 ± 1.7	*0.312*	2.79 ± 1.5	2.0 ± 1.6	*0.036**	2.7 ± 1.5	2.3 ± 1.7	*0.317*

GrA, grand average; CC, curve concavity; PPPD, pre vs. post-PAS difference; RRs, responders; NRs; non-responders; MMSE, Mini-Mental State Examination; MoCA, Montreal Cognitive Assessment; ACE-R, Addenbrooke's Cognitive Examination revised; *p*, p-value of the one-way ANOVA; *$p < 0.05$. Error measurement is represented by ± standard deviation.

negative correlation between MoCA and CC ($r = -0.285$, $p = 0.013$) but not between MoCA and GrA ($r = 0.131$, $p = 0.261$). ACE-R and MMSE were not correlated with either CC (MMSE: $r = -0.040$, $p = 0.732$; ACE-R: $r = -0.134$, $p = 0.251$) or GrA (MMSE: $r = -0.086$, $p = 0.462$; ACE-R: $r = 0.080$, $p = 0.496$) (Figure 4). No significant correlations were detected between the two PAS plasticity indexes (GrA and CC) and the subcategories of MoCA and ACE-R.

4 Discussion

This work analyzed, for the first time, different plasticity indexes that can reflect the PAS-induced LTP phenomena and the cognitive status of aged, healthy subjects. Overall, the results of the present study showed that CC is the PAS plasticity index that is able to better discriminate between RRs and NRs, as demonstrated by its consistency, high ORs, and sensibility in the discrimination of RRs and NRs to the PAS protocol.

In addition, CC was the only PAS plasticity index that was able to describe the cognitive status in a group of aged, healthy subjects, as demonstrated by its significant correlation with the MoCA score, which was, in turn, significantly different between RRs and NRs.

Notably, LTP is a key mechanism of synaptic plasticity, where specifically stimulated synaptic connections are strengthened following high-frequency stimulation and near-synchronous activation of both pre- and post-synaptic neurons (Malenka and Bear, 2004; Kandel et al., 2014). PAS is widely used in humans to study LTP at the cortical level, and it should determine a rapidly evolving (<30 min) and long-lasting (>60 min) increase in cortical excitability, resulting in an increase in MEP amplitude (Stefan et al., 2000; 2002). Due to its features, LTP–PAS effects should be observed as a long-lasting and non-isolated phenomenon (Malenka and Bear, 2004; Kandel et al., 2014), as defined by a curve-shaped trend, determined by a transient initial increment in the cortical excitability, until it returns to baseline levels. According to this point of view, that GrA is the most-used PAS-plasticity index in literature could be the result of an increase of M1 excitability rather than an LTP phenomenon. In fact, GrA is determined by the mean value of the MEP obtained at post-PAS time points (Wolters et al., 2005; Müller-Dahlhaus et al., 2008; Lahr et al., 2016; Minkova et al., 2019), which strongly influence it. For instance, for a substantial increase in MEP amplitude in only one time point, it may strongly influence the final GrA value. In addition, MEP changes at a single time point could reflect a simple change in cortical excitability rather than a plastic effect in M1 (Stefan et al., 2000). The calculation of PPPD and CC considered this point of view. In fact, PPPD discriminates RRs only when at least two out of the four post-PAS MEP amplitudes were significantly higher than baseline MEP values, thus individuating RRs only if the change in MEP amplitude was consistently present in two time

10.3389/fphys.2025.1625137

TABLE 4 Demographic, neurophysiological, and cognitive values of the sample by decade and responsiveness to the PAS protocol.

	Decade	Responsiveness	Numerosity	Sex	RMT	Baseline MEP	MMSE score	MoCA score	ACE-R score
GrA	50–59	RRs	9	6 F–3 M	43.3 ± 7.1	0.9 ± 0.6	28.6 ± 0.8	25.7 ± 1.9	91.9 ± 4.2
		NRs	4	4 M	39.0 ± 2.6	1.2 ± 0.4	28.4 ± 1.6	26.1 ± 2.9	91.2 ± 5.9
	60–69	RRs	24	13 F–11 M	45.5 ± 8.4	0.8 ± 0.4	29.0 ± 1.0	26.8 ± 2.2	95.3 ± 3.5
		NRs	11	3 F–8 M	45.4 ± 7.1	1.0 ± 0.7	29.4 ± 1.0	25.5 ± 2.4	94.3 ± 5.2
	70–79	RRs	17	10 F–7 M	46.0 ± 9.5	0.9 ± 0.6	28.8 ± 1.3	26.2 ± 3.2	96.2 ± 4.5
		NRs	7	4 F–3 M	43.4 ± 8.8	0.9 ± 0.7	29.5 ± 0.6	27.1 ± 2.2	96.2 ± 3.3
	80–89	RRs	3	1 F–2 M	46.0 ± 10.0	1.1 ± 0.4	29.2 ± 1.1	25.5 ± 1.0	103.2 ± 6.7
		NRs	1	M	66.0	0.45	27.1	22.5	94.6
CC	50–59	RRs	9	7 F–2 M	44.0 ± 6.4	0.9 ± 0.6	28.8 ± 0.9	26.6 ± 1.9	93.3 ± 4.5
		NRs	4	3 F–1 M	37.5 ± 3.4	1.2 ± 0.4	28.0 ± 1.2	24.3 ± 1.7	88.8 ± 3.0
	60–69	RRs	21	12 F–9 M	45.9 ± 7.8	0.8 ± 0.6	29.3 ± 0.9	26.9 ± 1.1	95.7 ± 3.2
		NRs	14	4 F–10 M	44.9 ± 8.4	0.8 ± 0.4	28.9 ± 1.1	25.6 ± 2.3	93.9 ± 5.0
	70–79	RRs	16	10 F–6 M	42.2 ± 8.0	0.7 ± 0.4	29.0 ± 1.3	27.2 ± 3.0	96.6 ± 3.8
		NRs	8	4 F–4 M	50.9 ± 9.0	1.3 ± 1.0	29.1 ± 0.8	25.2 ± 2.7	95.4 ± 4.7
	80–89	RRs	2	2 M	51.0 ± 7.0	1.0 ± 0.5	29.2 ± 1.6	25.5 ± 1.4	104.1 ± 9.1
		NRs	2	1 F–1 M	51.0 ± 21.2	0.9 ± 0.6	28.1 ± 1.4	24.0 ± 2.1	98.0 ± 4.9
PPPD	50–59	RRs	7	6 F–1 M	42.6 ± 8.0	1.0 ± 0.7	28.3 ± 0.6	25.5 ± 2.0	90.8 ± 3.7
		NRs	6	4 F–2 M	41.3 ± 4.3	1.0 ± 0.5	28.8 ± 1.4	26.3 ± 2.3	93.2 ± 5.4
	60–69	RRs	20	11 F–9 M	45.4 ± 8.5	0.8 ± 0.4	29.0 ± 1.0	27.0 ± 2.1	95.3 ± 3.8
		NRs	15	5 F–10 M	45.5 ± 7.5	0.9 ± 0.7	29.3 ± 0.9	25.6 ± 2.4	94.6 ± 4.5
	70–79	RRs	10	5 F–5 M	43.1 ± 7.6	1.2 ± 0.7	29.2 ± 1.2	27.0 ± 3.4	96.9 ± 4.9
		NRs	14	9 F–5 M	46.6 ± 10.1	0.7 ± 0.6	29.0 ± 1.1	26.1 ± 2.7	95.7 ± 3.5
	80–89	RRs	3	1 F–2 M	46.0 ± 10.0	1.1 ± 0.4	29.2 ± 1.1	25.5 ± 1.0	103.2 ± 6.7
		NRs	1	M	66.0	0.45	27.1	22.5	94.6

RMT, resting motor threshold; MEP, motor-evoked potential; MMSE, Mini-Mental State Examination; MoCA, Montreal Cognitive Assessment; ACE-R, Addenbrooke's Cognitive Examination revised; GrA, grand average; CC, curve concavity; PPPD, pre vs. post-PAS difference; RRs, responders; NRs; non-responders. Error measurement is represented by ± standard deviation.

points, which is in agreement with the existence of a long-lasting phenomenon. This was also supported by the high specificity shown in the contingency table model (Table 2), where GrA was used as a reference index since it is the most widely used index of PAS plasticity in literature (Wolters et al., 2005; Müller-Dahlhaus et al., 2008; Lahr et al., 2016; Minkova et al., 2019). Along the same line, CC was able to well-describe the LTP–PAS effects. In particular, CC was calculated through the polynomial function of the curve obtained from the MEP amplitudes assessed in all the five time points considered. A negative value (negative concavity) identified RRs, while a positive value (positive concavity) determined NRs. Due to its mathematical characteristics, CC describes the whole phenomenon. Therefore, to produce a negative concavity, the phenomenon should be long-lasting and not dependent on an isolated change in MEP amplitude. This observation was also supported by the high sensibility of CC (Table 2) that, although showing less specificity than PPPD, it had higher sensibility.

Notably, when dealing with the contingency model, sensibility identifies the ability of an index to more accurately discriminate subjects that do not respond to the PAS protocol; meanwhile,

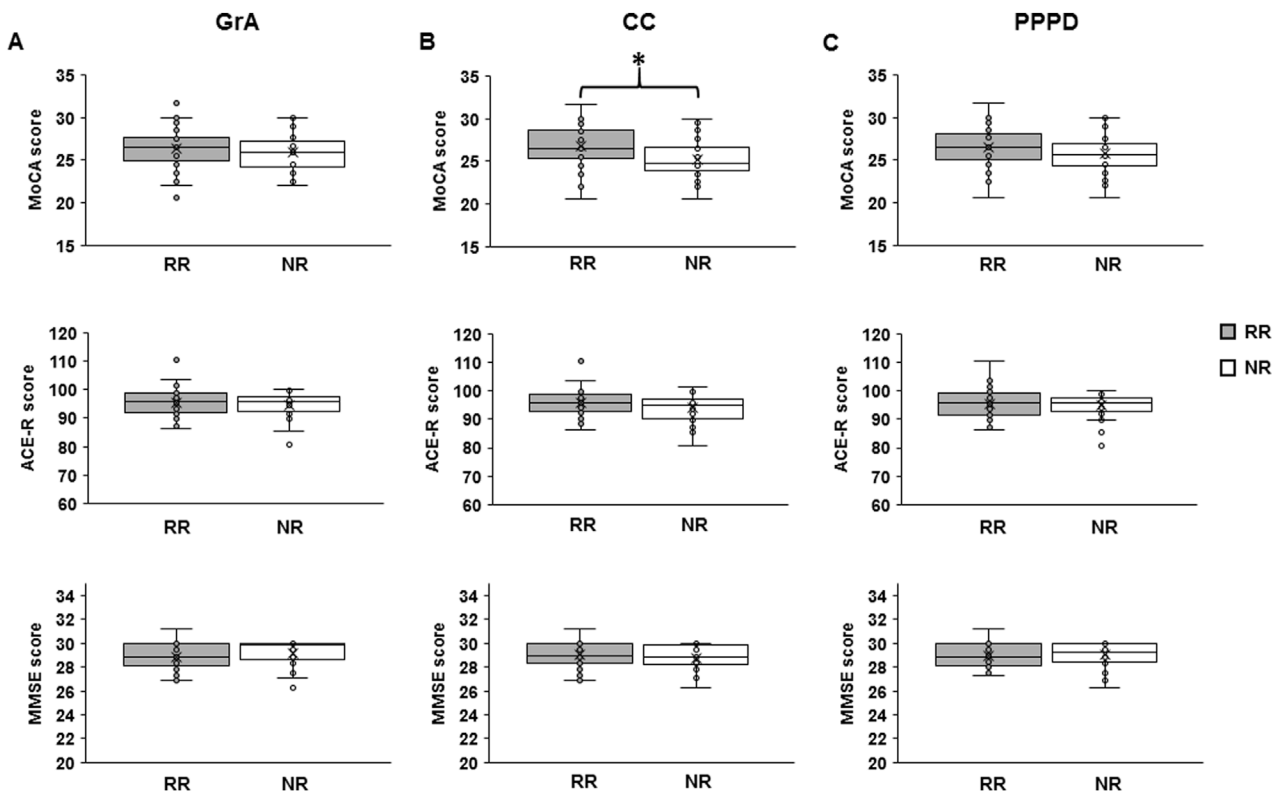

FIGURE 3
Differences in cognitive skills between responders (RRs) and non-responders (NRs) to the PAS protocol. The boxplots show the mean value of the Montreal Cognitive Assessment (MoCA), Addenbrooke's Cognitive Examination revised (ACE-R), and Mini-Mental State Examination (MMSE) scores in RRs and NRs when using grand average (GrA) **(A)**, curve concavity (CC) **(B)**, and pre- vs. post-PAS difference (PPPD) **(C)** as the discrimination indexes for the responsiveness to PAS. The continuous line in the boxplots represents the median value, while the ' × ' symbol represents the mean value of the group. Dots represent individual data. *$p < 0.05$.

specificity describes the index characteristic to better discriminate the RRs to the PAS protocol (Zweig and Campbell, 1993; Kallner, 2018). The analysis showed that the PPPD index has a high specificity since it identifies fewer RRs than CC and GrA (Table 1), determining the increased accuracy in the identification of the RRs in reference to GrA but less accuracy for the identification of NRs, as determined by the reduced OR compared to that of GrA. In contrast, CC demonstrated a higher sensibility than PPPD, with no ORs difference compared to that of GrA, suggesting its good capability in the correct discrimination of the NRs. Therefore, it is likely that the most accurate identification of RRs may be made by PPPD, as determined by the few false RRs in the contingency table (Table 2) and the analysis of robustness, while CC is able to better discriminate the NRs as GrA, as shown by few false NRs (Table 2) and the analysis of robustness. Although both PPPD and CC differently discriminated responsiveness to the PAS protocol and described the LTP phenomenon well, these indexes rely on MEP recordings from at least three time points, which could be time-consuming. Compared to GrA and PPPD, CC appears to be a better index to describe cognitive status, as demonstrated by the correlation with the MoCA score and the difference in MoCA between RRs and NRs.

Overall, the CC and PPPD PAS plasticity indexes can serve as reliable measures of PAS-induced plasticity across different contexts.

Based on the calculation of the ICC and OR, it is likely that CC is consistent in the assessment of PAS effects at least as much as GrA, and it is useful when the investigation is focused on the whole long-lasting plastic phenomenon. In fact, this can help not only to determine whether the PAS effects occurred or not but also its occurrence in a long-lasting post-PAS period. Moreover, in light of the relation found between CC and cognitive scores, this index appears to also be useful in studies that would correlate neurophysiological and cognitive aspects. The curve estimate regression model detected a weak goodness of fit between raw MEPs and the curve underpinning CC. The low R2 can likely be attributed to the intrinsic inter- and intra-subject variability of the MEP amplitude, which reflects fluctuations in cortical excitability during the experiments and, thus, requires several measure repetitions (Rossini et al., 2015).

On the other hand, the high specificity of PPPD makes it perfect for finding RRs with high reliability, even if it results in fewer RRs than with other indexes. This may be useful in studies with large samples, allowing analyses that are only focused on RRs, and for evaluating few post-PAS time points (at least two).

As mentioned before, compared to GrA and PPPD, CC seems to be a better index to describe the cognitive status, as

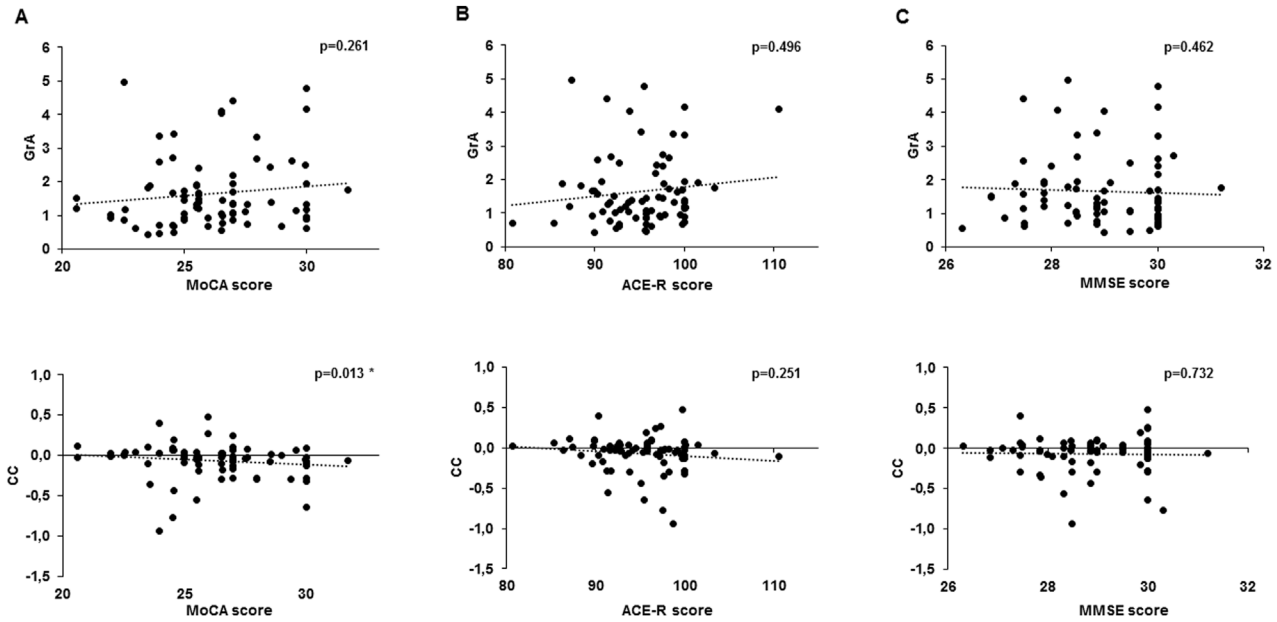

FIGURE 4
Correlation analysis between cognitive test scores and PAS plasticity indexes. The chart shows a correlation between the Montreal Cognitive Assessment (MoCA) **(A)**, Addenbrooke's Cognitive Examination revised (ACE-R) **(B)**, and Mini-Mental State Examination (MMSE) **(C)** with the grand average (GrA) (upper line) and curve concavity (CC) (bottom line). Dotted lines express the trending line of the correlation. $^{*}p < 0.05$.

demonstrated by the correlation with the MoCA score and the difference in MoCA between RRs and NRs. This observation is in contrast with those of previous studies that failed to detect any significant difference in cognitive status between RRs and NRs (Schättin et al., 2018; Minkova et al., 2019). These studies used the GrA, which did not correlate with cognitive status in our study as well. The significant correlation observed between CC and MoCA can be explained by CC characteristics, describing a curve-shaped trend of the long-lasting PAS plasticity effect, differently from the GrA. This finding suggests that CC may represent a useful index to investigate PAS-induced plastic events in humans in relation to cognitive scores, at least in healthy, aged subjects.

It is well known that synaptic plasticity is strongly connected to cognitive status. Previous studies found that cognitive decline is associated with altered connectivity between brain areas and reduced synaptic plasticity (Bassi et al., 2019). Moreover, it has been previously suggested that cognitive reserve may be intimately related to cortical excitability and cortical plasticity (Freitas et al., 2013; Palermo et al., 2025). Cognitive reserve allows cognitive functions to be maintained—or minimally impaired—in the elderly population and can enable individuals to sustain more neuropathological insults before they manifest cognitive decline (Freitas et al., 2013). It has been hypothesized that the gradual change in the relationship between altered cortical excitability and cognitive performance reflects the point at which hyperexcitability becomes compensatory and detrimental to individuals experiencing cognitive impairments, related to an increasing impediment in the allocation of cognitive resources (Palermo et al., 2025). The cognitive reserve serves to prolong functioning and delay the reaching of this critical point, additionally influencing the magnitude of plastic changes. For example, in patients with mild Alzheimer's disease (AD) with the same degree of cognitive decline, highly educated patients (higher cognitive reserve) have less advanced pathological and functional brain changes (Kemppainen et al., 2008), which suggests that the clinical manifestation of advanced AD pathology is delayed in individuals with higher educational attainment. Adaptive (or compensatory) network plasticity might, thus, represent the neurobiological substrate of cognitive reserve, and our results are in line with those of these studies, suggesting CC as a potential plasticity index to possibly assess cognitive reserve both in pathological and healthy aging populations.

In the present study, aged subjects were investigated, which rules out a possible ceiling effect in the results of neuropsychological tests when performed by young people. However, the lack of difference in ACE-R and MMSE scores between RRs and NRs suggests that the difference found when using MoCA to discriminate responsiveness to PAS could be because of the different types of the neuropsychological tests used. Previous findings observed that among the tests that are useful to discriminate the cognitive status between healthy and pathological subjects, MoCA is the most reliable and sensible one (Nasreddine et al., 2005). For this reason, it could be suggested that total ACE-R and MMSE failed to be associated with cortical plasticity and discriminate responsiveness to PAS because of their lower sensitivity than MoCA. Finally, RRs had higher memory skills than NRs, as demonstrated by MoCA and ACE-R subcategory analysis, only when using CC as the discriminative PAS-plasticity index. This result is in line with the literature describing how plasticity phenomena are the mechanisms underlining memory function. In this light, CC may strongly represent a key tool to investigate the relation between cognitive functions and plasticity in humans.

However, it has to be noted that responsiveness to a plasticity protocol could be influenced by several factors such as alertness (Kamke et al., 2012), attentional state (Stefan et al., 2004), stimulation intensity (Müller-Dahlhaus et al., 2008), genetic traits (Cheeran et al., 2008; Missitzi et al., 2011; Peña-Gomez et al., 2012; Fried et al., 2017), cortical thickness (List et al., 2013), and microstructural properties of white matter (Klöppel et al., 2008). Previous studies focusing on genetic factors found that polymorphism of the brain-derived neurotrophic factor gene (BDNF) (Cheeran et al., 2008; Fried et al., 2017) discriminated between RRs and NRs to repetitive TMS. BDNF has a variety of roles in cognition (Velioglu et al., 2021), and it has been shown to modulate NMDAR-dependent LTP in animal models (Figurov et al., 1996). Although a previous study failed to find a relation between BDNF polymorphism and PAS responsiveness (Minkova et al., 2019), future studies may try to relate the frequency of BDNF polymorphism with PAS responsiveness using CC as the PAS plasticity index.

The categorization and comparison of responsiveness to the PAS protocol across studies remain challenging, largely because of the heterogeneity of the protocols and their analysis in the existing literature. Future studies should focus on filling this gap by incorporating multiple post-PAS assessment time points, selecting PAS-induced plasticity indices that are best aligned with the specific study objectives, and increasing the sample size. These methodological features would help to minimize the influence of NRs on the overall findings, thereby allowing a more targeted investigation of RRs and potentially providing insights into PAS responsiveness in the context of cognitive decline.

4.1 Limitation of the study

We acknowledge that this study has some limitations. First, the study is not sham-controlled due to the absence of a true PAS-sham protocol available in the literature. However, future studies should reach a consensus on standardized protocols to more effectively assess PAS effects.

Additionally, a real gold standard for synaptic plasticity assessment is not available for comparison and to calculate the specificity and sensibility of the new PAS indexes. In fact, the comparison in terms of sensibility and selectivity between CC and PPPD as PAS plasticity indexes is referenced to GrA (the most used in literature), which does not represent a real observation of plastic changes in the brain. Without an external or clinical benchmark, the current results largely reflect the internal consistency between metrics.

In the present study, PAS effects have been investigated until 30 min after paired stimuli delivery. However, because of the high inter- and intra-subject variability, it is possible that some subjects may respond to the protocol after this time window. Hence, it appears to be worthwhile for future studies to investigate responsiveness to PAS after 30 min in subjects who do not respond in the first 30 min. Finally, future studies should investigate how some genetic and anatomical features of the subjects may influence responsiveness to the PAS protocol and the magnitude of the PAS-effect.

5 Conclusion

In conclusion, CC may represent a potential PAS-plasticity index that is useful for describing cortical plasticity and cognitive skills in humans, with a possible practical application in patients with cognitive impairment, namely, Alzheimer's disease.

Data availability statement

The data that support the findings of this study are made available from the corresponding author, upon reasonable request.

Ethics statement

The studies involving humans were approved by Sardinia Ethics Committee Prot. number PG/2023/5172, 06/04/2023. The studies were conducted in accordance with the local legislation and institutional requirements. The participants provided their written informed consent to participate in this study.

Author contributions

NL: Conceptualization, Writing – original draft, Writing – review and editing, Data curation, Formal Analysis, Investigation, Methodology, Visualization. FG: Conceptualization, Data curation, Formal Analysis, Investigation, Methodology, Visualization, Writing – original draft, Writing – review and editing, Validation. MZ: Data curation, Investigation, Visualization, Writing – original draft, Writing – review and editing. LV: Investigation, Visualization, Writing – review and editing. AC: Investigation, Visualization, Writing – review and editing, Project administration, Resources. CO: Investigation, Visualization, Writing – review and editing, Data curation. PO: Data curation, Investigation, Visualization, Writing – review and editing. MP: Data curation, Investigation, Visualization, Writing – review and editing, Methodology, Supervision. FD: Supervision, Writing – review and editing, Conceptualization, Funding acquisition, Project administration, Resources, Writing – original draft.

Funding

The author(s) declare that financial support was received for the research and/or publication of this article. This work was funded by Unione Europea, Next Generation EU, PNRR M6C2, Investimento 2.1 Valorizzazione e potenziamento della ricerca biomedica del SSN, PNRR-MAD-2022-12376667, CUP H83C22000720006.

Conflict of interest

The authors declare that the research was conducted in the absence of any commercial or financial relationships that could be construed as a potential conflict of interest.

Correction note

This article has been corrected with minor changes. These changes do not impact the scientific content of the article.

Generative AI statement

The author(s) declare that no Generative AI was used in the creation of this manuscript.

Any alternative text (alt text) provided alongside figures in this article has been generated by Frontiers with the support of artificial intelligence and reasonable efforts have been made to ensure accuracy, including review by the authors wherever possible. If you identify any issues, please contact us.

Publisher's note

References

Bassi, M. S., Iezzi, E., Gilio, L., Centonze, D., and Buttari, F. (2019). Synaptic plasticity shapes brain connectivity: implications for network topology. *Int. J. Mol. Sci.* 20 (24), 6193. doi:10.3390/ijms20246193

Battaglia, F., Wang, H. Y., Ghilardi, M. F., Gashi, E., Quartarone, A., Friedman, E., et al. (2007). Cortical plasticity in alzheimer's disease in humans and rodents. *Biol. Psychiatry* 62 (12), 1405–1412. doi:10.1016/j.biopsych.2007.02.027

Babyak, M. A. (2004). Whatyou may not be what you get: a brief, nontechnical introduction to overfitting in regression-type-models. *Psychosom. Med.* 66 (3), 411–421. doi:10.1097/01.psy.0000127692.23278.a9

Bhandari, A., Lissemore, J. I., Rajji, T. K., Mulsant, B. H., Cash, R. F. H., Noda, Y., et al. (2018). Assessment of neuroplasticity in late-life depression with transcranial magnetic stimulation. *J. Psychiatric Res.* 105 (1), 63–70. doi:10.1016/j.jpsychires.2018.08.022

Carson, R. G., and Kennedy, N. C. (2013). Modulation of human corticospinal excitability by paired associative stimulation. *Front. Hum. Neurosci.* 7 (DEC), 823–828. doi:10.3389/fnhum.2013.00823

Cheeran, B., Talelli, P., Mori, F., Koch, G., Suppa, A., Edwards, M., et al. (2008). A common polymorphism in the brain-derived neurotrophic factor gene (BDNF) modulates human cortical plasticity and the response to rTMS. *J. Physiology* 586 (23), 5717–5725. doi:10.1113/jphysiol.2008.159905

Cirillo, J., Lavender, A. P., Ridding, M. C., and Semmler, J. G. (2009). Motor cortex plasticity induced by paired associative stimulation is enhanced in physically active individuals. *J. Physiology* 587 (24), 5831–5842. doi:10.1113/jphysiol.2009.181834

Citri, A., and Malenka, R. C. (2008). Synaptic plasticity: multiple forms, functions, and mechanisms. *Neuropsychopharmacology* 33 (1), 18–41. doi:10.1038/sj.npp.1301559

Di Lorenzo, F., Motta, C., Casula, E. P., Bonnì, S., Assogna, M., Caltagirone, C., et al. (2020). LTP-Like cortical plasticity predicts conversion to dementia in patients with memory impairment. *Brain Stimul.* 13 (5), 1175–1182. doi:10.1016/j.brs.2020.05.013

Fathi, D., Ueki, Y., Mima, T., Koganemaru, S., Nagamine, T., Tawfik, A., et al. (2010). Effects of aging on the human motor cortical plasticity studied by paired associative stimulation. *Clin. Neurophysiol.* 121 (1), 90–93. doi:10.1016/j.clinph.2009.07.048

Figurov, A., Pozzo-Miller, L. D., Olafsson, P., Wang, T., and Lu, B. (1996). Regulation of synaptic responses to high-frequency stimulation and LTP by neurotrophins in the hippocampus. *Nature* 381 (6584), 706–709. doi:10.1038/381706a0

Folstein, M. F., Folstein, S. E., and McHugh, P. R. (1975). Mini-mental state. A practical method for grading the cognitive state of patients for the clinician. *J. Psychiatric Res.* 12 (3), 189–198. doi:10.1016/0022-3956(75)90026-6

Freitas, C., Farzan, F., and Pascual-Leone, A. (2013). Assessing brain plasticity across the lifespan with transcranial magnetic stimulation: why, how, and what is the ultimate goal? *Front. Neurosci.* 7 (7 APR), 42–17. doi:10.3389/fnins.2013.00042

Fried, P. J., Jannati, A., Davila-Pérez, P., and Pascual-Leone, A. (2017). Reproducibility of single-pulse, paired-pulse, and intermittent theta-burst TMS measures in healthy aging, Type-2 diabetes, and Alzheimer's disease. *Front. Aging Neurosci.* 9 (AUG), 263–13. doi:10.3389/fnagi.2017.00263

Ginatempo, F., Loi, N., Manca, A., Rothwell, J. C., and Deriu, F. (2022). Is it possible to compare inhibitory and excitatory intracortical circuits in face and hand primary motor cortex? *J. Physiology* 600 (15), 3567–3583. doi:10.1113/JP283137

Kallner, A. (2018). 'Bayes' theorem, the ROC diagram and reference values: definition and use in clinical diagnosis. *Biochem. Medica* 28 (1), 010101–010110. doi:10.11613/BM.2018.010101

Kamke, M. R., Hall, M. G., Lye, H. F., Sale, M. V., Fenlon, L. R., Carroll, T. J., et al. (2012). Visual attentional load influences plasticity in the human motor cortex. *J. Neurosci.* 32 (20), 7001–7008. doi:10.1523/JNEUROSCI.1028-12.2012

Kandel, E. R., Dudai, Y., and Mayford, M. R. (2014). The molecular and systems biology of memory. *Cell* 157 (1), 163–186. doi:10.1016/j.cell.2014.03.001

Karabanov, A., Thielscher, A., and Siebner, H. R. (2016). Transcranial brain stimulation: closing the loop between brain and stimulation. *Curr. Opin. Neurology* 29 (4), 397–404. doi:10.1097/WCO.0000000000000342

Kemppainen, N. M., Aalto, S., Karrasch, M., Någren, K., Savisto, N., Oikonen, V., et al. (2008). Cognitive reserve hypothesis: pittsburgh compound B and fluorodeoxyglucose positron emission tomography in relation to education in mild Alzheimer's disease. *Ann. Neurology* 63 (1), 112–118. doi:10.1002/ana.21212

Klöppel, S., Bäumer, T., Kroeger, J., Koch, M. A., Büchel, C., Münchau, A., et al. (2008). The cortical motor threshold reflects microstructural properties of cerebral white matter. *NeuroImage* 40 (4), 1782–1791. doi:10.1016/j.neuroimage.2008.01.019

Lahr, J., Peter, J., Minkova, L., Lauer, E., Reis, J., Heimbach, B., et al. (2016). No difference in paired associative stimulation induced cortical neuroplasticity between patients with mild cognitive impairment and elderly controls. *Clin. Neurophysiol.* 127 (2), 1254–1260. doi:10.1016/j.clinph.2015.08.010

Lee, M. D., and Wagenmakers, E. J. (2014). *Bayesian cognitive modelling: a practical course*. Cambridge, England: Cambridge University Press.

List, J., Kübke, J. C., Lindenberg, R., Külzow, N., Kerti, L., Witte, V., et al. (2013). Relationship between excitability, plasticity and thickness of the motor cortex in older adults. *NeuroImage* 83, 809–816. doi:10.1016/j.neuroimage.2013.07.033

Malenka, R. C., and Bear, M. F. (2004). LTP and LTD: an embarrassment of riches. *Neuron* 44 (1), 5–21. doi:10.1016/j.neuron.2004.09.012

Meder, A., Liepelt-Scarfone, I., Sulzer, P., Berg, D., Laske, C., Preische, O., et al. (2021). Motor cortical excitability and paired-associative stimulation-induced plasticity in amnestic mild cognitive impairment and Alzheimer's disease. *Clin. Neurophysiol.* 132 (9), 2264–2273. doi:10.1016/j.clinph.2021.01.011

Minkova, L., Peter, J., Abdulkadir, A., Schumacher, L. V., Kaller, C. P., Nissen, C., et al. (2019). Determinants of inter-individual variability in corticomotor excitability induced by paired associative stimulation. *Front. Neurosci.* 13 (JUL), 841–14. doi:10.3389/fnins.2019.00841

Mioshi, E., Dawson, K., Mitchell, J., Arnold, R., and Hodges, J. R. (2006). 'The Addenbrooke ' s cognitive examination revised (ACE-R): a brief cognitive test battery for dementia screening. *Int. J. Geriatr. Psychiatry* 21 (December 2005), 1078–1085. doi:10.1002/gps.1610

Missitzi, J., Gentner, R., Geladas, N., Politis, P., Karandreas, N., Classen, J., et al. (2011). Plasticity in human motor cortex is in part genetically determined. *J. Physiology* 589 (2), 297–306. doi:10.1113/jphysiol.2010.200600

Müller-Dahlhaus, J. F. M., Orekhov, Y., Liu, Y., and Ziemann, U. (2008). Interindividual variability and age-dependency of motor cortical plasticity induced by paired associative stimulation. *Exp. Brain Res.* 187 (3), 467–475. doi:10.1007/s00221-008-1319-7

Murman, D. L. (2015). The impact of age on cognition. *Seminars Hear.* 36 (3), 111–121. doi:10.1055/s-0035-1555115

Nasreddine, Z. S., Phillips, N. A., Bédirian, V., Charbonneau, S., Whitehead, V., Collin, I., et al. (2005). The Montreal cognitive assessment, MoCA: a brief screening tool for mild cognitive impairment. *Brief. Methodol. Rep.* 53 (4), 695–699. doi:10.1111/j.1532-5415.2005.53221.x

Palermo, S., Di Fazio, C., Scaliti, E., Stanziano, M., Nigri, A., and Tamietto, M. (2025). Cortical excitability and the aging brain: toward a biomarker of cognitive resilience. *Front. Psychol.* 16 (February), 1542880–1542888. doi:10.3389/fpsyg.2025.1542880

Peña-Gomez, C., Solé-Padullés, C., Clemente, I. C., Junqué, C., Bargalló, N., Bosch, B., et al. (2012). APOE status modulates the changes in network connectivity induced by brain stimulation in non-demented elders. *PLoS ONE* 7 (12), e51833. doi:10.1371/journal.pone.0051833

Ridding, M., and Taylor, J. (2001). Mechanisms of motor-evoked potential facilitation following prolonged dual peripheral and central stimulation in humans. *J. Physiology* 537 (2), 623–631. doi:10.1111/j.1469-7793.2001.00623.x

Rossi, S., Antal, A., Bestmann, S., Bikson, M., Brewer, C., Brockmöller, J., et al. (2021). Safety and recommendations for TMS use in healthy subjects and patient populations, with updates on training, ethical and regulatory issues: expert guidelines. *Clin. Neurophysiol.* 132 (1), 269–306. doi:10.1016/j.clinph.2020.10.003

Rossini, P. M., Burke, D., Chen, R., Cohen, L. G., Daskalakis, Z., Di Iorio, R., et al. (2015). Non-invasive electrical and magnetic stimulation of the brain, spinal cord, roots and peripheral nerves: basic principles and procedures for routine clinical and research application: an updated report from an I.F.C.N. committee. *Clin. Neurophysiol.* 126 (6), 1071–1107. doi:10.1016/j.clinph.2015.02.001

Sale, M. V., Ridding, M. C., and Nordstrom, M. A. (2007). Factors influencing the magnitude and reproducibility of corticomotor excitability changes induced by paired associative stimulation. *Exp. Brain Res.* 181 (4), 615–626. doi:10.1007/s00221-007-0960-x

Schättin, A., Gennaro, F., Egloff, M., Vogt, S., and de Bruin, E. D. (2018). Physical activity, nutrition, cognition, neurophysiology, and short-time synaptic plasticity in healthy older adults: a cross-sectional study. *Front. Aging Neurosci.* 10 (August), 242–15. doi:10.3389/fnagi.2018.00242

Singh, A. M., Neva, J. L., and Staines, W. R. (2014). Acute exercise enhances the response to paired associative stimulation-induced plasticity in the primary motor cortex. *Exp. Brain Res.* 232 (11), 3675–3685. doi:10.1007/s00221-014-4049-z

Stefan, K., Kunesch, E., Cohen, L. G., Benecke, R., and Classen, J. (2000). Induction of plasticity in the human motor cortex by paired associative stimulation. *Brain* 123 (3), 572–584. doi:10.1093/brain/123.3.572

Stefan, K., Kunesch, E., Benecke, R., Cohen, L. G., and Classen, J. (2002). Mechanisms of enhancement of human motor cortex excitability induced by interventional paired associative stimulation. *J. Physiology* 543 (2), 699–708. doi:10.1113/jphysiol.2002.023317

Stefan, K., Wycislo, M., and Classen, J. (2004). Modulation of associative human motor cortical plasticity by attention. *J. Neurophysiology* 92 (1), 66–72. doi:10.1152/jn.00383.2003

Tecchio, F., Zappasodi, F., Pasqualetti, P., Gennaro, L. D., Pellicciari, M. C., Ercolani, M., et al. (2008). Age dependence of primary motor cortex plasticity induced by paired associative stimulation. *Clin. Neurophysiol.* 119 (3), 675–682. doi:10.1016/j.clinph.2007.10.023

Terranova, C., Carmen, T., SantAngelo, A., Antonino, S., Morgante, F., Francesca, M., et al. (2013). Impairment of sensory-motor plasticity in mild Alzheimer's disease. *Brain Stimul.* 6 (1), 62–66. doi:10.1016/j.brs.2012.01.010

Velioglu, H. A., Hanoglu, L., Bayraktaroglu, Z., Toprak, G., Guler, E. M., Bektay, M. Y., et al. (2021). Left lateral parietal rTMS improves cognition and modulates resting brain connectivity in patients with Alzheimer's disease: possible role of BDNF and oxidative stress. *Neurobiol. Learn. Mem.* 180 (February), 107410. doi:10.1016/j.nlm.2021.107410

Wessel, M. J., Zimerman, M., and Hummel, F. C. (2015). Non-invasive brain stimulation: an interventional tool for enhancing behavioral training after stroke. *Front. Hum. Neurosci.* 9 (MAY), 265. doi:10.3389/fnhum.2015.00265

Wischnewski, M., and Schutter, D. J. L. G. (2016). Efficacy and time course of paired associative stimulation in cortical plasticity: implications for neuropsychiatry. *Clin. Neurophysiol.* 127 (1), 732–739. doi:10.1016/j.clinph.2015.04.072

Wolters, A., Sandbrink, F., Schlottmann, A., Kunesch, E., Stefan, K., Cohen, L. G., et al. (2003). A temporally asymmetric Hebbian rule governing plasticity in the human motor cortex. *J. Neurophysiology* 89 (5), 2339–2345. doi:10.1152/jn.00900.2002

Wolters, A., Schmidt, A., Schramm, A., Zeller, D., Naumann, M., Kunesch, E., et al. (2005). Timing-dependent plasticity in human primary somatosensory cortex. *J. Physiology* 565 (3), 1039–1052. doi:10.1113/jphysiol.2005.084954

Ziemann, U., Ilić, T. V., Iliać, T. V., Pauli, C., Meintzschel, F., and Ruge, D. (2004). Learning modifies subsequent induction of long-term potentiation-like and long-term depression-like plasticity in human motor cortex. *J. Neurosci.* 24 (7), 1666–1672. doi:10.1523/JNEUROSCI.5016-03.2004

Zweig, M. H., and Campbell, G. (1993). Receiver-operating characteristic (ROC) plots: a fundamental evaluation tool in clinical medicine. *Clin. Chem.* 39 (4), 561–577. doi:10.1093/clinchem/39.4.561

frontiers | Frontiers in Physiology

TYPE Review
PUBLISHED 01 October 2025
DOI 10.3389/fphys.2025.1675598

OPEN ACCESS

EDITED BY
Myriam Catalano,
Sapienza University of Rome, Italy

REVIEWED BY
Luana Fioriti,
Mario Negri Institute for Pharmacological Research (IRCCS), Italy
Leigh Plant,
Northeastern University, United States

*CORRESPONDENCE
Claudio Grassi,
claudio.grassi@unicatt.it

RECEIVED 29 July 2025
ACCEPTED 19 September 2025
PUBLISHED 01 October 2025

CITATION
Bertozzi A, Toscanelli W, Castellitto G, Grassi C and Colussi C (2025) SUMOylation balance: a key determinant in synapse physiology. *Front. Physiol.* 16:1675598. doi: 10.3389/fphys.2025.1675598

SUMOylation balance: a key determinant in synapse physiology

Alessia Bertozzi[1], Walter Toscanelli[1], Giuditta Castellitto[2], Claudio Grassi[1,3]* and Claudia Colussi[2]

[1]Department of Neuroscience, Università Cattolica del Sacro Cuore, Rome, Italy, [2]Istituto di Analisi dei Sistemi ed Informatica "Antonio Ruberti", National Research Council, Rome, Italy, [3]Fondazione Policlinico Universitario Agostino Gemelli IRCCS, Rome, Italy

Neuronal communication relies on the precise regulation of synaptic compartments, where protein activity, localization, and turnover are tightly controlled. Among the mechanisms ensuring this regulation, post-translational modifications (PTMs) play a central role. SUMOylation, the covalent attachment of Small Ubiquitin-like Modifier (SUMO) proteins to target substrates, has emerged as a dynamic key PTM in the nervous system, modulating synaptic structure and function. Target SUMOylation occurs through an enzymatic cascade and requires the presence of a consensus sequence. Reversible addition of SUMO monomers or chains may contribute to distinct functional outcomes changing the conformation of the protein thus favoring/inhibiting molecular interaction among proteins or stabilizing the protein inhibiting degradation or influencing subcellular localization. All these SUMO dependent effects are crucial in the regulation of the tiny and highly specialized synaptic compartments to achieve spatiotemporal control for proper neurotransmission and synaptic plasticity in response to environmental stimuli. Dysregulation of this system has been implicated in various neurological disorders, including Alzheimer's disease, where imbalances in SUMO1 versus SUMO2/3 levels contribute to synaptic dysfunction. As such, comprehension of SUMO related mechanisms may give important insights into both physiological regulation of synapses and potential therapeutic approaches for neurodegenerative diseases. Thus, in this review we will first introduce the enzymatic cascade of SUMOylation and its impact on protein function, then we will focus on its role within the synaptic compartment. Finally, we will discuss the therapeutic potential of modulating SUMOylation in Alzheimer's disease as example of neurodegenerative disorders.

KEYWORDS

SUMOylation, synapse, Alzheimer's disease, post-translational modifications, neuron

Introduction

The ability of neurons to transmit electrical impulse is based on their specialized structure that derives from a highly cellular polarization associated with the asymmetric distribution of proteins, RNA and organelles. Specifically, at the level of synapses, the functional units where an electrical signal is converted into biochemical changes, fine tuning of processes is achieved by multiple mechanisms based on proper temporal and spatial activation of the key players. Indeed, synapses are tiny but very complex

compartments that modulate neurotransmission by altering their shape, size, and protein/RNA content. At the level of pre-synaptic zone, neurotransmitter release is based on the formation of different synaptic vesicle (SVs) pools grouped on the basis of their availability for exocytosis: (i) the readily releasable pool (RRP), comprising about 1% of SVs, which rapidly fuses with the plasma membrane in response to an action potential; (ii) a recycling pool, accounting for 10%–20% of SVs, which participates in neurotransmission during moderate physiological stimulation and replenishes the RRP; and (iii) a large reserve pool (RP), making up 80%–90% of SVs, thought to serve as a storage compartment located away from the active zone. The dynamic interchange among these different pools is orchestrated by synapsins, a family of phosphoproteins that regulate the tethering and release of SVs from the actin cytoskeleton (Longhena et al., 2021). On the postsynaptic zone, the clustering of receptors and channels is facilitated by post synaptic density proteins, including PSD95, along with several enzymes involved in actin polymerization. These elements contribute to changes in spine morphology and modulate the postsynaptic response to stimuli (Hlushchenko et al., 2016).

Despite the limited space within synaptic structures, their fine regulation is ensured by both local protein synthesis and axonal transport (anterograde and retrograde) of various synaptic precursors, since the primary biosynthetic machinery resides in the soma and dendritic compartments, often located far from the synapse (Rizalar et al., 2021). In addition to the modulation of the transport of proteins and RNA necessary for these zones, regulation is based on the control of protein activity, protein-protein interaction and balance between protein stability and degradation, mainly achieved by post-translational modifications (PTMs). Among these, the Small ubiquitin-like modifier (SUMO) conjugation (SUMOylation) is emerging as dynamic PTM involved in the regulation of synaptic proteins thus contributing to the modulation of synapse structure and function as well as to synaptic transmission and plasticity. In this context, we will explore the physiological impact of SUMOylation and how its dysregulation plays a central role in Alzheimer's disease, serving as a representative example of neurodegenerative disorders.

SUMOylation enzymatic pathway

Proteins undergoing SUMOylation are modified by the covalent attachment of the SUMO peptides, which are small proteins ranging from 10 to 20 kDa. To date five paralogs have been identified: SUMO1, SUMO2, SUMO3, SUMO4, and SUMO5 with only SUMO1-3 being expressed in the brain. SUMO2 and 3 have 95% of homology and are often collectively referred to as SUMO2/3. In contrast, they share only about 45% homology with SUMO1, indicating functional divergence. While SUMO 4 and 5 are less characterized and their implication in pathophysiological processes is still under investigation, SUMO1-3 are well-established as key regulators of neuronal function (Matsuzaki et al., 2015; Datwyler et al., 2011).

Indeed, regulation of SUMOylation balance (SUMO1 versus SUMO2/3) or levels (SUMOylation versus deSUMOylation) is a crucial determinant of neuronal development and differentiation (Pronot et al., 2021; Bernstock et al., 2019; Du et al., 2020) plasticity (Du et al., 2020) and synaptic transmission (Martin et al., 2007). This balance is maintained through the interplay between the SUMOylation cascade and the deSUMOylating enzymes, which include three main families of serine proteases (SENP, sentrin-specific protease; deSUMOylating isopeptidase; USPL1, ubiquitin-specific peptidase-like protein 1) that remove SUMO peptides from target proteins.

During the SUMOylation enzymatic cascade (Figure 1), SUMO proteins are covalently attached to the target substrates via a sequential reaction that involves: maturation of the SUMO protein that consists in the cleavage of the C-terminus, operated by SUMO-specific proteases, that expose the Gly-Gly motif (SUMO-GG), necessary for SUMO ligation (Johnson et al., 1997); activation of the mature SUMO achieved through the binding of the SUMO-GG to the E1 enzyme (SAE1/SAE2) in an ATP-dependent manner; transfer of the activated complex to the active cysteine site of Ubc9 that facilitates SUMO attachment to the target with the assistance of the E3 ligase enzyme. While Ubc9 is the only E2 enzyme identified so far, a growing number of E3 ligases have been characterized. They can be grouped on the basis of structure and activity domains:

1. The SP-RING domain family that comprises PIAS proteins (PIAS1-4) whose ligation activity is dependent on the presence of the E2 enzyme (Jackson, 2001); Beyond SUMOylation, PIAS proteins are also involved in other cellular processes such as transcriptional regulation, DNA repair, and nuclear-cytoplasmic transport (Rytinki et al., 2009; Galanty et al., 2009; Sachdev et al., 2001; Kagey et al., 2003; Pichler et al., 2002).
2. The TRIM (Tripartite Motif) superfamily includes proteins characterized by the presence of a tripartite motif responsible for E3 ligase activity. These proteins also present additional domains such as B-box and coiled-coil domains important for self-aggregation and additional functions in immunity (Ozato et al., 2008).
3. The SIM-Containing SUMO E3 Ligases, lack both RING and TRIM motifs and mediate SUMOylation through a SUMO-interacting motif (SIM). SIM is a short sequence of hydrophobic residues flanked by serine or acidic residues typically located at either the N- or C-terminus. This motif allows non-covalent interactions between SUMOylated proteins and their binding partners. Nucleoporin RanBP2 (Pichler et al., 2002), a component of the nuclear pore, and Pc2, a component of polycomb group (PcG), both belong to this category (Merrill et al., 2010; Reverter and Lima, 2005). Interestingly, within the nuclear pore complex, the nucleoporin 153 has been reported to anchor the deSUMOylating enzymes SENP1 and 2 (Chow et al., 2012) thereby contributing to balance the RanBP2-dependent SUMOylation of nuclear transcription and epigenetic factors as well as proteins destined for export to the cytoplasm.
4. Non canonical E3 ligase activity has also been identified in several proteins that lack the RING or TRIM domains and do not possess a SIM module. In these cases, the specific region for SUMOylation activity has yet to be fully characterized. Among these proteins, the histone deacetylase 4 (HDAC4) and 7 (HDAC7) have been identified as SUMO E3 ligases. HDAC7 has been shown to promote the SUMOylation of Promyelocytic leukemia protein (PML)

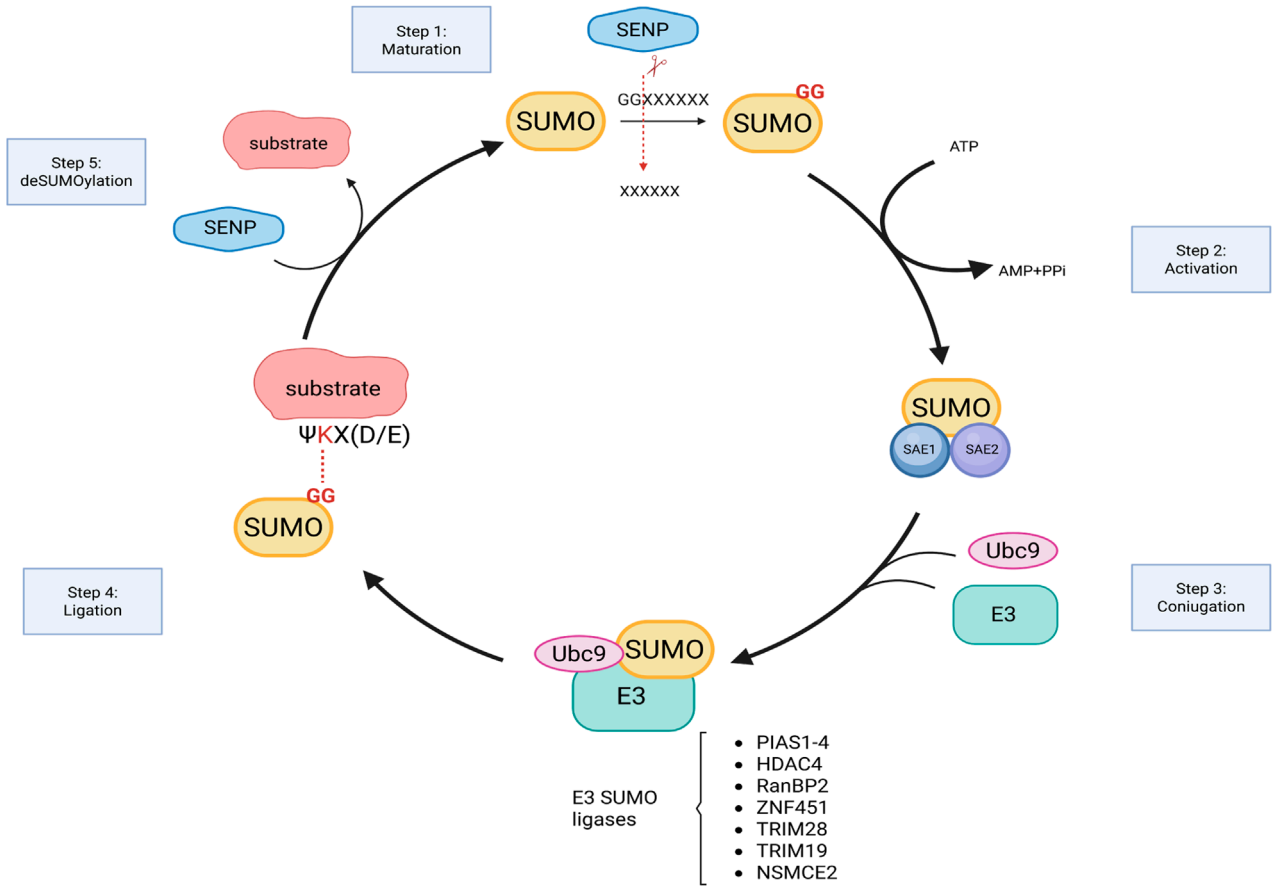

FIGURE 1
Graphical representation of SUMOylation enzymatic cascade. SUMO, synthesized as precursor, is cleaved by SENPs to expose diglycine (GG) motif of SUMO at the C-terminus. Mature SUMO, bound to E1 activating enzymes, is then ready to be conjugated to the target by the sequential action of Ubc9 and E3 ligase enzymes (examples are listed). SUMO attachment is reversible and is catalyzed by SENPs. Figure created with Biorender.

thereby facilitating the formation of PML nuclear bodies (Gao et al., 2008). HDAC4, on the other hand, has a broader range of identified SUMOylation targets. For instance, it inhibits NF-kb interacting with Ubc9 and by increasing the SUMOylation of the inhibitory subunit IkBa (Yang et al., 2020); suppresses androgen receptor by its SUMOylation (Yang et al., 2011); stabilizes SIRT1 and delays senescence (Han et al., 2016); inhibits MEF activation through SUMOylation (Zhao et al., 2005). More recently, HDAC4 has been identified as E3 ligase regulating SUMO2/3 levels in the synaptic compartment (Colussi et al., 2023).

Importantly, for both HDAC7 and HDAC4, the SUMO ligase activity is independent from their deacetylase activity, although the precise domains responsible for SUMOylation remain to be defined.

Pharmacological modulation of SUMOylation

Given the central role of SUMOylation in physiology and its deregulation in several neurodegenerative diseases, numerous inhibitors and activators have been developed with the aim of promoting neuroprotection. In pathological contexts, depending on the substrate and the type of SUMO added (SUMO1 versus SUMO2/3), SUMO conjugation can be either beneficial or detrimental. A wide range of small molecules with inhibitory activity against the E1 and E2 SUMOylation enzymes have been identified; however, no inhibitors targeting SUMO-E3 ligases have been discovered to date. The compounds identified include natural products, peptidomimetics, and synthetic derivatives obtained through virtual screening (for an extensive review see ref. (Brackett and Blagg, 2021).

For example, among the inhibitors of the E1 enzyme are both natural products (e.g., ginkgolic acid, anacardic acid, tannic acid) and synthetic compounds (e.g., phenyl urea, pyrazole urea, and thiazole urea) that block the formation of the E1–SUMO complex (Fukuda et al., 2009; Kumar et al., 2013). Other molecules, instead, induce conformational changes that prevent the binding of E1 with ATP and SUMO (Lv et al., 2018).

The second step of the SUMOylation cascade is carried out by Ubc9, the only known E2 enzyme. Natural inhibitors of this enzyme include spectomycin B1, chaetochromin A, and viomellein (Hirohama et al., 2013). The flavone 2-D08 also targets Ubc9 by

inhibiting the transfer of SUMO from Ubc9 to the substrate (Kim et al., 2013). Synthetic derivatives of the SUMO consensus region have also been used to develop peptides capable of competing with SUMO1 for Ubc9 binding.

So far, relatively few studies have focused on the development of SUMO activators compared to SUMO inhibitors. One of the first molecules identified as a SUMO activator is a negative regulator of miR-182 and miR-183, whose inhibition leads to a global increase in both SUMO1 and SUMO2/3 levels (Bernstock et al., 2016). This molecule also demonstrated neuroprotective effects *in vitro*.

N106 is another small molecule identified through screening, which selectively enhances SUMO1-ylation of the cardiac sarcoplasmic reticulum calcium ATPase (SERCA2a). Treatment with N106 was shown to restore cardiac function in a mouse model of heart failure (Kho et al., 2015). Notably, the authors did not observe a significant increase in overall SUMO1-ylation following N106 treatment, with only limited additional targets affected in cardiomyocytes. Nevertheless, since the mechanism of action of this molecule involves activation of the E1 enzyme, it is possible that other targets may be identified in different organs, such as the brain, which could be exploited to modulate neuronal function.

In a subsequent study, using a high-throughput homogeneous time-resolved fluorescence (HTRF) assay, several SUMO activators were identified, belonging to three chemical classes: quinolines, benzothiazoles, and aminothiazoles (Krajnak and Dahl, 2018). The degree of SUMO activation varied among these classes and their subtypes (43% for quinolines, 38% for benzothiazoles, and 53% for aminothiazoles). Nevertheless, all optimized compounds within each category demonstrated *in vitro* neuroprotection against ER stress-induced cell death, suggesting potential therapeutic applications for neurodegenerative diseases. Another way to increase SUMOylation is by blocking SENPs, thereby preventing the removal of SUMO from proteins (Albrow et al., 2011; Wang et al., 2020). Recently, this class of small molecules has also demonstrated neuroprotective effects in brain ischemia, where drug-induced increases in both SUMO1- and SUMO2/3-conjugated proteins improved recovery following stroke. Further studies will be necessary to evaluate the potential use of these compounds in the context of neurodegeneration as well (Yang et al., 2016).

Important steps toward the *in vivo* use of all these promising compounds, whether activators or inhibitors, include determining their bioavailability, tissue solubility, ability to cross the blood-brain barrier, and, in some cases, identifying the specific SUMO enzyme (E1, E2, or E3) they target. Moreover, deregulation of the SUMO machinery in disease may result in either a global increase in SUMO1 or SUMO2/3 conjugation, or selective SUMOylation/deSUMOylation of specific targets. Therefore, it is crucial to assess how these small molecules affect both global and target-specific SUMOylation, as well as their potential off-target effects.

Effects of SUMOylation on protein function

Some proteins are modified exclusively by SUMO1 or SUMO2/3, while others can undergo both modifications via the same catalytic pathway. Typically, SUMO1 is added as single unit to the substrate (mono-SUMOylation), whereas SUMO2/3 units are attached as chains (poly-SUMOylation). However, in certain cases SUMO1 itself can be further be modified by the addition of SUMO2/3 chains (Vertegaal et al., 2006) (Figure 2A). Modification occurs preferentially at a consensus site defined as (Ψ-K-X-[(D/E] (Tatham et al., 2001), where the lysine to be SUMOylated (K) is preceded by a large hydrophobic residue Ψ, while X can be any residue followed by aspartate or glutamate (D/E) (Rodriguez et al., 2001). Nevertheless, it has been observed that SUMOylation may occur in other non-canonical consensus (Hietakangas et al., 2006). Furthermore, PTMs in surrounding sequence or targeting the same lysine may enhance or compete with SUMOylation. For instance, acetylation and SUMOylation can be mutually exclusive when they target the same lysine, whereas phosphorylation of a nearby serine residue can enhance SUMOylation (Sapetschnig et al., 2002).

Addition of SUMO to the target protein changes its inter- and/or intramolecular interactions, often inducing conformational changes that may mask or expose nuclear localization/export (NLS/NES) sequences, or change affinity for specific transporters/adaptors thereby influencing transport between the nucleus and cytoplasm or direction through particular cellular compartments (e.g., dendritic spines). For example, SUMOylation of the serine/threonine kinase GSK3β, a key player in neuronal morphology, synapse formation and neuroinflammation, leads to its nuclear import (Eun Jeoung et al., 2008). Local translation at synapses depends on the availability of specific mRNAs that are packed and transported along the axons by the microtubule network. The RNA-binding protein La recognizes specific tagged-mRNA and transport them in anterograde or retrograde direction depending on its SUMOylation status (van Niekerk et al., 2007). SUMOylated La is dedicated to retrograde transport towards the nucleus, while deSUMOylated La allows anterograde transport by binding to kinesin. Changes in functional modulation (Figure 2B) are also common effects after SUMOylation. If SUMO modification of the protein/enzyme occurs close to the active site it may inhibit the activity by blocking substrate access or may enhance the activation by stabilizing a catalytically favorable conformation. For example, SUMO1 conjugation at lysine 430 within the catalytic domain of protein phosphatase 5 (PP5), activated during stress-induced signaling, regulates its enzymatic activity and substrate release (Sager et al., 2024). SUMOylation can also enhance or inhibit interactions with binding partners. SUMO-dependent modification of the interaction with cofactors or regulatory proteins, as well as prevention of other activatory/inhibitory PTMs (e.g., ubiquitination, phosphorylation) may likewise modify protein activity. Moreover, many proteins can bind SUMO non-covalently through SUMO-interacting motif (SIM), a sequence containing a hydrophobic core flanked by acidic or phosphorylatable serine residues. The SUMO/SIM interaction acts as a platform for other partners thus expanding the protein network fundamental for the assembly of large molecular transcriptional complexes involved in epigenetic regulation. HDAC4 dependent SUMO1-ylation of MeCP2, for example, activates the HDAC4/MeCP2 repressive complex during neuroinflammation (Li Puma et al., 2023), while SUMO-1 modified RAD51 promotes Sp1 transcriptional activity (Wu et al., 2025).

In general, SUMOylation increases protein stability by preventing ubiquitination at the same lysine residue, thereby protecting the protein from proteasomal degradation (Wei et al., 2025).

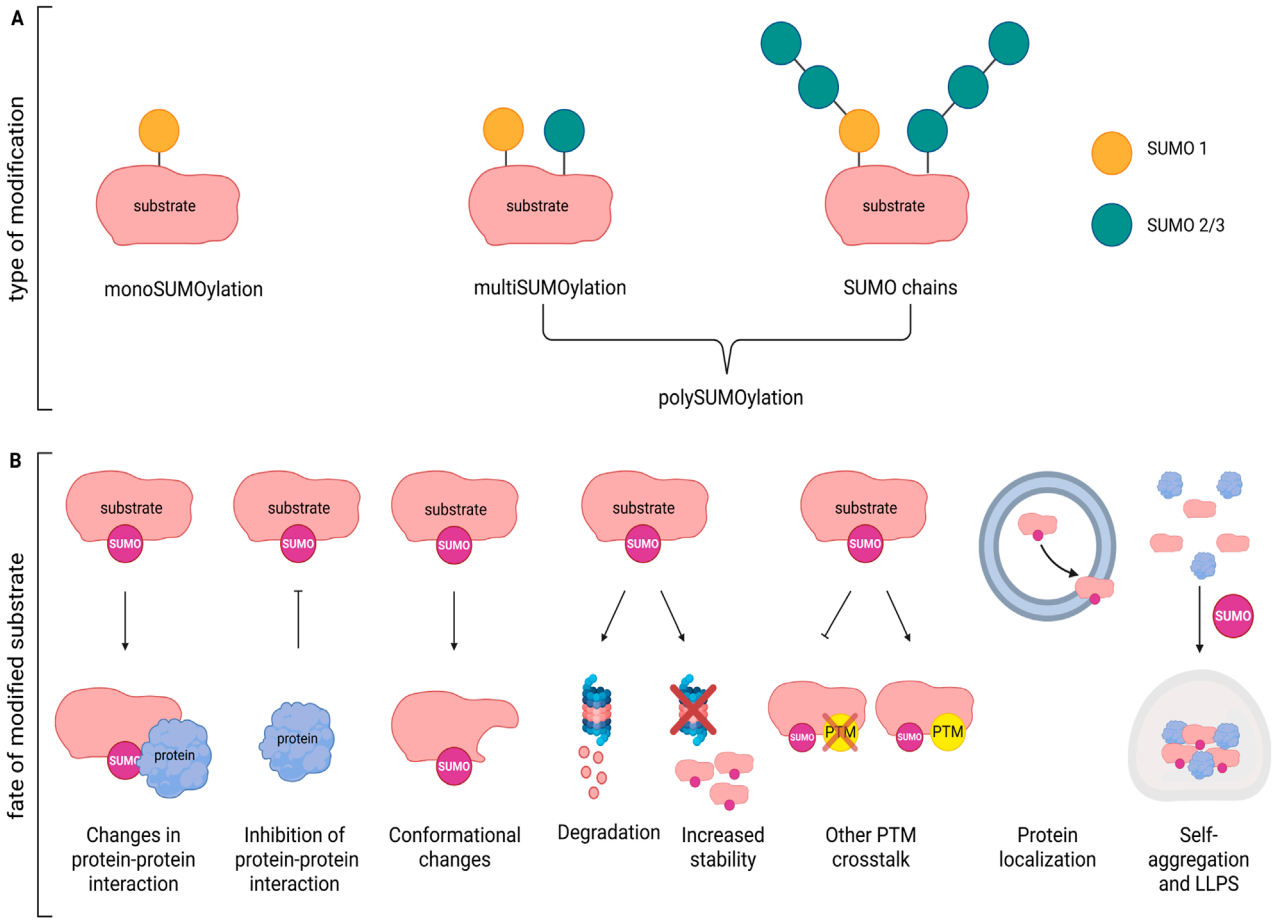

FIGURE 2
Effects of SUMOylation on protein function. **(A)** Example of mono- and poly-SUMOylation by SUMO1, SUMO2/3 or both on a substrate. **(B)** Substrate modification by SUMO may modify protein function in multiple ways: inducing changes in protein-protein interaction; inhibiting protein binding; determining conformational changes; affecting stability/degradation; favoring or inhibiting other PTMs; modulating protein localization; modifying self-aggregation capacity and formation of LLPS. Figure created with Biorender.

In other contexts, stress-driven SUMOylation, may dramatically alter protein solubility and promote self-aggregation, especially in proteins with intrinsically disordered domains, that are more prone to condensate and to be incorporated into stress granules, dynamic RNA-containing condensates (Verde et al., 2025). For example, preventing SUMO2/3-ylation of TDP43, a protein involved in amyotrophic lateral sclerosis and frontotemporal dementia, prevents its cytosolic aggregation and formation of stress granules. However, the formation of molecular condensate is not always deleterious. In fact, it can serve as a mechanism to compartmentalize groups of proteins or enzymatic pathways within small, membrane-less regions via liquid-liquid phase separation (LLPS) (Guzikowski and Kavalali, 2024), a process that may be particularly crucial at the level of the synaptic nanodomains.

Overall, these findings underscore the critical role of SUMOylation in a wide range of biological processes, including those essential for neuronal function. Dysregulation of SUMOylation may therefore contribute to the pathogenesis of various neurological disorders.

SUMOylation dependent regulation of synapse function

Functional aspects

SUMOylation is highly abundant in the nucleus and indeed many SUMO substrates, including transcription factors and co-regulators, were first identified in this compartment (Vertegaal, 2022).

Also, the SUMOylation machinery including E1-E3 enzymes and SENP proteases are present in the nucleus and are localized in the nuclear matrix where they play roles in processes such as chromosome segregation (Chen et al., 2024). Additionally, components of the SUMOylation system are associated with the nuclear pore complex (Chow et al., 2012; Ptak et al., 2025), where protein import and export are tightly coupled with SUMOylation, significantly influencing protein localization and function. For example, nuclear localization of the Downstream regulatory element antagonist modulator (DREAM), a multifunctional Ca^{2+}-sensitive protein, occurs upon SUMO1-ylation and enables its repressive

activity on several targets including sodium/calcium exchanger isoform 3 (NCX3), brain-derived neurotrophic factor (BDNF), prodynorphin, and c-fos (Palczewska et al., 2011). Furthermore, SUMOylation of TDP-43, a nuclear RNA-binding protein that forms toxic aggregates in amyotrophic lateral sclerosis and frontotemporal dementia patients, promotes its nuclear export and aggregation in the cytoplasm within stress granules (Maraschi et al., 2021).

Although less abundant outside the nucleus, SUMOylation plays a key role in synaptic function and development. SUMOylation enzymes and SENPs have been shown to localize not only in the cytoplasm but also specifically at synapses. For example, SENP5 immunoreactivity has been observed both in the postsynaptic spines and at the presynaptic zone (Akiyama et al., 2018), while by means of super-resolution microscopy the colocalization of SUMO1, SUMO2/3, and Ubc9 with pre- and post-synaptic markers was demonstrated (Colnaghi et al., 2019). The dynamic role of SUMOylation at synapse is also indicated by estrogen-dependent redistribution of Ubc9 and its interaction with PSD95 and synaptophysin in the Brain of APP/PS1 mice, a model of AD, and cortical neurons as revealed by immunofluorescence and co-immunoprecipitation (Lai et al., 2017).

HDAC4, an enzyme with low deacetylase activity, has recently been described as a new E3 ligase enzyme that localizes at synapses. It modulates the enrichment of PSD95 at the post-synaptic membrane by increasing its SUMO2/3ylation conjugation thus promoting synaptic transmission (Colussi et al., 2023). Moreover, activity-dependent Ubc9 localization to dendritic spines has been observed downstream metabotropic glutamate 5 receptors (mGlu5R) activation, process that leads to increased synaptic SUMOylation (Loriol et al., 2014).

In the same context, activity-induced Akt1 SUMO1-ylation has been reported as necessary for activation of the ERK1/2-BDNF/Arc signalling cascade, which supports LTP and long-lasting excitatory synaptic responses (Meng et al., 2021). Spatiotemporal regulation of synapse SUMOylome is crucial not only during normal synaptic activity but also throughout development and synaptogenesis. Indeed, proteomic studies on the developing brain have shown that the SUMO2/3-ylome of the synaptic compartment is enriched in neurotransmitter receptors, adhesion molecules, scaffolding proteins, molecules involved in vesicular trafficking and cytoskeleton rearrangement, all necessary for synapse maturation (Pronot et al., 2021).

To date, numerous pre- and post-synaptic proteins, including ion channels, receptors and transducers have been identified as either SUMO substrate or SUMO-interacting protein widening the complexity of the SUMOylome network that regulates these highly specialized compartments.

On the presynaptic side, several proteins involved in the synaptic vesicle cycle are modulated by SUMOylation. Synapsin I, one of the main regulators of synaptic vesicle pool availability, is subject of SUMO1 modification that increases its binding to SVs and promotes their reclustering after stimulation thereby contributing to the maintenance of the reserve pool (Tang et al., 2015). Of note, synapsin I is also target of many kinases and can be phosphorylated at various sites, critical for its interaction with actin and SVs, or for their release in the fine-tuning of synapsin I function (Longhena et al., 2021).

Efficient and controlled exocytosis of SVs is also regulated by the SUMO1 conjugation of the Rab3-interacting molecule 1α (RIM1α). This modification promotes the clustering of $Ca_V2.1$ calcium channels, so enhancing Ca^{2+} influx required for vesicle release (Girach et al., 2013). SV fusion with the plasma membrane is regulated by the interaction of SNARE proteins, located on both the SV and the presynaptic membrane at the active zone. SUMO1-ylation of Syntaxin1, a core component of the SNARE complex, increases its interaction with other SNARE proteins promotes endocytosis, suggesting an additional role for SUMO-modified Syntaxin1 in regulating the rate of neurotransmitter vesicle recycling (Craig et al., 2015). However, SUMO1-ylation can also have detrimental effects on synaptic function. In a study using mice with a neuronal restricted SUMO1 expression, the authors found an altered basal synaptic transmission and impaired presynaptic function that were associated with increased SUMO1-ylation of synaptotagmin-1 (Matsuzaki et al., 2015). Although the precise role of SUMOylation on synaptotagmin-1 was not fully elucidated, these findings suggest that that elevated SUMO1-ylation may have a role in altered neuronal function and neurodegenerative disease mechanisms.

According to the most recent models of presynaptic compartmentalization, synaptic vesicles (SVs) and the proteins involved in the entire SV cycle, including exocytosis and endocytosis, are organized into distinct or overlapping membrane-less assemblies based on liquid-liquid phase separation that is driven by the presence of disordered regions and SUMOylation (Zhang et al., 2024). This suggests that presynaptic protein SUMOylation may be essential for the formation of dynamic sub-synaptic protein clusters, enabling the fine-tuning of the SV cycle in response to neuronal activity and external stimuli.

The postsynaptic zone is another small yet highly specialized compartment, responsible for receiving neurotransmitter and converting the chemical signal into electrical one. The more specialized region is the post synaptic density (PSD), a protein-dense structure that gathers receptors, signaling molecules and scaffold proteins, many of which have been found to be SUMO2/3ylated by a proteomic approach in rat brains at the post-natal day 14 (Pronot et al., 2021). For example, β-catenin, PSD95, SynGAP, SAPAP3, Homer1, CaMKII, Neuroligin and N-Cadherin have all been found to undergo SUMOylation, although the functional consequences of these modifications remain largely unexplored. More recently, in adult mice, SUMO2/3-ylation of PSD95, the core component of PSD, has been observed. This modification is regulated by a cytoplasmic pool of HDAC4, which acts as an E3 ligase. SUMOylation of PSD95 was shown to promote its anchoring to the postsynaptic membrane, suggesting a role in stabilizing synaptic architecture (Colussi et al., 2023).

Membrane remodeling at the post synaptic density zone is fundamental to structural changes in dendritic spines and include receptor membrane trafficking, cytoskeletal rearrangement and activation of several signaling pathways that coordinate these processes (Hotulainen and Hoogenraad, 2010; Nishiyama and Yasuda, 2015; Spence and Soderling, 2015). Many of the proteins involved in actin remodeling and spine morphology regulation are modulated by SUMOylation. For example, CaMKII (calcium/calmodulin-dependent protein kinase II) activated by increased Ca^{2+} influx upon synaptic stimulation, phosphorylates several targets including the activity-regulated cytoskeleton-associated protein (Arc) that plays a key role in driving actin

remodeling. Upon stimulation, Arc mRNA is rapidly translated locally at synapse and undergoes dynamic mono-SUMO1-ylation that is necessary for its interaction with the actin binding protein debrin (DaSilva et al., 2016; Lyford et al., 1995; Nair et al., 2017). Furthermore, Arc interacts with cofilin, one of the main proteins that regulates actin polymerization (Messaoudi et al., 2007). On the contrary, deSUMOylated Arc is associated with decreased F-actin stabilization and spine size (Newpher et al., 2018).

Kainate receptors (KARs) represent another example of SUMO-regulated receptors. KARs are glutamate receptors that, depending on the neuronal type, present a distribution at pre- and post-synaptic sites and in extrasynaptic regions. Their signalling may occur either as ionotropic channels or metabotropic receptors based on G protein-coupled signals. Due to this broad distribution and functional versatility, KAR are modulators of neuronal excitability and synaptic transmission. These receptors are composed of tetrameric assemblies of different subunits (GluK1-5), among which the Gluk2 subunit is regulated by multiple PTMs including SUMO1-ylation (Martin et al., 2007). Indeed, Gluk2 SUMO1-ylation is necessary for receptor internalization upon agonist binding. Interestingly, interplay among SUMOylation, phosphorylation and palmitoylation coordinates KAR surface expression and activity-dependent endocytosis. Under basal (unstimulated) conditions, palmitoylation of GluK2 inhibits both phosphorylation and SUMOylation, thereby stabilizing the receptor at the plasma membrane. However, upon kainate stimulation, Gluk2 is depalmitoylated and undergoes phosphorylation and SUMOylation that in turn stimulates internalization (Yucel et al., 2023; Chamberlain et al., 2012; Konopacki et al., 2011).

K2P family channels form K^+ selective pores that regulate the background flux of potassium ions that are key determinants of the resting membrane potential. Two homomeric or heteromeric subunits (there are 145 genes so far identified) assembly to form the pore (Plant et al., 2012; Lopes et al., 2001). Although it has been object of debate, it has been demonstrated that a basal SUMO1-ylation of the K2P1 isoform maintains the channel in an inactive state (Rajan et al., 2005). Accordingly, a co-localization of K2P1, SAE1, and Ubc9 was observed at the plasma membrane, and conjugation of SUMO1 to the ε-amino group of Lys274 was also confirmed by a proteomic approach (Plant et al., 2010). Furthermore, when SUMOylated-K2P1 is associated with K2P3 or K2P9 subunits at the surface of cerebellar granule neurons their response to stimuli is suppressed indicating a more wide effect of SUMOylation on these channels (Plant et al., 2012).

The regulatory role of SUMOylation on potassium channel was also demonstrated by means of SENP2-deficient mice that exhibit seizures and sudden death (Qi et al., 2014). In this model deficiency of SENP2 led to hyper-SUMOylation of Kv1.1 and Kv7.2/Kv7.3 channels. Changes in SUMO levels however affected only Kv7.2/Kv7.3 channels causing a reduction in depolarizing M-current responsible for neuronal hyperexcitability.

Several sodium channel isoforms ($Na_V1.1$, $Na_V1.2$, and $Na_V1.6$) are present in mature neurons with a specific spatiotemporal distribution that ensures proper onset and propagation of action potential (AP). In particular, $Na_V1.2$ channels, located in the proximal part of the axon initial segment, where AP originates, is responsible for backpropagation of AP to the soma/dendrites important for synaptic strength and the coordination of synaptic inputs (Markram et al., 1997).

SUMO1-ylation of $Na_V1.2$ has recently found as critical modification able to increase action potential backpropagation from the AIS providing a new layer of complexity in the modulation of synaptic integration and plasticity (Kotler et al., 2023). Additionally, SUMO1-ylation of $Na_V1.2$ channels occurs in response to brain hypoxia and allows a neuroprotective response to this stress increasing sodium current (Plant et al., 2016).

Overall, these works outline the role of sodium channel SUMOylation as important means to modulate neuronal response to different stimuli.

Structural aspects

The type and the magnitude of synaptic transmission rely on the signalling generated between the pre- and post-synaptic compartments which is strongly influenced by the shape, size, and organization of these specialized sites. For example, several structural proteins and their regulators contribute to the maturation, stabilization, or retraction of dendritic spines. These formations are enriched in actin filaments and microtubules which are continuously modulated in terms of polymerization, organization, stability, and turnover ensuring rapid response to stimuli. Activity-dependent changes in actin polymerization enable spines to change shape, enlarge or become stabilized thus supporting learning processes and memory storage (Kasai et al., 2003).

The calcium/calmodulin-dependent serine protein kinase (CASK) belongs to the family of the membrane-associated guanylate kinase (MAGUK) proteins. CASK has been identified as a key element inducing actin nucleation, assembly and spine formation through its interaction with the adhesion protein 4.1 (Biederer and Sudhof, 2001). However, it has been shown that SUMO1-ylation of CASK at lys 679, alters the binding site for protein 4.1 reducing the formation of the complex actin/protein4.1/CASK that leads to a decrease in the number and size of spines (Chao et al., 2008).

Other studies indicate that the control of actin at the level of spines may be obtained by regulating its transcription. Indeed, local translation within these small compartments is fundamental for achieving precise spatial and temporal regulation of structural and signaling proteins. Specifically, actin interacts in neurons with the prion-like cytoplasmic polyadenylation element-binding protein 3 (CPEB3) (Stephan et al., 2015), that is an RNA binding protein identified as an important modulator of long-term synaptic plasticity in the hippocampus (Fioriti et al., 2015).

Under basal conditions CPEB3 is SUMO2/3-ylated, remains soluble and acts as repressor of mRNA translation (Drisaldi et al., 2015). Upon neuronal stimulation, CPEB3 is deSUMOylated and undergoes aggregation which promotes the translation of its target mRNAs, including actin, ultimately influencing spine structure and synaptic plasticity (Gu et al., 2020).

Dynamic interaction of actin with the microtubule cytoskeleton is another key element in maintaining spine morphology and maturation of synapses (Dent and Gertler, 2003). In this context, Spastin is a protease that fragments microtubules in an ATP dependent manner when SUMO1-ylated at K427. Conversely, its deSUMOylation leads to microtubule stability (Ji et al.,

2020). Since only dynamic microtubules can enter the dendritic spines and regulate F-actin levels it is evident that SUMOylation balance of Spastin is crucial for maintaining microtubule polymerization dynamics.

Altogether, the coordinated regulation of both structural and functional elements is fundamental for the remodeling and maturation of dendritic spines, processes that are essential for synaptic plasticity and, ultimately, cognitive function.

Deregulation of SUMOylation in Alzheimer's disease

Thanks to its dynamic nature, SUMOylation enables the rapid and reversible modification of protein function in response to signals occurring well before changes in gene expression. This mechanism underlies several neuronal processes including the regulation of synaptic transmission and plasticity (Loriol et al., 2012; Watanabe et al., 2008). Indeed, increase in SUMO1 conjugation and in Ubc9 levels characterize the early developing brain while activity-dependent higher SUMOylation and redistribution of the SUMO machinery occur both at the level of pre- and post-synaptic compartments facilitating neuronal signal transmission (Loriol et al., 2013). In addition, SUMOylation-dependent changes are necessary for long-term synaptic plasticity (LTP). Indeed, following stimulation, SUMO2/3 levels transiently peak, but acute inhibition of SUMOylation impairs both LTP and hippocampal-dependent learning (Lee et al., 2014).

Because of its key role in modulating protein function and neuronal signaling, disruption of SUMOylation homeostasis, whether through excessive conjugation or impaired deSUMOylation, is linked to several neurological disorders including Alzheimer's disease (AD). AD is the most common neurodegenerative disorder in the elderly characterized by increased deposition of amyloid beta (Aβ), which accumulates in plaques, and by increased levels of phosphorylated tau leading to the formation of neurofibrillary tangles. Synaptic failure is an early event in the pathogenesis of the disease that represents the best correlate of disease progression and is considered a key determinant of its severity (Selkoe, 2002; Reddy et al., 2005).

Dysregulation of SUMOylation has been observed in Alzheimer's disease (AD) patients and demonstrated across multiple animal models of pathology. Both human subjects and AD models show an altered global SUMOylation profile, with generally elevated levels of SUMO1 and reduced levels of SUMO2/3 (Li et al., 2003; Lee et al., 2014). Elevated SUMO1 levels have also been detected in plasma samples from AD patients, suggesting a potential role as a biomarker (Cho et al., 2015). Importantly, deregulation of SUMO balance was linked to impaired LTP and hippocampal-dependent learning and memory (Lee et al., 2014). Accordingly, transgenic mice with SUMO1 restricted overexpression in the brain exhibited altered basal synaptic transmission and impaired presynaptic function (Matsuzaki et al., 2015). Of note, altered SUMOylation has been observed both in post-mortem AD brain and in presymptomatic patients (Mandel and Agarwal, 2022) thus suggesting that changes in SUMOylation is more a chronic status rather than an acute episode.

Focusing on the SUMOylation of specific targets, several reports have shown its impact on the two pathological AD hallmarks, Aβ and tau. Amyloid beta is generated through the amyloidogenic processing pathway that involves that sequential cleavage of the amyloid precursor protein (APP) by β-site APP cleaving enzyme (BACE), followed by γ-secretase (Wolfe and Haass, 2001). Different effects on Aβ deposition and aggregation have been reported depending on the type of SUMO modification and protein targets involved. Increasing the SUMO3 expression in an *in vitro* system, for example, induced a reduction of Aβ production (Li et al., 2003) and APP SUMO1 conjugation at lysines 587 and 595, close to the site of BACE cleavage, reduced Aβ aggregation (Zhang and Sarge, 2008). Conversely, SUMO1-ylation of BACE1 at lysine 501 enhanced the enzyme's protease activity and stability, resulting in elevated Aβ production (Bao et al., 2018). Tau is a microtubule associated protein that undergoes aggregation in several neurodegenerative disorders including AD. This protein is target of many PTMs, in particular phosphorylations, that change its solubility and promote aggregation. Recent advances led to the discovery that interplay among different PTMs can either exacerbate or mitigate tau aggregation and its associated pathology. Specifically, SUMO1-ylation of tau increased the level of its phosphorylation while reducing its solubility (Wada et al., 2024). Conversely, SUMO2 modification of tau enhances its solubility and reduces tau-dependent pathological effects (Zhang et al., 2023).

Additional evidence of the contrasting effects resulting from the imbalance of SUMO1- and SUMO2/3-conjugated proteins is provided from the altered localization and function of the E3 ligase enzyme HDAC4. In AD, where HDAC4 is mislocalized from synapses and accumulates in the nucleus, there is a reduction in the SUMO2/3-ylation of PSD95, one of its targets, that is associated with the loss of membrane localization of several proteins important for synaptic transmission such as CaMKII, GluA1, N-cadherin (Colussi et al., 2023). HDAC4 nuclear accumulation also characterizes an AD-like model induced by neuroinflammation. In this model, HDAC4 mediates the SUMO1 conjugation of the transcriptional repressor MeCP2, resulting in the formation of a multimeric complex containing HDAC4 and MeCP2 that suppresses the expression of synaptic genes (Li Puma et al., 2023).

Based on these data several research groups developed strategies to modulate SUMOylation as a means of restoring synaptic function. Downregulation of SUMO1-ylation in the synaptosomal compartment successfully normalized impaired glutamate release further highlighting the detrimental effects of elevated SUMO1 levels (Marcelli et al., 2017). Conversely, AD mice (APP) either overexpressing SUMO2 or treated with a brain-penetrant recombinant SUMO2 showed a recovery in cognitive and synaptic impairment along with reduced amyloid pathology suggesting that a pharmacological approach may be a promising therapeutic tool (Fioriti et al., 2025). Similarly, viral induced expression of SUMO2 rescued neuronal toxicity in mice overexpressing the mutant form of tau (Orsini et al., 2024).

Conclusion

Protein modification through SUMOylation plays a crucial role in regulating their function inducing conformational changes or

masking/exposing sites critical for protein-protein interaction or influencing other post-translational modifications (PTMs). These actions collectively affect protein stability, degradation, solubility, and activity. Synaptic function is regulated by SUMOylation both at the nuclear level and directly at synapses, where an increasing number of proteins have been identified as SUMO targets. Consequently, alteration in SUMO machinery, frequently observed in many neurodegenerative diseases, may have a central role in disease pathogenesis. Specifically in AD, reducing SUMO1-ylation or increasing SUMO2-ylation demonstrated a beneficial effect on synaptic function suggesting that targeting SUMOylation could represent a promising therapeutic approach for restoring synaptic health in AD.

Author contributions

AB: Writing – original draft. WT: Writing – original draft. GC: Writing – original draft. CG: Conceptualization, Writing – review and editing. CC: Conceptualization, Writing – original draft, Writing – review and editing.

Funding

The author(s) declare that financial support was received for the research and/or publication of this article. We acknowledge the financial support of "Ricerca Corrente 2025" from Fondazione Policlinico Universitario "A. Gemelli" IRCCS to CG. This work was partially supported by the Grant PRIN PNRR 2022 P20222WFZ3 to CC.

Conflict of interest

The authors declare that the research was conducted in the absence of any commercial or financial relationships that could represent a potential conflict of interest.

Generative AI statement

The author(s) declare that no Generative AI was used in the creation of this manuscript.

Any alternative text (alt text) provided alongside figures in this article has been generated by Frontiers with the support of artificial intelligence and reasonable efforts have been made to ensure accuracy, including review by the authors wherever possible. If you identify any issues, please contact us.

Publisher's note

References

Akiyama, H., Nakadate, K., and Sakakibara, S. I. (2018). Synaptic localization of the SUMOylation-regulating protease SENP5 in the adult mouse brain. *J. Comp. Neurol.* 526, 990–1005. doi:10.1002/cne.24384

Albrow, V. E., Ponder, E. L., Fasci, D., Bekes, M., Deu, E., Salvesen, G. S., et al. (2011). Development of small molecule inhibitors and probes of human SUMO deconjugating proteases.

Bao, J., Qin, M., Mahaman, Y. A. R., Zhang, B., Huang, F., Zeng, K., et al. (2018). BACE1 SUMOylation increases its stability and escalates the protease activity in Alzheimer's disease. *Proc. Natl. Acad. Sci. U. S. A.* 115, 3954–3959. doi:10.1073/pnas.1800498115

Bernstock, J. D., Lee, Y. J., Peruzzotti-Jametti, L., Southall, N., Johnson, K. R, Maric, D., et al. (2016). A novel quantitative high-throughput screen identifies drugs that both activate SUMO conjugation via the inhibition of microRNAs 182 and 183 and facilitate neuroprotection in a model of oxygen and glucose deprivation. *J. Cereb. Blood. Flow. Metab.* 36, 426–41.

Bernstock, J. D., Peruzzotti-Jametti, L., Leonardi, T., Vicario, N., Ye, D., Lee, Y. J., et al. (2019). SUMOylation promotes survival and integration of neural stem cell grafts in ischemic stroke. *EBioMedicine* 42, 214–224. doi:10.1016/j.ebiom.2019.03.035

Biederer, T., and Sudhof, T. C. (2001). CASK and protein 4.1 support F-actin nucleation on neurexins. *J. Biol. Chem.* 276, 47869–47876. doi:10.1074/jbc.M105287200

Brackett, C. M., and Blagg, B. S. J. (2021). Current status of SUMOylation inhibitors. *Curr. Med. Chem.* 28, 3892–3912. doi:10.2174/0929867327666200810135039

Chamberlain, S. E., Gonzalez-Gonzalez, I. M., Wilkinson, K. A., Konopacki, F. A., Kantamneni, S., Henley, J. M., et al. (2012). SUMOylation and phosphorylation of GluK2 regulate kainate receptor trafficking and synaptic plasticity. *Nat. Neurosci.* 15, 845–852. doi:10.1038/nn.3089

Chao, H. W., Hong, C. J., Huang, T. N., Lin, Y. L., and Hsueh, Y. P. (2008). SUMOylation of the MAGUK protein CASK regulates dendritic spinogenesis. *J. Cell Biol.* 182, 141–155. doi:10.1083/jcb.200712094

Chen, Z., Luo, J., Zhang, Y., Zheng, S., Zhang, H., Huang, Y., et al. (2024). SUMOylation is enriched in the nuclear matrix and required for chromosome segregation. *J. Biol. Chem.* 300, 105547. doi:10.1016/j.jbc.2023.105547

Cho, S. J., Yun, S. M., Lee, D. H., Jo, C., Ho Park, M., Han, C., et al. (2015). Plasma SUMO1 protein is elevated in Alzheimer's disease. *J. Alzheimers Dis.* 47, 639–643. doi:10.3233/JAD-150103

Chow, K. H., Elgort, S., Dasso, M., and Ullman, K. S. (2012). Two distinct sites in Nup153 mediate interaction with the SUMO proteases SENP1 and SENP2. *Nucleus* 3, 349–358. doi:10.4161/nucl.20822

Colnaghi, L., Russo, L., Natale, C., Restelli, E., Cagnotto, A., Salmona, M., et al. (2019). Super resolution microscopy of SUMO proteins in neurons. *Front. Cell Neurosci.* 13, 486. doi:10.3389/fncel.2019.00486

Colussi, C., Aceto, G., Ripoli, C., Bertozzi, A., Li Puma, D. D., Paccosi, E., et al. (2023). Cytoplasmic HDAC4 recovers synaptic function in the 3×Tg mouse model of Alzheimer's disease. *Neuropathol. Appl. Neurobiol.* 49, e12861. doi:10.1111/nan.12861

Craig, T. J., Anderson, D., Evans, A. J., Girach, F., and Henley, J. M. (2015). SUMOylation of Syntaxin1A regulates presynaptic endocytosis. *Sci. Rep.* 5, 17669. doi:10.1038/srep17669

Dasilva, L. L., Wall, M. J., Almeida, L. P. D., Wauters, S. C., Januario, Y. C., Muller, J., et al. (2016). Activity-regulated cytoskeleton-associated protein controls AMPAR endocytosis through a direct interaction with clathrin-adaptor protein 2. *eNeuro* 3, ENEURO.0144–15.2016. doi:10.1523/ENEURO.0144-15.2016

Datwyler, A. L., Lattig-Tunnemann, G., Yang, W., Paschen, W., Lee, S. L., Dirnagl, U., et al. (2011). SUMO2/3 conjugation is an endogenous neuroprotective mechanism. *J. Cereb. Blood Flow. Metab.* 31, 2152–2159. doi:10.1038/jcbfm.2011.112

Dent, E. W., and Gertler, F. B. (2003). Cytoskeletal dynamics and transport in growth cone motility and axon guidance. *Neuron* 40, 209–227. doi:10.1016/s0896-6273(03)00633-0

Drisaldi, B., Colnaghi, L., Fioriti, L., Rao, N., Myers, C., Snyder, A. M., et al. (2015). SUMOylation is an inhibitory constraint that regulates the prion-like aggregation and activity of CPEB3. *Cell Rep.* 11, 1694–1702. doi:10.1016/j.celrep.2015.04.061

DU, C. P., Wang, M., Geng, C., Hu, B., Meng, L., Xu, Y., et al. (2020). Activity-induced SUMOylation of neuronal nitric oxide synthase is associated with plasticity of synaptic transmission and extracellular signal-regulated kinase 1/2 signaling. *Antioxid. Redox Signal* 32, 18–34. doi:10.1089/ars.2018.7669

Eun Jeoung, L., Sung Hee, H., Jaesun, C., Sung Hwa, S., Kwang Hum, Y., Min Kyoung, K., et al. (2008). Regulation of glycogen synthase kinase 3beta functions by modification of the small ubiquitin-like modifier. *Open Biochem. J.* 2, 67–76. doi:10.2174/1874091X00802010067

Fioriti, L., Myers, C., Huang, Y. Y., Li, X., Stephan, J. S., Trifilieff, P., et al. (2015). The persistence of hippocampal-based memory requires protein synthesis mediated by the prion-like protein CPEB3. *Neuron* 86, 1433–1448. doi:10.1016/j.neuron.2015.05.021

Fioriti, L., Wijesekara, N., Argyrousi, E. K., Matsuzaki, S., Takamura, H., Satoh, K., et al. (2025). Genetic and pharmacologic enhancement of SUMO2 conjugation prevents and reverses cognitive impairment and synaptotoxicity in a preclinical model of Alzheimer's disease. *Alzheimers Dement.* 21, e70030. doi:10.1002/alz.70030

Fukuda, I., Ito, A., Hirai, G., Nishimura, S., Kawasaki, H., Saitoh, H., et al. (2009). Ginkgolic acid inhibits protein SUMOylation by blocking formation of the E1-SUMO intermediate. *Chem Biol.* 16, 133–40.

Galanty, Y., Belotserkovskaya, R., Coates, J., Polo, S., Miller, K. M., and Jackson, S. P. (2009). Mammalian SUMO E3-ligases PIAS1 and PIAS4 promote responses to DNA double-strand breaks. *Nature* 462, 935–939. doi:10.1038/nature08657

Gao, C., Ho, C. C., Reineke, E., Lam, M., Cheng, X., Stanya, K. J., et al. (2008). Histone deacetylase 7 promotes PML sumoylation and is essential for PML nuclear body formation. *Mol. Cell Biol.* 28, 5658–5667. doi:10.1128/MCB.00874-08

Girach, F., Craig, T. J., Rocca, D. L., and Henley, J. M. (2013). RIM1α SUMOylation is required for fast synaptic vesicle exocytosis. *Cell Rep.* 5, 1294–1301. doi:10.1016/j.celrep.2013.10.039

Gu, X., Schafer, N. P., Wang, Q., Song, S. S., Chen, M., Waxham, M. N., et al. (2020). Exploring the F-actin/CPEB3 interaction and its possible role in the molecular mechanism of long-term memory. *Proc. Natl. Acad. Sci. U. S. A.* 117, 22128–22134. doi:10.1073/pnas.2012964117

Guzikowski, N. J., and Kavalali, E. T. (2024). Functional specificity of liquid-liquid phase separation at the synapse. *Nat. Commun.* 15, 10103. doi:10.1038/s41467-024-54423-7

Han, X., Niu, J., Zhao, Y., Kong, Q., Tong, T., and Han, L. (2016). HDAC4 stabilizes SIRT1 via sumoylation SIRT1 to delay cellular senescence. *Clin. Exp. Pharmacol. Physiol.* 43, 41–46. doi:10.1111/1440-1681.12496

Hietakangas, V., Anckar, J., Blomster, H. A., Fujimoto, M., Palvimo, J. J., Nakai, A., et al. (2006). PDSM, a motif for phosphorylation-dependent SUMO modification. *Proc. Natl. Acad. Sci. U. S. A.* 103, 45–50. doi:10.1073/pnas.0503698102

Hirohama, M., Kumar, A., Fukuda, I., Matsuoka, S., Igarashi, Y., Saitoh, H., et al. (2013). Spectomycin B1 as a novel SUMOylation inhibitor that directly binds to SUMO E2. *ACS. Chem. Biol.* 8, 2635–2642.

Hlushchenko, I., Koskinen, M., and Hotulainen, P. (2016). Dendritic spine actin dynamics in neuronal maturation and synaptic plasticity. *Cytoskelet. Hob.* 73, 435–441. doi:10.1002/cm.21280

Hotulainen, P., and Hoogenraad, C. C. (2010). Actin in dendritic spines: connecting dynamics to function. *J. Cell Biol.* 189, 619–629. doi:10.1083/jcb.201003008

Jackson, P. K. (2001). A new RING for SUMO: wrestling transcriptional responses into nuclear bodies with PIAS family E3 SUMO ligases. *Genes Dev.* 15, 3053–3058. doi:10.1101/gad.955501

Ji, Z. S., Liu, Q. L., Zhang, J. F., Yang, Y. H., Li, J., Zhang, G. W., et al. (2020). SUMOylation of spastin promotes the internalization of GluA1 and regulates dendritic spine morphology by targeting microtubule dynamics. *Neurobiol. Dis.* 146, 105133. doi:10.1016/j.nbd.2020.105133

Johnson, E. S., Schwienhorst, I., Dohmen, R. J., and Blobel, G. (1997). The ubiquitin-like protein Smt3p is activated for conjugation to other proteins by an Aos1p/Uba2p heterodimer. *EMBO J.* 16, 5509–5519. doi:10.1093/emboj/16.18.5509

Kagey, M. H., Melhuish, T. A., and Wotton, D. (2003). The polycomb protein Pc2 is a SUMO E3. *Cell* 113, 127–137. doi:10.1016/s0092-8674(03)00159-4

Kasai, H., Matsuzaki, M., Noguchi, J., Yasumatsu, N., and Nakahara, H. (2003). Structure-stability-function relationships of dendritic spines. *Trends Neurosci.* 26, 360–368. doi:10.1016/S0166-2236(03)00162-0

Kim, Y. S., Nagy, K., Keyser, S., and Schneekloth, J. S. (2013). An electrophoretic mobility shift assay identifies a mechanistically unique inhibitor of protein sumoylation. *Chem. Biol.* 20, 604–613.

Kho, C., Lee, A., Jeong, D., Oh, J. G., Gorski, P. A., Fish, K., et al. (2015). Small-molecule activation of SERCA2a SUMOylation for the treatment of heart failure. *Nat. Commun.* 6, 7229.

Konopacki, F. A., Jaafari, N., Rocca, D. L., Wilkinson, K. A., Chamberlain, S., Rubin, P., et al. (2011). Agonist-induced PKC phosphorylation regulates GluK2 SUMOylation and kainate receptor endocytosis. *Proc. Natl. Acad. Sci. U. S. A.* 108, 19772–19777. doi:10.1073/pnas.1111575108

Kotler, O., Khrapunsky, Y., Shvartsman, A., Dai, H., Plant, L. D., Goldstein, S. A. N., et al. (2023). SUMOylation of Na(V)1.2 channels regulates the velocity of backpropagating action potentials in cortical pyramidal neurons. *Elife* 12, e81463. doi:10.7554/eLife.81463

Krajnak, K., and Dahl, R. (2018). Small molecule SUMOylation activators are novel neuroprotective agents. *Bioorg. Med. Chem. Lett.* 28, 405–409.

Kumar, A., Ito, A., Hirohama, M., Yoshida, M., and Zhang, K. Y. (2013). Identification of sumoylation activating enzyme 1 inhibitors by structure-based virtual screening. *J. Chem. Inf. Model.* 53, 809–2.

Lai, Y. J., Liu, L., Hu, X. T., He, L., and Chen, G. J. (2017). Estrogen modulates ubc9 expression and synaptic redistribution in the brain of APP/PS1 mice and cortical neurons. *J. Mol. Neurosci.* 61, 436–448. doi:10.1007/s12031-017-0884-2

Lee, L., Dale, E., Staniszewski, A., Zhang, H., Saeed, F., Sakurai, M., et al. (2014). Regulation of synaptic plasticity and cognition by SUMO in normal physiology and Alzheimer's disease. *Sci. Rep.* 4, 7190. doi:10.1038/srep07190

Li, Y., Wang, H., Wang, S., Quon, D., Liu, Y. W., and Cordell, B. (2003). Positive and negative regulation of APP amyloidogenesis by sumoylation. *Proc. Natl. Acad. Sci. U. S. A.* 100, 259–264. doi:10.1073/pnas.0235361100

Li Puma, D. D., Colussi, C., Bandiera, B., Puliatti, G., Rinaudo, M., Cocco, S., et al. (2023). Interleukin 1β triggers synaptic and memory deficits in Herpes simplex virus type-1-infected mice by downregulating the expression of synaptic plasticity-related genes via the epigenetic MeCP2/HDAC4 complex. *Cell Mol. Life Sci.* 80, 172. doi:10.1007/s00018-023-04817-5

Longhena, F., Faustini, G., Brembati, V., Pizzi, M., Benfenati, F., and Bellucci, A. (2021). An updated reappraisal of synapsins: structure, function and role in neurological and psychiatric disorders. *Neurosci. Biobehav Rev.* 130, 33–60. doi:10.1016/j.neubiorev.2021.08.011

Lopes, C. M., Zilberberg, N., and Goldstein, S. A. (2001). Block of Kcnk3 by protons. Evidence that 2-P-domain potassium channel subunits function as homodimers. *J. Biol. Chem.* 276, 24449–24452. doi:10.1074/jbc.C100184200

Loriol, C., Parisot, J., Poupon, G., Gwizdek, C., and Martin, S. (2012). Developmental regulation and spatiotemporal redistribution of the sumoylation machinery in the rat central nervous system. *PLoS One* 7, e33757. doi:10.1371/journal.pone.0033757

Loriol, C., Khayachi, A., Poupon, G., Gwizdek, C., and Martin, S. (2013). Activity-dependent regulation of the sumoylation machinery in rat hippocampal neurons. *Biol. Cell* 105, 30–45. doi:10.1111/boc.201200016

Loriol, C., Casse, F., Khayachi, A., Poupon, G., Chafai, M., Deval, E., et al. (2014). mGlu5 receptors regulate synaptic sumoylation via a transient PKC-dependent diffusional trapping of Ubc9 into spines. *Nat. Commun.* 5, 5113. doi:10.1038/ncomms6113

Lv, Z., Yuan, L., Atkison, J. H., Williams, K. M., Vega, R., Sessions, E. H., et al. (2018). Molecular mechanism of a covalent allosteric inhibitor of SUMO E1 activating enzyme. *Nat. Commun.* 9, 5145.

Lyford, G. L., Yamagata, K., Kaufmann, W. E., Barnes, C. A., Sanders, L. K., Copeland, N. G., et al. (1995). Arc, a growth factor and activity-regulated gene, encodes a novel cytoskeleton-associated protein that is enriched in neuronal dendrites. *Neuron* 14, 433–445. doi:10.1016/0896-6273(95)90299-6

Mandel, N., and Agarwal, N. (2022). Role of SUMOylation in neurodegenerative diseases. *Cells* 11, 3395. doi:10.3390/cells11213395

Maraschi, A., Gumina, V., Dragotto, J., Colombrita, C., Mompean, M., Buratti, E., et al. (2021). SUMOylation regulates TDP-43 splicing activity and nucleocytoplasmic distribution. *Mol. Neurobiol.* 58, 5682–5702. doi:10.1007/s12035-021-02505-8

Marcelli, S., Ficulle, E., Iannuzzi, F., Kovari, E., Nistico, R., and Feligioni, M. (2017). Targeting SUMO-1ylation contrasts synaptic dysfunction in a mouse model of Alzheimer's disease. *Mol. Neurobiol.* 54, 6609–6623. doi:10.1007/s12035-016-0176-9

Markram, H., Lubke, J., Frotscher, M., and Sakmann, B. (1997). Regulation of synaptic efficacy by coincidence of postsynaptic APs and EPSPs. *Science* 275, 213–215. doi:10.1126/science.275.5297.213

Martin, S., Nishimune, A., Mellor, J. R., and Henley, J. M. (2007). SUMOylation regulates kainate-receptor-mediated synaptic transmission. *Nature* 447, 321–325. doi:10.1038/nature05736

Matsuzaki, S., Lee, L., Knock, E., Srikumar, T., Sakurai, M., Hazrati, L. N., et al. (2015). SUMO1 affects synaptic function, spine density and memory. *Sci. Rep.* 5, 10730. doi:10.1038/srep10730

Meng, L., DU, C. P., Lu, C. Y., Zhang, K., Li, L., Yan, J. Z., et al. (2021). Neuronal activity-induced SUMOylation of Akt1 by PIAS3 is required for long-term potentiation of synaptic transmission. *FASEB J.* 35, e21769. doi:10.1096/fj.202002728R

Merrill, J. C., Melhuish, T. A., Kagey, M. H., Yang, S. H., Sharrocks, A. D., and Wotton, D. (2010). A role for non-covalent SUMO interaction motifs in Pc2/CBX4 E3 activity. *PLoS One* 5, e8794. doi:10.1371/journal.pone.0008794

Messaoudi, E., Kanhema, T., Soule, J., Tiron, A., Dagyte, G., Da Silva, B., et al. (2007). Sustained Arc/Arg3.1 synthesis controls long-term potentiation consolidation through

regulation of local actin polymerization in the dentate gyrus *in vivo*. *J. Neurosci.* 27, 10445–10455. doi:10.1523/JNEUROSCI.2883-07.2007

Nair, R. R., Patil, S., Tiron, A., Kanhema, T., Panja, D., Schiro, L., et al. (2017). Dynamic Arc SUMOylation and selective interaction with F-Actin-Binding protein drebrin A in LTP consolidation *in vivo*. *Front. Synaptic Neurosci.* 9, 8. doi:10.3389/fnsyn.2017.00008

Newpher, T. M., Harris, S., Pringle, J., Hamilton, C., and Soderling, S. (2018). Regulation of spine structural plasticity by Arc/Arg3.1. *Semin. Cell Dev. Biol.* 77, 25–32. doi:10.1016/j.semcdb.2017.09.022

Nishiyama, J., and Yasuda, R. (2015). Biochemical computation for spine structural plasticity. *Neuron* 87, 63–75. doi:10.1016/j.neuron.2015.05.043

Orsini, F., Pascente, R., Martucci, A., Palacino, S., Fraser, P., Arancio, O., et al. (2024). SUMO2 rescues neuronal and glial cells from the toxicity of P301L Tau mutant. *Front. Cell Neurosci.* 18, 1437995. doi:10.3389/fncel.2024.1437995

Ozato, K., Shin, D. M., Chang, T. H., and Morse, H. C. (2008). TRIM family proteins and their emerging roles in innate immunity. *Nat. Rev. Immunol.* 8, 849–860. doi:10.1038/nri2413

Palczewska, M., Casafont, I., Ghimire, K., Rojas, A. M., Valencia, A., Lafarga, M., et al. (2011). Sumoylation regulates nuclear localization of repressor DREAM. *Biochim. Biophys. Acta* 1813, 1050–1058. doi:10.1016/j.bbamcr.2010.11.001

Pichler, A., Gast, A., Seeler, J. S., Dejean, A., and Melchior, F. (2002). The nucleoporin RanBP2 has SUMO1 E3 ligase activity. *Cell* 108, 109–120. doi:10.1016/s0092-8674(01)00633-x

Plant, L. D., Dementieva, I. S., Kollewe, A., Olikara, S., Marks, J. D., and Goldstein, S. A. (2010). One SUMO is sufficient to silence the dimeric potassium channel K2P1. *Proc. Natl. Acad. Sci. U. S. A.* 107, 10743–10748. doi:10.1073/pnas.1004712107

Plant, L. D., Zuniga, L., Araki, D., Marks, J. D., and Goldstein, S. A. (2012). SUMOylation silences heterodimeric TASK potassium channels containing K2P1 subunits in cerebellar granule neurons. *Sci. Signal* 5, ra84. doi:10.1126/scisignal.2003431

Plant, L. D., Marks, J. D., and Goldstein, S. A. (2016). SUMOylation of Na(V)1.2 channels mediates the early response to acute hypoxia in central neurons. *Elife* 5, e20054. doi:10.7554/eLife.20054

Pronot, M., Kieffer, F., Gay, A. S., Debayle, D., Forquet, R., Poupon, G., et al. (2021). Proteomic identification of an endogenous synaptic SUMOylome in the developing rat brain. *Front. Mol. Neurosci.* 14, 780535. doi:10.3389/fnmol.2021.780535

Ptak, C., Saik, N. O., and Wozniak, R. W. (2025). Ulp1 association with nuclear pore complexes is required for the maintenance of global SUMOylation. *Mol. Biol. Cell* 36, ar81. doi:10.1091/mbc.E24-12-0563

Qi, Y., Wang, J., Bomben, V. C., Li, D. P., Chen, S. R., Sun, H., et al. (2014). Hyper-SUMOylation of the Kv7 potassium channel diminishes the M-current leading to seizures and sudden death. *Neuron* 83, 1159–1171. doi:10.1016/j.neuron.2014.07.042

Rajan, S., Plant, L. D., Rabin, M. L., Butler, M. H., and Goldstein, S. A. (2005). Sumoylation silences the plasma membrane leak K+ channel K2P1. *Cell* 121, 37–47. doi:10.1016/j.cell.2005.01.019

Reddy, P. H., Mani, G., Park, B. S., Jacques, J., Murdoch, G., Whetsell, W., JR., et al. (2005). Differential loss of synaptic proteins in Alzheimer's disease: implications for synaptic dysfunction. *J. Alzheimers Dis.* 7, 103–180. doi:10.3233/jad-2005-7203

Reverter, D., and Lima, C. D. (2005). Insights into E3 ligase activity revealed by a SUMO-RanGAP1-Ubc9-Nup358 complex. *Nature* 435, 687–692. doi:10.1038/nature03588

Rizalar, F. S., Roosen, D. A., and Haucke, V. (2021). A presynaptic perspective on transport and assembly mechanisms for synapse formation. *Neuron* 109, 27–41. doi:10.1016/j.neuron.2020.09.038

Rodriguez, M. S., Dargemont, C., and Hay, R. T. (2001). SUMO-1 conjugation *in vivo* requires both a consensus modification motif and nuclear targeting. *J. Biol. Chem.* 276, 12654–12659. doi:10.1074/jbc.M009476200

Rytinki, M. M., Kaikkonen, S., Pehkonen, P., Jaaskelainen, T., and Palvimo, J. J. (2009). PIAS proteins: pleiotropic interactors associated with SUMO. *Cell Mol. Life Sci.* 66, 3029–3041. doi:10.1007/s00018-009-0061-z

Sachdev, S., Bruhn, L., Sieber, H., Pichler, A., Melchior, F., and Grosschedl, R. (2001). PIASy, a nuclear matrix-associated SUMO E3 ligase, represses LEF1 activity by sequestration into nuclear bodies. *Genes Dev.* 15, 3088–3103. doi:10.1101/gad.944801

Sager, R. A., Backe, S. J., Dunn, D. M., Heritz, J. A., Ahanin, E., Dushukyan, N., et al. (2024). SUMOylation of protein phosphatase 5 regulates phosphatase activity and substrate release. *EMBO Rep.* 25, 4636–4654. doi:10.1038/s44319-024-00250-2

Sapetschnig, A., Rischitor, G., Braun, H., Doll, A., Schergaut, M., Melchior, F., et al. (2002). Transcription factor Sp3 is silenced through SUMO modification by PIAS1. *EMBO J.* 21, 5206–5215. doi:10.1093/emboj/cdf510

Selkoe, D. J. (2002). Alzheimer's disease is a synaptic failure. *Science* 298, 789–791. doi:10.1126/science.1074069

Spence, E. F., and Soderling, S. H. (2015). Actin out: regulation of the synaptic cytoskeleton. *J. Biol. Chem.* 290, 28613–28622. doi:10.1074/jbc.R115.655118

Stephan, J. S., Fioriti, L., Lamba, N., Colnaghi, L., Karl, K., Derkatch, I. L., et al. (2015). The CPEB3 protein is a functional prion that interacts with the actin cytoskeleton. *Cell Rep.* 11, 1772–1785. doi:10.1016/j.celrep.2015.04.060

Tang, L. T., Craig, T. J., and Henley, J. M. (2015). SUMOylation of synapsin Ia maintains synaptic vesicle availability and is reduced in an autism mutation. *Nat. Commun.* 6, 7728. doi:10.1038/ncomms8728

Tatham, M. H., Jaffray, E., Vaughan, O. A., Desterro, J. M., Botting, C. H., Naismith, J. H., et al. (2001). Polymeric chains of SUMO-2 and SUMO-3 are conjugated to protein substrates by SAE1/SAE2 and Ubc9. *J. Biol. Chem.* 276, 35368–35374. doi:10.1074/jbc.M104214200

Van Niekerk, E. A., Willis, D. E., Chang, J. H., Reumann, K., Heise, T., and Twiss, J. L. (2007). Sumoylation in axons triggers retrograde transport of the RNA-binding protein La. *Proc. Natl. Acad. Sci. U. S. A.* 104, 12913–12918. doi:10.1073/pnas.0611562104

Verde, E. M., Antoniani, F., Mediani, L., Secco, V., Crotti, S., Ferrara, M. C., et al. (2025). SUMO2/3 conjugation of TDP-43 protects against aggregation. *Sci. Adv.* 11, eadq2475. doi:10.1126/sciadv.adq2475

Vertegaal, A. C. O. (2022). Signalling mechanisms and cellular functions of SUMO. *Nat. Rev. Mol. Cell Biol.* 23, 715–731. doi:10.1038/s41580-022-00500-y

Vertegaal, A. C., Andersen, J. S., Ogg, S. C., Hay, R. T., Mann, M., and Lamond, A. I. (2006). Distinct and overlapping sets of SUMO-1 and SUMO-2 target proteins revealed by quantitative proteomics. *Mol. Cell Proteomics* 5, 2298–2310. doi:10.1074/mcp.M600212-MCP200

Wada, H., Maruyama, T., and Niikura, T. (2024). SUMO1 modification of 0N4R-tau is regulated by PIASx, SENP1, SENP2, and TRIM11. *Biochem. Biophys. Rep.* 39, 101800. doi:10.1016/j.bbrep.2024.101800

Wang, Z., Liu, Y., Zhang, J., Ullah, S., Kang, N., Zhao, Y., et al. (2020). Benzothiophene-2-carboxamide derivatives as SENPs inhibitors with selectivity within SENPs family. *Eur. J. Med. Chem.* 204, 112553.

Watanabe, M., Takahashi, K., Tomizawa, K., Mizusawa, H., and Takahashi, H. (2008). Developmental regulation of Ubc9 in the rat nervous system. *Acta Biochim. Pol.* 55, 681–686. doi:10.18388/abp.2008_3027

Wei, X., Wang, B., Yang, Y., Fang, Z., Yi, C., Zhang, L., et al. (2025). Crosstalk between SUMOylation and ubiquitination controls the stability of transcription factor zinc finger protein 24: a novel antitumor mechanism in bladder cancer. *Oncogene* 44, 2762–2777. doi:10.1038/s41388-025-03450-9

Wolfe, M. S., and Haass, C. (2001). The Role of presenilins in gamma-secretase activity. *J. Biol. Chem.* 276, 5413–5416. doi:10.1074/jbc.R000026200

Wu, Y., Lin, B., Xie, Z., Huang, J., Qiu, Y., Chen, X., et al. (2025). SUMOylation of RAD51 upregulates GOLPH3 expression and promotes cisplatin resistance in colon cancer cells by Sp1 transcriptional activity. *Biochem. Pharmacol.* 236, 116888. doi:10.1016/j.bcp.2025.116888

Yang, W., Sheng, H., and Wang, H. (2016). Targeting the SUMO pathway for neuroprotection in brain ischaemia. *Stroke. Vasc. Neurol.* 1, 101–107.

Yang, Y., Tse, A. K., Li, P., Ma, Q., Xiang, S., Nicosia, S. V., et al. (2011). Inhibition of androgen receptor activity by histone deacetylase 4 through receptor SUMOylation. *Oncogene* 30, 2207–2218. doi:10.1038/onc.2010.600

Yang, Q., Tang, J., Xu, C., Zhao, H., Zhou, Y., Wang, Y., et al. (2020). Histone deacetylase 4 inhibits NF-κB activation by facilitating IκBα sumoylation. *J. Mol. Cell Biol.* 12, 933–945. doi:10.1093/jmcb/mjaa043

Yucel, B. P., Al Momany, E. M., Evans, A. J., Seager, R., Wilkinson, K. A., and Henley, J. M. (2023). Coordinated interplay between palmitoylation, phosphorylation and SUMOylation regulates kainate receptor surface expression. *Front. Mol. Neurosci.* 16, 1270849. doi:10.3389/fnmol.2023.1270849

Zhang, Y. Q., and Sarge, K. D. (2008). Sumoylation of amyloid precursor protein negatively regulates Abeta aggregate levels. *Biochem. Biophys. Res. Commun.* 374, 673–678. doi:10.1016/j.bbrc.2008.07.109

Zhang, Z. Y., Harischandra, D. S., Wang, R., Ghaisas, S., Zhao, J. Y., Mcmonagle, T. P., et al. (2023). TRIM11 protects against tauopathies and is down-regulated in Alzheimer's disease. *Science* 381, eadd6696. doi:10.1126/science.add6696

Zhang, W., Li, Z., Wang, X., and Sun, T. (2024). Phase separation is regulated by post-translational modifications and participates in the developments of human diseases. *Heliyon* 10, e34035. doi:10.1016/j.heliyon.2024.e34035

Zhao, X., Sternsdorf, T., Bolger, T. A., Evans, R. M., and Yao, T. P. (2005). Regulation of MEF2 by histone deacetylase 4- and SIRT1 deacetylase-mediated lysine modifications. *Mol. Cell Biol.* 25, 8456–8464. doi:10.1128/MCB.25.19.8456-8464.2005

frontiers | Frontiers in Physiology

TYPE Review
PUBLISHED 09 October 2025
DOI 10.3389/fphys.2025.1671271

OPEN ACCESS

EDITED BY
Roberto Piacentini,
Catholic University of the Sacred Heart, Italy

REVIEWED BY
Christian Hansel,
The University of Chicago, United States
Taegon Kim,
Korea Institute of Science and Technology, Republic of Korea

*CORRESPONDENCE
Stefano Masoli,
stefano.masoli@unipv.it
Egidio D'Angelo,
dangelo@unipv.it

RECEIVED 22 July 2025
ACCEPTED 19 September 2025
PUBLISHED 09 October 2025

CITATION
Masoli S, Rizza MF, Moccia F and D'Angelo E (2025) The spiny relationship between parallel fibers, climbing fibers, and Purkinje cells. *Front. Physiol.* 16:1671271. doi: 10.3389/fphys.2025.1671271

The spiny relationship between parallel fibers, climbing fibers, and Purkinje cells

Stefano Masoli[1]*, Martina Francesca Rizza[1], Francesco Moccia[2] and Egidio D'Angelo[1,3]*

[1]Department of Brain and Behavioral Sciences, University of Pavia, Pavia, Italy, [2]Department of Medicine and Health Sciences "V. Tiberio", University of Molise, Campobasso, Italy, [3]Digital Neuroscience Center, IRCCS Mondino Foundation, Pavia, Italy

Cerebellar Purkinje cells are one of the most complex neurons in the central nervous system and are well known for their extensive dendritic tree dotted by dendritic spines. PC spines receive excitatory synapses from parallel and climbing fibers and, although their morphological properties are comparable to those of other neuronal types, they show distinct extracellular and intracellular regulatory properties. Purkinje cell spine protrusion and helical patterning do not require nearby axons, as e.g., in pyramidal cells. Instead, Purkinje cell spines require structural proteins located on parallel and climbing fibers for their stabilisation and maintenance. The total spine number is influenced by scaffold proteins and eventually reflects the total dendritic length and local spine density. Purkinje cell spines were supposed to range up to over 10^5 in rodents and 10^6 in humans, but recent experimental data show that spines are less numerous than initially thought. Instead, they are endowed with mechanisms designed to improve their efficiency and differentiation. Some spines are double-headed, thereby enhancing Purkinje cell responses when the companion parallel fiber is stimulated. Other spines are single-headed and presumably endowed with slow neurotransmission mechanisms. Latest experimental data showed that glial cells modulate spines activity after a task or learning. Eventually, these multiple mechanisms can make each spine crucial in its own way for synaptic pattern recognition. In this review, we present the most recent advancements on Purkinje cell spines spanning their biochemical, structural, and functional properties, both in mice and humans, and propose a recalculation of the effective complement of spines and their activation by parallel fibers.

KEYWORDS

Purkinje cell, cerebellum, spines, synapses, history, parallel fibers

Introduction

The first description of "protoplasmic processes," currently called dendrites, was reported by Golgi in 1883, using his newly developed Golgi-method staining (Golgi, 1883; Bentivoglio et al., 2019). Five years later, the first image of cerebellar Purkinje cells (PC) spines was published by Santiago Ramón y Cajal but, until this seminal work, spines were discarded as staining artifacts (Ramón y Cajal, 1888; Yuste, 2015; Defelipe, 2025). Spines are small protrusions of a neuron cell membrane, canonically described with a mushroom-like shape, which can be observed on the dendrites and, sometimes, also on

the soma (Lackey et al., 2024). These protrusions are usually elicited by a nearby axon and consolidated through synaptic activity, but there are exceptions to this rule. Spines are quite common in the central nervous system (CNS) and can be found on both excitatory neurons, such as pyramidal neurons (PN) (Davidson et al., 2020), and inhibitory neurons, such as the PC (Lee et al., 2004; Lee et al., 2005), striatal medium spiny neurons (Lanciego et al., 2012), and dopaminergic neurons (Jang et al., 2015). Their primary role is to create a confined space in which a tightly interconnected biochemical machinery can modulate the strength of the postsynaptic responses (Nimchinsky et al., 2002). Cerebellar PCs are inhibitory neurons most known for expressing a huge quantity of spines on their extensive dendritic tree. Their spines retain most of the properties common to other neuronal types, but they also exhibit critical differences. Spines in PN are primarily generated and consolidated through synaptic activity, while in PCs, internal and external control proteins are required. Moreover, the presence of 10^3–10^5 spines on PC dendrites brought about issues of how they are generated, maintained, consolidated, silenced, and raised hypotheses on mechanisms that might limit their extensive coding space (Marr, 1969; Albus, 1971). It was proposed that not all spines have a presynaptic partner, that some are silent or covered by glial processes, and that some others generate only slow responses mediated by metabotropic glutamate receptors 1 (mGluR1). Recent experiments showed that the number of spines is lower than previously thought, with 30–50 thousand synapses in mice and 300–500 thousand synapses in humans. However, several spines receive more than one parallel fiber (PF) and glial cells would not silence spines but make them more specific for certain activities. Therefore, PC spines are endowed with complex mechanisms that eventually fine-tune neurotransmission and synaptic plasticity. This review considers the most recent experimental advancements on PC spines and the plethora of proteins that are involved in balancing this delicate system.

Cerebellum: Purkinje and granule cells

The cerebellum is highly convoluted and, in humans, it can account for approximately 80% of the neocortex surface (Sereno et al., 2020). It is divided into 10 lobules, and each lobule is composed of 3 layers, termed granular (GL), molecular (ML) and Purkinje cell layer (PL). The GL contains the tightly packed granule cells (GrC) (Nguyen et al., 2023) and the sparser Golgi (GoC), Lugaro and Unipolar Brush cells, with the latter located primarily in the vestibular lobuli (lobuli IX and X). The PL contains the soma of PCs, the soma of Bergmann glia (BG) and the candelabrum cells (Osorno et al., 2022). The ML contains multiple types of inhibitory interneurons, the PFs, climbing fibers (CF) and the extensive dendritic arborisation of PCs (Figure 1). The ML is the location where the extensive territory occupied by PF synapses intermingles with the territory occupied by a few thousands of CF synapses.

Cerebellar GrCs, in conjunction with PCs, form the conserved primary input/output pathway of the cerebellar network (van der Heijden and Sillitoe, 2021). These neurons evolved millions of years before the first PN appeared in a nervous system and, during their long life, acquired characteristics that differentiate them from other neuronal cell types. One of these

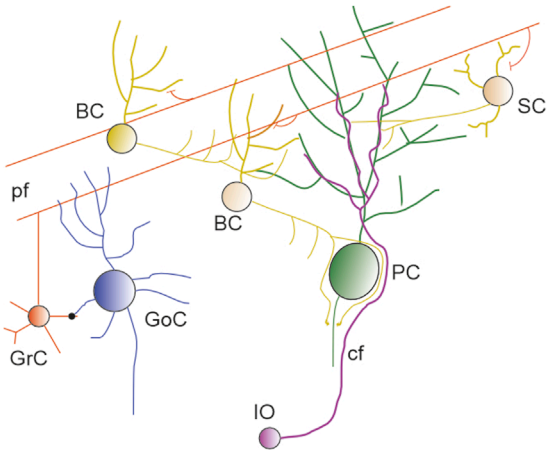

FIGURE 1
The cerebellar network. Schematics of the circuit showing GrC and PF (red), SC and BC (yellow and orange), PC (green), IO neuron and CF (violet), Golgi cells (blu).

differences was recently highlighted by studying the amount of unmethylated DNA contained in their nuclei. This amount was unusually high for neurons, making them closer to glial cells (Tian et al., 2022; Tan et al., 2023).

The Purkinje cell

PCs were described in 1837 by Johannes Evangelista Purkinje (Purkinje, 1837; Zárský, 2012; VoŽeh, 2015), who used the most advanced optical microscope available in the nineteenth century. Unfortunately, the limitations in the staining process restricted his study to the somatic region. Only in 1888, Santiago Ramón y Cajal, using an improved Golgi staining, described PC dendritic tree and spines (Golgi, 1883; Ramón y Cajal, 1888; Yuste, 2015).

It is one of the oldest neurons of the CNS and appeared in cartilaginous fishes 400 million years ago (Hibi et al., 2017; Mokhtar, 2020). These neurons are mostly known for their extensive and elaborated dendritic trees dotted by tens of thousands of spines. Even though not all species exhibit highly intricate dendritic trees (O'Brien and Unwin, 2006), they all have in common the presence of dendritic spines. This means that, over time, certain morphological properties were adapted by the evolution, while others were improved to support complex behaviour. Recent technical advancement showed that PCs are not a single family limited to just Zebrin- and Zebrin+ but there are multiple variants in zebrafish (Magnus et al., 2023) and up to eleven PC subtypes in mice (Khouri-Farah et al., 2025). In humans, the morphological evolution led to up to three distinct trees attached to the same soma (Busch and Hansel, 2023).

The importance of PCs as a computational powerhouse, in connection with the excitatory input transmitted from GrCs and the remainder of the neurons forming the cerebellar network, can be summarised by the wide range of abilities showed by the cerebellum. It is a motor coordination system (movement, balance) (Morton and Bastian, 2004), it is involved in higher cognition (Schmahmann,

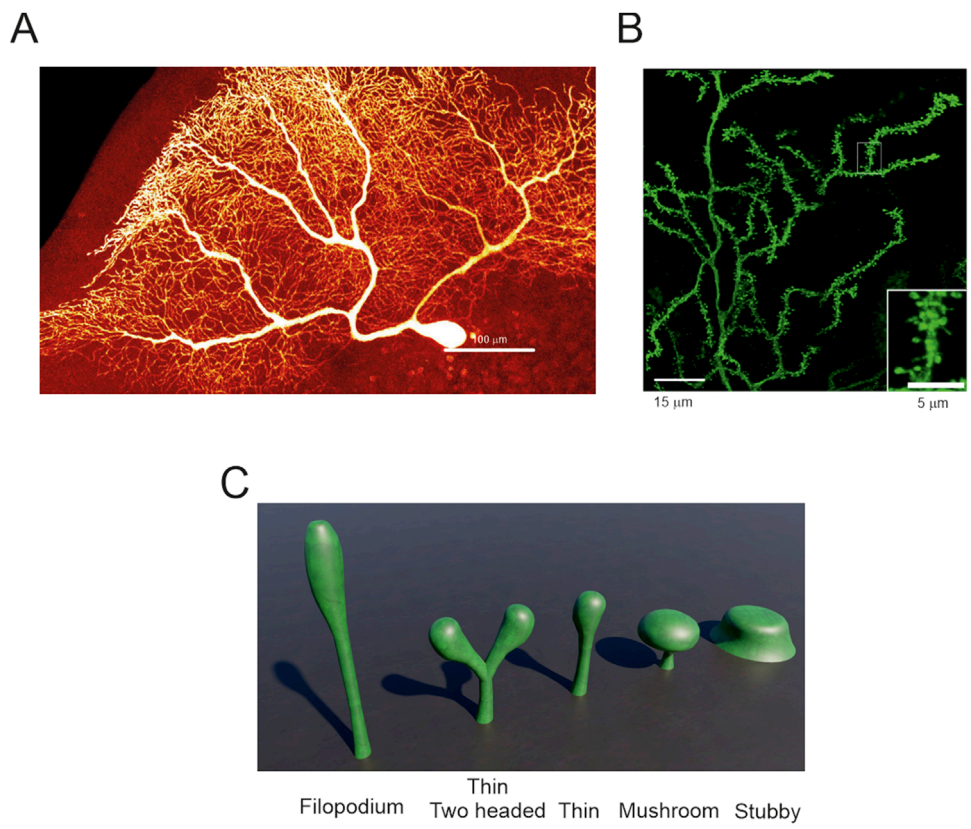

FIGURE 2
Purkinje cells spines – **(A)** Human PC reconstructed from post-mortem tissue (Masoli et al., 2024). At this resolution, spines are not evident. **(B)** Zoom-in of a portion the image in A showing spines decorating the dendrites. The inset further enlarges a dendrite crowded with many spines (modified from (Masoli et al., 2024)). **(C)** Typical spine shapes that can be found in PCs and in other neuronal types. The most common is the thin spine shape and, in PCs, 15% can have two heads (image built with Blender 3.6).

2019), fear responses (Liu et al., 2010), language (Desmond and Fiez, 1998), emotion and sociality (Van Overwalle, 2024). Spinocerebellar ataxias (SCAs), which are progressive, degenerative, genetic diseases, are linked to multiple DNA mutations leading to various degrees of PC malfunctioning. In some cases mutations are so extreme to cause PC death through suppression of their intrinsic firing by hyperexcited ML interneurons (SCA1), by a reduction in Cav2.1 calcium (Ca^{2+}) channel activity (SCA3), or a reduction of potassium (K^{+}) channels currents (SCA6) (Hills et al., 2013; Hoxha et al., 2018; Huang and Verbeek, 2019; Egorova et al., 2023; Zhu et al., 2024). The cerebellar involvement in neurodegeneration was reported in Alzheimer's disease (Mavroudis et al., 2019) and in Parkinsonism, where PC axonal dysfunction contributes to essential tremor (Schmahmann, 2019). Numerous physiological, biochemical and morphological studies of single cerebellar cells have been performed extensively on rodents, both in healthy and diseased conditions. The same approach can be used in humans only in very specific cases for ethical and technical reasons. This limitation can be mitigated by using non-invasive techniques that, although not providing the same quality data as single-cell recordings, can provide information useful to compare mice and humans. Unfortunately, as recently reported, the cerebellum is not taken into consideration in neurodegenerative disorders and is often neglected in multiple imaging studies (Wang et al., 2025).

The granule cell, ascending axon and parallel fibers

Mice GrCs have a compact morphology with just three to six dendrites (Nguyen et al., 2023) and occasional branches (Houston et al., 2017). Some examples of the human GrC were reconstructed from *ex vivo* tissues, showing only three dendrites and a soma comparable in size with mice (Jacobs et al., 2014). The small dimension of the somato-dendritic sections makes them the most common neuron in the entire CNS (Tan et al., 2023). Their thin axon is split into an ascending axon (AA) followed by two PFs oriented in opposite directions (Palay and Chan-Palay, 1974b; Huang and Huang, 1998; Heck and Sultan, 2002). When an AA enters the ML, it can make synapses with multiple spines of the same PC, with AA/PF ratio in the order of 5%–10% (Lu et al., 2009). Instead, PFs can reach over 3 mm length in rats (Huang and Huang, 1998) and an average of 6.64 mm length in rhesus monkeys (Mugnaini, 1983). These fibers are canonically reported to make a single synaptic contact with a single spine of each PC they encounter. Recently it was shown that a single PF can make two or even more contacts with spines located in different locations of the same dendritic tree (Loschky et al., 2022). Even though PF intersect multiple PCs along their pathway, they only establish a stable connection with approximately half of them (Nguyen et al., 2023; Park et al., 2023).

There are few sources estimating the total number of PFs. An *in vivo* study using a sparse labelling method showed 540 PFs for a 200 × 200 μm^2 section, accounting for just 0.38% of PFs in that section (Wilms and Häusser, 2015). The estimation for the total number of PF was about 142.000, which was in the same range as previously reported (Palay and Chan-Palay, 1974a). Another recent measurement performed on a 175 × 122 × 50 μm^3 EM slab reported 33.900 (Park et al., 2023), which was suggested to account for 76.9% of the total number of PFs passing through the section. The total number of PF that can hypothetically pass through the section could reach 42.500 PFs. This variation in the number of PFs depends on the conformation of each lobulus and differences in the ML thickness between each sulcus, apex and the tissue in-between them. The changes in the ML thickness were studied in human sections showing that most lobuli have a thickness between 300 and 340 μm (Zheng et al., 2023). The smallest thickness was identified in lobule X (170 ± 80 μm), while lobules I and II showed the maximum thickness (360 ± 110 μm). In human sections of 200 μm × 160 μm, the estimated total number of PFs was 33.515 ± 36.261 (Kuo et al., 2011). Despite the large range of variation, the upper bound estimates are consistent with previous reports. More experiments will be required to elucidate the variability of PF number in each lobule, in both human and rodents as well as in health and disease.

Purkinje cell spine properties

PCs are endowed with tens of thousands of spines that follow a helical pattern along the dendrites (O'Brien and Unwin, 2006; Parajuli et al., 2020) (Figures 2A,B). During mice development and until P20, spines are also expressed on the soma. They direct the CFs in the translocation process from the soma to the dendrites and *vice versa* for BC collaterals (Ichikawa et al., 2011). The requirement of having an intrinsic system to manage the spine distribution is a reflection of a profound difference with other neuronal types. PC spines follow the "Sotelo model," which states that spines are intrinsically generated during the first and second week of development and a nearby axon is not required for their protrusion (Sotelo and Dusart, 2009; Dusart and Flamant, 2012; Verslegers et al., 2014). In contrast, PNs and other neuronal types follow the "Millers–Peters model," which states that a spine can be protruded only when an axon and a dendrite are within a certain distance (Yuste and Bonhoeffer, 2004). It is a critical difference since a PC generates tens of thousands of PF - spine pairs with the ability to elaborate a near-infinite number of synaptic patterns. This supposed limitless in input/output could interfere with the encoding/decoding process in deep cerebellar nuclei (DCN), vestibular nuclei, and their transmission to the red nucleus and thalamus (Pugh and Raman, 2005; Gilbert and Rasmussen, 2025).

One neck, not always a single head

The most stereotyped spine shape is called "mushroom" since it looks like a mushroom. It is canonically used to illustrate the morphological, biochemical and biophysical properties of a spine because there is a clear distinction between two adjacent regions called "neck" and "head" (Risher et al., 2014). The neck is generated by the outward bending of the cellular membrane followed by the head, which forms its terminal part. The mushroom-like shape has a neck and a head of similar length, but the head is significantly wider than the neck. When the difference between neck and head diameters is small, and the neck is multiple times longer than the head, the spine is called "thin". If the difference in diameter and length between neck and head are non-existent, the spine is called "stubby". When a spine does not show a clear separation between neck and head, it is called a "filopodium" (Li et al., 2023) (Figure 2C). A recent clustering analysis showed that spines should not be classified in predefined categories because they are a "continuum of shapes" with multiple intermediate forms (Pchitskaya and Bezprozvanny, 2020).

In rats, 75% of PC spines were described "thin" and only 25% were stubby, mushroom-like or with more than one head (branched) (Lee et al., 2004). A similar proportion was identified in mouse and human morphologies, with a higher number of thin spines compared to stubby, mushroom, and branched spines (Busch and Hansel, 2025). A recent technical advancement allowed to discern that 15% of spines in awake mice, and 7% in sleeping mice, have two heads on a single neck and in rarer cases, even three heads for a single neck (Loschky et al., 2022). Branched spines with similar features were also described in mouse and human PCs (Busch and Hansel, 2025) and in mouse hippocampal neurons (Mohrmann et al., 2024) suggesting a possible conserved property. Moreover, a rare "spine cluster" was uncovered in human morphologies, in which a single giant head showed multiple swellings acting as single spine heads (Busch and Hansel, 2025). Currently, it is not known if each head of the "spine cluster" contains an active synapse.

The other important part of the spine, the neck, can be wrongly classified by the low resolution of two photon microscopy and optical microscopes. This issue can increase the total number of stubby spines compared to the other known types (Tønnesen et al., 2014). In the majority of neuronal types, spines, necks and heads lay on the same plane but, in PCs, some heads can reach a 60° angle compared to the neck (Parajuli et al., 2020). Post Synaptic Densities (PSDs) are usually placed at the top centre of the postsynaptic membrane, but PC spines can angle their heads so the PSD can switch position and be placed even on the side of the head. With this flexibility, they can generate more occasions to find a nearby PF to establish a contact (Parajuli et al., 2020).

Total surface area and dendritic length

In mammals, the width covered by PC dendritic trees passes from an average of 180 μm in P27 mice (Wilms and Häusser, 2015), to 300 μm in P90 Guinea pigs (Rapp et al., 1994) and to an average of 700 μm in 50–90 years old humans (Jacobs et al., 2014; Masoli et al., 2024; Busch and Hansel, 2025). The extensive dendritic tree in conjunction with rather large soma, averaging 20 μm in P27 mice and 35 μm in adult humans (Masoli et al., 2024), restricts the number of PCs to about 0.5% of all the neurons in the cerebellum (Tan et al., 2023). The total dendritic length, along with the linear spine density, is widely used to calculate the total spine number, which can vary among the cells. Since PCs are embedded in a 3D space, they do

not occupy it entirely but are constrained by multiple parameters. The location in a lobule (apex or sulcus) (Nedelescu and Abdelhack, 2013) and the thickness of the ML (Liu et al., 2021; Zheng et al., 2023) dictate the overall shape of the dendrites and their extension. The same space contains other neurons (Stellate cells, Basket cells, candelabrum cells), fibers (PFs and CFs) and glial cells (Bergmann glia). Moreover, the cerebellar microvasculature contributes to the overall reduction of the space available for dendritic expansion. These factors can all limit the extension of their dendritic tree and the total number of spines. As summarized in Table 1, the total dendritic length can range from an average of 2,782.59 ± 671.12 µm in P27 mice (Masoli et al., 2024) to 7,900 µm in P63 mice (Gao et al., 2011; Takeo et al., 2021). In humans, it can range from 9,507 ± 1,053.13 µm (Mavroudis et al., 2021) to 63,645 ± 4,572 µm (Busch and Hansel, 2025). In all cases, the reported dendritic length may be underestimated due to the incomplete reconstruction of some thin dendrites. According to the data in Table 1, the variability reported above, and the type of technique used to reconstruct dendrites and spines (Li et al., 2023), the most common dendritic length ranges between 4,000 and 7,000 µm in mice and between 30,000 and 70,000 µm in humans. The human datasets are still very limited, and there are cases in which the total length amounts to only 10,000 µm, despite the use of good quality tissue sources and technique (Masoli et al., 2024).

Spine number per unit length

The number of spines for linear micron can vary between different studies, depending on the overall quality of the tissue and/or the techniques used. Usually, the number of spines is calculated from single dendritic branches using an optical microscope or from digitised images using confocal microscopes (Li et al., 2023). The stacked images, with the aid of specific software, can be reconstructed into a file and visualised with a computer to better study the distribution of spines in a 3D space (Gao et al., 2011; Busch and Hansel, 2025). The most cited estimates reported 4.5 spines/µm in feline PCs (Palkovits et al., 1971) and 17.2 spines/µm in rats (Napper and Harvey, 1988). While most reconstructions reported an average of 2 spines/µm, other studies reported 1.4 spines/µm (Gao et al., 2011) or up to 5.1 ± 0.61 (Busch and Hansel, 2025) or 7.1 ± 1.693 spines/µm (Parajuli et al., 2020). The spine number per unit length did not show associations with mice treatment, learning tasks or enriched environment, which are factors known to stimulate spinogenesis (Gelfo et al., 2016; Stevenson et al., 2021). Neither age nor animal strain appeared to exert an effect. Similar values were reported in human PCs, although with a limited number of investigations showing an average of 2 spines/µm. Recent human reconstructions showed an average of 6.9 ± 0.77 spines/µm (Busch and Hansel, 2025). The average distribution of spines, taken from various publications, is summarised in Table 2. The spine number per unit length obtained with most recent techniques and high-quality tissue can range between 4 and 8 spines/µm. In human, as previously discussed, the range was shown to range between 6 and 7 spines/µm (Busch and Hansel, 2025). It is not yet possible to define if 6 spines/µm is the lowest value since similar analyses were performed on high-quality tissue and yielded 2 spines/µm (Masoli et al., 2024). The human datasets do not yet cover the entire cerebellum, and regional differences can be a lot more critical compared to mice.

Spine number estimates

Early estimates of PC spines

One of the first estimates of the number of PC spines ranged between 80,000 and 100,000 spines in the feline cerebellum (Palkovits et al., 1971). This value was estimated considering 4.5 spines/µm, which matches current studies on rodents. However, the total dendritic tree length was not provided, making it difficult to assess the number of spines. Another estimate was performed on rat PCs and proposed 17.2 spines/µm. This value was multiplied by a total dendritic length of 9,941.5 µm, which was an average value obtained from a previous study (Palay and Chan-Palay, 1974a) yielding 175,000 spines per PC (Napper and Harvey, 1988). Compared to common spine estimation techniques, this approach was not based on the number of spines/µm but on an equation using spine volume densities as the main parameter (Napper and Harvey, 1988). This estimation, which is often used for reference, does not match the majority of experimental recordings and, even in the best cases, it is six-seven times larger than reality. Based on these numbers, many authors estimated that human PCs could reach up to one million spines or even more (Huang et al., 2014), but this value has recently been disproven (Busch and Hansel, 2025).

Estimates based on the latest experimental data

As detailed in Table 1, the most common quantification of the spine density in mice and humans is 2 spines/µm. The average mouse dendritic length is approximately 5,000 µm, which, with 2 spines/µm, gives space to a maximum of 10,000 spines. Based on recent detailed morphological reconstructions, the spine number per unit length in mice can range up to 5.1 ± 0.61 (Busch and Hansel, 2025) or even 7.1 ± 1.693 (Parajuli et al., 2020) spines/µm. Even in these cases, with the same 5,000 µm dendritic length, the maximum number of spines increases up to a value ranging between 25,000 and 35,000 spines. Taking into consideration the longest recorded mouse dendritic tree (7,900 µm) (Takeo et al., 2021), and the highest number of spines/µm (7 ± 1.693) (Parajuli et al., 2020), the total number would reach 55,300 spines. Using the maximum spine density (6.81 ± 0.77 spines/µm) (Busch and Hansel, 2025) and the maximum dendritic length (63,645 ± 4,572 µm) (Busch and Hansel, 2025) reported in the human tissue, a similar calculation yields ~470,000 spines, which is still only 47% of the proposed estimate of about one million. The estimates provided in Table 1 are primarily obtained from pieces of spiny dendrites and overlook differences in spine distribution due to regional variability or the absence of spines on main dendritic trunks. The most recent experimental data (Busch and Hansel, 2025) showed that human spines cover more dendritic length (95%) compared to mice (87%). This could mean that human PC have more spiny dendrites even in presence of multiple main trunks stemming from the soma.

TABLE 1 Total dendritic length and age. The table shows the age and the total dendritic length, which in some cases were estimated from graphs. The range is rather variable from 2 mm to 8 mm in mice. The variability is similar in human but on an order of magnitude more ranging from 9 mm to 67 mm.

Dendritic length (μm) (e = estimate from graphs)	Age	Paper
Mice		
2,782.59 ± 671.12	P27	Masoli et al. (2024)
4,430 ± 30	Various ages	Kumar et al. (2016)
6,004 ± 831	10–12 weeks	Busch and Hansel (2025)
7,000 (e)	P21	Liu et al. (2022)
2,500 (e)	P10	Takeo et al. (2021)
5,100 (e)	P14	
7,500 (e)	P21	
7,900 (e)	P63	
7,500 (e)	5–6 weeks	Gao et al. (2011)
Rats		
5,620.25 ± 2,504.09	P12-P21	Roth and Hausser (2001)
Humans		
10,500 (e)	Average 73	Mavroudis et al. (2019)
11,658.5 ± 5,734.2	Elderly	Louis et al. (2014)
(Vermis) 9,507 ± 1053.13	65.6 ± 6.0	Mavroudis et al. (2021)
(Hemispheres) 10,757.3 ± 1,666.24		
20,166.96 ± 15,248.58	50 and 90	Masoli et al. (2024)
63,645 ± 4,572	Various ages (>37)	Busch and Hansel (2025)

Fewer spines than expected but more critical than hypothesised

Based on the information given above, the total spine number is lower than the most cited estimations, but this reduction may not be a negative factor after all. The question turns into how synaptic integration over fewer spines can generate an effective response able to modulate DCN and the vestibular nucleus (Gilbert and Rasmussen, 2025). Due to the initial estimate of a very high number of spines, one argument used to reduce their total number was that ~90% of them had no presynaptic partner, i.e., they were silent (Isope and Barbour, 2002). This hypothesis has recently been challenged by the discovery that 92.7% of spines do present a synapse (Loschky et al., 2022). Thus, the number of spines is lower than initially thought, but the number of spines featuring a synaptic connection is significantly higher. This evidence is in accordance with recent estimates leveraging advanced recording techniques to show that, in mice, there are up to 42,000 PFs (Park et al., 2023), which would yield about 40,000 synaptic pairs (PF–spine) if 93% of them synapsed with a PC. In close agreement, a recent estimate of spine density and total dendritic length (Liu et al., 2022) allowed to calculate the number of ~35,000 spines, which we will use for all subsequent calculations (Figure 3).

A critical point is that not all the connected spines appear to have the same functional properties. Approximately 15.1% ± 3.6% of all spines are double-headed, receive one PF per head, and have been suggested to be more "eloquent" compared to the typical single headed spine (Loschky et al., 2022). The response of two or more PFs on the same spine can be elicited by the synchronous activation of GrCs, increasing their overall postsynaptic current and potentially resulting in a somatic response. Moreover, 16% of single-headed spines, which express mGluR1 mediated slow responses, may be critical in the overall synaptic pattern recognition. By combining this observation, 7% of synapses would remain orphan and therefore fully silent, 15% double-headed and fast-responding, and 78% single-headed, either slow-responding (16%) or partially

10.3389/fphys.2025.1671271

TABLE 2 Spines distribution in literature. The table contains experimental values collected in the literature about the average number of spines, the animal type and the age. Not all these data was available in the mentioned papers.

Number/micron linear	Type	Age	Paper
Mice			
1	C57/Bl6	Various	Kumar et al. (2016)
2	B6.Cg-Tg (Thy1-YFP)16Jrs/J	1-month old	Loschky et al. (2022)
2	Atoh1	P14	van der Heijden et al. (2021)
2	-	Adult	Peter et al. (2016)
2	C57BL/6N	4–6weeks	Toledo et al. (2019)
2	C57Bl6	(culture)	Campeau et al. (2013)
2	TLR4 knockout	4 months	Zhu et al. (2024)
2.2	C57BL/6N	6–12-18months	Hoxha et al. (2017)
2.7	Atxn2-CAG100-knock	9months	Arsović et al. (2020)
2–3	C57BL	3–10weeks	Sugawara et al. (2013)
3	Sv129 3 C57Bl/6	P78 to P204	Vecellio et al. (2000)
4.5 superficial	C57BL/6N Cas 9	P21	Liu et al. (2022)
5.5 deep			Liu et al. (2022)
5.1 ± 0.61	C57BL/6J	10–12 weeks	Busch and Hansel (2025)
7.10 ± 1.693	C57BL/6 male	12 weeks	Parajuli et al. (2020)
Rat			
1.1	-	5 weeks	Huang et al. (2012)
1.9			Huang et al. (2012)
2.07 ± 0.42 (Proximal)	Colture	-	Heintz et al. (2016)
2.93 ± 0.88 (Distal)			Heintz et al. (2016)
Camel			
1.2 and 2.2	-	-	Al-Hussain et al. (2022)
Human			
0.937 ± 0.93 (vermis)		65.6 ± 6.0 years old	Mavroudis et al. (2021)
0.98 ± 0.68 (Hemispheres)			Mavroudis et al. (2021)
1	-	Elderly	Louis et al. (2014)
1	-	Everage 73 years old	Mavroudis et al. (2019)
2	-	50 and 90 years old	Masoli et al. (2024)
6.81 ± 0.77 (Average) 5.37 ± 0.82 (Thin head) 0.49 ± 0.44 (large mushroom)	-	Various ages	Busch and Hansel (2025)

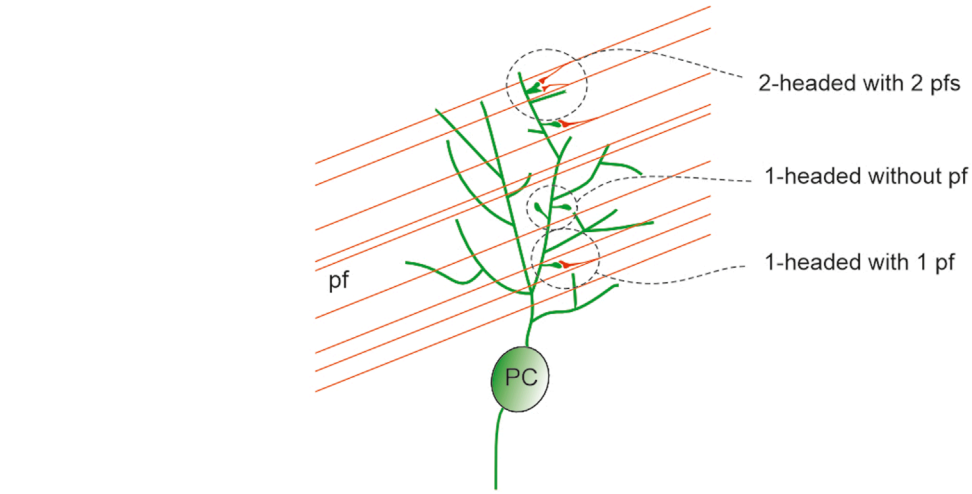

		x	y	z
	Spine counts	% spines	# spines	# pf
a	Total number	**100**	**35000**	
b	With pf	**92.7**	32445	
c	2-headed with 2 pfs	**15**	5250	10500
d	1-headed with 1 pf	78	27195	27195
e	1-headed without pf	7	2555	
f	Total number of pf crossing the PC dendritic tree			75390

FIGURE 3
Total spine number and parallel fibers interaction – Schematics of PFs passing through the PC dendritic tree and of their connectivity with the PC spines. The insets illustrate the three main types of spine contacts. The table shows calculations of the number of spines (green) and PFs (red). Numbers in bold are derived from literature. The total number of spines, 35000, was taken from (Liu et al., 2022), the percentage of spines contacted by PFs and of double-headed spines was taken from (Loschky et al., 2022). The number of PFs crossing the PC dendritic tree is calculated assuming a contact rate of 50% (Park et al., 2023).

silenced by glial cells (see below). This picture yields an estimate of up to a maximum of 85% putative silent synapses, approaching earlier estimates of 90% (Isope and Barbour, 2002; Brunel et al., 2004), but redefining their nature to include, in addition to null responses, also slow and partial responses.

As a special morphological feature of PCs, each spine is surrounded by BG, which forms multiple types of peri-synaptic astrocytic processes (PAPs) (Tao-Cheng, 2025). This affects the computation of active spines since glial cells can remodel spine structure by nibbling pieces of the spine membrane, a process that was reported to modulate their activity after learning (Morizawa et al., 2022). This is in contrast to another hypothesis, claiming that glia covered spines to make them unresponsive (Lippman Bell et al., 2010).

In aggregate, the count of active spines on the PC dendritic tree is complicated not just by the anatomical connectivity but also by specific processes that can regulate their effectiveness. To summarise, even though the average number of spines is probably ~35,000 in mice and ~360,000 in humans, 93% are connected to a presynaptic partner, 15% (double-headed) have high efficiency, while 78% (single-headed) have low efficiency (either modulated by glial PAPs or generating slow metabotropic responses). Similarly, the number of PFs effectively conveying information to a PC is also difficult to establish. It has been reported that PCs make synapses only with about half of the PFs traversing their dendrites (Nguyen et al., 2023; Park et al., 2023), amounting to ~76,000 PFs crossing the PC dendritic tree, with ~27,000 synapsing on double-headed spines and ~10,000 synapsing on single-headed synapses (Figure 3).

Molecular properties of Purkinje cell spines

Even thou the total spine number is lower than the original estimates, it does not detract from the fact that each spine is

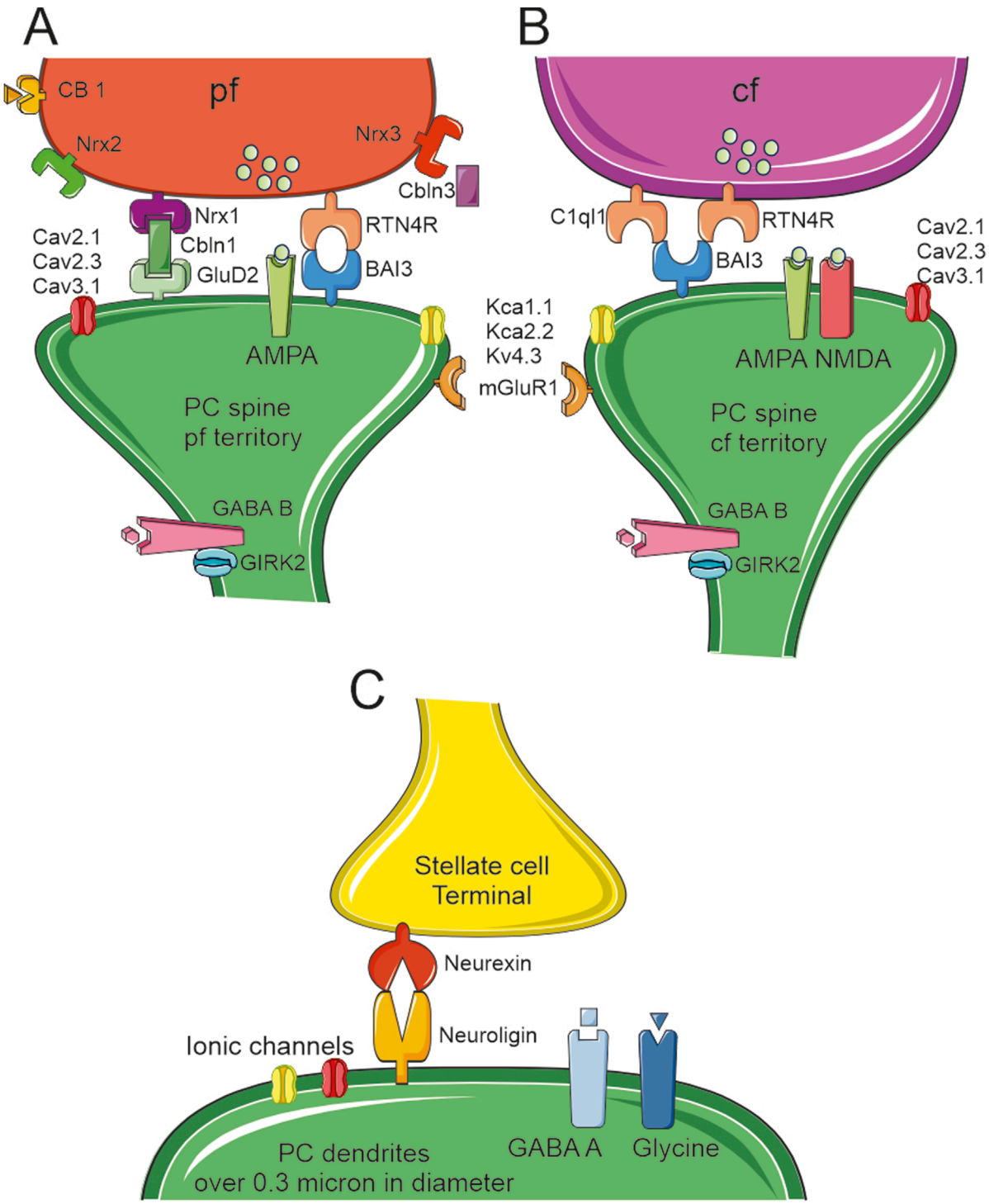

FIGURE 4
Proteins linking the pre and post synaptic sides. Schematic drawing of the main molecular components of PC spine synapses. **(A)**The PF terminal expresses three types of neurexin (nrx1-2–3) with nrx1 linked to the postsynaptic GluD2 through cerebellin (Cbln3). This is the main system that keeps PF and PC spines connected together. A second system, RTN4R and BAI3, can be found in some PF–PC synapses (although this complex is more typically expressed in CF–PC synapses). These spines expressed AMPA receptors, three types of Ca^{2+}channels (Cav2.1, Cav2.3, Cav3.1), and three types of K^{+}channels (KCa1.1, KCa2.2 and Kv4.3). The GABAB receptor is expressed on the spine neck along with GIRK2. **(B)**The CF terminal expresses RTN4R and C1ql1 linked to the postsynaptic BAI3. This is the main system that keeps CF and PC spines connected together. The CF spines express both AMPA and NMDA receptors, and (possibly) the same three types of $Ca^{2+}$and K^{+}channels as the PF spines. As in PF spines, CF spines express the GABA B receptor and GIRK2 on the spine neck. **(C)**The stellate cell synaptic terminals end on PCs dendrites and they are kept in place by presynaptic Neurexin and postsynaptic Neuroligin. The postsynaptic side hosts GABAA and Glycine receptors. PCs dendrites have multiple types of ionic channels that can change depending on their diameters [for reference supplemental materials (Masoli et al., 2024)].

covered and contains multiple protein types and enzymes. These can be broadly subdivided into: a) structural proteins, which are fundamental to preserve the connection with the presynaptic side (i.e., PF and CF) through a series of transmembrane and secreted proteins; b) ionic channels and synaptic receptors, which allow the generation of action potentials and local increases in the intracellular Ca^{2+} concentration; and c) structural proteins and enzymes involved in the control of synaptic plasticity, Ca^{2+} buffering and receptors turnover.

Structural proteins between spines and parallel fibers

The tripartite complex that stabilises PF-PC spines require: a) the GluD2 receptor on the spine surface, b) the neuropeptide cerebellin (Cbln1), and c) the presynaptic cell adhesion protein neurexin (Nrxn) on the PF membrane (Paul et al., 2024).

The GluD2 receptor

A critical structural protein is the GluD2 receptor (Kakegawa et al., 2009; Burada et al., 2022), whose structure was recently reconstructed with cryo-EM microscopy (Burada et al., 2020). GluD2 is a member of the glutamate receptor (iGluR) family encoded by the *GRID2* gene and has long been regarded as an "orphan" receptor, as it is not gated by glutamate (Naur et al., 2007; Yuzaki and Aricescu, 2017; Brunetti et al., 2024). It can act as an ionotropic receptor only in the Lurcher mutation (p.Ala654Thr), in which the protein quaternary structure is twisted in a constitutively open state (Selimi et al., 2003). This abnormal open state can be closed by D-serine or Glycine (Itoh and Yuzaki, 2024) and enhanced by extracellular Ca^{2+} (Hansen et al., 2009). In both cases, the alteration in GluD2 activity can push PCs into a hyper-excited state that ultimately leads to cell death in about two post-natal weeks. When the cerebellum is still immature, D-serine released by BG is critical to generate long-term depression (LTD) because GluD2 regulates the trafficking of AMPA (α-amino-3-hydroxy-5-methyl-4-isoxazole propionate) receptors (Kakegawa et al., 2011). The receptor is primarily expressed in cerebellar PCs (Itoh and Yuzaki, 2024), while it is less abundant in cerebral and hippocampal neurons (Konno et al., 2014). In all cases, GluD2 promotes synaptogenesis (Khan, 2017), thereby increasing the number of spines (Spanaki et al., 2024). GluD2 stabilises spines and promotes postsynaptic LTD both in the immature and mature cerebellum (Kakegawa et al., 2011). Deletion of GRID2 causes ataxia in humans (Hills et al., 2013) and can be rescued in mouse cultures by injections of GluD1 in the PC soma (Ryu et al., 2012). Another critical activity performed by GluD2 is the separation of territories occupied by PF synapses and CF synapses. Its absence causes the aberrant development of CF collaterals and synapses in the PF territory (Ichikawa et al., 2016).

The adaptor protein complex 2 (AP-2) and Glutamate Receptor Delta 2 Interacting Protein 1 (GRID2IP) were recently found to be critical for the balance of PF-CF territories. Loss of the two AP-2 isogenes, i.e., Ap2a1 and Ap2a2, in PCs causes the degradation of GRID2IP and an increased expression of GluD2. This reduces the CF-PC territory and increases the PF-PC territory, making PCs more excitable. This leads to morphological degeneration, early PC death and Spino Cerebellar Ataxia type 1 (SCA1) (Tolve et al., 2025).

Cerebellin, an adaptor protein

There are four variants of the secreted protein Cbln, which are encoded by four genes (*Cbln1-4*) (Südhof, 2023). They can interact with both GluD1 and GluD2 and with the various Nrxn isoforms only if these contain an insert in the alternatively spliced sequence 4 (SS4) (Uemura et al., 2010). The first Cbln, as suggested by the name, was discovered in the cerebellum: it is secreted by cerebellar GrCs and interacts with Nrxn to form the tripartite complex that stabilizes PF-PC synapses. Cbln1 expression is quite low at birth, but it undergoes a 20-fold increase and thereby becomes the most expressed cerebellar isoform during the postnatal development. Conversely, Cbln2 is highly expressed before birth but is strongly downregulated during the postnatal phase and reaches a very low expression level in adulthood (Seigneur and Südhof, 2017). Cbln4 has a slim expression in the cerebellum, but it was recently shown that it is the first Cbln isoform downregulated in SCA2 (Arsović et al., 2020) followed by Cbln3, which is highly critical for the maintenance of PF-PC synapses. Cbln3 cannot be secreted from PFs unless it associates with Cbln1 and, when it reaches the synaptic cleft, accumulates and modulates Cbln1 activity. This activity was explored in mice with a KO for Cbln3, which increased sevenfold the expression of Cbln1. Instead, the KO of Cbln1 completely eliminated Cbln3 from the synaptic cleft (Bao et al., 2006; Iijima et al., 2007; Larsen, 2021). Cbln1 is also critical for downregulating the formation of inhibitory synapses, mainly from SCs, on the PC dendritic tree (Ito-Ishida et al., 2014b) (see the inhibitory section). It has recently been discovered that Cbln1 and GluD2 are not only critical for maintaining spines and their presynaptic partners, but even for the dendritic tree development. A total KO of GluD2 does not influence the shape of PC trees, but a sparse KO or an increase in Clbn1 and GluD2 proteins disrupts the morphological properties of PCs (Takeo et al., 2021).

Neurexin, type I cell adhesion protein

Three isoforms of Nrxn are encoded by three genes (*Nrxn1-3*) but they are highly rearranged through alternative splicing (Fuccillo et al., 2015; Südhof, 2017). Nrxns are so important for the survival of GrCs that a KO of these proteins is fatal even in cell cultures. This condition was reversed by the application of brain derived nerve factor (BDNF) and partially rescued by insulin-like growth factor-1 (IGF-1) (Uemura et al., 2022). BDNF is a neurotrophic factor that is postulated to have an autocrine or paracrine activity on GrCs axons. This substance is released by GrCs axon under control of Nrxns. They are critical for the creation of the presynaptic machinery, which is activity-induced through action potential-dependent Ca^{2+} entry. Multiple combinations of *Nrxn* KO showed that the different isoforms are interchangeable since the cerebellum shows no structural defects when only two out of three Nrxn isoforms (Nrxn1/2, Nrxn2/3 and Nrxn1/3) are genetically deleted (Uemura et al., 2022). Nrxn2 was found to be critically involved with Cbln1 in the regulation of GrCs axonal guidance and growth. These proteins act as cues during development and elongation of the axon in an autocrine manner (Han et al., 2022) Figure 4A.

Scaffold proteins between spines and climbing fibers

CFs are the terminal part of axons belonging to neurons located in the inferior olive nucleus. These fibers are critical to deliver the graded control correction signals capable of changing PC activity through the activation of PF-PC synaptic plasticity (Hansel et al., 2001; Coesmans et al., 2004; Jörntell and Hansel, 2006; Hoxha et al., 2016; Boele et al., 2018). The majority of PCs in mice shows a single trunk stemming from the soma, but PCs with two trunks stemming from the soma can be found in lobuli IX and X (Nedelescu et al., 2018). This is even more evident in human reconstructions, where three distinct branches were frequently observed (Busch and Hansel, 2023; 2025; Masoli et al., 2024). Similar to the previously defined tripartite complex, a complex of two proteins is required to stabilise a CF on PC spines: a) the secreted C1ql1 complement family protein and b) the brain angiogenesis inhibitor 3 (BAI3/ADGRB3) protein, which is an orphan receptor of the adhesion G-protein-coupled receptors (GPCR) (Sigoillot et al., 2015). Both GluD2 and BAI3 can be found in the immature PCs when the PF and CF synaptic territories are not yet defined. After the stabilisation of the synaptic territories, some spines belonging to the PF territory keep BAI3 on their membrane surface and connect RTN4R located on the PF presynaptic side (Paul et al., 2024). The presence of a single winner CF has been proved wrong for humans (Busch and Hansel, 2023) since there can be more than one depending on the number of main trunks. In some cases, more than one CF has been observed in rodents too (Nishiyama and Linden, 2004; Piochon et al., 2014). To guide the rodent CFs shift, transient somatic spines are generated lasting only until P20 and used by both CF and BC axon collaterals (Ichikawa et al., 2011). After P21, only the winner CF can be found on dendritic spines, showing a larger volume, extensive PSD and more AMPA receptors compared to somatic spines and dendritic spines of the looser CF. This process is coordinated by the Rab3-interacting molecule RIM, which can also be found in PFs (Nitta et al., 2025). Progranulin release by PCs acts as a retrograde signal activating sort1, which increases the release probability of the presynaptic terminals of the CF that have translocated from the soma to the dendrites (Uesaka et al., 2018). Dysregulation of either C1ql1 or BAI3 in the adult allows the formation of new synaptic contacts between nearby CF branches and the upper part of PC dendritic tree (Aimi et al., 2023). The KO of either Cbln1 or C1ql1 causes the disruption of at least 50% of PF and CF synapses (Paul et al., 2024). As observed upon the KO of GluD2, the absence of Cbln1 disrupts the CF territory, increasing its presence in territories normally occupied by PF synapses Figure 4B.

How structural proteins control inhibitory synapses

Early work described that BC collaterals interact with PC somatic spines for 2 weeks until P20 (Ichikawa et al., 2011). After this point in the development, no other evidence of inhibitory interneurons synapsing with PC spines was provided, not even SCs, which make synapses directly with dendrites. This is different compared with the morphological reconstructions and electrophysiological recordings performed in PNs, in which some spines are dedicated to receiving inhibitory synapses (Boivin and Nedivi, 2018). The absence of SC synapses on PC spines is due to the same Cbln1 that controls the PF territory. The number of SC and CF synapses was significantly increased in cerebellar slices from Clbn1/DluD2-deficient mice (Ito-Ishida et al., 2014a). This investigation further showed that the lack of Cbln1 also increased the density of the Vesicular Gaba Transporter (VGAT)-positive puncta, which are a marker of GABA- and glycine-containing inhibitory terminals (although with some regional differences in P11 mice). Since Cbln1-GluD2 signalling can control the territory occupied by VGAT, this finding confirms that the PF-PC synapses can hetero-synaptically control the generation and stabilisation of molecular layer interneurons (MLI)-PC synapses (Ito-Ishida et al., 2014a). Cbln1 finely regulates synaptogenesis through the Src-family protein tyrosine kinase (SFK) pathway (Ito-Ishida et al., 2014b). PC-expressed Neuroligin can interact with Nrxn expressed by MLI to generate the complex that stabilises these synapses (Südhof, 2008; Zhang et al., 2015; Park et al., 2018). The absence of Neuroligin or Nrxn can impair mature synapses but is not involved in synaptogenesis, which has been recently attributed to Dystroglycan. SC synapses cannot be found on spines since they do not co-localise with markers of excitatory synapses (Jahncke et al., 2025). Global KO of Neuroligin 2 reduced the inhibitory input from MLIs to PCs and suppressed pruning of CF synapses (Suk et al., 2025) (Figure 4C).

Ionic channels and receptors in PC spines

The majority of synaptic receptors, ionic channels and internal biochemical pathways which control the postsynaptic plasticity are within the conglomerate of scaffolding proteins forming the PSD (Harris and Stevens, 1988; Cramer and Gao, 2013; Chen et al., 2022).

Ionic channels

PCs are endowed with multiple voltage-dependent ionic channels distributed over the different cell compartments (Masoli et al., 2015). Some channels have an axosomatic expression, but the majority are somato-dendritic. Some have a higher expression on the proximal part of dendritic trees, whereas others cover the entire tree, including dendritic spines. The most known ionic channel, the P-type high voltage-activated (HVA) Ca^{2+} channel (Cav2.1) can be found everywhere and can act alone or cluster with big (BK, KCa1.1) and small conductance Ca^{2+}-dependent K^+ channels (SK2, KCa2.2) (Indriati et al., 2013; Luján et al., 2018a). The modulation of the spike amplitude is under control of A-type K^+ channel (Kv4.3) and the rebound excitation from negative potential is modulated by a low voltage-activated (LVA) Ca^{2+} channel (Cav3.1) (Otsu et al., 2014; Alfaro-Ruíz et al., 2020). The R-type HVA Ca^{2+} channel (Cav2.3) is found in spines, but is not critical in controlling the overall PC electrical responses (Otsu et al., 2014).

The physical length and the absence of voltage-dependent sodium or Ca^{2+} channels from the necks (Araya et al., 2006) can generate a local filtering system. The G-protein inward-rectifier K^+ channels 2 (GIRK2), expressed on both necks and heads (Luján et al., 2018b), could also act as a modulatory system. It can shunt the forward propagation of weak signals from the spine to the rest of the dendrite and, at the same, filter the back propagating spikes from the axosomatic compartments by promoting membrane hyperpolarization.

Ionotropic receptors (AMPA, NMDA)

The majority of neurons express both AMPA and NMDA receptors on their spines, whereas PCs express a majority of spines with only AMPA receptors. The absence of postsynaptic NMDA receptors can be due their presynaptic expression on PF (Schonewille et al., 2021). Postsynaptic NMDA receptors are instead expressed by spines belonging to the CF territory (Piochon et al., 2007; 2010). The AMPA receptor subtype expressed by human PC spines comprises all the known subunits (GluR1 – GluR4) in their flip and flop splice variants (Tomiyama et al., 1999). The highest expression was reported for GluR1 (Castejón and Dailey, 2009), GluR2 (Liu et al., 2010) and GluR3 (Loschky et al., 2022). AMPA receptors in PCs are almost impermeable to Ca^{2+} ions, since they contain the GluR2 subunit. This subunit is critical for the AMPA assembly since it controls receptor kinetics, conductance of single-channel, and Ca^{2+} permeability. The passage of Ca^{2+} is limited by the presence of an arginine residue at position 607 (R607) that introduces an additional positive charge in the pore (Isaac et al., 2007). According to recent experiments, Ca^{2+} permeability can be modulated by the transmembrane AMPAR regulatory protein (TARP) and cornichon auxiliary subunits, modifying the known properties of GluR2 subunits (Miguez-Cabello et al., 2025). The paired pulse facilitation of AMPA receptors differ depending on the source of the presynaptic innervation: AMPA receptors expressed by spines belonging to the PF territory present a strong facilitation (Schmidt, 2019), whereas those expressed in the CF territory showed a strong depression after a single pulse (Zhang et al., 2020). This difference has been proven, not only with electrophysiological approaches but also by assessing the expression of the glutamate transporters Vglut1 and Vglut2. The former is associated with the majority of PFs and the latter only with CFs (Mao et al., 2022). These AMPA receptors are assisted primarily by NMDA GluN2A subunits and, to a lesser extent, by GluN2B subunits (Renzi and Cull-Candy, 2007). GluN2A has a high opening probability that facilitates Ca^{2+} entry, whereas GluN2B has half the value of GluN2A opening probability but shows longer openings (Santucci and Raghavachari, 2008). These receptors, along with Cav2.1 Ca^{2+} channels, play a critical role in Ca^{2+}-dependent facilitation and depression (Kim et al., 2008; Benton and Raman, 2009; Adams et al., 2010).

PCs synthesise and release glutamate from their dendrites until the fourth postnatal week (Crépe et al., 2011). This autocrine activity on spine receptors is useful for depolarisation-induced suppression of excitation (DSE), and for depolarisation-induced potentiation of inhibition (DPI) (Crépe et al., 2011). Glial cells are usually in charge of clearing the excessive glutamate from the cleft, and this is one of the multiple activities performed by BG, which expresses the glutamate transporter EAAT2. Contrary to other neuronal types, PCs express the EAAT4 transporter in the spine perisynaptic region (Dehnes et al., 1998; Tao-Cheng, 2025). In postischemic mice, the low expression of this transporter causes excitotoxicity and cell death (Yamashita et al., 2006).

Three members of the ionotropic P2X receptors ($P2X_2$, $P2X_4$, and $P2X_6$), which are non-selective cation channels gated by ATP, have been detected on spines belonging only to PF territory (Rubio and Soto, 2001). These ionotropic receptors mediate both membrane depolarization and Ca^{2+} influx in some regions of the CNS (Mut-Arbona and Sperlágh, 2023), but their physiological role in cerebellar PCs is yet to be determined.

Metabotropic receptors (GABAB, mGluR1)

Compared to PNs, PCs do not have spines capable of receiving inhibitory inputs from GABAergic interneurons. However, spines belonging to both PF and CF territories express extra synaptic GABAB receptors, which can cluster with GIRK2 channels on spine necks and with Cav2.1. The activation of GABAB receptors enhances the depression of the synaptic currents (AMPA-mediated fast synaptic currents and mGluR-mediated slow synaptic currents) induced by glutamate in spine heads (Tabata and Kano, 2006) and is responsible for PC hyperpolarization (Luján et al., 2018b). The presence of GABAB receptors, GIRK2 ionic channels, and the correlation between neck lengths and electrical activity (Araya et al., 2006) could generate a filtering property that could reduce the noise to signal ratio of each spine.

Another major player in generating slow responses is mGluR1. The CF that wins the competition and becomes stabilised on PC specific main trunk is under control of mGluR1 located on spines, AMPA receptors located on PFs and NMDA receptors located on MLI (Nakayama et al., 2024). The cannabinoid receptor CB1 is located on the presynaptic PF (Buceta et al., 2020) and is stimulated by mGluR1 through a signalling cascade that generates 2-arachidonoylglycerol (2-AG) and anandamide as retrograde messengers (Marcaggi, 2015; Hoxha et al., 2016). This pathway is critical because it reduces the release probability of PF in a Ca^{2+}- and glutamate-dependent manner (Safo et al., 2006). Accordingly, mGluR1 stimulates phospholipase Cβ (PLCβ) to cleave phosphatidylinositol-4,5-bisphosphate (PIP_2) into inositol-1,4,5-trisphosphate (IP_3) and diacylglycerol (DAG) (Negri et al., 2020). DAG is hydrolyzed into 2-AG by DAG lipase and can thus serve as a retrograde messenger to reduce glutamate release from PFs (Safo et al., 2006). While DAG promotes the inhibitory inputs at the PF-PC synapse, the other branch of the signalling cascade, i.e., IP_3, maintains the presynaptic function by inducing the secretion of BDNF, which acts as a retrograde messenger to increase the glutamate release probability (Furutani et al., 2006). The chronic suppression of mGluR1 and IP_3 profoundly reduce the release probability. A similar activity can be induced by applications of BDNF (Furutani et al., 2006). The weight of DAG vs. IP_3 signalling at the PF-PC synapse could depend on their different rates of degradation upon PLCβ activation (Raghu et al., 2019; Joensuu et al., 2020).

Inside a PC spine

The intracellular molecular mechanisms of PC spines are highly specialized and include several enzymatic cascades, molecular motors, and a specialization of the endoplasmic reticulum (ER) called spine apparatus. These are instrumental in ensuring spine neurotransmission, plasticity, and motility.

Cytoplasmic molecules and the spine apparatus

The ER in PC dendritic spines is central to Ca^{2+} dynamics and synaptic plasticity. It regulates intracellular Ca^{2+} homeostasis, which is essential for synaptic function and plasticity. The ER network extends into the dendrites and spines with specialised sub domains, such as spine-associated ER and smooth ER tubules,

contribute to localised Ca^{2+} dynamics. The ER serves as a major Ca^{2+} store, modulating LTD and other forms of synaptic plasticity in PCs. Ryanodine receptors (RyRs) and IP_3 receptors (IP_3Rs) play key roles in Ca^{2+} release from the ER. This Ca^{2+} regulation is crucial for the function of cerebellar circuits, impacting motor learning, since the ER interacts with synaptic receptors, including AMPA and mGluRs (Konietzny et al., 2023). Synaptopodin is an actin-associated protein highly expressed in neuronal dendritic spines. It is known to organise the spine apparatus, a special form of the ER inside dendritic spines. It plays an important role in Ca^{2+} signalling and synaptic plasticity. Synaptopodin is mainly found in cortical PNs (especially in the hippocampus and neocortex), but it is not expressed in PCs. PCs have other types of ER structures in their spines (such as spine smooth ER) (Mundel et al., 1997; Deller et al., 2000; Vlachos et al., 2009; Wagner et al., 2011).

A recent investigation revealed that PIP_2 can be primarily located in PC spines and GrC presynaptic active zones (Eguchi et al., 2023). As explained above, during glutamatergic stimulation, mGluR1 stimulates PLCβ to cleave PIP_2 into DAG and IP_3, which releases ER Ca^{2+} by activating IP_3Rs. IP_3-induced ER Ca^{2+} release can then be amplified by Ca^{2+}-induced Ca^{2+} release (CICR) through RyRs and lead to a dramatic reduction in the ER Ca^{2+} concentration ($[Ca^{2+}]_{ER}$). Stromal interaction molecule (STIM) proteins, namely, STIM1 and STIM2, can, respectively, detect large and small decreases in the $[Ca^{2+}]_{ER}$; once activated, STIM proteins oligomerize and translocate to ER-plasma membrane junctions, known as *puncta*, where they bind to and gate the Ca^{2+}-permeable channel, Orai1. This mechanism is known as store-operated Ca^{2+} entry (SOCE) and is primarily responsible for refilling ER Ca^{2+} in neurons (Moccia et al., 2015). STIM1 is abundantly expressed in cerebellar PCs (Klejman et al., 2009) and a recent investigation reported that it is preferentially localized in the dendritic subsurface cisterns of the ER in mouse PCs (Nomura et al., 2025). Orai1 is also highly expressed in cerebellar PCs from several species, including human, rat and Cynomolgus monkey (Guzman et al., 2014), but it is still unclear whether it contributes to SOCE. In this view, PCs are also enriched with Orai2 (Skibinska-Kijek et al., 2009), which may serve as a dominant negative regulator of Orai1 (Kito et al., 2015; Yoast et al., 2020), thereby strongly limiting Orai1-mediated Ca^{2+} entry in PCs. However, STIM1 can interact with many other components of the Ca^{2+} handling machinery (Moccia et al., 2015), including Cav1.2 channels (Wang et al., 2010), NMDA receptors (Gruszczynska-Biegala et al., 2020), AMPA receptors (Gruszczynska-Biegala et al., 2016), and members of Transient Receptor Potential (TRP) superfamily of non-selective cation channels, such as TRP Canonical 1 (TRPC1) and TRPC3 (Zeng et al., 2008; Lee et al., 2014). TRPC1 and TRPC3 are both expressed in PCs, but only TRPC3 can be gated by STIM1 in response to IP_3-dependent ER Ca^{2+} release (Hartmann et al., 2008). A series of investigations has unambiguously demonstrated that STIM1-gated TRPC3-containing channels mediated mGluR1-dependent slow synaptic excitatory postsynaptic currents ($EPSP_{slow}$) in cerebellar PCs (Hartmann et al., 2014; Gui et al., 2024). STIM1 maintains the ER Ca^{2+} pool that it mobilized during dendritic mGluR1 signalling to ensure motor coordination (Hartmann et al., 2014), regulates PC intrinsic excitability by interacting with Sarco-Endoplasmic Reticulum Ca^{2+}-ATPase (SERCA) to clear intracellular Ca^{2+} and fine-tune the recruitment of Ca^{2+}-dependent conductances (Ryu et al., 2017), and is crucial for the memory consolidation of the vestibulo-ocular reflex (Jang et al., 2020). The major expression of STIM1 and SERCA2 was detected at the dendritic level with little to no presence on spines. Conversely, two other critical receptors for the release of Ca^{2+} from the smooth ER (SER), RyR1 and IP_3R1, were expressed on spines. The former had a lower spine expression compared to the somato-dendrites compartments, while the latter was highly expressed in spines (Nomura et al., 2025). An early study showed that the rapid replenishment of the ER Ca^{2+} store within the spine is driven by the intraluminal redistribution of dendritic Ca^{2+} (Okubo et al., 2015). This observation suggests that the ER within the spine neck does not represent a significant barrier to Ca^{2+} diffusion and that the absence of STIM1 impairs the overall ER Ca^{2+} dynamics in PCs. The neuronal ER functions act as an intracellular tunnel to redistribute stored Ca^{2+} within the neurons and as a leaky integrator of Ca^{2+} spike-inducing synaptic inputs (Okubo et al., 2015). This separation can lead to two distinct levels of synaptic plasticity; one strictly located on the dendritic level and one confined in each spine. This compartmentalized Ca^{2+} regulation is critical for cerebellar function and motor coordination.

Cytoskeleton

The cytoskeleton within the dendritic spines of PCs is primarily composed of filamentous actin (F-actin), which provides structural support and facilitates synaptic plasticity. Several key proteins regulate the organization and dynamics of this actin cytoskeleton: 1) Myosin XVI is a motor protein that interacts with the WAVE Regulatory Complex (WRC) to modulate actin dynamics in PC spines. Inhibition of the WRC accelerates F-actin turnover, resulting in altered spine morphology and reduced structural plasticity (Roesler et al., 2019). 2) Cortactin is predominantly localized near the postsynaptic density and sub-membrane regions of PC spines, and plays a role in actin filament branching and stabilization. Its distribution in these spines differs from that in forebrain neurons, suggesting region-specific functions in synaptic architecture (Szabó et al., 2021). 3) CaMKIIβ (Ca^{2+}/Calmodulin-Dependent Protein Kinase II Beta) is the most abundant protein in the PSD and it is involved in synaptic plasticity through the phosphorylation of multiple NMDA subunits (Kennedy, 2000). This kinase also promotes spine formation and elongation through its F-actin binding activity (Okamoto et al., 2007). Activation of group I mGluRs, i.e., mGluR1 and mGluR5, triggers protein kinase C (PKC)-mediated phosphorylation of CaMKIIβ, leading to its dissociation from F-actin. This mechanism prevents excessive spine development and maintains proper spine morphology in mature PCs (Sugawara et al., 2017). 4) Myosin-Va is a motor protein responsible for transporting the ER into dendritic spines of PCs. The presence of ER in spines is essential for synaptic plasticity, and myosin-Va facilitates this process by pulling the ER into spines along actin filaments (Wagner et al., 2011).

These proteins collectively contribute to the dynamic regulation of the actin cytoskeleton in PC spines, influencing their structure and function in cerebellar synaptic plasticity (for a comparison, see Table 3).

TABLE 3 Comparison of ER related properties. Differences between cortex, hippocampus and Purkinje cells.

Feature	Pyramidal neuron (neocortex)	Pyramidal neuron (hippocampus)	Purkinje cell (cerebellum)
Spine Apparatus	Present (Space-filling ER structure) (Mundel et al., 1997; Deller et al., 2000)	Present complex multilamellar structure (Deller et al., 2000; Spacek and Harris, 1997)	Absent or extremely rare (Deller et al., 2000)
Smooth ER in Spines	Present, associated with spine apparatus (Deller et al., 2000)	Present, highly structured, contributes to spine apparatus (Spacek and Harris, 1997)	Present simpler tubular ER without a spine apparatus (Martone et al., 1993)
Synaptopodin Expression	High; essential for spine apparatus (Mundel et al., 1997; Deller et al., 2000)	High; essential for forming spine apparatus (Mundel et al., 1997; Deller et al., 2000)	Very low or absent (Deller et al., 2000)
Other Actin-Associated Proteins	Actin-binding proteins (e.g., α-actinin) (Mundel et al., 1997)	α-actinin, drebrin, important for actin/ER organization (Mundel et al., 1997)	Other cytoskeletal proteins; synaptopodin absent (Martone et al., 1996)
Main Function of ER	Ca^{2+} storage, buffering, and plasticity (supports LTP) (Spacek and Harris, 1997)	Ca^{2+} storage, modulation of synaptic plasticity (supports LTP) (Spacek and Harris, 1997)	Ca^{2+} buffering for LTD, especially after parallel fiber activation (Llano et al., 1991)
Synaptic Plasticity Linked to ER	Supports LTP (Spacek and Harris, 1997; Deller et al., 2000)	Supports LTP — local Ca^{2+} release needed for strengthening synapses (Spacek and Harris, 1997; Deller et al., 2000)	Supports LTD — local Ca^{2+} dynamics required for weakening synapses (Konnerth et al., 1992)
ER Complexity	Complex, multilayered spine apparatus (Spacek and Harris, 1997)	Highly complex, stacked cisternae (spine apparatus) (Spacek and Harris, 1997)	Simple, fine tubular ER network (Martone et al., 1993)
Calcium Release Mechanisms	IP3 receptors and ryanodine receptors on spine ER (Sharp et al., 1993)	IP3 receptors and ryanodine receptors on spine ER (Sharp et al., 1993)	IP3-mediated Ca^{2+} release; ryanodine receptors also present (Finch and Augustine, 1998)

Purkinje cell spine regulation

Parallel fibers (anti-Hebbian) and climbing fibers (Hebbian) long-term potentiation and depression

PC dendrites receive excitatory inputs from PFs and CFs and the spines are instrumental in generating specific forms of long-term synaptic plasticity, including long-term potentiation (LTP) and LTD. While synaptic plasticity at CF – spine synapses follows the Hebbian rules, the PF – spine synapse present both LTD and LTP based on a non-Hebbian plasticity rule (Roberts and Leen, 2010; Piochon et al., 2012; Runge et al., 2020). The general synaptic plasticity rule (Lisman, 1989; Shouval et al., 2002; Pali et al., 2025) dictates that LTP is generated by low Ca^{2+} concentrations and LTD by high concentrations. LTD at PF - PC synapses consists of an activity-dependent long-lasting reduction in synaptic strength (Roberts and Leen, 2010; Nishiyama and Yasuda, 2015). Coincidence of PF stimulation (glutamate release) and CF activation (membrane depolarisation and Ca^{2+} influx) triggers LTD (Piochon et al., 2012; Daida et al., 2024). This leads to an influx of Ca^{2+} via voltage-gated Ca^{2+} channels and to Ca^{2+} release from the endogenous ER stores through the CICR process (Harvey-Girard et al., 2010). Glutamate released from PFs activates mGluR1 to produce IP_3 production, thereby promoting IP_3-induced Ca^{2+} release from the spine apparatus (Hartmann et al., 2011). A high localised Ca^{2+} concentration, together with PKC activation, induces AMPA receptor (GluA2 subunit) internalisation from the postsynaptic membrane, weakening synaptic transmission (Lisman, 1989). LTD is essential for motor learning, such as eye-blink conditioning and adaptation of the vestibulo-ocular reflex (Sharp et al., 1993; Finch and Augustine, 1998; Hansel et al., 2001; Ito, 2001). Moderate PF activation without strong CF co-activation leads to protein kinase A (PKA) stimulation and enhances AMPA receptor phosphorylation, promoting their insertion or stabilisation at the postsynaptic membrane, involving the activation of phosphatases, such as protein phosphatase 1 (PP1) and PP2B (calcineurin) (Lewis and Maler, 2002). The nitric oxide (NO)/soluble guanylyl cyclase/cyclinc guanosine monophosphate (cGMP) signalling pathway has also been implicated (Lev-Ram et al., 2002). Unlike LTD, where a large, spatially localised Ca^{2+} rise triggers depression, LTP requires smaller, slower Ca^{2+} elevations that fails to engage the higher threshold LTD pathway. LTP may help counterbalance LTD, maintaining synaptic homeostasis and contributing to fine-tuning of motor commands (Martone et al., 1993; Spacek and Harris, 1997; Lev-Ram et al., 2002; Coesmans et al., 2004). The presynaptic protein RIM1, in connection with Rab3-interacting molecule, is necessary for LTP to occur between PFs and PC (Uriu et al., 2010). It should also be noted that also presynaptic forms of synaptic plasticity also exist at the PF-PC synapse but are not considered here (Hansel et al., 2001).

How to modulate a spine: presynaptic release probability

There are various substances that can module the overall synaptic strength without the need to physically eliminate the PF-spine synapse. The endocannabinoids, which are produced by PCs and act as a retrograde signal, interact with the presynaptic side, reducing the release probability through CB1 receptors (Safo et al., 2006). A critical presynaptic protein termed RIM1 is important in the control and recruitment of presynaptic Ca^{2+} channels (Kaeser and Regehr, 2014). This protein is activated by progranulin generated by PCs and, acting as a diffusible signal, leads instead to an increase in release probability. This strengthening of the synaptic activity was recorded during the stage in which a CF becomes the winner with its translocation from somatic to dendritic spines (Uriu et al., 2010; Nitta et al., 2025). The presynaptic NMDA receptors are involved in the production of NO, which, compared to many other neuronal types, is not produced by the postsynaptic side (D'Angelo, 2014; Mapelli et al., 2017). NO may influence the postsynaptic Ca^{2+} dynamics and thereby change the overall strength of the presynaptic side, pushing the synapse into LTP (Schonewille et al., 2021). The structural proteins between PF and spines are critical, but the axon itself can define if a presynaptic active site needs to be stabilized or abolished (Aiken and Holzbaur, 2024). Based on the type of signals that need to be elaborated by a specific PCs, it is possible that the synapse is initially established between PF and PC and a certain point in the development, the presynaptic side itself is pruned.

How to modulate a spine: postsynaptic properties

As previously defined (see chapter "Spine number estimates"), to reduce the impact of the large number of spines and their low response it was assumed the absence of fast AMPA receptor-mediated responses, and the presence of a majority of mGluR1/TRPC3-mediated slow synaptic currents (Jin et al., 2007). These slow EPSC, lasting up to hundreds of milliseconds, were recently shown to change greatly depending on the lobuli (Thomas et al., 2024). Slow responses could be elicited in spines with only one head to preserve the PF-spine synapse, to convey support information, or to maintain the synapse active when no relevant information is transmitted. This model is supported by the recent discovery that branched spines are more "eloquent" compared to single-headed spines (Loschky et al., 2022). Another way to reduce the number spines, without physical deletion, is through GABAB receptors located peri synaptically and on spine necks. These receptors are connected with GIRK2 channels that can act as a filter for small intensity presynaptic activation or by slow responses elicited by mGluR1. The PF – spine synapse follows an anti-Hebbian rule to generate short and long-term potentiation (Lev-Ram et al., 2002; Piochon et al., 2012). This is in agreement with the evidence that postsynaptic Ca^{2+} needs to remain low to generate LTP, while it must increase by coincident activation of CFs to generate LTD.

Dynamic changes in morphological conformation

A property that was studied in layer 5 PN showed that the length of spine necks electrically isolates the heads from the dendrites. This activity was recorded using Spine Uncaging Potentials and showed a correlation between the neck lengths and electrical activity recorded at the somatic level. Longer necks had more impact on the activity, even reaching a complete silencing of the post-synaptic potentials, where shorted neck allowed post-synaptic potential transmission (Araya et al., 2006). When a synaptic contact is established, its shape does not change even during LTD activity (Sdrulla and Linden, 2007). This view was recently challenged with a new experimental procedure showing that, besides changing their shape, the entire dendritic spine can be retracted and regenerated along the day/night cycle (Loschky et al., 2022). An *in vivo* experimental procedure further showed that PC spine size can be changed by a process that required the endocytosis of some spine membrane by BG (Morizawa et al., 2022). This process was marked by increased activity of BGs after training and learning.

Spine modification in diseases

Spine properties can be greatly modified in the presence of mutations that dysregulate various signalling pathways, thereby resulting in severe neurological diseases. In many cases, the PC dendritic tree can change its shape, branching points and overall arborisation. The dendritic trees are subject to marked modifications as exemplified by the atrophy observed in PCs of Weaver mice and in ectopic PCs of Reeler mice. In both mouse models, the presence of spines is unaffected by the mutations, but their linear count is lower compared to controls (Yuste and Bonhoeffer, 2004). In essential tremor, a human parkinsonism characterized by localised axon swelling, there is a reduction in the complexity of PC dendritic tree with just a small reduction in spine number per unit length (Louis et al., 2014). In Staggerer mice, which are missing the retinoid-related orphan receptor α (RORα), the animal is ataxic (SCA1) and PCs show stunted trees with parts of them completely devoid of spines (Mitsumura et al., 2011). Some remnants of the PF-PC connectivity can be observed with excitatory synapses made directly on the dendritic surface. Another ataxia (SCA2) is caused by polyglutamine expansion in Ataxin-2 (ATXN2) and its activity on CaMKIIα and CaMKIV signalling with a reduction in spine length and spine density (Arsović et al., 2020). A point mutation in the protein kinase C gamma (PKCγ), involved in SCA14, showed that it has a limited impact on spinogenesis except if it is upregulated. In the latter case, it causes the reduction of the number of spines, their length and overall maturity (Sziber et al., 2025). In human schizophrenia, a decrease in spine density was observed, but with no information about changes to the spine shape (Mavroudis et al., 2017). This specific mutation is yet to be replicated in animal models.

Conclusions and computational implications

Although the number of spines appears to be lower than initially thought, this is not expected to hamper the encoding capabilities of PCs. Indeed, instead of having ~90% silent synapses out of 100000, there would be a maximum of 85% inactive or poorly active synapse out of 35,000. The more "eloquent" double-headed spines would be 15% of the total, i.e., ~5,000 in mouse

and ~40,000 in human PCs contribute more to the modularity of cerebellar organisation (Streng et al., 2025) compared to the single-headed spines. We recently compared PCs in mice and humans (Masoli et al., 2024), showing that the human/mouse spine head ratio (7.5) could determine the computing capability of the neurons. This number compared well with other metrics like the dendritic surface ratio (5.5) and dendritic complexity index (6.5), as well as with dendritic transfer impedance computed for clusters of spines that can effectively impact spike generation in the PC axonal initial segment (6.5) with 1-ms time resolution. This suggested that the increased number of contacts was almost entirely transformed into effective combinations of input patterns that can regulate spike generation in the soma, akin to the linear encoding in a perceptron (Brunel et al., 2004; Walter et al., 2009). The maximum computational capacity, which depends on the number of alternative states established by the dendrites, turned out to be 2^8 for mice and 2^{51} for human (Masoli et al., 2024). It remains to be determined whether these figures would change by making assumptions about spine efficiency, e.g., following the arguments reported here. The electrical isolation generated by the spine neck, the large number of thin spines, and the hyperpolarizing activity of GABAB/GIRK2 channels suggest that each spine may individually influence the overall neuronal encoding activity. This is because of the reduction in the noise/signal ratio, allowing the transmission of strong excitatory activity concentrated on few spines. It should be noted that, owing to the redundancy of dendritic combinations, some output spike patterns may be mutually indistinguishable on the temporal resolution scale of the neuron. Ad hoc simulations using PC computational models with spines may allow the calculation of the combinatorial capacity in human and mouse PCs under more realistic assumptions, for example, that segments are not fully active or inactive or that spine independence is incomplete, or that individual spines have specific and differentiated neurotransmission properties reflecting modulatory, plastic, or pathological states (Rieke, 1999; London et al., 2002; Arleo et al., 2010).

Author contributions

SM: Conceptualization, Writing – original draft, Writing – review and editing. MR: Writing – original draft, Writing – review and editing. FM: Writing – original draft, Writing – review and editing. ED'A: Funding acquisition, Writing – original draft, Writing – review and editing, Validation, Methodology.

Funding

The author(s) declare that financial support was received for the research and/or publication of this article. SM - National Recovery and Resilience Plan (NRRP), project IR00011-EBRAINS-Italy funded by the European Union–NextGenerationEU (Project IR0000011, CUP B51E22000150006, "EBRAINS-Italy").

Acknowledgments

MFR - The Virtual Brain Twin Project has received funding from the European Union's Research and Innovation Program Horizon Europe under grant agreement No. 101137289. ED'A - Work supported by #NEXTGENERATIONEU (NGEU) and funded by the Ministry of University and Research (MUR), National Recovery and Resilience Plan (NRRP), project MNESYS (PE0000006) – A Multiscale integrated approach to the study of the nervous system in health and disease (DN. 1553 11.10.2022). The European Union's Horizon Europe Programme under the Specific Grant Agreement No. 101147319 (EBRAINS 2.0 Project). Figure 4 - Image provided by Servier Medical Art (https://smart.servier.com/), licensed under CC BY 4.0 (https://creativecommons.org/licenses/by/4.0/).

Conflict of interest

The authors declare that the research was conducted in the absence of any commercial or financial relationships that could be construed as a potential conflict of interest.

The author(s) declared that they were an editorial board member of Frontiers, at the time of submission. This had no impact on the peer review process and the final decision.

Generative AI statement

The author(s) declare that no Generative AI was used in the creation of this manuscript.

Any alternative text (alt text) provided alongside figures in this article has been generated by Frontiers with the support of artificial intelligence and reasonable efforts have been made to ensure accuracy, including review by the authors wherever possible. If you identify any issues, please contact us.

Publisher's note

References

Adams, P., Rungta, R., Garcia, E., van den Maagdenberg, A. M. J. M., MacVicar, B. A., and Snutch, T. P. (2010). Contribution of calcium-dependent facilitation to synaptic plasticity revealed by migraine mutations in the P/Q-type calcium channel. *Proc.* 107, 18694–18699. doi:10.1073/pnas.1009500107

Aiken, J., and Holzbaur, E. L. F. (2024). Spastin locally amplifies microtubule dynamics to pattern the axon for presynaptic cargo delivery. *Curr. Biol.* 34, 1687–1704.e8. doi:10.1016/j.cub.2024.03.010

Aimi, T., Matsuda, K., and Yuzaki, M. (2023). C1ql1-Bai3 signaling is necessary for climbing fiber synapse formation in mature Purkinje cells in coordination with neuronal activity. *Mol. Brain* 16, 61–17. doi:10.1186/s13041-023-01048-4

Al-Hussain, S. M., Yousuf, M. S., Hani, A. B., Zaqout, S., Djouhri, L., and Mustafa, A. G. (2022). A Golgi study of neurons in the camel cerebellum (*Camelus dromedarius*). *Anat. Rec.* 305, 1264–1276. doi:10.1002/ar.24742

Albus, J. S. (1971). A theory of cerebellar function. *Math. Biosci.* 10, 25–61. doi:10.1016/0025-5564(71)90051-4

Alfaro-Ruíz, R., Aguado, C., Martín-Belmonte, A., Moreno-Martínez, A. E., and Luján, R. (2020). Cellular and subcellular localisation of kv4-associated kchip proteins in the rat cerebellum. *Int. J. Mol. Sci.* 21, 6403–6419. doi:10.3390/ijms21176403

Araya, R., Jiang, J., Eisenthal, K. B., and Yuste, R. (2006). The spine neck filters membrane potentials. *Proc. Natl. Acad. Sci. U. S. A.* 103, 17961–17966. doi:10.1073/pnas.0608755103

Arleo, A., Nieus, T., Bezzi, M., D'Errico, A., D'Angelo, E., and Coenen, O. (2010). How synaptic release probability shapes neuronal transmission: information-theoretic analysis in a cerebellar granule cell. *Neural comput.* 22, 2031–2058. doi:10.1162/NECO_a_00006-Arleo

Arsović, A., Halbach, M. V., Canet-Pons, J., Esen-Sehir, D., Döring, C., Freudenberg, F., et al. (2020). Mouse ataxin-2 expansion downregulates camkii and other calcium signaling factors, impairing granule—purkinje neuron synaptic strength. *Int. J. Mol. Sci.* 21, 6673–36. doi:10.3390/ijms21186673

Bao, D., Pang, Z., Morgan, M. A., Parris, J., Rong, Y., Li, L., et al. (2006). Cbln1 is essential for interaction-dependent secretion of Cbln3. *Mol. Cell. Biol.* 26, 9327–9337. doi:10.1128/mcb.01161-06

Bentivoglio, M., Cotrufo, T., Ferrari, S., Tesoriero, C., Mariotto, S., Bertini, G., et al. (2019). The original histological slides of camillo golgi and his discoveries on neuronal structure. *Front. Neuroanat.* 13, 3–13. doi:10.3389/fnana.2019.00003

Benton, M. D., and Raman, I. M. (2009). Stabilization of Ca current in Purkinje neurons during high-frequency firing by a balance of Ca-dependent facilitation and inactivation. *Channels (Austin).* 3, 393–401. doi:10.4161/chan.3.6.9838

Boele, H. J., Peter, S., Ten Brinke, M. M., Verdonschot, L., Ijpelaar, A. C. H., Rizopoulos, D., et al. (2018). Impact of parallel fiber to Purkinje cell long-term depression is unmasked in absence of inhibitory input. *Sci. Adv.* 4, eaas9426–eaas9429. doi:10.1126/sciadv.aas9426

Boivin, J. R., and Nedivi, E. (2018). Functional implications of inhibitory synapse placement on signal processing in pyramidal neuron dendrites. *Curr. Opin. Neurobiol.* 51, 16–22. doi:10.1016/j.conb.2018.01.013

Brunel, N., Hakim, V., Isope, P., Nadal, J. P., and Barbour, B. (2004). Optimal information storage and the distribution of synaptic weights: perceptron versus Purkinje cell. *Neuron* 43, 745–757. doi:10.1016/j.neuron.2004.08.023

Brunetti, V., Soda, T., Berra-Romani, R., De Sarro, G., Guerra, G., Scarpellino, G., et al. (2024). Two signaling modes are better than one: flux-independent signaling by ionotropic glutamate receptors is coming of age. *Biomedicines* 12, 880. doi:10.3390/biomedicines12040880

Buceta, I., Elezgarai, I., Rico-Barrio, I., Gerrikagoitia, I., Puente, N., and Grandes, P. (2020). Deletion of the cannabinoid CB1 receptor impacts on the ultrastructure of the cerebellar parallel fiber-Purkinje cell synapses. *J. Comp. Neurol.* 528, 1041–1052. doi:10.1002/cne.24808

Burada, A. P., Vinnakota, R., and Kumar, J. (2020). The architecture of GluD2 ionotropic delta glutamate receptor elucidated by cryo-EM. *J. Struct. Biol.* 211, 107546. doi:10.1016/j.jsb.2020.107546

Burada, A. P., Vinnakota, R., Bharti, P., Dutta, P., Dubey, N., and Kumar, J. (2022). Emerging insights into the structure and function of ionotropic glutamate delta receptors. *Br. J. Pharmacol.* 179, 3612–3627. doi:10.1111/bph.15313

Busch, S. E., and Hansel, C. (2023). Climbing fiber multi-innervation of mouse Purkinje dendrites with arborization common to human. *Science* 381, 420–427. doi:10.1126/science.adi1024

Busch, S. E., and Hansel, C. (2025). eLife Assessment: non-allometric expansion and enhanced compartmentalization of Purkinje cell dendrites in the human cerebellum. doi:10.7554/eLife.105013.2.sa3

Campeau, J. L., Wu, G., Bell, J. R., Rasmussen, J., and Sim, V. L. (2013). Early increase and late decrease of Purkinje cell dendritic spine density in prion-infected organotypic mouse cerebellar cultures. *PLoS One* 8, e81776–e81777. doi:10.1371/journal.pone.0081776

Castejón, O. J., and Dailey, M. E. (2009). Immunohistochemistry of GluR1 subunits of AMPA receptors of rat cerebellar nerve cells. *Biocell* 33, 71–80. doi:10.32604/biocell.2009.33.071

Chen, X., Du, Y., Broussard, G. J., Kislin, M., Yuede, C. M., Zhang, S., et al. (2022). Transcriptomic mapping uncovers Purkinje neuron plasticity driving learning. *Nature* 605, 722–727. doi:10.1038/s41586-022-04711-3

Coesmans, M., Weber, J. T., De Zeeuw, C. I., and Hansel, C. (2004). Bidirectional parallel fiber plasticity in the cerebellum under climbing fiber control. *Neuron* 44, 691–700. doi:10.1016/j.neuron.2004.10.031

Cramer, S., Gao, W., Chen, G., and Ebner, T. J. (2013). Reevaluation of the beam and radial hypotheses of parallel fiber action in the cerebellar cortex. *J. Neurosci.* 33, 11412–11424. doi:10.1523/JNEUROSCI.0711-13.2013

Crépe, F., Galante, M., Habbas, S., McLean, H., and Danie, H. (2011). Role of the vesicular transporter VGLUT3 in retrograde release of glutamate by cerebellar Purkinje cells. *J. Neurophysiol.* 105, 1023–1032. doi:10.1152/jn.00736.2010

Daida, A., Kurotani, T., Yamaguchi, K., Takahashi, Y., and Ichinohe, N. (2024). Different numbers of conjunctive stimuli induce LTP or LTD in mouse cerebellar purkinje cell. *Cerebellum* 23, 2297–2307. doi:10.1007/s12311-024-01726-6

Davidson, A. M., Mejiá-Gómez, H., Jacobowitz, M., and Mostany, R. (2020). Dendritic spine density and dynamics of layer 5 pyramidal neurons of the primary motor cortex are elevated with aging. *Cereb. Cortex* 30, 767–777. doi:10.1093/cercor/bhz124

Defelipe, J. (2025). Cajal and the discovery of the Golgi method: a neuroanatomist ' s dream. *Anat. Sci. Int.* doi:10.1007/s12565-025-00840-7

Dehnes, Y., Chaudhry, F. A., Ullensvang, K., Lehre, K. P., Storm-Mathisen, J., and Danbolt, N. C. (1998). The glutamate transporter EAAT4 in rat cerebellar Purkinje cells: a glutamate-gated chloride channel concentrated near the synapse in parts of the dendritic membrane facing astroglia. *J. Neurosci.* 18, 3606–3619. doi:10.1523/jneurosci.18-10-03606.1998

Deller, T., Merten, T., Roth, S. U., Mundel, P., and Frotscher, M. (2000). Actin-associated protein synaptopodin in the rat hippocampal formation: localization in the spine neck and close association with the spine apparatus of principal neurons. *J. Comp. Neurol.* 418, 164–181. doi:10.1002/(SICI)1096-9861(20000306)418:2<164::AID-CNE4>3.0.CO;2-0

Desmond, J. E., and Fiez, J. A. (1998). Neuroimaging studies of the cerebellum: language, learning and memory. *Trends Cogn. Sci.* 2, 355–362. doi:10.1016/S1364-6613(98)01211-X

Dusart, I., and Flamant, F. (2012). Profound morphological and functional changes of rodent Purkinje cells between the first and the second postnatal weeks: a metamorphosis? *Front. Neuroanat.* 6, 11. doi:10.3389/fnana.2012.00011

D'Angelo, E. (2014). *The organization of plasticity in the cerebellar cortex: from synapses to control.* 1st ed. Elsevier B.V. doi:10.1016/B978-0-444-63356-9.00002-9

Egorova, P. A., Marinina, K. S., and Bezprozvanny, I. B. (2023). Chronic suppression of STIM1-mediated calcium signaling in Purkinje cells rescues the cerebellar pathology in spinocerebellar ataxia type 2. *Biochim. Biophys. Acta - Mol. Cell Res.* 1870, 119466. doi:10.1016/j.bbamcr.2023.119466

Eguchi, K., Le Monnier, E., and Shigemoto, R. (2023). Nanoscale phosphoinositide distribution on cell membranes of mouse cerebellar neurons. *J. Neurosci.* 43, 4197–4216. doi:10.1523/JNEUROSCI.1514-22.2023

Finch, E. A., and Augustine, G. J. (1998). Local calcium signalling by inositol-1,4,5-trisphosphate in Purkinje cell dendrites. *Nature* 396, 753–756. doi:10.1038/25541

Fuccillo, M. V., Földy, C., Gökce, Ö., Rothwell, P. E., Sun, G. L., Malenka, R. C., et al. (2015). Single-cell mRNA profiling reveals cell-type-specific expression of neurexin isoforms. *Neuron* 87, 326–340. doi:10.1016/j.neuron.2015.06.028

Furutani, K., Okubo, Y., Kakizawa, S., and Iino, M. (2006). Postsynaptic inositol 1,4,5-trisphosphate signaling maintains presynaptic function of parallel fiber-Purkinje cell synapses via BDNF. *Proc. Natl. Acad. Sci. U. S. A.* 103, 8528–8533. doi:10.1073/pnas.0600497103

Gao, Y., Perkins, E. M., Clarkson, Y. L., Tobia, S., Lyndon, A. R., Jackson, M., et al. (2011). β-III spectrin is critical for development of purkinje cell dendritic tree and spine morphogenesis. *J. Neurosci.* 31, 16581–16590. doi:10.1523/JNEUROSCI.3332-11.2011

Gelfo, F., Florenzano, F., Foti, F., Burello, L., Petrosini, L., and De Bartolo, P. (2016). Lesion-induced and activity-dependent structural plasticity of Purkinje cell dendritic spines in cerebellar vermis and hemisphere. *Brain Struct. Funct.* 221, 3405–3426. doi:10.1007/s00429-015-1109-5

Gilbert, M., and Rasmussen, A. (2025). The cerebellar deep nuclei: a patch for rate codes? *Front. Neural Circuits* 19, 1548123–14. doi:10.3389/fncir.2025.1548123

Golgi, C. (1883). Sulla fina anatomia degli organi centrali del sistema nervoso. *Riv. Sper. Freniatr.*

Gruszczynska-Biegala, J., Sladowska, M., and Kuznicki, J. (2016). AMPA receptors are involved in store-operated calcium entry and interact with STIM proteins in rat primary cortical neurons. *Front. Cell. Neurosci.* 10, 251. doi:10.3389/fncel.2016.00251

Gruszczynska-Biegala, J., Strucinska, K., Maciag, F., Majewski, L., Sladowska, M., and Kuznicki, J. (2020). STIM protein-NMDA2 receptor interaction decreases NMDA-dependent calcium levels in cortical neurons. *Cells* 9, 160. doi:10.3390/cells9010160

Gui, L., Tellios, V., Xiang, Y.-Y., Feng, Q., Inoue, W., and Lu, W.-Y. (2024). Neuronal nitric oxide synthase regulates cerebellar parallel fiber slow EPSC in purkinje neurons by modulating STIM1-gated TRPC3-containing channels. *Cerebellum* 23, 1867–1881. doi:10.1007/s12311-024-01683-0

Guzman, R., Valente, E. G., Pretorius, J., Pacheco, E., Qi, M., Bennett, B. D., et al. (2014). Expression of ORAII, a plasma membrane resident subunit of the CRAC channel, in rodent and non-rodent species. *J. Histochem. Cytochem.* 62, 864–878. doi:10.1369/0022155414554926

Han, P., She, Y., Yang, Z., Zhuang, M., Wang, Q., Luo, X., et al. (2022). Cbln1 regulates axon growth and guidance in multiple neural regions. *PLOS Biol.* 20, e3001853. doi:10.1371/journal.pbio.3001853

Hansel, C., Linden, D. J., and D'Angelo, E. (2001). Beyond parallel fiber LTD: the diversity of synaptic and non-synaptic plasticity in the cerebellum. *Nat. Neurosci.* 4, 467–475. doi:10.1038/87419

Hansen, K. B., Naur, P., Kurtkaya, N. L., Kristensen, A. S., Gajhede, M., Kastrup, J. S., et al. (2009). Modulation of the dimer interface at ionotropic glutamate-like receptor delta2 by D-serine and extracellular calcium. *J. Neurosci.* 29, 907–917. doi:10.1523/JNEUROSCI.4081-08.2009

Harris, K. M., and Stevens, J. K. (1988). Dendritic spines of rat cerebellar Purkinje cells: serial electron microscopy with reference to their biophysical characteristics. *J. Neurosci.* 8, 4455–4469. doi:10.1523/JNEUROSCI.08-12-04455.1988

Hartmann, J., Dragicevic, E., Adelsberger, H., Henning, H. A., Sumser, M., Abramowitz, J., et al. (2008). TRPC3 channels are required for synaptic transmission and motor coordination. *Neuron* 59, 392–398. doi:10.1016/j.neuron.2008.06.009

Hartmann, J., Henning, H. A., and Konnerth, A. (2011). mGluR1/TRPC3-mediated synaptic transmission and calcium signaling in mammalian central neurons. *Cold Spring Harb. Perspect. Biol.* 3, a006726–16. doi:10.1101/cshperspect.a006726

Hartmann, J., Karl, R. M., Alexander, R. P. D., Adelsberger, H., Brill, M. S., Rühlmann, C., et al. (2014). STIM1 controls neuronal Ca^{2+} signaling, mGluR1-dependent synaptic transmission, and cerebellar motor behavior. *Neuron* 82, 635–644. doi:10.1016/j.neuron.2014.03.027

Harvey-Girard, E., Lewis, J., and Maler, L. (2010). Burst-induced anti-hebbian depression acts through short-term synaptic dynamics to cancel redundant sensory signals. *J. Neurosci.* 30, 6152–6169. doi:10.1523/JNEUROSCI.0303-10.2010

Heck, D., and Sultan, F. (2002). Cerebellar structure and function: making sense of parallel fibers. *Hum. Mov. Sci.* 21, 411–421. doi:10.1016/s0167-9457(02)00123-9

Heintz, T. G., Eva, R., and Fawcett, J. W. (2016). Regional regulation of purkinje cell dendritic spines by integrins and Eph/ephrins. *PLoS One* 11, e0158558–15. doi:10.1371/journal.pone.0158558

Hibi, M., Matsuda, K., Takeuchi, M., Shimizu, T., and Murakami, Y. (2017). Evolutionary mechanisms that generate morphology and neural-circuit diversity of the cerebellum. *Dev. Growth Differ.* 59, 228–243. doi:10.1111/dgd.12349

Hills, L. B., Masri, A., Konno, K., Kakegawa, W., Lam, A. T. N., Lim-Melia, E., et al. (2013). Deletions in GRID2 lead to a recessive syndrome of cerebellar ataxia and tonic upgaze in humans. *Neurology* 81, 1378–1386. doi:10.1212/WNL.0b013e3182a841a3

Houston, C. M., Diamanti, E., Diamantaki, M., Kutsarova, E., Cook, A., Sultan, F., et al. (2017). Exploring the significance of morphological diversity for cerebellar granule cell excitability. *Sci. Rep.* 7, 46147. doi:10.1038/srep46147

Hoxha, E., Tempia, F., Lippiello, P., and Miniaci, M. C. (2016). Modulation, plasticity and pathophysiology of the parallel fiber-purkinje cell synapse. *Front. Synaptic Neurosci.* 8, 35–16. doi:10.3389/fnsyn.2016.00035

Hoxha, E., Gabriele, R. M. C., Balbo, I., Ravera, F., Masante, L., Zambelli, V., et al. (2017). Motor deficits and cerebellar atrophy in Elovl5 knock out mice. *Front. Cell. Neurosci.* 11, 343–11. doi:10.3389/fncel.2017.00343

Hoxha, E., Balbo, I., Miniaci, M. C., and Tempia, F. (2018). Purkinje cell signaling deficits in animal models of ataxia. *Front. Synaptic Neurosci.* 10, 6–17. doi:10.3389/fnsyn.2018.00006

Huang, C. ming, and Huang, R. H. (1998). Measuring parallel fiber length in the rat cerebellum. *Brain Res.* 801, 211–215. doi:10.1016/S0006-8993(98)00444-2

Huang, C., Gammon, S. J., Dieterle, M., Huang, R. H., Likins, L., Ricklefs, R. E., et al. (2014). Dramatic increases in number of cerebellar granule-cell-Purkinje-cell synapses across several mammals. *Mamm. Biol.*79, 163–169. doi:10.1016/j.mambio.2013.12.003

Huang, M., and Verbeek, D. S. (2019). Why do so many genetic insults lead to Purkinje Cell degeneration and spinocerebellar ataxia? *Neurosci. Lett.* 688, 49–57. doi:10.1016/j.neulet.2018.02.004

Huang, T.-Y., Lin, L.-S., Cho, K.-C., Chen, S.-J., Kuo, Y., Yu, L., et al. (2012). Chronic treadmill exercise in rats delicately alters the Purkinje cell structure to improve motor performance and toxin resistance in the cerebellum. *J. Appl. Physiol.* 113, 889–895. doi:10.1152/japplphysiol.01363.2011

Ichikawa, R., Yamasaki, M., Miyazaki, T., Konno, K., Hashimoto, K., Tatsumi, H., et al. (2011). Developmental switching of perisomatic innervation from climbing fibers to basket cell fibers in cerebellar Purkinje cells. *J. Neurosci.* 31, 16916–16927. doi:10.1523/JNEUROSCI.2396-11.2011

Ichikawa, R., Sakimura, K., and Watanabe, M. (2016). GluD2 endows parallel fiber-purkinje cell synapses with a high regenerative capacity. *J. Neurosci.* 36, 4846–4858. doi:10.1523/JNEUROSCI.0161-16.2016

Iijima, T., Miura, E., Matsuda, K., Kamekawa, Y., Watanabe, M., and Yuzaki, M. (2007). Characterization of a transneuronal cytokine family Cbln - regulation of secretion by heteromeric assembly. *Eur. J. Neurosci.* 25, 1049–1057. doi:10.1111/j.1460-9568.2007.05361.x

Indriati, D. W., Kamasawa, N., Matsui, K., Meredith, A. L., Watanabe, M., and Shigemoto, R. (2013). Quantitative localization of Cav2.1 (P/Q-type) voltage-dependent calcium channels in Purkinje cells: somatodendritic gradient and distinct somatic coclustering with calcium-activated potassium channels. *J. Neurosci.* 33, 3668–3678. doi:10.1523/JNEUROSCI.2921-12.2013

Isaac, J. T. R. R., Ashby, M., and McBain, C. J. (2007). The role of the GluR2 subunit in AMPA receptor function and synaptic plasticity. *Neuron* 54, 859–871. doi:10.1016/j.neuron.2007.06.001

Isope, P., and Barbour, B. (2002). Properties of unitary granule cell Purkinje cell synapses in adult rat cerebellar slices. *J. Neurosci.* 22, 9668–9678. doi:10.1523/JNEUROSCI.22-22-09668.2002

Ito, M. (2001). Cerebellar long-term depression: characterization, signal transduction, and functional roles. *Physiol. Rev.* 81, 1143–1195. doi:10.1152/physrev.2001.81.3.1143

Ito-Ishida, A., Kakegawa, W., Kohda, K., Miura, E., Okabe, S., and Yuzaki, M. (2014a). Cbln1 downregulates the formation and function of inhibitory synapses in mouse cerebellar Purkinje cells. *Eur. J. Neurosci.* 39, 1268–1280. doi:10.1111/ejn.12487

Ito-Ishida, A., Okabe, S., and Yuzaki, M. (2014b). The role of Cbln1 on Purkinje cell synapse formation. *Neurosci. Res.* 83, 64–68. doi:10.1016/j.neures.2014.01.009

Itoh, M., and Yuzaki, M. (2024). The hidden face of GluD1 at inhibitory synapses. *Cell Res.* 34, 405–406. doi:10.1038/s41422-024-00931-6

Jacobs, B., Johnson, N. L., Wahl, D., Schall, M., Maseko, B. C., Lewandowski, A., et al. (2014). Comparative neuronal morphology of the cerebellar cortex in afrotherians, carnivores, cetartiodactyls, and primates. *Front. Neuroanat.* 8, 24. doi:10.3389/fnana.2014.00024

Jahncke, J. N., Schnell, E., and Wright, K. M. (2025). Distinct functional domains of Dystroglycan regulate inhibitory synapse formation and maintenance in cerebellar Purkinje cells. *Commun. Biol.* 8, 878. doi:10.1038/s42003-025-08323-1

Jang, M., Bum Um, K., Jang, J., Jin Kim, H., Cho, H., Chung, S., et al. (2015). Coexistence of glutamatergic spine synapses and shaft synapses in substantia nigra dopamine neurons. *Sci. Rep.* 5, 14773–16. doi:10.1038/srep14773

Jang, D. C., Shim, H. G., and Kim, S. J. (2020). Intrinsic plasticity of cerebellar purkinje cells contributes to motor memory consolidation. *J. Neurosci.* 40, 4145–4157. doi:10.1523/JNEUROSCI.1651-19.2020

Jin, Y., Kim, S. J., Kim, J., Worley, P. F., and Linden, D. J. (2007). Long-term depression of mGluR1 signaling. *Neuron* 55, 277–287. doi:10.1016/j.neuron.2007.06.035

Joensuu, M., Wallis, T. P., Saber, S. H., and Meunier, F. A. (2020). Phospholipases in neuronal function: a role in learning and memory? *J. Neurochem.* 153, 300–333. doi:10.1111/jnc.14918

Jörntell, H., and Hansel, C. (2006). Synaptic memories upside down: bidirectional plasticity at cerebellar parallel fiber-purkinje cell synapses. *Neuron* 52, 227–238. doi:10.1016/j.neuron.2006.09.032

Kaeser, P. S., and Regehr, W. G. (2014). Molecular mechanisms for synchronous, asynchronous, and spontaneous neurotransmitter release. *Annu. Rev. Physiol.* 76, 333–363. doi:10.1146/annurev-physiol-021113-170338

Kakegawa, W., Miyazaki, T., Kohda, K., Matsuda, K., Emi, K., Motohashi, J., et al. (2009). The N-terminal domain of GluD2 (GluRdelta2) recruits presynaptic terminals and regulates synaptogenesis in the cerebellum *in vivo*. *J. Neurosci.* 29, 5738–5748. doi:10.1523/JNEUROSCI.6013-08.2009

Kakegawa, W., Miyoshi, Y., Hamase, K., Matsuda, S., Matsuda, K., Kohda, K., et al. (2011). D-Serine regulates cerebellar LTD and motor coordination through the δ glutamate receptor. *Nat. Neurosci.* 14, 603–613. doi:10.1038/nn.2791

Kennedy, M. B. (2000). Signal-processing machines at the postsynaptic density. *Sci. 80* 290, 750–754. doi:10.1126/science.290.5492.750

Khan, M. Z. (2017). Ionotropic glutamate receptors (iGluRs) of the delta family (GluD1 and GluD2) and synaptogenesis. *Alex. J. Med.* 53, 201–206. doi:10.1016/j.ajme.2016.09.003

Khouri-Farah, N., Guo, Q., Perry, T. A., Dussault, R., and Li, J. Y. H. (2025). FOXP genes regulate Purkinje cell diversity and cerebellar morphogenesis. *Nat. Neurosci.* 4, 1–21. doi:10.1038/s41593-025-02042-w

Kim, E. Y., Rumpf, C. H., Fujiwara, Y., Cooley, E. S., Van Petegem, F., and Minor, D. L. (2008). Structures of CaV2 Ca2+/CaM-IQ domain complexes reveal binding modes that underlie calcium-dependent inactivation and facilitation. *Structure* 16, 1455–1467. doi:10.1016/j.str.2008.07.010

Kito, H., Yamamura, H., Suzuki, Y., Yamamura, H., Ohya, S., Asai, K., et al. (2015). Regulation of store-operated Ca2+ entry activity by cell cycle dependent up-regulation of Orai2 in brain capillary endothelial cells. *Biochem. Biophys. Res. Commun.* 459, 457–462. doi:10.1016/j.bbrc.2015.02.127

Klejman, M. E., Gruszczynska-Biegala, J., Skibinska-Kijek, A., Wisniewska, M. B., Misztal, K., Blazejczyk, M., et al. (2009). Expression of STIM1 in brain and puncta-like co-localization of STIM1 and ORAI1 upon depletion of Ca(2+) store in neurons. *Neurochem. Int.* 54, 49–55. doi:10.1016/j.neuint.2008.10.005

Konietzny, A., Wegmann, S., and Mikhaylova, M. (2023). The endoplasmic reticulum puts a new spin on synaptic tagging. *Trends Neurosci.* 46, 32–44. doi:10.1016/j.tins.2022.10.012

Konnerth, A., Dreessen, J., and Augustine, G. J. (1992). Brief dendritic calcium signals initiate long-lasting synaptic depression in cerebellar Purkinje cells. *Proc. Natl. Acad. Sci. U. S. A.* 89, 7051–7055. doi:10.1073/pnas.89.15.7051

Konno, K., Matsuda, K., Nakamoto, C., Uchigashima, M., Miyazaki, T., Yamasaki, M., et al. (2014). Enriched expression of GluD1 in higher brain regions and its involvement in parallel fiber-interneuron synapse formation in the cerebellum. *J. Neurosci.* 34, 7412–7424. doi:10.1523/JNEUROSCI.0628-14.2014

Kumar, A., Paeger, L., Kosmas, K., Kloppenburg, P., Noegel, A. A., and Peche, V. S. (2016). Neuronal actin dynamics, spine density and neuronal dendritic complexity are regulated by CAP2. *Front. Cell. Neurosci.* 10, 180–17. doi:10.3389/fncel.2016.00180

Kuo, S.-H., Faust, P. L., Vonsattel, J.-P. G., Ma, K., and Louis, E. D. (2011). Parallel fiber counts and parallel fiber integrated density are similar in essential tremor cases and controls. *Acta Neuropathol.* 121, 287–289. doi:10.1007/s00401-010-0776-9

Lackey, E. P., Moreira, L., Norton, A., Hemelt, M. E., Osorno, T., Nguyen, T. M., et al. (2024). Specialized connectivity of molecular layer interneuron subtypes leads to disinhibition and synchronous inhibition of cerebellar Purkinje cells. *Neuron* 112, 2333–2348.e6. doi:10.1016/j.neuron.2024.04.010

Lanciego, J. L., Luquin, N., and Obeso, J. A. (2012). Functional neuroanatomy of the basal ganglia. *Cold Spring Harb. Perspect. Med.* 2, a009621–20. doi:10.1101/cshperspect.a009621

Larsen, K. (2021). The porcine cerebellin gene family. *Gene* 799, 145852. doi:10.1016/j.gene.2021.145852

Lee, K. J., Kim, H., Kim, T. S., Park, S. H., and Rhyu, I. J. (2004). Morphological analysis of spine shapes of Purkinje cell dendrites in the rat cerebellum using high-voltage electron microscopy. *Neurosci. Lett.* 359, 21–24. doi:10.1016/j.neulet.2004.01.071

Lee, K. J., Kim, H., and Rhyu, I. J. (2005). The roles of dendritic spine shapes in Purkinje cells. *Cerebellum* 4, 97–104. doi:10.1080/14734220510007842

Lee, K. P., Choi, S., Hong, J. H., Ahuja, M., Graham, S., Ma, R., et al. (2014). Molecular determinants mediating gating of Transient Receptor Potential Canonical (TRPC) channels by stromal interaction molecule 1 (STIM1). *J. Biol. Chem.* 289, 6372–6382. doi:10.1074/jbc.M113.546556

Lev-Ram, V., Wong, S. T., Storm, D. R., and Tsien, R. Y. (2002). A new form of cerebellar long-term potentiation is postsynaptic and depends on nitric oxide but not cAMP. *Proc. Natl. Acad. Sci. U. S. A.* 99, 8389–8393. doi:10.1073/pnas.122206399

Lewis, J. E., and Maler, L. (2002). Dynamics of electrosensory feedback: short-term plasticity and inhibition in a parallel fiber pathway. *J. Neurophysiol.* 88, 1695–1706. doi:10.1152/jn.2002.88.4.1695

Li, B. Z., Sumera, A., Booker, S. A., and McCullagh, E. A. (2023). Current best practices for analysis of dendritic spine morphology and number in neurodevelopmental disorder research. *ACS Chem. Neurosci.* 14, 1561–1572. doi:10.1021/acschemneuro.3c00062

Lippman Bell, J. J., Lordkipanidze, T., Cobb, N., and Dunaevsky, A. (2010). Bergmann glial ensheathment of dendritic spines regulates synapse number without affecting spine motility. *Neuron Glia Biol.* 6, 193–200. doi:10.1017/S1740925X10000165

Lisman, J. (1989). A mechanism for the Hebb and the anti-Hebb processes underlying learning and memory. *Proc. Natl. Acad. Sci. U. S. A.* 86, 9574–9578. doi:10.1073/pnas.86.23.9574

Liu, Y., Formisano, L., Savtchouk, I., Takayasu, Y., Szabo, G., Zukin, R. S., et al. (2010). A single fear-inducing stimulus induces a transcription-dependent switch in synaptic AMPAR phenotype. *Nat. Neurosci.* 13, 223–231. doi:10.1038/nn.2474

Liu, C. J., Ammon, W., Siless, V., Fogarty, M., Wang, R., Atzeni, A., et al. (2021). Quantification of volumetric morphometry and optical property in the cortex of human cerebellum at micrometer resolution. *Neuroimage* 244, 118627. doi:10.1016/j.neuroimage.2021.118627

Liu, Z., Jiang, M., Liakath-Ali, K., Sclip, A., Ko, J., Zhang, R. S., et al. (2022). Deletion of Calsyntenin-3, an atypical cadherin, suppresses inhibitory synapses but increases excitatory parallel-fiber synapses in cerebellum. *Elife* 11, e70664–35. doi:10.7554/eLife.70664

Llano, I., Dreessen, J., Kano, M., and Konnerth, A. (1991). Intradendritic release of calcium induced by glutamate in cerebellar Purkinje cells. *Neuron* 7, 577–583. doi:10.1016/0896-6273(91)90370-f

London, M., Schreibman, A., Haäusser, M., Larkum, M. E., and Segev, I. (2002). The information efficacy of a synapse. *Nat. Neurosci.* 5, 332–340. doi:10.1038/nn826

Loschky, S. S., Spano, G. M., Marshall, W., Schroeder, A., Nemec, K. M., Schiereck, S. S., et al. (2022). Ultrastructural effects of sleep and wake on the parallel fiber synapses of the cerebellum. *Elife* 11, e84199–26. doi:10.7554/ELIFE.84199

Louis, E. D., Lee, M., Babij, R., Ma, K., Cortés, E., Vonsattel, J. P. G., et al. (2014). Reduced Purkinje cell dendritic arborization and loss of dendritic spines in essential tremor. *Brain* 137, 3142–3148. doi:10.1093/brain/awu314

Lu, H., Esquivel, A. V., and Bower, J. M. (2009). 3D electron microscopic reconstruction of segments of rat cerebellar Purkinje cell dendrites receiving ascending and parallel fiber granule cell synaptic inputs. *J. Comp. Neurol.* 514, 583–594. doi:10.1002/cne.22041

Luján, R., Aguado, C., Ciruela, F., Arus, X. M., Martín-Belmonte, A., Alfaro-Ruiz, R., et al. (2018a). SK2 channels associate with mGlu1α receptors and CaV2.1 channels in purkinje cells. *Front. Cell. Neurosci.* 12, 311–316. doi:10.3389/fncel.2018.00311

Luján, R., Aguado, C., Ciruela, F., Cózar, J., Kleindienst, D., de la Ossa, L., et al. (2018b). Differential association of GABAB receptors with their effector ion channels in Purkinje cells. *Brain Struct. Funct.* 223, 1565–1587. doi:10.1007/s00429-017-1568-y

Magnus, G., Xing, J., Zhang, Y., and Han, V. Z. (2023). Diversity of cellular physiology and morphology of Purkinje cells in the adult zebrafish cerebellum. *J. Comp. Neurol.* 531, 461–485. doi:10.1002/cne.25435

Mao, H., Mediavilla, T., Estévez-Silva, H., Marcellino, D., and Sultan, F. (2022). Increase of vesicular glutamate transporter 2 co-expression in the deep cerebellar nuclei related to skilled reach learning. *Brain Res.* 1782, 1–8. doi:10.1016/j.brainres.2022.147842

Mapelli, L., Gagliano, G., Soda, T., Laforenza, U., Moccia, F., and D'Angelo, E. U. (2017). Granular layer neurons control cerebellar neurovascular coupling through an NMDA receptor/NO-dependent system. *J. Neurosci.* 37, 1340–1351. doi:10.1523/JNEUROSCI.2025-16.2016

Marcaggi, P. (2015). Cerebellar endocannabinoids: retrograde signaling from purkinje cells. *Cerebellum* 14, 341–353. doi:10.1007/s12311-014-0629-5

Marr, D. (1969). A theory of cerebellar cortex. *J. Physiol.* 202, 437–470. doi:10.1113/jphysiol.1969.sp008820

Martone, M. E., Zhang, Y., Simpliciano, V. M., Carragher, B. O., and Ellisman, M. H. (1993). Three-dimensional visualization of the smooth endoplasmic reticulum in purkinje cell dendrites. *J. Neurosci.* 13, 4636–4646. doi:10.1523/jneurosci.13-11-04636.1993

Martone, M. E., Pollock, J. A., Jones, Y. Z., and Ellisman, M. H. (1996). Ultrastructural localization of dendritic messenger RNA in adult rat hippocampus. *J. Neurosci.* 16, 7437–7446. doi:10.1523/jneurosci.16-23-07437.1996

Masoli, S., Solinas, S., and D'Angelo, E. (2015). Action potential processing in a detailed Purkinje cell model reveals a critical role for axonal compartmentalization. *Front. Cell. Neurosci.* 9, 47–22. doi:10.3389/fncel.2015.00047

Masoli, S., Sanchez-Ponce, D., Vrieler, N., Abu-Haya, K., Lerner, V., Shahar, T., et al. (2024). Human Purkinje cells outperform mouse Purkinje cells in dendritic complexity and computational capacity. *Commun. Biol.* 7, 5. doi:10.1038/s42003-023-05689-y

Mavroudis, I. A., Petrides, F., Manani, M., Chatzinikolaou, F., Ciobică, A. S., Pădurariu, M., et al. (2017). Purkinje cells pathology in schizophrenia. A morphometric approach. *Rom. J. Morphol. Embryol.* 58, 419–424.

Mavroudis, I., Petridis, F., Kazis, D., Njau, S. N., Costa, V., and Baloyannis, S. J. (2019). Purkinje cells pathology in Alzheimer's disease. *Am. J. Alzheimers. Dis. Other Demen.* 34, 439–449. doi:10.1177/1533317519859200

Mavroudis, I., Kazis, D., Petridis, F., Chatzikonstantinou, S., Karantali, E., Njau, S., et al. (2021). Morphological and morphometric changes in the Purkinje cells of patients with essential tremor. *Exp. Ther. Med.* 23, 167–168. doi:10.3892/etm.2021.11090

Miguez-Cabello, F., Wang, X.-T., Yan, Y., Brake, N., Alexander, R. P. D., Perozzo, A. M., et al. (2025). GluA2-containing AMPA receptors form a continuum of Ca2+-permeable channels. *Nature* 641, 537–544. doi:10.1038/s41586-025-08736-2

Mitsumura, K., Hosoi, N., Furuya, N., and Hirai, H. (2011). Disruption of metabotropic glutamate receptor signalling is a major defect at cerebellar parallel fibre-Purkinje cell synapses in staggerer mutant mice. *J. Physiol.* 589, 3191–3209. doi:10.1113/jphysiol.2011.207563

Moccia, F., Zuccolo, E., Soda, T., Tanzi, F., Guerra, G., Mapelli, L., et al. (2015). Stim and Orai proteins in neuronal Ca(2+) signaling and excitability. *Front. Cell. Neurosci.* 9, 153. doi:10.3389/fncel.2015.00153

Mohrmann, L., Seebach, J., Missler, M., and Rohlmann, A. (2024). Distinct alterations in dendritic spine morphology in the absence of β-neurexins. *Int. J. Mol. Sci.* 25, 1285. doi:10.3390/ijms25021285

Mokhtar, D. M. (2020). Patterns of organization of cerebellum and spinal cord of the red-tail shark (*Epalzeorhynchos bicolor*): histological, morphometrical, and immunohistochemical studies. *Microsc. Microanal.* 26, 1255–1263. doi:10.1017/S1431927620024563

Morizawa, Y. M., Matsumoto, M., Nakashima, Y., Endo, N., Aida, T., Ishikane, H., et al. (2022). Synaptic pruning through glial synapse engulfment upon motor learning. *Nat. Neurosci.* 25, 1458–1469. doi:10.1038/s41593-022-01184-5

Morton, S. M., and Bastian, A. J. (2004). Cerebellar control of balance and locomotion. *Neuroscientist* 10, 247–259. doi:10.1177/1073858404263517

Mugnaini, E. (1983). The length of cerebellar parallel fibers in chicken and rhesus monkey. *J. Comp. Neurol.* 220, 7–15. doi:10.1002/cne.902200103

Mundel, P., Reiser, J., Borja, A. Z. M., Pavenstädt, H., Davidson, G. R., Kriz, W., et al. (1997). Rearrangements of the cytoskeleton and cell contacts induce process formation during differentiation of conditionally immortalized mouse podocyte cell lines. *Exp. Cell Res.* 236, 248–258. doi:10.1006/excr.1997.3739

Mut-Arbona, P., and Sperlágh, B. (2023). P2 receptor-mediated signaling in the physiological and pathological brain: from development to aging and disease. *Neuropharmacology* 233, 109541. doi:10.1016/j.neuropharm.2023.109541

Nakayama, H., Miyazaki, T., Abe, M., Yamazaki, M., Kawamura, Y., Choo, M., et al. (2024). Direct and indirect pathways for heterosynaptic interaction underlying developmental synapse elimination in the mouse cerebellum. *Commun. Biol.* 7, 806–813. doi:10.1038/s42003-024-06447-4

Napper, R. M. A., and Harvey, R. J. (1988). Quantitative study of the Purkinje cell dendritic spines in the rat cerebellum. *J. Comp. Neurol.* 274, 158–167. doi:10.1002/cne.902740203

Naur, P., Hansen, K. B., Kristensen, A. S., Dravid, S. M., Pickering, D. S., Olsen, L., et al. (2007). Ionotropic glutamate-like receptor delta2 binds D-serine and glycine. *Proc. Natl. Acad. Sci. U. S. A.* 104, 14116–14121. doi:10.1073/pnas.0703718104

Nedelescu, H., and Abdelhack, M. (2013). Comparative morphology of dendritic arbors in populations of purkinje cells in mouse sulcus and apex. *Neural Plast.* 2013, 948587. doi:10.1155/2013/948587

Nedelescu, H., Abdelhack, M., and Pritchard, A. T. (2018). Regional differences in Purkinje cell morphology in the cerebellar vermis of male mice. *J. Neurosci. Res.* 96, 1476–1489. doi:10.1002/jnr.24206

Negri, S., Faris, P., Pellavio, G., Botta, L., Orgiu, M., Forcaia, G., et al. (2020). Group 1 metabotropic glutamate receptors trigger glutamate-induced intracellular Ca2+ signals and nitric oxide release in human brain microvascular endothelial cells. *Cell. Mol. Life Sci.* 77, 2235–2253. doi:10.1007/s00018-019-03284-1

Nguyen, T. M., Thomas, L. A., Rhoades, J. L., Ricchi, I., Yuan, X. C., Sheridan, A., et al. (2023). Structured cerebellar connectivity supports resilient pattern separation. *Nature* 613, 543–549. doi:10.1038/s41586-022-05471-w

Nimchinsky, E. A., Sabatini, B. L., and Svoboda, K. (2002). Structure and function of dendritic spines. *Annu. Rev. Physiol.* 64, 313–353. doi:10.1146/annurev.physiol.64.081501.160008

Nishiyama, H., and Linden, D. J. (2004). Differential maturation of climbing fiber innervation in cerebellar vermis. *J. Neurosci.* 24, 3926–3932. doi:10.1523/JNEUROSCI.5610-03.2004

Nishiyama, J., and Yasuda, R. (2015). Biochemical computation for spine structural plasticity. *Neuron* 87, 63–75. doi:10.1016/j.neuron.2015.05.043

Nitta, A., Yamasaki, M., Miyazaki, T., Konno, K., Yoshimura, H., and Watanabe, M. (2025). Molecular and anatomical strengthening of "winner" climbing fiber synapses in developing mouse purkinje cells. *J. Neurosci.* 45, e2156242025. doi:10.1523/JNEUROSCI.2156-24.2025

Nomura, S., Yamasaki, M., Miyazaki, T., Konno, K., and Watanabe, M. (2025). Preferential localization of STIM1 to dendritic subsurface ER structures in mouse purkinje cells. *J. Neurosci.* 45, e1829242025. doi:10.1523/JNEUROSCI.1829-24.2025

Okamoto, K. I., Narayanan, R., Lee, S. H., Murata, K., and Hayashi, Y. (2007). The role of CaMKII as an F-actin-bundling protein crucial for maintenance of dendritic spine structure. *Proc. Natl. Acad. Sci. U. S. A.* 104, 6418–6423. doi:10.1073/pnas.0701656104

Okubo, Y., Suzuki, J., Kanemaru, K., Nakamura, N., Shibata, T., and Iino, M. (2015). Visualization of Ca2+ filling mechanisms upon synaptic inputs in the endoplasmic reticulum of cerebellar purkinje cells. *J. Neurosci.* 35, 15837–15846. doi:10.1523/JNEUROSCI.3487-15.2015

Osorno, T., Rudolph, S., Nguyen, T., Kozareva, V., Nadaf, N. M., Norton, A., et al. (2022). Candelabrum cells are ubiquitous cerebellar cortex interneurons with specialized circuit properties. *Nat. Neurosci.* 25, 702–713. doi:10.1038/s41593-022-01057-x

Otsu, Y., Marcaggi, P., Feltz, A., Isope, P., Kollo, M., Nusser, Z., et al. (2014). Activity-dependent gating of calcium spikes by A-type K+ channels controls climbing fiber signaling in purkinje cell dendrites. *Neuron* 84, 137–151. doi:10.1016/j.neuron.2014.08.035

O'Brien, J., and Unwin, N. (2006). Organization of spines on the dendrites of Purkinje cells. *Proc. Natl. Acad. Sci. U. S. A.* 103, 1575–1580. doi:10.1073/pnas.0507884103

Palay, S. L., and Chan-Palay, V. (1974a). *Cerebellar cortex*. Berlin, Heidelberg: Springer Berlin Heidelberg. doi:10.1007/978-3-642-65581-4

Palay, S. L., and Chan-Palay, V. (1974b). "Granule cells," in *Cerebellar cortex: cytology and organization* (Berlin, Heidelberg: Springer Berlin Heidelberg), 63–99. doi:10.1007/978-3-642-65581-4_3

Pali, E., Masoli, S., Di Domenico, D., Sorbo, T., Prestori, F., and D'Angelo, E. (2025). Coincidence detection between apical and basal dendrites drives STDP in cerebellar Golgi cells. *Commun. Biol.* 8, 731–16. doi:10.1038/s42003-025-08153-1

Palkovits, M., Magyar, P., and Szentágothai, J. (1971). Quantitative histological analysis of the cerebellar cortex in the cat. 3. Structural organization of the molecular layer. *Brain Res.* 34, 1–18. doi:10.1016/0006-8993(71)90347-7

Parajuli, L. K., Urakubo, H., Takahashi-Nakazato, A., Ogelman, R., Iwasaki, H., Koike, M., et al. (2020). Geometry and the organizational principle of spine synapses along a dendrite. *eNeuro* 7, 0248–20.2020. doi:10.1523/ENEURO.0248-20.2020

Park, D., Bae, S., Yoon, T. H., and Ko, J. (2018). Molecular mechanisms of synaptic specificity: spotlight on hippocampal and cerebellar synapse organizers. *Mol. Cells* 41, 373–380. doi:10.14348/molcells.2018.0081

Park, C., Gim, J., Bahn, S., Kim, G. H., Im, Y., Lee, S.-H., et al. (2023). A cerebellar disinhibitory circuit supports synaptic plasticity. *Bioarxiv*. doi:10.1101/2023.09.15.557147

Paul, M. A., Sigoillot, S. M., Marti, L., Urra Quiroz, F. J., Delagrange, M., Cheung, H. W., et al. (2024). Stepwise molecular specification of excitatory synapse diversity onto cerebellar Purkinje cells. *Nat. Neurosci.* 28, 308–319. doi:10.1038/s41593-024-01826-w

Pchitskaya, E., and Bezprozvanny, I. (2020). Dendritic spines shape analysis—classification or clusterization? Perspective. *Front. Synaptic Neurosci.* 12, 31. doi:10.3389/fnsyn.2020.00031

Peter, S., Ten Brinke, M. M., Stedehouder, J., Reinelt, C. M., Wu, B., Zhou, H., et al. (2016). Dysfunctional cerebellar Purkinje cells contribute to autism-like behaviour in Shank2-deficient mice. *Nat. Commun.* 7, 12627. doi:10.1038/ncomms12627

Piochon, C., Irinopoulou, T., Brusciano, D., Bailly, Y., Mariani, J., and Levenes, C. (2007). NMDA receptor contribution to the climbing fiber response in the adult mouse Purkinje cell. *J. Neurosci.* 27, 10797–10809. doi:10.1523/JNEUROSCI.2422-07.2007

Piochon, C., Levenes, C., Ohtsuki, G., and Hansel, C. (2010). Purkinje cell NMDA receptors assume a key role in synaptic gain control in the mature cerebellum. *J. Neurosci.* 30, 15330–15335. doi:10.1523/JNEUROSCI.4344-10.2010

Piochon, C., Kruskal, P., Maclean, J., and Hansel, C. (2012). Non-Hebbian spike-timing-dependent plasticity in cerebellar circuits. *Front. Neural Circuits* 6, 124. doi:10.3389/fncir.2012.00124

Piochon, C., Kloth, A. D., Grasselli, G., Titley, H. K., Nakayama, H., Hashimoto, K., et al. (2014). Cerebellar plasticity and motor learning deficits in a copy-number variation mouse model of autism. *Nat. Commun.* 5, 5586. doi:10.1038/ncomms6586

Pugh, J. R., and Raman, I. M. (2005). GABAA receptor kinetics in the cerebellar nuclei: evidence for detection of transmitter from distant release sites. *Biophys. J.* 88, 1740–1754. doi:10.1529/biophysj.104.055814

Purkinje, jan E. (1837). Neueste Untersuchungen aus der Nerven-und Hirnanatomie. *Amtlicher Ber. über Versamml. Ges. Dtsch. Naturforscher Aerzte*, 177–180.

Raghu, P., Joseph, A., Krishnan, H., Singh, P., and Saha, S. (2019). Phosphoinositides: regulators of nervous system function in health and disease. *Front. Mol. Neurosci.* 12, 208. doi:10.3389/fnmol.2019.00208

Ramón y Cajal, S. (1888). Estructura de los centros nerviosos de las aves. *Rev. Trimest. Histol. Norm. Patològica* 1, 1–10.

Rapp, M., Segev, I., and Yarom, Y. (1994). Physiology, morphology and detailed passive models of Guinea-pig cerebellar Purkinje cells. *J. Physiol.* 474, 101–118. doi:10.1113/jphysiol.1994.sp020006

Renzi, F., and Cull-Candy, S. G. (2007). Climbing-fibre activation of NMDA receptors in Purkinje cells of adult mice. *J. Physiol.* 585, 91–101. doi:10.1113/jphysiol.2007.141531

Rieke, F. (1999). *Spikes: exploring the neural code*. Cambridge, Mass: MIT.

Risher, W. C., Ustunkaya, T., Alvarado, J. S., and Eroglu, C. (2014). Rapid golgi analysis method for efficient and unbiased classification of dendritic spines. *PLoS One* 9, e107591. doi:10.1371/journal.pone.0107591

Roberts, P. D., and Leen, T. K. (2010). Anti-Hebbian spike-timing-dependent plasticity and adaptive sensory processing. *Front. Comput. Neurosci.* 4, 156–11. doi:10.3389/fncom.2010.00156

Roesler, M. K., Lombino, F. L., Freitag, S., Schweizer, M., Hermans-Borgmeyer, I., Schwarz, J. R., et al. (2019). Myosin XVI regulates actin cytoskeleton dynamics in dendritic spines of purkinje cells and affects presynaptic organization. *Front. Cell. Neurosci.* 13, 330. doi:10.3389/fncel.2019.00330

Roth, A., and Hausser, M. (2001). Compartmental models of rat cerebellar Purkinje cells based on simultaneous somatic and dendritic patch-clamp recordings. *J. Physiol.* 535, 445–472. doi:10.1111/j.1469-7793.2001.00445.x

Rubio, M. E., and Soto, F. (2001). Distinct localization of P2X receptors at excitatory postsynaptic specializations. *J. Neurosci.* 21, 641–653. doi:10.1523/jneurosci.21-02-00641.2001

Runge, K., Cardoso, C., and de Chevigny, A. (2020). Dendritic spine plasticity: function and mechanisms. *Front. Synaptic Neurosci.* 12, 36. doi:10.3389/fnsyn.2020.00036

Ryu, K., Yokoyama, M., Yamashita, M., and Hirano, T. (2012). Induction of excitatory and inhibitory presynaptic differentiation by GluD1. *Biochem. Biophys. Res. Commun.* 417, 157–161. doi:10.1016/j.bbrc.2011.11.075

Ryu, C., Jang, D. C., Jung, D., Kim, Y. G., Shim, H. G., Ryu, H.-H., et al. (2017). STIM1 regulates somatic Ca2+ signals and intrinsic firing properties of cerebellar purkinje neurons. *J. Neurosci.* 37, 8876–8894. doi:10.1523/JNEUROSCI.3973-16.2017

Safo, P., Cravatt, B., and Regehr, W. (2006). Retrograde endocannabinoid signaling in the cerebellar cortex. *Cerebellum* 5, 134–145. doi:10.1080/14734220600791477

Santucci, D. M., and Raghavachari, S. (2008). The effects of NR2 subunit-dependent NMDA receptor kinetics on synaptic transmission and CaMKII activation. *PLoS Comput. Biol.* 4, e1000208. doi:10.1371/journal.pcbi.1000208

Schmahmann, J. D. (2019). The cerebellum and cognition. *Neurosci. Lett.* 688, 62–75. doi:10.1016/j.neulet.2018.07.005

Schmidt, H. (2019). Control of presynaptic parallel fiber efficacy by activity-dependent regulation of the number of occupied release sites. *Front. Syst. Neurosci.* 13, 30–36. doi:10.3389/fnsys.2019.00030

Schonewille, M., Girasole, A. E., Rostaing, P., Mailhes-Hamon, C., Ayon, A., Nelson, A. B., et al. (2021). NMDARs in granule cells contribute to parallel fiber-Purkinje cell synaptic plasticity and motor learning. *Proc. Natl. Acad. Sci. U. S. A.* 118, e2102635118–e2102635119. doi:10.1073/pnas.2102635118

Sdrulla, A. D., and Linden, D. J. (2007). Double dissociation between long-term depression and dendritic spine morphology in cerebellar Purkinje cells. *Nat. Neurosci.* 10, 546–548. doi:10.1038/nn1889

Seigneur, E., and Südhof, T. C. (2017). Cerebellins are differentially expressed in selective subsets of neurons throughout the brain. *J. Comp. Neurol.* 525, 3286–3311. doi:10.1002/cne.24278

Selimi, F., Lohof, A. M., Heitz, S., Lalouette, A., Jarvis, C. I., Bailly, Y., et al. (2003). Lurcher GRID2-induced death and depolarization can Be dissociated in cerebellar Purkinje cells. *Neuron* 37, 813–819. doi:10.1016/S0896-6273(03)00093-X

Sereno, M. I., Diedrichsen, J., Tachrount, M., Testa-Silva, G., D Arceuil, H., and De Zeeuw, C. (2020). The human cerebellum has almost 80% of the surface area of the neocortex. *Proc. Natl. Acad. Sci. U. S. A.* 117, 19538–19543. doi:10.1073/pnas.2002896117

Sharp, A. H., McPherson, P. S., Dawson, T. M., Aoki, C., Campbell, K. P., and Snyder, S. H. (1993). Differential immunohistochemical localization of inositol 1,4,5-trisphosphate- and ryanodine-sensitive Ca2+ release channels in rat brain. *J. Neurosci.* 13, 3051–3063. doi:10.1523/jneurosci.13-07-03051.1993

Shouval, H. Z., Bear, M. F., and Cooper, L. N. (2002). A unified model of NMDA receptor-dependent bidirectional synaptic plasticity. *Proc. Natl. Acad. Sci. U. S. A.* 99, 10831–10836. doi:10.1073/pnas.152343099

Sigoillot, S. M., Iyer, K., Binda, F., González-Calvo, I., Talleur, M., Vodjdani, G., et al. (2015). The secreted protein C1QL1 and its receptor Bai3 control the synaptic connectivity of excitatory inputs converging on cerebellar purkinje cells. *Cell Rep.* 10, 820–832. doi:10.1016/j.celrep.2015.01.034

Skibinska-Kijek, A., Wisniewska, M. B., Gruszczynska-Biegala, J., Methner, A., and Kuznicki, J. (2009). Immunolocalization of STIM1 in the mouse brain. *Acta Neurobiol. Exp. (Wars).* 69, 413–428. doi:10.55782/ane-2009-1753

Sotelo, C., and Dusart, I. (2009). Intrinsic versus extrinsic determinants during the development of Purkinje cell dendrites. *Neuroscience* 162, 589–600. doi:10.1016/j.neuroscience.2008.12.035

Spacek, J., and Harris, K. M. (1997). Three-dimensional organization of smooth endoplasmic reticulum in hippocampal CA1 dendrites and dendritic spines of the immature and mature rat. *J. Neurosci.* 17, 190–203. doi:10.1523/jneurosci.17-01-00190.1997

Spanaki, C., Sidiropoulou, K., Petraki, Z., Diskos, K., Konstantoudaki, X., Volitaki, E., et al. (2024). Glutamate-specific gene linked to human brain evolution enhances synaptic plasticity and cognitive processes. *iScience* 27, 108821. doi:10.1016/j.isci.2024.108821

Stevenson, M. E., Nazario, A. S., Czyz, A. M., Owen, H. A., and Swain, R. A. (2021). Motor learning rapidly increases synaptogenesis and astrocytic structural plasticity in the rat cerebellum. *Neurobiol. Learn. Mem.* 177, 107339. doi:10.1016/j.nlm.2020.107339

Streng, M. L., Carter, R. E., Kottke, B. W., Togneri, K., Wasserman, E., Rajendran, V., et al. (2025). Purkinje cell spatial correlation dynamics are key to cerebellar cortical contributions to behavior. *J. Neurosci.* 45, e1915242025. doi:10.1523/JNEUROSCI.1915-24.2025

Südhof, T. C. (2008). Neuroligins and neurexins link synaptic function to cognitive disease. *Nature* 455, 903–911. doi:10.1038/nature07456

Südhof, T. C. (2017). Synaptic neurexin complexes: a molecular code for the logic of neural circuits. *Cell* 171, 745–769. doi:10.1016/j.cell.2017.10.024

Südhof, T. C. (2023). Cerebellin–neurexin complexes instructing synapse properties. *Curr. Opin. Neurobiol.* 81, 102727. doi:10.1016/j.conb.2023.102727

Sugawara, T., Hisatsune, C., Le, T. D., Hashikawa, T., Hirono, M., Hattori, M., et al. (2013). Type 1 inositol trisphosphate receptor regulates cerebellar circuits by maintaining the spine morphology of purkinje cells in adult mice. *J. Neurosci.* 33, 12186–12196. doi:10.1523/JNEUROSCI.0545-13.2013

Sugawara, T., Hisatsune, C., Miyamoto, H., Ogawa, N., and Mikoshiba, K. (2017). Regulation of spinogenesis in mature Purkinje cells via mGluR/PKC-mediated phosphorylation of CaMKII. *Proc. Natl. Acad. Sci. U. S. A.* 114, E5256-E5265–E5265. doi:10.1073/pnas.1617270114

Suk, E., Lai, K., and Uesaka, N. (2025). Reduced GABAergic inhibition and impaired synapse elimination by neuroligin-2 deletion from Purkinje cells of the developing cerebellum, 1–18. doi:10.3389/fncir.2025.1530141

Szabó, L. E., Marcello, G. M., Süth, M., Sótonyi, P., and Rácz, B. (2021). Distribution of cortactin in cerebellar Purkinje cell spines. *Sci. Rep.* 11, 1375–11. doi:10.1038/s41598-020-80469-w

Sziber, Z., Torrents-Solé, P., Kovacevic, A., and Kapfhammer, J. P. (2025). Protein kinase C gamma regulates Purkinje cell dendritic spine development in a mouse model of spinocerebellar ataxia. *Exp. Neurol.* 393, 115377. doi:10.1016/j.expneurol.2025.115377

Tabata, T., and Kano, M. (2006). GABAB receptor-mediated modulation of glutamate signaling in cerebellar Purkinje cells. *Cerebellum* 5, 127–133. doi:10.1080/14734220600788911

Takeo, Y. H., Shuster, S. A., Jiang, L., Hu, M. C., Luginbuhl, D. J., Rülicke, T., et al. (2021). GluD2-and Cbln1-mediated competitive interactions shape the dendritic arbors of cerebellar Purkinje cells. *Neuron* 109, 629–644.e8. doi:10.1016/j.neuron.2020.11.028

Tan, L., Shi, J., Moghadami, S., Parasar, B., Wright, C. P., Seo, Y., et al. (2023). Lifelong restructuring of 3D genome architecture in cerebellar granule cells. *Science* 381, 1112–1119. doi:10.1126/science.adh3253

Tao-Cheng, J.-H. (2025). Ultrastructural characterization of peri-synaptic astrocytic processes around cerebellar Purkinje spines under resting and stimulated conditions. *Mol. Brain* 18, 28. doi:10.1186/s13041-025-01198-7

Thomas, R. E., Mudlaff, F., Schweers, K., Farmer, W. T., and Suvrathan, A. (2024). Heterogeneity in slow synaptic transmission diversifies purkinje cell timing. *J. Neurosci.* 44, e0455242024. doi:10.1523/JNEUROSCI.0455-24.2024

Tian, W., Zhou, J., Bartlett, A., Zeng, Q., Liu, H., Castanon, R. G., et al. (2022). Epigenomic complexity of the human brain revealed by single-cell DNA methylomes and 3D genome structures. *bioRxiv* 11.30, 518285. doi:10.1101/2022.11.30.518285

Toledo, A., Lang, F., Doengi, M., Morrison, H., Stein, V., and Baader, S. L. (2019). Merlin modulates process outgrowth and synaptogenesis in the cerebellum. *Brain Struct. Funct.* 224, 2121–2142. doi:10.1007/s00429-019-01897-7

Tolve, M., Tutas, J., Özer-Yildiz, E., Klein, I., Petzold, A., Fritz, V. J., et al. (2025). The endocytic adaptor AP-2 maintains Purkinje cell function by balancing cerebellar parallel and climbing fiber synapses. *Cell Rep.* 44, 115256. doi:10.1016/j.celrep.2025.115256

Tomiyama, M., Palacios, J. M., Cortés, R., and Mengod, G. (1999). Flip and flop variants of AMPA receptor subunits in the human cerebellum: implication for the selective vulnerability of Purkinje cells. *Synapse* 31, 163–167. doi:10.1002/(SICI)1098-2396(199902)31:2<163::AID-SYN10>3.0.CO;2-H

Tønnesen, J., Katona, G., Rózsa, B., and Nägerl, U. V. (2014). Spine neck plasticity regulates compartmentalization of synapses. *Nat. Neurosci.* 17, 678–685. doi:10.1038/nn.3682

Uemura, T., Lee, S. J., Yasumura, M., Takeuchi, T., Yoshida, T., Ra, M., et al. (2010). Trans-synaptic interaction of GluRdelta2 and Neurexin through Cbln1 mediates synapse formation in the cerebellum. *Cell* 141, 1068–1079. doi:10.1016/j.cell.2010.04.035

Uemura, T., Suzuki-Kouyama, E., Kawase, S., Kurihara, T., Yasumura, M., Yoshida, T., et al. (2022). Neurexins play a crucial role in cerebellar granule cell survival by organizing autocrine machinery for neurotrophins. *Cell Rep.* 39, 110624. doi:10.1016/j.celrep.2022.110624

Uesaka, N., Abe, M., Konno, K., Yamazaki, M., Sakoori, K., Watanabe, T., et al. (2018). Retrograde signaling from progranulin to Sort1 counteracts synapse elimination in the developing cerebellum. *Neuron* 97, 796–805. doi:10.1016/j.neuron.2018.01.018

Uriu, Y., Kiyonaka, S., Miki, T., Yagi, M., Akiyama, S., Mori, E., et al. (2010). Rab3-interacting molecule γ isoforms lacking the rab3-binding domain induce long lasting currents but block neurotransmitter vesicle anchoring in voltage-dependent P/Q-type Ca2+ channels. *J. Biol. Chem.* 285, 21750–21767. doi:10.1074/jbc.M110.101311

van der Heijden, M. E., and Sillitoe, R. V. (2021). Interactions between purkinje cells and granule cells coordinate the development of functional cerebellar circuits. *Neuroscience* 462, 4–21. doi:10.1016/j.neuroscience.2020.06.010

van der Heijden, M. E., Lackey, E. P., Perez, R., Işleyen, F. S., Brown, A. M., Donofrio, S. G., et al. (2021). Maturation of Purkinje cell firing properties relies on neurogenesis of excitatory neurons. *Elife* 10, e68045–37. doi:10.7554/eLife.68045

Van Overwalle, F. (2024). Social and emotional learning in the cerebellum. *Nat. Rev. Neurosci.* 25, 776–791. doi:10.1038/s41583-024-00871-5

Vecellio, M., Schwaller, B., Meyer, M., Hunziker, W., and Celio, M. R. (2000). Alterations in Purkinje cell spines of calbindin D-28 k and parvalbumin knock-out mice. *Eur. J. Neurosci.* 12, 945–954. doi:10.1046/j.1460-9568.2000.00986.x

Verslegers, M., Van Hove, I., Dekeyster, E., Gantois, I., Hu, T. T., D'Hooge, R., et al. (2014). MMP-2 mediates Purkinje cell morphogenesis and spine development in the mouse cerebellum. *Brain Struct. Funct.* 220, 1601–1617. doi:10.1007/s00429-014-0747-3

Vlachos, A., Korkotian, E., Schonfeld, E., Copanaki, E., Deller, T., and Segal, M. (2009). Synaptopodin regulates plasticity of dendritic spines in hippocampal neurons. *J. Neurosci.* 29, 1017–1033. doi:10.1523/JNEUROSCI.5528-08.2009

VoŽeh, F. (2015). Jan Evangelista Purkyně and the cerebellum then and now. *Physiol. Res.* 64, S567–S584. doi:10.33549/physiolres.933231

Wagner, W., Brenowitz, S. D., and Hammer, J. A. (2011). Myosin-Va transports the endoplasmic reticulum into the dendritic spines of Purkinje neurons. *Nat. Cell Biol.* 13, 40–48. doi:10.1038/ncb2132

Walter, J. T., Dizon, M.-J., and Khodakhah, K. (2009). The functional equivalence of ascending and parallel fiber inputs in cerebellar computation. *J. Neurosci.* 29, 8462–8473. doi:10.1523/JNEUROSCI.5718-08.2009

Wang, Y., Deng, X., Mancarella, S., Hendron, E., Eguchi, S., Soboloff, J., et al. (2010). The calcium store sensor, STIM1, reciprocally controls Orai and CaV1.2 channels. *Science* 330, 105–109. doi:10.1126/science.1191086

Wang, B., Lebel, A., and Mello, A. M. D. (2025). Trends in Cognitive Sciences Ignoring the cerebellum is hindering progress in neuroscience. *Trends Cogn. Sci.* xx, 1–13. doi:10.1016/j.tics.2025.01.004

Wilms, C. D., and Häusser, M. (2015). Reading out a spatiotemporal population code by imaging neighbouring parallel fibre axons *in vivo*. *Nat. Commun.* 6, 6464. doi:10.1038/ncomms7464

Yamashita, A., Makita, K., Kuroiwa, T., and Tanaka, K. (2006). Glutamate transporters GLAST and EAAT4 regulate postischemic Purkinje cell death: an *in vivo* study using a cardiac arrest model in mice lacking GLAST or EAAT4. *Neurosci. Res.* 55, 264–270. doi:10.1016/j.neures.2006.03.007

Yoast, R. E., Emrich, S. M., Zhang, X., Xin, P., Johnson, M. T., Fike, A. J., et al. (2020). The native ORAI channel trio underlies the diversity of Ca2+ signaling events. *Nat. Commun.* 11, 2444. doi:10.1038/s41467-020-16232-6

Yuste, R. (2015). The discovery of dendritic spines by Cajal. *Front. Neuroanat.* 9, 18–6. doi:10.3389/fnana.2015.00018

Yuste, R., and Bonhoeffer, T. (2004). Genesis of dendritic spines: insights from ultrastructural and imaging studies. *Nat. Rev. Neurosci.* 5, 24–34. doi:10.1038/nrn1300

Yuzaki, M., and Aricescu, A. R. (2017). A GluD coming-of-age story. *Trends Neurosci.* 40, 138–150. doi:10.1016/j.tins.2016.12.004

Zárský, V. (2012). Jan Evangelista Purkyně/Purkinje (1787-1869) and the establishment of cellular physiology–Wrocław/Breslau as a central European cradle for a new science. *Protoplasma* 249, 1173–1179. doi:10.1007/s00709-012-0407-5

Zeng, W., Yuan, J. P., Kim, M. S., Choi, Y. J., Huang, G. N., Worley, P. F., et al. (2008). STIM1 gates TRPC channels, but not Orai1, by electrostatic interaction. *Mol. Cell* 32, 439–448. doi:10.1016/j.molcel.2008.09.020

Zhang, B., Chen, L. Y., Liu, X., Maxeiner, S., Lee, S.-J., Gokce, O., et al. (2015). Neuroligins sculpt cerebellar purkinje-cell circuits by differential control of distinct classes of synapses. *Neuron* 87, 781–796. doi:10.1016/j.neuron.2015.07.020

Zhang, R. S., Liakath-Ali, K., and Südhof, T. C. (2020). Latrophilin-2 and latrophilin-3 are redundantly essential for parallel-fiber synapse function in cerebellum. *Elife* 9, e54443–21. doi:10.7554/eLife.54443

Zheng, J., Yang, Q., Makris, N., Huang, K., Liang, J., Ye, C., et al. (2023). Three-Dimensional digital reconstruction of the cerebellar cortex: lobule thickness, surface area measurements, and layer architecture. *Cerebellum* 22, 249–260. doi:10.1007/s12311-022-01390-8

Zhu, J., Qiu, W., Wei, F., Zhang, J., Yuan, Y., Liu, L., et al. (2024). Toll-like receptor 4 deficiency in Purkinje neurons drives cerebellar ataxia by impairing the BK channel-mediated after-hyperpolarization and cytosolic calcium homeostasis. *Cell Death Dis.* 15, 594. doi:10.1038/s41419-024-06988-w

Frontiers in Physiology

Understanding how an organism's components work together to maintain a healthy state

The second most-cited physiology journal, promoting a multidisciplinary approach to the physiology of living systems - from the subcellular and molecular domains to the intact organism and its interaction with the environment.

Discover the latest Research Topics

See more →

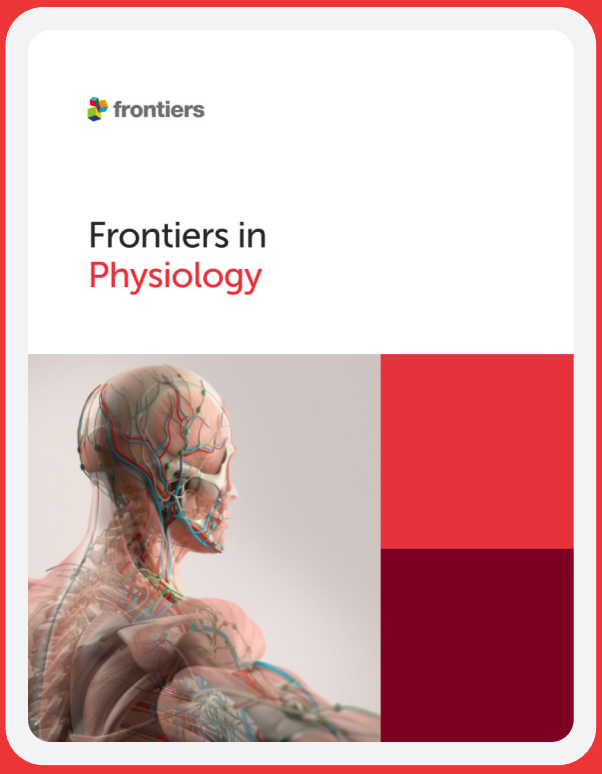

Frontiers

Avenue du Tribunal-Fédéral 34
1005 Lausanne, Switzerland
frontiersin.org

Contact us

+41 (0)21 510 17 00
frontiersin.org/about/contact